공학박사학위논문

다중 연결된 직사각 박판보에 관한 고차 보 이론 기반의 통합 해석 연구

Unified Higher-Order Beam Analysis for Multiply-Connected Thin-Walled Box Beams

2016년 2월

서울대학교 대학원

기계항공공학부

최 수 민

ABSTRACT

Unified Higher-Order Beam Analysis for Multiply-Connected Thin-walled Box Beams

Soomin Choi
School of Mechanical and Aerospace Engineering
The Graduate School
Seoul National University

Both the consideration of significant higher-order deformation degrees and the derivation of exact matching conditions among field variables at a joint are required to establish a one-dimensional beam model applicable to thin-walled box beam systems. Especially when three or more box beams are multiply-connected at a joint, significantly flexible behavior is observed near the joint that dominates the structural responses of the entire system. Moreover, the flexibility of the joint varies considerably depending on the number of beam members connected at the joint and the joint angles among the members. Because of the difficulties, no one-dimensional beam analysis method has yet been proposed that can capture the structural responses of the box beams-joint systems accurately. With this

background, this study proposes a unified one-dimensional higher-order beam analysis approach for the first time that is applicable to the multiply-connected box beams-joint systems under both out-of-plane loads and in-plane loads. It is worth mentioning that the concept of so-called “edge resultants” as well as conventional (sectional) resultants are employed to derive physically correct equilibrium conditions at a joint and that the exact joint matching conditions are theoretically derived by applying an energy method to the equilibrium conditions. The derived matching conditions are valid even when any number of beams meet at any angle. In addition, higher-order deformation degrees (e.g. bending warping, bending distortion, and etc.) are newly introduced or redefined that are essential to represent the exact joint flexibility of considered systems. The accuracy and validity of the proposed analysis method are checked by comparing the present approach based results and the shell analysis results for various box beams-joint systems.

Keywords: thin-walled box beam, higher-order beam theory, joint equilibrium, joint matching condition

Student Number: 2009-20732

CONTENTS

LIST OF TABLES

LIST OF FIGURES

CHAPTER 1.
OVERVIEW

Thin-walled closed beams show relatively high bending and torsional rigidities compared to other types of beams with identical mass, and thus those beams have been widely used as principle load carrying members of automotive body structures to meet the requirements of lightweight vehicle design. Because of their hollow cross-section, however, cross-sectional deformations are easily accompanied when those beams are deformed, and the cross-sectional deformations cause highly flexible and complicated behavior of the thin-walled closed beams. Especially when three or more thin-walled closed beams meet at a joint, the cross-sectional deformations of those beams are further amplified near the joint, and thus significantly flexible behavior determining the rigidity of whole structure is observed near the joint. Meanwhile, classical beam theories such as Euler or Timoshenko beam theory cannot deal with those significant flexibilities caused by cross-sectional deformations, and for this reason, and for this reason, some difficulties that the classical beam theories overestimate the stiffness of automotive body structure, e.g. under body structure and side frame shown in Figs. 1(a, b) have been founded (one can see those difficulties by comparing the classical beam analysis results with the accurate results obtained by ABAQUS shell analysis given in Figs. 2(a, b)).

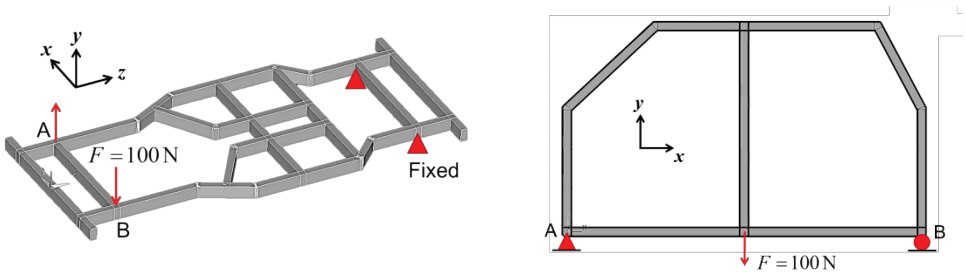

(a) (b)

Fig. 1.1 multiply-connected thin-walled beam structures (a) underbody structure, (b) side frame.

From those difficulties of the classical beam theories, there have been efforts to develop one-dimensional beam analysis applicable to multiply-connected thin-walled closed beam structures such as automobile body structures. Initial studies employed the classical beam theories and expressed the joint flexibilities by introducing some artificial joint models composed of rigid sections and rotational springs. Thereafter, some analysis approaches based on the classical beam theories introduced joint stiffness elements obtained from the detailed shell joint model as a way to involve the joint flexibilities in their approaches. Recently, higher-order beam theories considering significant cross-sectional deformations as additional degrees of freedom have been developed, and some analysis method theoretically expressing the joint flexibilities without using artificial concepts have been proposed based on the higher-order beam theories (the detailed descriptions with respect to those previous studies are given in Chapters. 2~4). Despite all these efforts, however, there is no one-dimensional beam analysis method consistently

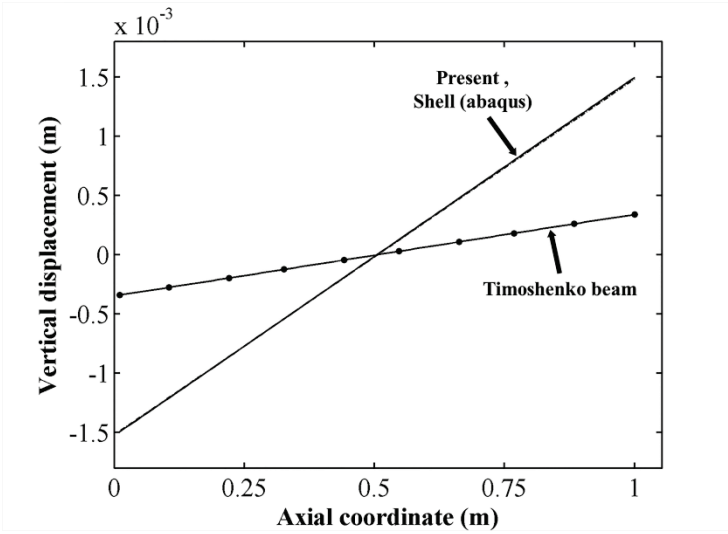

(a)

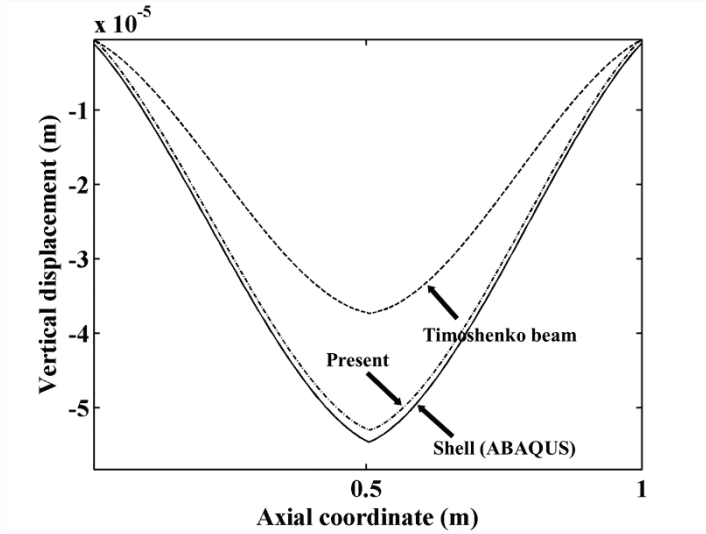

(b)

Fig. 1.2 (a) analysis results of the vertical displacement (in *y* direction) for Beam AB in Fig. 1.1(a), (b) analysis results of vertical displacement (in *y* direction) for Beam AB in Fig. 1.1(b)..

applicable to various multiply-connected thin-walled closed beams because the flexible responses of the joints vary considerably depending on the number of beams connected to the joint, the joint angles among those beams and the dimensions of cross-sections of those beams. With this background, therefore, a higher-order beam analysis method consistently applicable to various multiply-connected thin-walled box beams will be proposed for the first time in this study.

The underbody structure of vehicle subjected to out-of-plane loads is shown in Fig. 1(a), and the torsional rigidity of the underbody structure can be evaluated under the given boundary condition. To exactly interpret multiply-connected box beams under out-of-plane loads such as the problem given in Fig. 1(a), the higher-order beam theory considering torsional warping and distortional deformations of box beam cross-section as independent field variables in addition to rigid body motions of cross-section, i.e. vertical displacement, bending/shear rotation and torsional rotation is employed in this study. The key is finding exact matching conditions among all field variables of the box beams meeting at a joint. To determine theoretically correct joint matching conditions, we first derive exact matching conditions for two box beams meeting at an angled joint of magnitude ϕ; the joint matrix $\mathbf{T}(\phi)$ representing joint matching conditions is exactly derived by considering some essential conditions which $\mathbf{T}(\phi)$ must hold, and the detailed procedures are given in Chapter 2. Subsequently, the equilibrium conditions at a joint of multiply-connected box beams among generalized forces, which are work conjugates of the field variables, are derived from the joint matrix $\mathbf{T}(\phi)$, and

consequently the desired joint matching conditions for multiply-connected box beams are exactly derived by applying energy method to those equilibrium conditions (the detailed procedures are given in Chapter 3). Observing the results shown in Fig. 2(a), one can find that the proposed one-dimensional analysis can interpret the response on the underbody structure as accurately as ABAQUS shell analysis.

The side frame of vehicle subjected to in-plane loads is shown in fig. 1(b), and the bending rigidity of side frame can be calculated through the given boundary condition. One-dimensional analysis method for multiply-connected box beams subjected to in-plane loads such as the problem given in Fig. 1(b) is also developed in this study based on the approaches established in those studies concerning out-of-plane loads. Because the significant cross-sectional deformations inducing the joint flexibilities of multiply-connected box beams under in-plane loads are not clearly found, the cross-sectional deformations such as extensional warping, extensional distortion, bending warping, bending distortion and etc. are theoretically derived in this study, and a higher-order beam theory considering those cross-sectional deformations as independent field variables in addition to the rigid body motions of cross-section, i.e. longitudinal displacement, transverse displacement and in-plane bending/shear rotation is newly established (the details can be found in Chapter 4 and 5). Thereafter, the joint matrix $\mathbf{T}(\phi)$ representing the joint matching conditions for two box beams meeting at an angled joint of magnitude ϕ under in-plane loads is exactly derived by considering some essential

conditions $\mathbf{T}(\phi)$ must hold; in in-plane loading case, more considerations and cares are required because more cross-sectional deformations of further complicated deformation patterns are considered, and the detailed procedures are given in Chapter 4. Equilibrium conditions of generalized forces at a joint of multiply-connected box beams under in-plane loads are exactly derived from the matrix $\mathbf{T}(\phi)$, and exact joint matching conditions consistently applicable to multiply-connected box beams under in-plane loads are theoretically derived by applying energy method to those equilibrium conditions; the details are given in Chapter 5. Observing the results given in Fig. 2(b), one can also find that the proposed method can interpret the behavior of side frame as accurately as ABAQUS shell analysis.

As mentioned above, an exact higher-order beam analysis method for multiply-connected thin-walled box beams is newly developed in this study. In addition, theoretically correct equilibrium conditions of generalized forces and matching conditions of field variables at a joint of multiply-connected box beams are determined for the first time. The proposed derivation approaches of those conditions are expected to be an important building block for expanding the scope of structures that can be interpreted by using the higher-order beam analysis to multiply-connected three dimensional thin-walled closed beams.

CHAPTER 2.
Higher-Order Beam Analysis for Two Box Beams-Joint Systems Subjected to Out-of-Plane Bending and Torsion

2.1 Introduction

This work is concerned with the analysis of thin-walled box beams connected through angled joints under out-of-plane bending and torsion as depicted in Fig. 2.1. The analysis will be carried out by higher-order beam theories that employ five kinematic variables representing sectional warping (U) and distortion (χ) in addition to the standard Timoshenko kinematic variables such as vertical bending deflection (V), bending/shear rotation (β), and torsional rotation (θ). The displacements or deformations of the cross section of a box beam corresponding to the five kinematic variables are illustrated in Fig. 2.2. The importance of considering warping and distortion in thin-walled closed beams has been addressed in earlier investigations [1-9] and several forms of higher-order theories have been developed for straight box beams [1, 3, 5, 8, 10, 11].

Nevertheless, there is no box beam theory based theoretical method to exactly match the degrees of freedom at an angle joint where two straight box beams are connected. The significant local effects appearing near joints of thin-walled box beams have been pointed out in several investigations [12–16]. The joint-related

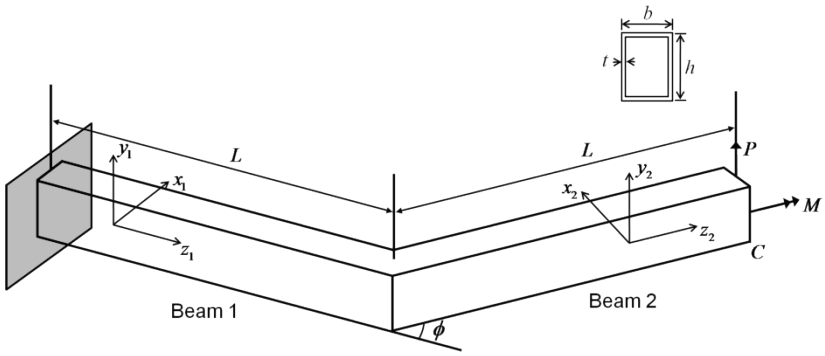

Fig. 2.1 Thin-walled box beams connected at an angled joint.

investigations using a higher-order beam theory were first given by Jang et al. [17-19], but the approach used an approximate technique that minimizes the difference between three-dimensional displacements in the sections of two beams connected at an angled joint. On the contrary, we aim to derive the *exact* condition relating the field variables of one box beam to those of another box beam at the joint using a higher-order beam theory [20].

In deriving the joint matching condition, we will employ the higher-order beam theory given in [17] which employs the above-mentioned five field variables. The joint matching condition can be expressed by a 5×5 transformation matrix $\mathbf{T}(\phi)$ (ϕ: joint angle) relating $\mathbf{U}_1$ and $\mathbf{U}_2$ as $\mathbf{U}_2=\mathbf{T}(\phi)\cdot\mathbf{U}_1$ where $\mathbf{U}_p=\{V,\ \beta,\ \theta,\ U,\ \chi\}_p^{\mathrm{T}}$ ($p=1,\ 2$) is the field variable vector of Beam p. For a later use, we introduce the symbol $\mathbf{F}_p=\{P,\ M,\ H,\ B,\ Q\}_p^{\mathrm{T}}$ to denote the generalized force vector, which is the work conjugate of $\mathbf{U}_p$. Here, P, M, and H denote vertical

shear force, bending moment, and twisting moment, respectively. Note that they all have resultants. On the other hand, the bimoment B and transverse bimoment Q have no resultant, i.e., they represent self-equilibrated terms. In case of the Euler or Timoshenko beam, a 3×3 transformation matrix involving only $\{V,\ \beta,\ \theta\}$ can be derived only by considering equilibrium conditions. Since warping and distortion that are self-equilibrated deformations are also used in a thin-walled box beam theory, however, additional conditions must be used. To derive all components of the 5×5 $\mathbf{T}$ matrix, we propose to consider the following three additional conditions in addition to the equilibrium conditions.

(1) Because B_1 and Q_1 have no resultant, P_2, M_2, and H_2 should not be coupled with B_1 and Q_1 at the joint of two box beams.

(2) At the so-called intersection points of two box beams at an angled joint, the three- dimensional displacements should be continuous.

(3) A fundamental transformation rule $\mathbf{T}(\phi)\cdot\mathbf{T}(-\phi)=\mathbf{I}$ ($\mathbf{I}$: identity matrix) must be satisfied for any value of ϕ.

(4) Another fundamental transformation identity $\mathbf{T}(\phi)\cdot\mathbf{T}(\phi)=\mathbf{T}(2\phi)$ must hold.

Conditions (3) and (4) seem to be trivial, but they play critical roles in determine all 5×5 elements exactly.

To check the validity of the derived transformation matrix $\mathbf{T}(\phi)$, two case

problems will be examined. Because the problems to be considered were also solved by an approximate method, the accuracy by the present exact condition may be better demonstrated. The converged finite element results obtained with the ANSYS shell elements [21] will be used as the reference results.

2.2 Higher-Order Beam Theory for Straight Box Beams

A higher-order beam theory for a rectangular box beam in [10, 17] will briefly explained as a basis for all subsequent analyses. As depicted in Fig. 2.2, each edge has its own coordinate (n, s); the tangential coordinate, s, is measured along the contour (or center line) of the wall starting from the center, and the normal coordinate, n, is measured by the outward normal distance from the contour. The three-dimensional displacements of a point on the contour can be expressed in terms of the five one-dimensional field variables, $\mathbf{U} = \{V,\ \beta,\ \theta,\ U,\ \chi\}^{\mathrm{T}}$, as

$$u_n(s,z) = \psi_n^V(s)V(z) + \psi_n^\beta(s)\beta(z) + \psi_n^\theta(s)\theta(z) + \psi_n^U(s)U(z) + \psi_n^\chi(s)\chi(z) \quad (2.1a)$$

$$u_s(s,z) = \psi_s^V(s)V(z) + \psi_s^\beta(s)\beta(z) + \psi_s^\theta(s)\theta(z) + \psi_s^U(s)U(z) + \psi_s^\chi(s)\chi(z) \quad (2.1b)$$

$$u_z(s,z) = \psi_z^V(s)V(z) + \psi_z^\beta(s)\beta(z) + \psi_z^\theta(s)\theta(z) + \psi_z^U(s)U(z) + \psi_z^\chi(s)\chi(z) \quad (2.1c)$$

where z is the axial coordinate, and u_s, u_n, and u_z are the tangential, normal, and axial displacements of the point on the contour, respectively. In Eq. (2.1), $\psi_i^\alpha(s)$ $(i = n,\ s,\ z;\ \alpha = V,\ \beta,\ \theta,\ U,\ \chi)$ represent the deformation of the cross section along the i-coordinate corresponding to the unit magnitude of field variable α.

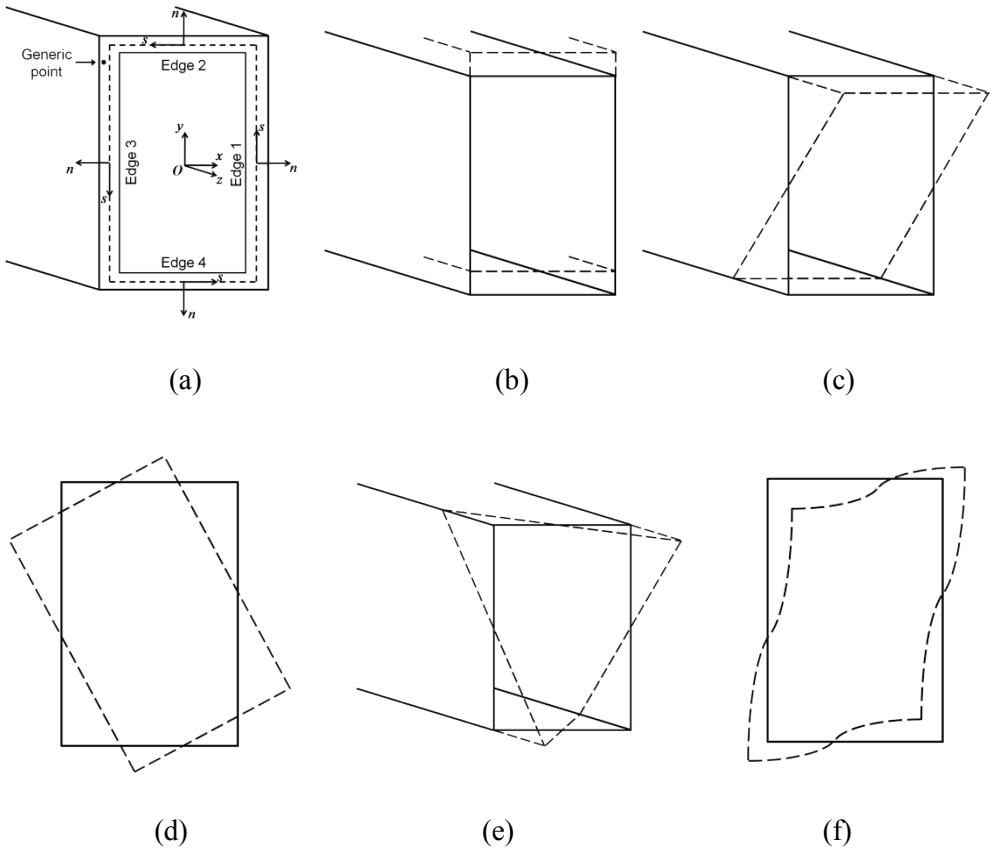

Fig. 2.2 (*a*) Coordinate system and (*b–f*) displacements/deformations of the beam section corresponding to the field variables (V, β, θ, U, χ).

The explicit expressions of $\psi_i^{\alpha}(s)$ are given in Appendix.

The three-dimensional displacements of a generic point located away from the contour by n on the cross section, $\{\tilde{u}_n,\ \tilde{u}_s,\ \tilde{u}_z\}$, can be written as

$$\tilde{u}_n(n,\ s,\ z) = u_n(s,\ z) = \psi_n^V \cdot V + \psi_n^\theta \cdot \theta + \psi_n^\chi \cdot \chi \tag{2.2a}$$

$$\tilde{u}_s(n,\ s,\ z) = u_s(s,\ z) - n\frac{du_n(s,\ z)}{ds} = \psi_s^V \cdot V + \psi_s^\theta \cdot \theta + \psi_s^\chi \cdot \chi - n\frac{d\psi_n^\chi}{ds} \cdot \chi \tag{2.2b}$$

$$\tilde{u}_z(n,\ s,\ z) = u_z(s,\ z) = \psi_z^{\beta} \cdot \beta + \psi_z^{U} \cdot U \tag{2.2c}$$

where the term $(-n\ du_n(s,z)/ds)$ in Eq. (2.2b) is needed to consider the bending effect of the cross-section wall.

One can derive the expressions for the dominant components of strain from $\{\varepsilon_{ss},\ \varepsilon_{sz},\ \varepsilon_{zz}\}$ Eq. (2.2a) and stress $\{\sigma_{ss},\ \sigma_{sz},\ \sigma_{zz}\}$ by using constitutive relation. Then, from the principle of minimum potential energy, one can derive the governing equations for V, β, θ, U, and χ (see [10, 17] for the explicit forms of equations) and also define the work conjugates of the field variables, $\mathbf{F} = \{P,\ M,\ H,\ B,\ Q\}^{\mathrm{T}}$:

$$\begin{aligned} P &= \int_A \sigma_{zs}\psi_s^{V} dA\ ,\ M = \int_A \sigma_{zz}\psi_s^{\beta} dA\ ,\ H = \int_A \sigma_{zs}\psi_s^{\theta} dA\ , \\ B &= \int_A \sigma_{zz}\psi_s^{U} dA\ ,\ Q = \int_A \sigma_{zs}\psi_s^{\chi} dA \end{aligned} \tag{2.3}$$

As defined in Introduction P, M, H, B, and Q denote the one-dimensional force measures representing vertical force, bending moment, twisting moment, bimoment, and transverse bimoment respectively.

2.3 Derivation of the Exact Joint Matching Condition

Thin-walled box beams (indicated by Beam 1 and Beam 2 in Fig. 2.1) meet each other at an angle of ϕ in the $x-z$ plane. The relation between the field variable vector $\mathbf{U}_1$ of Beam 1 and $\mathbf{U}_2$ of Beam 2 may be expressed in terms of a

transformation matrix $\mathbf{T}(\phi)$ such that

$$\mathbf{U}_2 = \mathbf{T}(\phi)\mathbf{U}_1 \tag{4.4a}$$

or

$$\begin{Bmatrix} V \\ \beta \\ \theta \\ U \\ \chi \end{Bmatrix}_2 = \begin{bmatrix} t_{11} & t_{12} & t_{13} & t_{14} & t_{15} \\ t_{21} & t_{22} & t_{23} & t_{24} & t_{25} \\ t_{31} & t_{32} & t_{33} & t_{34} & t_{35} \\ t_{41} & t_{42} & t_{43} & t_{44} & t_{45} \\ t_{51} & t_{52} & t_{53} & t_{54} & t_{55} \end{bmatrix} \begin{Bmatrix} V \\ \beta \\ \theta \\ U \\ \chi \end{Bmatrix}_1 \tag{4.4b}$$

The matrix $\mathbf{T}$ depends not only on ϕ but also on the box beam geometry (such as b (width), h (height), and t (thickness) defined in Fig. 2.1), but it will be simply written as $\mathbf{T}(\phi)$ to emphasize its dependence on ϕ.

Before using the four propositions given at the end of Introduction, we first recall the well-known relation. If $\mathbf{U}_2$ and $\mathbf{U}_1$ are related by $\mathbf{T}(\phi)$ by Eq. (2.4a), $\mathbf{F}_2$ and $\mathbf{F}_1$ are related as

$$\mathbf{F}_2 = \mathbf{T}^{*}\mathbf{F}_1 = \mathbf{T}^{-\mathrm{T}}(\phi)\mathbf{F}_1 \tag{2.5}$$

Equation (2.5) is the direct consequence of the virtual work conservation at the joint such that

$$\mathbf{F}_1^{\mathrm{T}}\delta\mathbf{U}_1 = \mathbf{F}_2^{\mathrm{T}}\delta\mathbf{U}_2 \tag{2.6}$$

where $\delta\mathbf{U}_p$ denotes the variation of $\mathbf{U}_p$ ($p = 1,\ 2$).

Another well-known relation is the force/moment equilibrium at a joint:

$$\begin{Bmatrix} P \\ M \\ H \end{Bmatrix}_2 = \begin{bmatrix} 1 & 0 & 0 \\ 0 & \cos\phi & -\sin\phi \\ 0 & \sin\phi & \cos\phi \end{bmatrix} \begin{Bmatrix} P \\ M \\ H \end{Bmatrix}_1 \tag{2.7}$$

Because B and Q represent self-equilibrated bimoments, they do not appear in the equilibrium relation, Eq. (2.7). Now let us consider the four conditions proposed in Introduction to determine all of the 5×5 components of $\mathbf{T}(\phi)$ [20].

2.3.1 Proposition 1: Consideration of No Resultant by *B* and *Q*

First of all, we observe that torsional (B) and transverse (Q) bimoments are in a state of self-equilibrium. This observation implies that the generalized force terms (P_2, M_2, H_2) in Beam 2 should not be affected by the self-equilibrated force terms (B_1, Q_1) of Beam 1. Therefore, the relations between $\mathbf{F}_1$ and $\mathbf{F}_2$ should be written as

$$\begin{Bmatrix} P \\ M \\ H \\ B \\ Q \end{Bmatrix}_2 = \begin{bmatrix} 1 & 0 & 0 & 0 & 0 \\ 0 & \cos\phi & -\sin\phi & 0 & 0 \\ 0 & \sin\phi & \cos\phi & 0 & 0 \\ \bullet & \bullet & \bullet & \bullet & \bullet \\ \bullet & \bullet & \bullet & \bullet & \bullet \end{bmatrix} \begin{Bmatrix} P \\ M \\ H \\ B \\ Q \end{Bmatrix}_1 \tag{2.8}$$

In Eq. (2.8), the zeros appearing inside the dotted rectangle are the consequences of the above-mentioned observation while 10 solid circles represent the elements to be determined. Noting that the transformation matrix appearing in Eq. (2.8) is $\mathbf{T}^*$,

which is equal to $\mathbf{T}^{-\mathrm{T}}$ by Eq. (2.5), one can show that the matrix $\mathbf{T}$ must take the following form;

$$\mathbf{T} = \begin{bmatrix} 1 & 0 & 0 & t_{14} & t_{15} \\ 0 & \cos\phi & -\sin\phi & t_{24} & t_{25} \\ 0 & \sin\phi & \cos\phi & t_{34} & t_{35} \\ 0 & 0 & 0 & t_{44} & t_{45} \\ 0 & 0 & 0 & t_{54} & t_{55} \end{bmatrix} \tag{2.9}$$

where the ten components of that the matrix $\mathbf{T}$ (t_{14}, t_{15},$\cdots$, t_{55}) are the quantities that cannot be determined from the equilibrium consideration.

2.3.2 Proposition 2: Three-Dimensional Displacement Continuity at the Intersection Points

In theory, the three-dimensional displacements at every point of the common interfacing region of Beams 1 and 2 should be continuous. However, it is not possible to strictly impose the continuity condition because only a finite number of one-dimensional field variables are used in the box beam theory. To use the one-dimensional beam theory for the joint, let us consider the top view of the connected beams in the $x-z$ plane in Fig. 2.3(a). Here, two beams are assumed to penetrate each other so that the centers of the cross sections of the two beams meet at Point *A*. From the three-dimensional view of the cross sections shown in Fig. 2.3(b), in fact, two beams meet at *A* and *B*. Note that Points *A* and *B* lie on Edge 2 and 4 of the contours (center lines) of two beam cross sections, respectively.

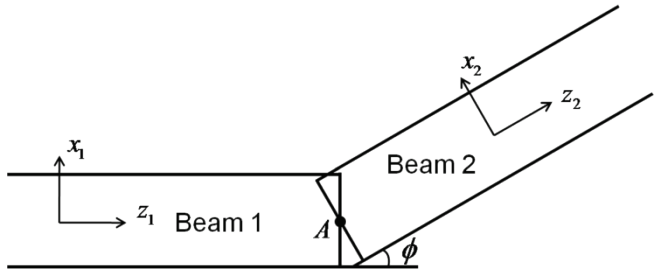

(a)

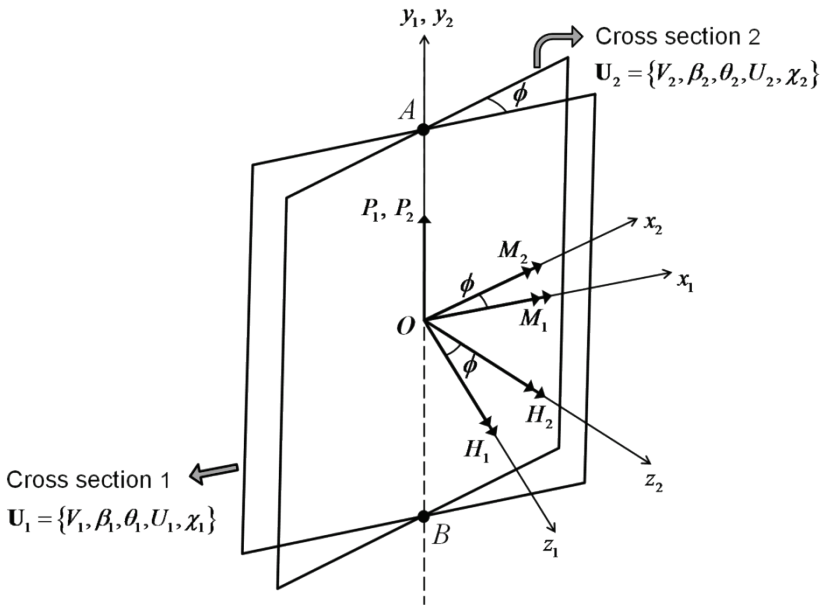

(b)

Fig. 2.3 (*a*) the top view of the beam centerlines in the *x*–*z* plane with an indication of the assumed common intersection point *A* (*b*) beam cross sections passing though the common intersection points *A* and *B* (The generalized force quantities having non-zero resultants are shown.).

Let us now consider the three-dimensional continuity at *A*:

$$(\tilde{u}_n \underset{\sim}{e}_n + \tilde{u}_s \underset{\sim}{e}_s + \tilde{u}_z \underset{\sim}{e}_z)_{\text{Beam 1}} = (\tilde{u}_n \underset{\sim}{e}_n + \tilde{u}_s \underset{\sim}{e}_s + \tilde{u}_z \underset{\sim}{e}_z)_{\text{Beam 2}} \tag{2.10}$$

where $\underset{\sim}{e}_q$ is the unit base vector along the local coordinate axis q ($q = n,\ s,\ z$).

Using the relation between $\underset{\sim}{e}_q\big|_{\text{Beam 1}}$ and $\underset{\sim}{e}_q\big|_{\text{Beam 2}}$ (see Fig. 2.3(b))

$$\underset{\sim}{e}_n\big|_{\text{Beam 1}} = \underset{\sim}{e}_n\big|_{\text{Beam 2}} \tag{2.11a}$$

$$\underset{\sim}{e}_s\big|_{\text{Beam 1}} = \underset{\sim}{e}_s\big|_{\text{Beam 2}} \cos\phi - \underset{\sim}{e}_z\big|_{\text{Beam 2}} \sin\phi \tag{2.11b}$$

$$\underset{\sim}{e}_z\big|_{\text{Beam 1}} = \underset{\sim}{e}_s\big|_{\text{Beam 2}} \sin\phi + \underset{\sim}{e}_z\big|_{\text{Beam 2}} \cos\phi \tag{2.11c}$$

the displacement components of Beams 1 and 2 are related at A as

$$\tilde{u}_n\big|_{\text{Beam 2}} = \tilde{u}_n\big|_{\text{Beam 1}} \tag{2.12a}$$

$$\tilde{u}_s\big|_{\text{Beam 2}} = \tilde{u}_s\big|_{\text{Beam 1}} \cos\phi + \tilde{u}_z\big|_{\text{Beam 1}} \sin\phi \tag{2.12b}$$

$$\tilde{u}_z\big|_{\text{Beam 2}} = -\tilde{u}_s\big|_{\text{Beam 1}} \sin\phi + \tilde{u}_z\big|_{\text{Beam 1}} \cos\phi \tag{2.12c}$$

To find the relations between $\mathbf{U}_1$ and $\mathbf{U}_2$ from Eq. (2.12), Eq. (2.2) and the formula in Appendix are used to calculate the displacement components at Point A of Beams 1 and 2:

$$\text{Point A}\big|_{\text{Beam 1}}:\ \tilde{u}_n = V_1,\ \tilde{u}_s = \frac{h}{2}\theta_1 - \frac{bh}{b+h}\chi_1,\ \tilde{u}_z = \frac{h}{2}\beta_1 \tag{2.13}$$

$$\text{Point A}\big|_{\text{Beam 2}}:\ \tilde{u}_n = V_2,\ \tilde{u}_s = \frac{h}{2}\theta_2 - \frac{bh}{b+h}\chi_2,\ \tilde{u}_z = \frac{h}{2}\beta_2 \tag{2.14}$$

Substituting Eqs. (2.13, 2.14) into Eq. (2.12) and using Eq. (2.4) with $\mathbf{T}$ in Eq. (2.9) yield

$$V_2 = V_1 \tag{2.15}$$

$$t_{24} = 0,\ t_{25} = \frac{2b}{b+h}\sin\phi \tag{2.16}$$

$$t_{34} = \frac{2b}{b+h}t_{54},\ t_{35} = \frac{2b}{b+h}(t_{55} - \cos\phi) \tag{2.17}$$

Inserting the results in Eqs. (2.15 – 2.17) into $\mathbf{T}(\phi)$ in Eq. (2.9) gives

$$\mathbf{T}(\phi) = \begin{bmatrix} 1 & 0 & 0 & 0 & 0 \\ 0 & \cos\phi & -\sin\phi & 0 & \frac{2b}{b+h}\sin\phi \\ 0 & \sin\phi & \cos\phi & \frac{2b}{b+h}t_{54} & \frac{2b}{b+h}(t_{55} - \cos\phi) \\ 0 & 0 & 0 & t_{44} & t_{45} \\ 0 & 0 & 0 & t_{54} & t_{55} \end{bmatrix} \tag{2.18}$$

Now $\mathbf{T}(\phi)$ has only 4 undetermined components: t_{44}, t_{45}, t_{54}, and t_{55}.

2.3.3 Proposition 3: Use of the Relation $\mathbf{T}(\phi)\cdot\mathbf{T}(-\phi) = \mathbf{I}$

Here, we use a fundamental relation $\mathbf{T}(\phi)\cdot\mathbf{T}(-\phi) = \mathbf{I}$ where $\mathbf{I}$ is an identity matrix. To find $\mathbf{T}(-\phi)$, the schematic figures shown in Fig. 2.4 will be used. Figure 2.4(a) shows two beams connected at a positive angle of ϕ while the first figure in Fig. 2.4(b) sketches two beams connected at a negative angle, $-\phi$. As indicated in Fig. 2.4(b), the two beams connected at a negative angle may be viewed as two beams connected at a positive angle of ϕ in a rotated coordinate system ($\tilde{x}, \tilde{y}, \tilde{z}$) by 180° from the (x, y, z) coordinate system such that

$$\tilde{x} = -x,\ \tilde{y} = -y,\ \text{and}\ \tilde{z} = z \tag{2.19}$$

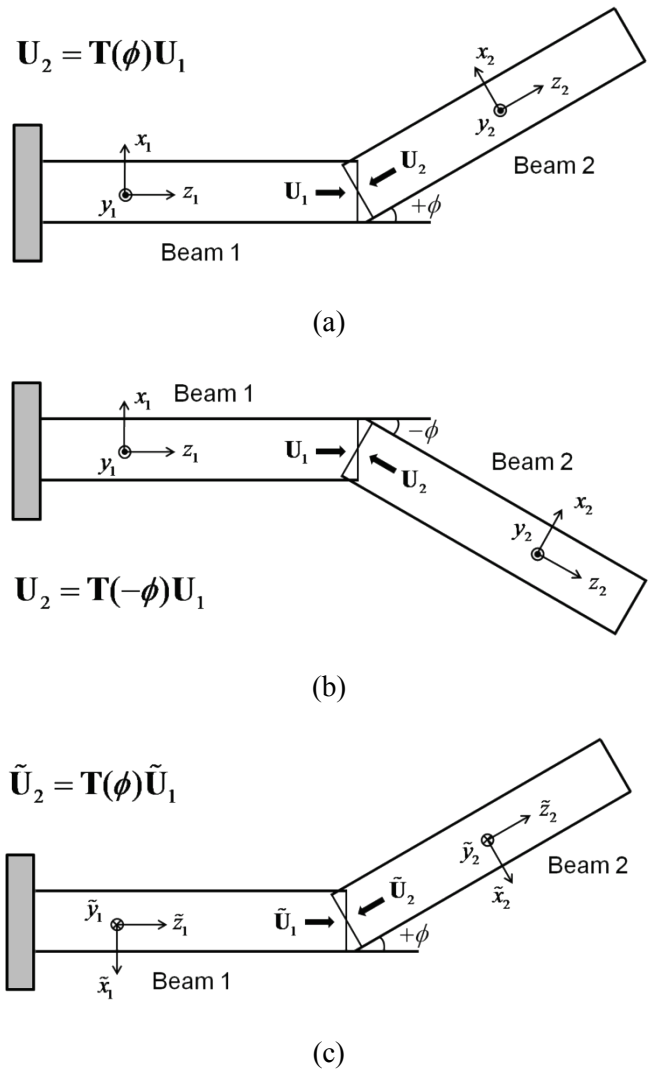

Fig. 2.4 Description of the procedure to obtain T($-\phi$): (*a*) T(ϕ) relation for a positive ϕ (*b*) T($-\phi$) defined for a negative ϕ, which can be derived from T(ϕ) defined in a different coordinate system.

If the field quantities defined in the ($\tilde{x}, \tilde{y}, \tilde{z}$) coordinate system are denoted by $\tilde{\mathbf{U}} = \{\tilde{V},\ \tilde{\beta},\ \tilde{\theta},\ \tilde{U},\ \tilde{\chi}\}^{\mathrm{T}}$, the relation between $\tilde{\mathbf{U}}_1$ and $\tilde{\mathbf{U}}_2$ is given by

$$\tilde{\mathbf{U}}_2 = \mathbf{T}(\phi)\tilde{\mathbf{U}}_1 \tag{2.20}$$

By examining the section displacements or deformations shown in Figs. 2.2 (b–f), one can show that

$$\tilde{V} = -V,\ \tilde{\beta} = -\beta,\ \tilde{\theta} = \theta,\ \tilde{W} = W,\ \tilde{\chi} = \chi \tag{2.21}$$

To find the last two relations in Eq. (2.21), one must note that the deformation patterns of W and χ shown in Figs. 2.2 (e; f) under the rotation produce the same deformation patterns, resulting in $\tilde{W} = W$ and $\tilde{\chi} = \chi$. Substituting Eq. (2.21) into Eq. (2.20) and doing some algebra to write Eq. (2.20) as $\mathbf{U}_2 = \mathbf{T}(-\phi)\mathbf{U}_1$ where $\mathbf{U} = \{+V,\ +\beta,\ \theta,\ U,\ \chi\}^{\mathrm{T}}$, one can identify $\mathbf{T}(-\phi)$ as

$$\mathbf{T}(-\phi) = \begin{bmatrix} 1 & 0 & 0 & 0 & 0 \\ 0 & \cos\phi & \sin\phi & -t_{24} & -t_{25} \\ 0 & -\sin\phi & \cos\phi & t_{34} & t_{35} \\ 0 & 0 & 0 & t_{44} & t_{45} \\ 0 & 0 & 0 & t_{54} & t_{55} \end{bmatrix} = \begin{bmatrix} 1 & 0 & 0 & 0 & 0 \\ 0 & \cos\phi & \sin\phi & 0 & -\frac{2b}{b+h}\sin\phi \\ 0 & -\sin\phi & \cos\phi & \frac{2b}{b+h}t_{54} & \frac{2b}{b+h}(t_{55} - \cos\phi) \\ 0 & 0 & 0 & t_{44} & t_{45} \\ 0 & 0 & 0 & t_{54} & t_{55} \end{bmatrix} \tag{2.22}$$

To use the fundamental transformation relation of $\mathbf{T}(\phi)\cdot\mathbf{T}(-\phi) = \mathbf{I}$, we multiply $\mathbf{T}(\phi)$ in Eq. (2.18) and $\mathbf{T}(-\phi)$ in Eq. (2.22):

$$\mathbf{T}(\phi)\cdot\mathbf{T}(-\phi) = \begin{bmatrix} 1 & 0 & 0 & 0 & 0 \\ 0 & 1 & 0 & 0 & 0 \\ 0 & 0 & 1 & \frac{2b}{b+h}t_{54}(t_{44}+t_{55}) & \frac{2b}{b+h}(t_{55}^2 + t_{54}t_{45} - 1) \\ 0 & 0 & 0 & t_{44}^2 + t_{45}t_{54} & t_{45}(t_{44}+t_{55}) \\ 0 & 0 & 0 & t_{54}(t_{44}+t_{55}) & t_{55}^2 + t_{45}t_{54} \end{bmatrix} \equiv \begin{bmatrix} 1 & 0 & 0 & 0 & 0 \\ 0 & 1 & 0 & 0 & 0 \\ 0 & 0 & 1 & 0 & 0 \\ 0 & 0 & 0 & 1 & 0 \\ 0 & 0 & 0 & 0 & 1 \end{bmatrix} \tag{2.23}$$

From Eq. (2.23), the following four relations for the undetermined components (t_{44}, etc.) are derived:

$$t_{44}^2 + t_{45}t_{54} = 1 \tag{2.24a}$$

$$t_{45}(t_{44} + t_{55}) = 0 \tag{2.24b}$$

$$t_{54}(t_{44} + t_{55}) = 0 \tag{2.24c}$$

$$t_{55}^2 + t_{45}t_{54} = 1 \tag{2.24d}$$

The solutions that satisfy Eq. (2.24) may not be unique. To deal with this issue, a fundamental multiplication relation valid for any transformation matrix is used as the following proposition, Proposition 4.

2.3.4 Proposition 4: Use of the Relation $\mathbf{T}(\phi)\cdot\mathbf{T}(\phi) = \mathbf{T}(2\phi)$

Finally, we consider another fundamental relation, $\mathbf{T}(\phi)\cdot\mathbf{T}(\phi) = \mathbf{T}(2\phi)$. By using Eq. (2.18), one can write $\mathbf{T}(\phi)\cdot\mathbf{T}(\phi)$ explicitly as

$$\mathbf{T}(\phi)\cdot\mathbf{T}(\phi) = \begin{bmatrix} 1 & 0 & 0 & 0 & 0 \\ 0 & \cos(2\phi) & -\sin(2\phi) & 0 & \frac{2b}{b+h}\sin(2\phi) \\ 0 & \sin(2\phi) & \cos(2\phi) & \frac{2b}{b+h}t_{54}(t_{44}+t_{55}) & \frac{2b}{b+h}((t_{55}^2 + t_{54}t_{45}) - \cos(2\phi)) \\ 0 & 0 & 0 & t_{44}^2 + t_{45}t_{54} & t_{45}(t_{44}+t_{55}) \\ 0 & 0 & 0 & t_{54}(t_{44}+t_{55}) & t_{55}^2 + t_{45}t_{54} \end{bmatrix} \tag{2.25}$$

Observe that the expressions involving t_{44}, t_{45}, t_{54}, and t_{55} in Eq. (2.25) are exactly the same as those derived as Eq. (2.24) from Proposition 3. Therefore, one

can finally express $\mathbf{T}(2\phi) = \mathbf{T}(\phi) \cdot \mathbf{T}(\phi)$ as, without any unknowns,

$$\mathbf{T}(2\phi) = \begin{bmatrix} 1 & 0 & 0 & 0 & 0 \\ 0 & \cos(2\phi) & -\sin(2\phi) & 0 & \frac{2b}{b+h}\sin(2\phi) \\ 0 & \sin(2\phi) & \cos(2\phi) & 0 & \frac{2b}{b+h}(1-\cos(2\phi)) \\ 0 & 0 & 0 & 1 & 0 \\ 0 & 0 & 0 & 0 & 1 \end{bmatrix} \tag{2.26}$$

Putting ϕ instead of 2ϕ in Eq. (2.26) yields the exact expression of $\mathbf{T}(\phi)$ such that

$$\begin{Bmatrix} V \\ \beta \\ \theta \\ U \\ \chi \end{Bmatrix}_2 = \mathbf{T}(\phi) \begin{Bmatrix} V \\ \beta \\ \theta \\ U \\ \chi \end{Bmatrix}_1 = \begin{bmatrix} 1 & 0 & 0 & 0 & 0 \\ 0 & \cos\phi & -\sin\phi & 0 & \frac{2b}{b+h}\sin\phi \\ 0 & \sin\phi & \cos\phi & 0 & \frac{2b}{b+h}(1-\cos\phi) \\ 0 & 0 & 0 & 1 & 0 \\ 0 & 0 & 0 & 0 & 1 \end{bmatrix} \begin{Bmatrix} V \\ \beta \\ \theta \\ U \\ \chi \end{Bmatrix}_1 \tag{2.27}$$

Equation (2.27) shows that the distortion (χ_1) of Beam 1 affects the bending/shear rotation (β_2) and torsional rotation (θ_2) of Beam 2 at the joint. On the other hand, the warping (U_1) of Beam 1 is not coupled with any other deformation but is directly transmitted only to the warping (U_2) of Beam 2. Although the final form of the transformation matrix $\mathbf{T}$ of the thin-walled box beam theory is simple and compact, the exact derivation is given here for the first time.

2.4 Numerical Examples

Two case studies, considered earlier by Jang et al. [19], will be performed to

demonstrate the accuracy and validity of the derived transformation $\mathbf{T}$. The present $\mathbf{T}$ matrix will be used in the one-dimensional finite element method employing the five kinematic variables. Since the higher-order box beam finite element implementation is a standard procedure, the detailed steps to obtain the numerical results will be omitted.

2.4.1 Case Study 1: Two Box Beams Connected at an Angled Joint

As the first case study, the beam structures shown in Fig. 2.1 are analyzed for various joint angles ϕ and aspect ratios of the cross section. Some of the beam dimensions are fixed to be $t = 2$ mm and $L = 1000$ mm and the material properties are E (Young's modulus) = 200 GPa and ν (Poisson's ratio) = 0.3. The one end of the structure is clamped and the other end, denoted as C, is subjected to a vertical force, $P = 100$ N. The cross section C is assumed to be rigid (no warping or distortion). To check the accuracy of the present approach using the derived $\mathbf{T}$ matrix, the displacements obtained by the proposed approach are compared with those by ANSYS shell elements [21]. The results are also compared with those based on the same higher-order beam theory incorporating the joint-displacement minimization technique (Jang et al. [19]). Also, the displacements by the standard Timoshenko beam elements are plotted for comparison.

Figure 2.5 shows the axial distributions of the five field variables for the case of

$b = 50$ mm, $h = 100$ mm, and $\phi = 60^\circ$. The numbers of the discretizing finite elements are 60 for the present beam analysis and 3,960 for the shell analysis. In Fig. 2.5, the results by the present approach are virtually identical to those by the shell calculation while the Timoshenko beam results are quite off from the shell results. Two-beam structures having different joint angles were also investigated and the numerical results are plotted in Fig. 2.6 and Fig. 2.7. The responses of the field variables for different aspect ratios of the cross section, $b = 50$ mm and $h = 150$ mm are also illustrated in Fig. 2.8. The results by the present approach agree well with the shell element results compared with the results by the Timoshenko theory and those by Jang et al. [19]. Although not presented here, the present approach was shown to produce accurate results for box beams of different aspect ratios with various joint angles.

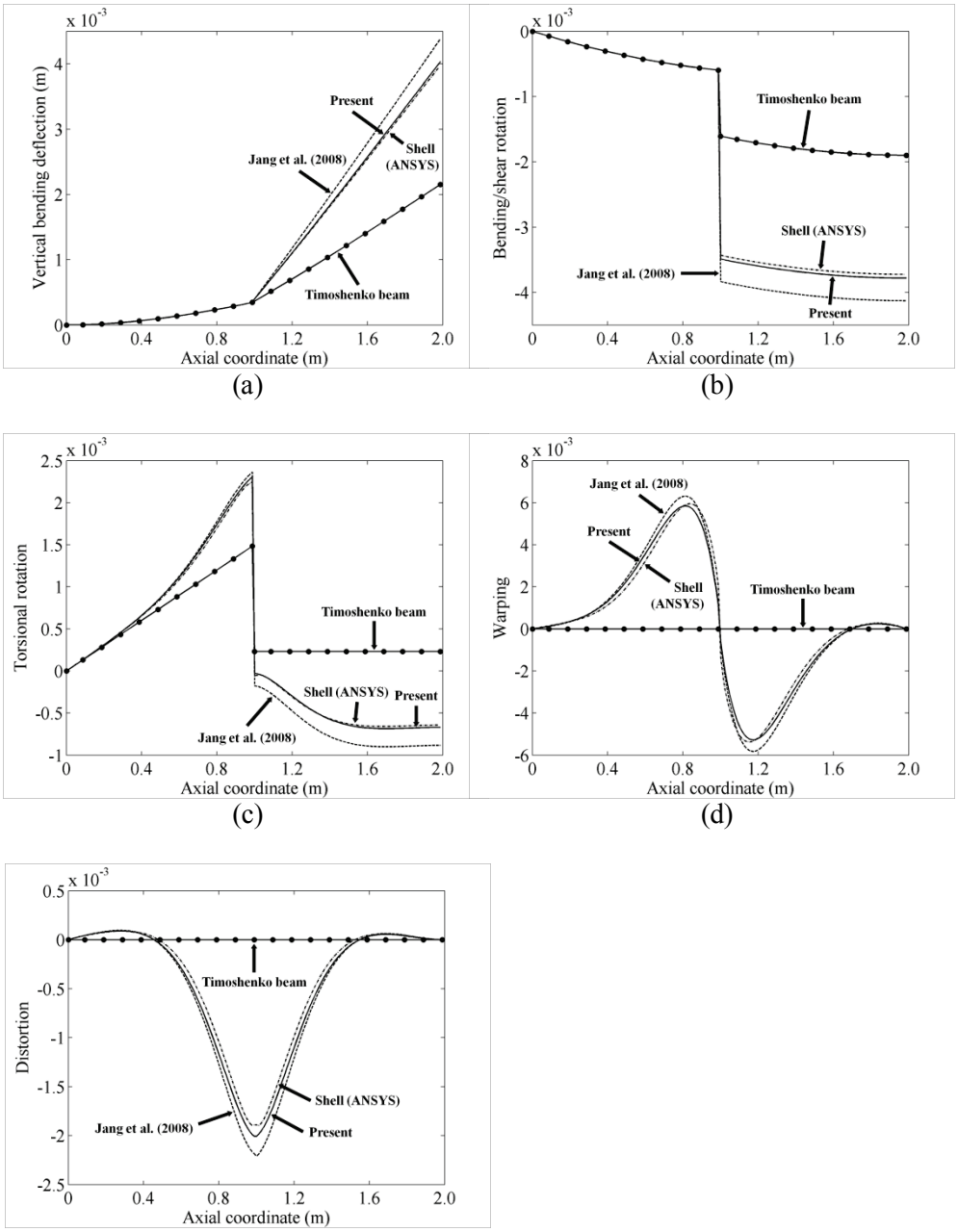

Fig. 2.5 Numerical results for the two-beam structure in Fig. 2.1 with b=50 mm, h=100 mm, ϕ=60°: (a) vertical bending deflection V, (b) bending/shear rotation β, (c) torsional rotation θ, (d) warping U, and (e) distortion χ.

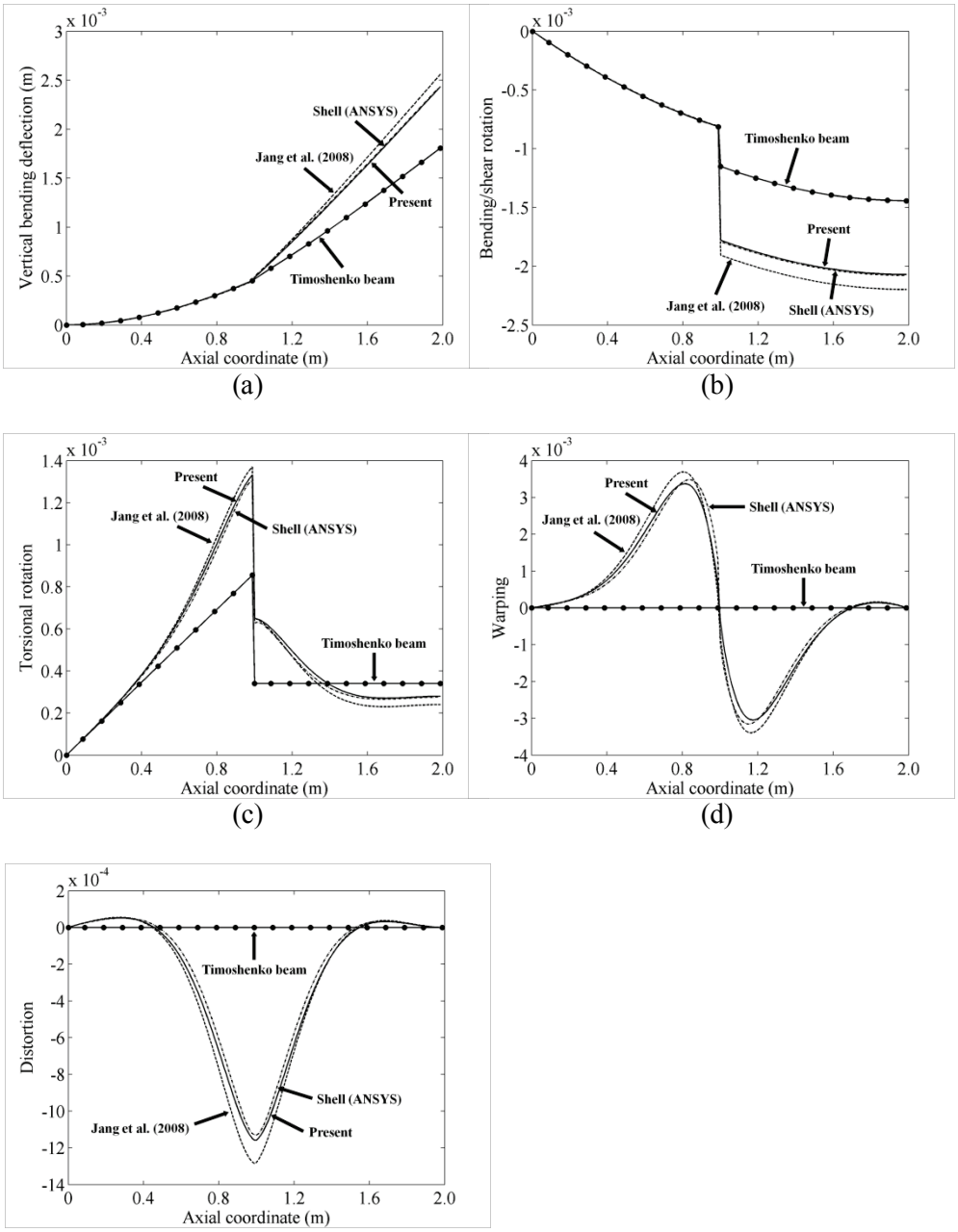

Fig. 2.6 Numerical results for the two-beam structure in Fig. 2.1 with b=50 mm, h=100 mm, ϕ =30°: (a) vertical bending deflection V, (b) bending/shear rotation β, (c) torsional rotation θ, (d) warping U, and (e) distortion χ.

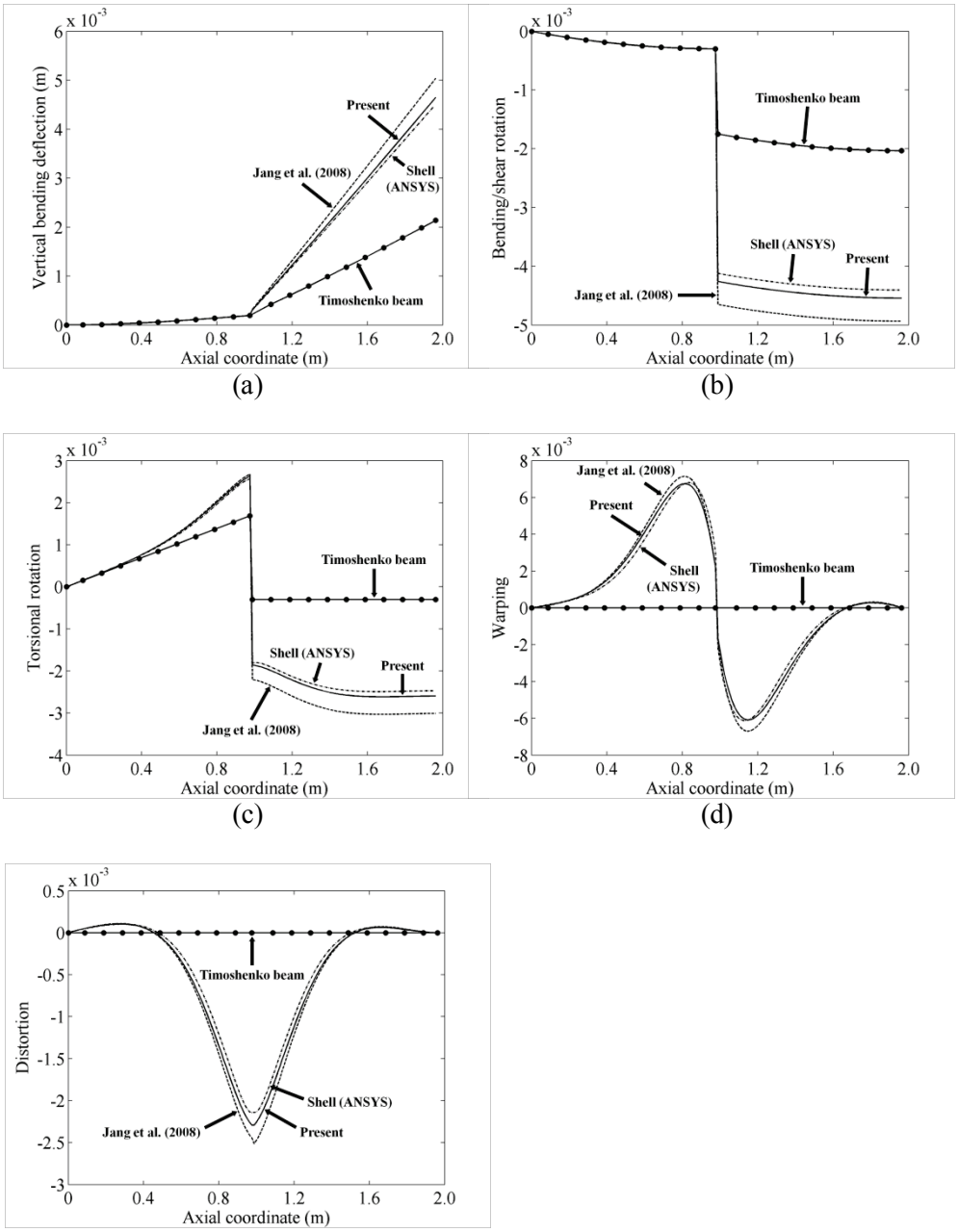

Fig. 2.7 Numerical results for the two-beam structure in Fig. 2.1 with b=50 mm, h=100 mm, ϕ =90°: (a) vertical bending deflection V, (b) bending/shear rotation β, (c) torsional rotation θ, (d) warping U, and (e) distortion χ.

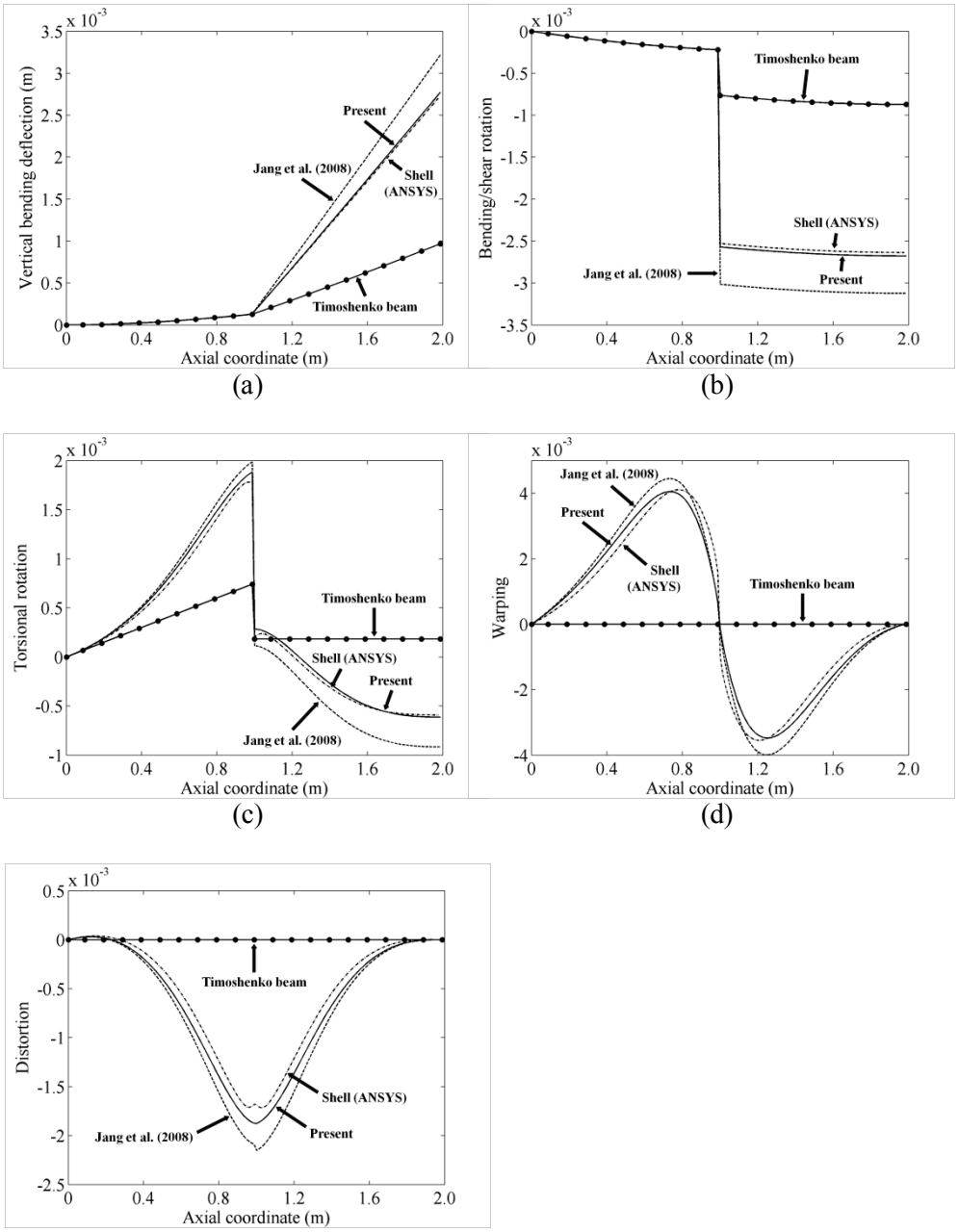

Fig. 2.8 Numerical results for the two-beam structure in Fig. 2.1 with b=50 mm, h=150 mm, ϕ =60°: (a) vertical bending deflection V, (b) bending/shear rotation β, (c) torsional rotation θ, (d) warping U, and (e) distortion χ.

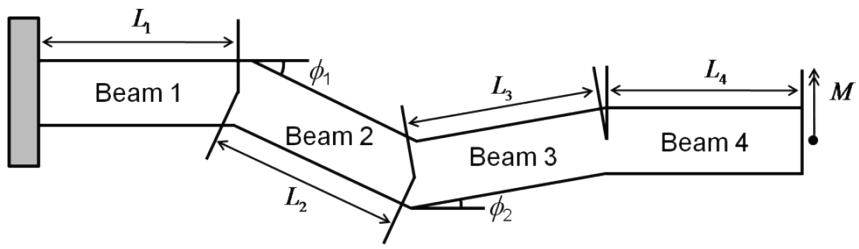

Fig. 2.9 A thin-walled beam structure having three angled joints under a bending moment M ($L_1 = L_2 = L_3 = L_4 = 1000$ mm, $\phi_1 = -45^o$, $\phi_2 = 20^o$, $M = -100$ Nm).

2.4.2 Case Study 2: Four Box Beams Serially Connected at Angled Joints

Figure 2.9 illustrates a structure of four thin-walled box beams connected at three joints. The dimensions of the cross sections of all beams are $b = 50$ mm, $h = 100$ mm, and $t = 2$ mm. The material properties are the same as those in the previous case study. The one end of the structure is clamped while the other end is subjected to a bending moment, $M = 100\ \mathrm{N \cdot m}$. The cross section of the loaded end is assumed to be rigid. Figure 2.10 shows that the axial variations of V, β, θ, U, and χ. Unlike the results predicted by the approach by Jang et al. [19] or the Timoshenko beam theory, the present results match the shell finite element results well. The studies with beams of other cross sectional geometries and joint angles also confirmed the superior accuracy of the thin-walled beam analysis using the exact transformation derived in the present work.

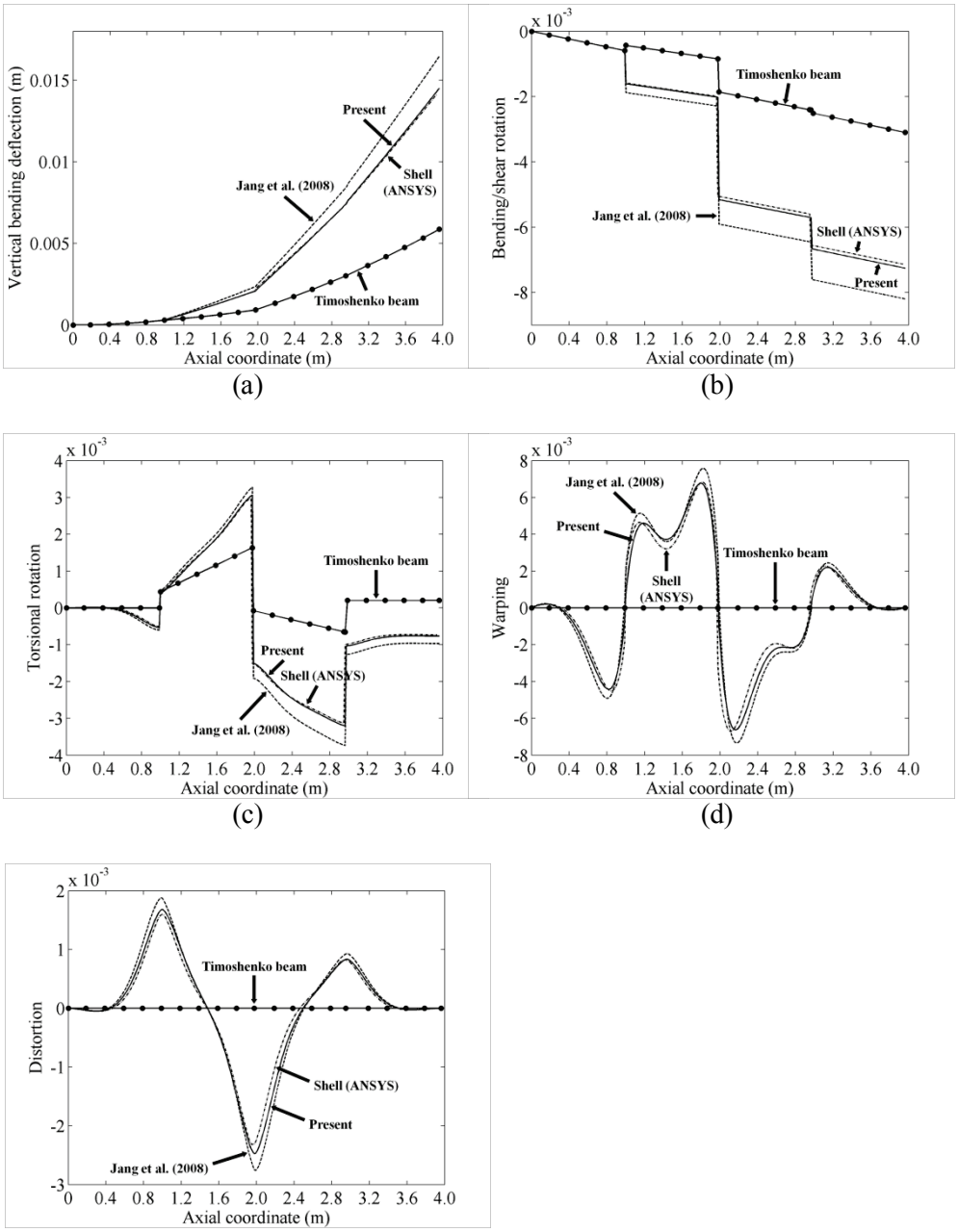

Fig. 2.10 Numerical results for the beam structure shown in Fig. 2.9: (*a*) vertical bending deflection V, (*b*) bending/shear rotation β, (*c*) torsional rotation θ, (*d*) warping U, and (e) distortion χ.

2.5 Conclusions

The transformation matrix relating the field variables of a higher-order thin-walled box beam theory at angled joints was derived in an exact form. The proposed conditions to determine unknown elements of the transformation matrix were shown to be sufficient for box beams connected at angled joints that are subject to out-of-plane and torsional loads. With the derived matrix, we were able to explain the interaction between the field variables of the two beams connected at an angle joint. Specifically, the distortion of one beam is coupled with the bending/shear and torsional rotations of the other while the warping deformation of one beams is not coupled with other field variables of the other beam but only with the warping deformation of the other beam. The present derivation of the joint matching condition is expected to serve as an important building block to expedite the research on higher-order beam theories for arbitrarily-shaped, connected thin-walled beams.

Appendix

The section shape functions ψ's are explicitly given. The index j indicates the edge number of the beam cross section.

$$\psi_n^V(s_j) = 0 \ \ (j = 1,\ 3) \ \text{ and } \ (-1)^{(j-2)/2} \ \ (j = 2,\ 4) \tag{2.A1}$$

$$\psi_s^V(s_j) = (-1)^{(j-1)/2} \ \ (j = 1,\ 3) \ \text{ and } \ 0 \ \ (j = 2,\ 4) \tag{2.A2}$$

$$\psi_z^V(s_j) = 0,\ \ \psi_n^\beta(s_j) = 0,\ \ \psi_s^\beta(s_j) = 0 \tag{2.A3, 4, 5}$$

$$\psi_z^{\beta}(s_j) = (-1)^{(j-1)/2} \mathrm{s}_i \quad (j = 1,\ 3) \ \text{ and } \ (-1)^{(j-2)/2} \frac{h}{2} \quad (j = 2,\ 4) \tag{2.A6}$$

$$\psi_n^{\theta}(s_j) = -s_j \tag{2.A7}$$

$$\psi_s^{\theta}(s_j) = \frac{b}{2} \quad (j = 1,\ 3) \ \text{ and } \ \frac{h}{2} \quad (j = 2,\ 4) \tag{2.A8}$$

$$\psi_z^{\theta}(s_j) = 0,\ \psi_n^{U}(s_j) = 0,\ \psi_s^{U}(s_j) = 0 \tag{2.A9, 10, 11}$$

$$\psi_z^{U}(s_j) = \frac{b}{2} s_j \quad (j = 1,\ 3) \ \text{ and } \ -\frac{h}{2} s_j \quad (j = 2,\ 4) \tag{2.A12}$$

$$\psi_n^{\chi}(s_j) = -\frac{4}{h(b+h)} s_j^3 + \frac{2b+h}{b+h} s_j \quad (j = 1,\ 3) \ \text{ and } \ \frac{4}{b(b+h)} s_j^3 - \frac{b+2h}{b+h} s_j \quad (j = 2,\ 4) \tag{2.A13}$$

$$\psi_s^{\chi}(s_j) = \frac{bh}{b+h} \quad (j = 1,\ 3) \ \text{ and } \ -\frac{bh}{b+h} \quad (j = 2,\ 4) \tag{2.A14}$$

$$\psi_z^{\chi}(s_j) = 0 \tag{2.A15}$$

where

$$-\frac{h}{2} \le s_1, s_3 \le \frac{h}{2} \ \text{ and } \ -\frac{b}{2} \le s_2, s_4 \le \frac{b}{2}$$

References

[1] Vlasov VZ. Thin-walled elastic beams. Jerusalem: Israel Program for Scientific Translations; 1961.

[2] Bazant Z, El Nimeiri M. Stiffness method for curved box girders at initial stress. J Struct Div 1974;100:2071-90.

[3] Mikkola MJ, Paavola J. Finite element analysis of box girders. J Struct Div 1980; 106: 1343-57.

[4] Boswell LF, Zhang SH. A box beam finite element for the elastic analysis of thin-walled structures. Thin-Walled Struct 1983;1:353-83.

[5] Maisel BI. Analysis of concrete box beams using small-computer capacity. London: Cement and Concrete Association; 1982.
[6] Zhang S H, Lyons LPR. A thin-walled box beam finite element for curved bridge analysis. Comput Struct 1984;18: 1035-46.
[7] Balch CD, Steele CR. Asymptotic solutions for warping and distortion of thin-walled box beams. J Appl Mech-Trans ASME 1987;54:165-73.
[8] Razaqpur AG, Li HG. A finite element with exact shape functions for shear lag analysis in multi-cell box girders. Comput Struct 1991;39:155-63.
[9] Boswell LF, Li Q. Consideration of the relationships between torsion, distortion and warping of thin-walled beams. Thin-Walled Struct 1995;21:147-61.
[10] Kim JH, Kim YY. Analysis of thin-walled closed beams with general quadrilateral cross sections. J Appl Mech-Trans ASME 1999;66:904-12.
[11] Kim JH, Kim YY. Thin-walled multicell beam analysis for coupled torsion, distortion, and warping deformations. J Appl Mech-Trans ASME 2001;68:260-9.
[12] Sumami Y, Yugawa T, Yoshida Y. Analysis of joint rigidity of in-plane bending of plane-joint structures. JSAE Review 1988;9:44-51.
[13] Sunami Y, Yugawa T, Yoshida Y. Analysis of the joint rigidity of the automotive body structure-out-of-plane bending of plane-joint structures. JSAE Review 1990;11:59-66.
[14] Lee K, Nikolaidis E. A two-dimensional model for joints in vehicle structures. Comput Struct 1992;45:775-84.
[15] Garro L, Vullo V. Deformations car body joints under operating conditions. SAE Technical Paper 1986; no. 861397.
[16] El-Sayed MEM. Calculation of joint spring rates using finite element formulation. Comput Struct 1989;33:977-81.
[17] Jang G-W, Kim KJ, Kim YY. Higher-order beam analysis of box beams connected at angled joints subject to out-of-plane bending and torsion. Int J Numer Methods Eng 2008;75:1361-84.
[18] Jang G-W, Kim YY. Higher-order in-plane bending analysis of box beams connected at an angled joint considering cross-sectional bending warping and distortion. Thin-Walled Struct 2009;47:1478-89.
[19] Jang G-W, Kim YY. Vibration analysis of piecewise straight thin-walled box beams without using artificial joint springs. J Sound Vibr 2009;326:647-70.
[20] Choi S, Jang G-W, Kim YY. Exact matching condition at a joint of thin-walled box beams under out-of-plane bending and torsion. J Appl Mech-Trans ASME 2012;79:051018.
[21] ANSYS Inc. ANSYS Structural Analysis Guide. 2007.

CHAPTER 3.
Higher-Order Beam Analysis for Multiply-Connected Box Beams-Joint Systems Subjected to Out-of-Plane Bending and Torsion

3.1 Introduction

The behavior of thin-walled box beams is quite flexible in comparison with the analysis result obtained by classical Euler and Timoshenko beam theories (see, e.g. [1, 2]) because cross-sectional deformations not covered by those classical theories easily appear in thin-walled box beams. Especially when those box beams meet at a joint, the magnitudes of cross-sectional deformations near the joint region are further amplified, and that causes the joint region to exhibit significant flexibilities. For this reason, the behavior of thin-walled box beam structures having joints shows big difference from the predicted result based on the classical beam theories. To overcome the difficulty that the classical beam theories overestimate stiffness for thin-walled box beam structures (or members), researchers have developed one-dimensional higher-order beam theories [3-10] that consider cross-sectional deformations as independent degrees of freedom. Because higher-order deformations such as warping and distortion do not produce any resultants, determining the joint matching relations among all the degrees of freedom of box beams connected at a joint is a difficult problem. Especially when the box beam

structures are subjected to out-of-plane bending and torsion, distortion is found to be complicatedly coupled with other degrees of freedom at the joint. However, there has been no dedicated research to investigate how they are coupled. In fact, there is no exact analysis method based on higher-order beam theories that is applicable to structures with “three” or more thin-walled box beams subjected to out-of-plane loads that are connected at a joint. With this background, we propose an exact analysis approach for the first time, applicable for cases of three or more box beams-joint structures under out-of-plane loads.

First, it is worth mentioning the previous researches trying to express the joint flexibilities of thin-walled box beam structures by using one-dimensional beam theories. Initial studies based on the classical beam theories introduced some joint models with rotational springs to account for those flexibilities [11-13]. El-Sayed [11] proposed a joint model with torsional springs to represent the flexible responses of a joint under out-of-plane loads, and Lee and Nikolaidis [12] proposed a joint model consisting of springs and rigid sections to consider additional joint coupling effects. Thereafter, Becker et al. [14] suggested a method using structural dynamics for evaluating the stiffness of a joint. Recently, Refs. [15, 16] proposed joint concept modeling approaches reducing the shell element based detailed joint into a super element through static or dynamic reduction techniques. However, the joint flexibilities caused by the cross-sectional deformations vary considerably depending on both the number of box beams connected to the joint and the joint angles among those box beams, and thus it is difficult to develop a consistent joint

model applicable to various joints by using the classical beam theories.

If there existed a beam theory considering the significant cross-sectional deformations as additional degrees of freedom, one can capture the flexible responses of thin-walled box beam members or structures without employing any artificial concepts. Vlasov [3] theoretically defined the warping deformation resulting from twisting moment as a sectorial coordinate, and established a beam theory for thin-walled beams including the warping as the additional degree of freedom. To handle stress analysis, buckling analysis, dynamic analysis, etc., by advanced beam theories, several analytic or semi-analytic methods have been proposed such as an approach based on Saint Venant's theory [17, 18], the variational asymptotic method [19-21], Carrera's unified formulation [22, 23], and the GBT cross-section analysis [24, 25]. Especially for thin-walled closed section beams including thin-walled box beams, Kim and Kim [6, 26-29] developed a higher-order beam theory interpreting torsional behavior of those beams correctly. In this regard, they recognized the importance of considering accurate distortional deformations in addition to the warping deformations and proposed a semi-analytical method to determine those cross-sectional modes. In recent years, developments of higher-order beam models have been reported to analyze the stress distribution or nonlinear behavior of thin-walled box beam members. Genoese et al. [8, 30] proposed a mixed beam model considering warping modes derived from their Saint Venant theory based approach and having a mixed formulation with the independent description of stress and displacement fields.

Ferradi and Cespedes [9, 31] proposed a method calculating distortion modes through the modal analysis of cross-section decomposed with beam elements and derived relevant warping modes by using their proposed equilibrium scheme. Vieira et al. [10, 32] derived a generalized eigenvalue problem calculating uncoupled warping modes through the assumption of in-plane rigid cross-sections and suggested a higher-order beam model considering those warping modes.

As higher-order beam theories including the effects of cross-sectional deformations were established, efforts to theoretically express the joint flexibilities of thin-walled beam structures have been followed. Especially concerning the joint of thin-walled open section beams, many researches defining the compatibility of degrees of freedom have been proposed [33-38]. Vacharajittiphan and Trahair [33] investigated the warping restraint/transmission at the joint of two I-section members and found the influence of distortion on the warping transmission. Baigent and Hancock [34] determined the equilibrium condition at the joint of two asymmetric section members by transforming force terms on the centroid and the shear center to the member origin axes and derived corresponding displacement relations at the joint including warping coupling effects. In addition, they proposed a modeling technique to consider the effects of different joint types and eccentric restraint. Based on the researches above, Basaglia et al. [37] have recently derived extended displacement relations applicable to the joint of multiple open section members and determined the warping transmission for various types of joint. Subsequently, they established a Generalized Beam Theory (GBT) based analysis

method interpreting various buckling behavior of thin-walled open section beam structures by considering additional displacement constraints at some specific points around the joint [38].

In thin-walled closed section beam structures, meanwhile, the complicated responses of joints are also induced by the distortional deformation. Therefore, the consideration of the effects of distortion as well as warping on the joint flexibilities is important. Especially in the case of box beams, the joint flexibilities observed under out-of-plane loads are mainly generated by the coupling of distortion with other degrees of freedom because the location of the centroid is identical to that of the shear center. Therefore, some efforts defining those effects of distortion have been made to express the joint flexibilities of box beams subjected to out-of-plane loads correctly [39-43]. Jang et al. [39-41] matched the displacements of two box beams connected at a joint on an imaginary joint section and determined joint matching conditions by solving an optimization problem which minimizes differences between the displacements of two box beams on the imaginary joint section. On the other hand, Choi et al. [42] proposed exact matching conditions at the joint of two box beams to capture the joint behavior comparable with that predicted by detailed shell analysis. In case of three or more box beams-joint structures, the methods for two box beams-joint structures in Refs. [39-42] may be used, but the joint stiffness is found to be overestimated. The reason is that the deformation of the joint is excessively constrained and thus higher-order deformations such as warping and distortion cannot be properly developed at the

joint.

From the observations above, a new approach to theoretically derive joint matching conditions is required in order to develop exact higher-order beam theory-based analysis applicable to three or more box beams-joint structures. Especially when the joint is defined as a point box beam members being connected to, similar to classical beam theories or Refs. [39-42], there is no research so far which gives exact matching conditions defined at that joint point. From the observation that two adjacent box beam members always share one common edge near the joint, Jang et al. [43] have recently proposed joint matching conditions defining three-dimensional displacement continuity between those two members along the actual location of common edge, and analyzed three box beams-joint structures under out-of-plane loads by employing those matching conditions. Since the joint is described as several scattered points, however, equilibriums of the resultant forces or moments cannot be held exactly at the joint, and that builds in errors in the analyses.

In this study, three or more box beams-joint structures under out-of-plane bending or torsion will be analyzed by using a higher-order beam theory. The unique contribution of this investigation is to derive the exact matching relations among all field variables of box beams meeting at the joint. Figure 3.1 shows a three or more box beams-joint structure. Only a portion of the structure, such as Beam i-1, Beam i, and Beam i+1 ($i \geq 2$) is depicted, for convenience. It is assumed that all the box beams in Fig. 3.1 are placed on the same plane, and also

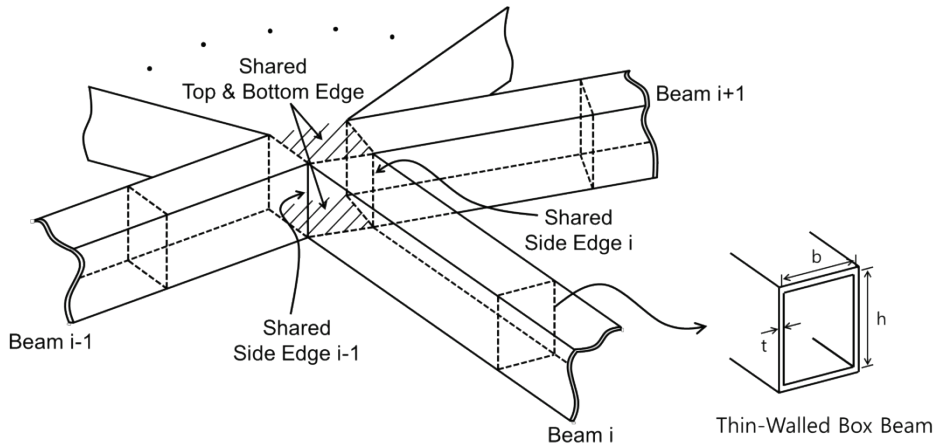

Fig. 3.1 Three or more thin-walled box beams-joint structures (only a portion of the structure such as Beam *i*-1, Beam *i*, and Beam *i*+1 ($i \geq 2$), is depicted, for convenience.).

assumed that their width, height, and thickness are equal to *b*, *h*, and *t*, respectively. In this study, in order to interpret the box beams-joint structure depicted in Fig. 3.1 by using the higher-order beam theory, the connectivity between box beams is modeled as shown in Fig. 3.2. As with the classical beam theories or Refs. [39-42], the point where all the box beams converge is defined as the joint (strictly speaking, the joint refers to the point where the central axes of box beams meet). Shared Side Edge *i*-1 in Fig. 3.1, which is shared by Beam *i*-1 and Beam *i* ($i \geq 2$), is extended and represented in Fig. 3.2 by Edge $M_{i-1}M'_{i-1}$ in Beam *i*-1 and Edge $N_iN'_i$ in Beam *i* separately. So, in this study, Edge $M_{i-1}M'_{i-1}$ and Edge $N_iN'_i$ are considered as if they were attached rigidly to each other (by an imaginary rigid body).

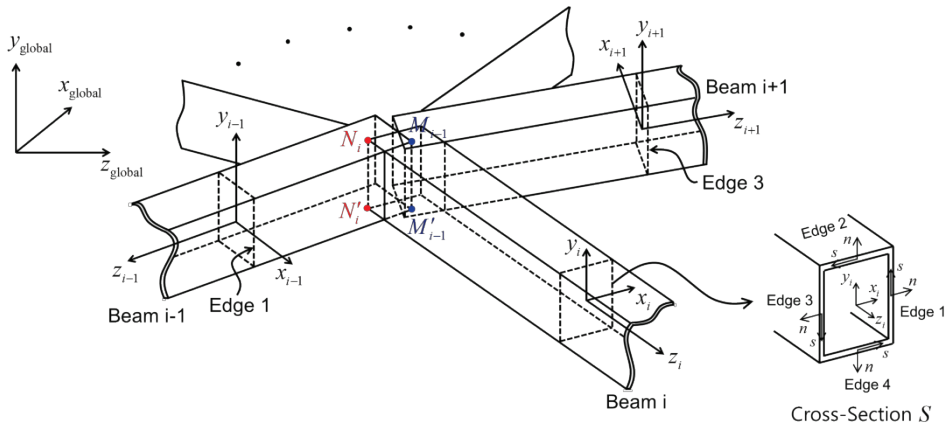

(a)

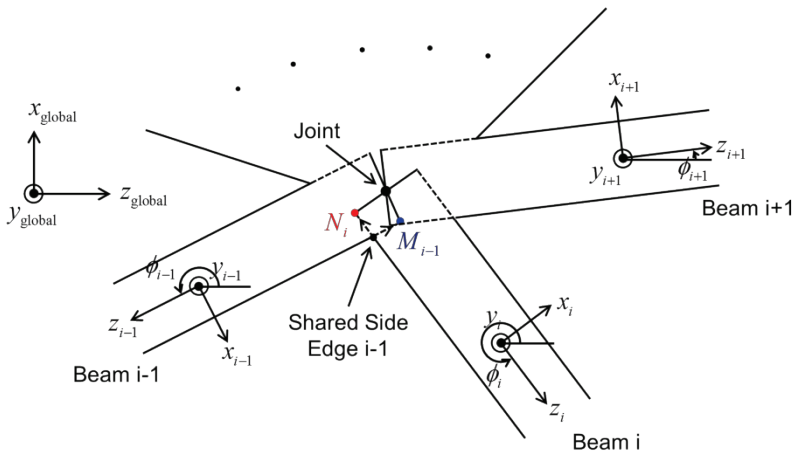

(b)

Fig. 3.2 (*a*) Beam modeling for the three or more box beams-joint structures (Edge $M_{i\text{-}1}M'_{i\text{-}1}$ of Beam *i*-1 and Edge N_iN_i' of Beam *i* ($i \geq 2$) are considered as if they were connected rigidly to each other (by an imaginary rigid body).), (*b*) the top view of beam modeling (Edge $M_{i\text{-}1}M'_{i\text{-}1}$ of Beam *i*-1 and Edge N_iN_i' of Beam *i* are extended and separated from Shared Side Edge *i*-1 ($i \geq 2$) in Fig. 3.1.).

Therefore, although Edge $M_{i-1}M'_{i-1}$ and Edge N_iN_i' are separated from each

other, both the equilibrium between the forces and the continuity between the displacements, which are generated at each of those edges, can be considered.

As mentioned above, the key of this study is to find joint matching conditions among field variables that can be applied to the three or more box beams-joint structure. To this end, joint equilibrium conditions among generalized forces, which are the work conjugates of the field displacement variables, will be precisely defined first. Then, taking into account the defined equilibrium conditions and the principle of virtual work together, joint matching conditions among field variables will be theoretically derived. In this process, note that the work conjugates of the field variables representing the cross-sectional warping and distortion do not generate any resultant forces or moments acting on the cross-section, but do generate stress resultants acting on each of the edges. Therefore, if the equilibriums on the edges (Edge $M_{i-1}M'_{i-1}$, Edge N_iN_i', etc.) are considered in addition to the resultant forces and moments equilibriums, then generalized forces equilibrium conditions which are consistently valid for the three or more box beams-joint structures can be determined. Although the purpose of this study is to derive equilibrium conditions or matching conditions applicable to the three or more box beams-joint structures, the derived conditions should also be valid for the two box beams-joint structures in order for this approach to be reasonable. According to this observation, we derive more generalized matching conditions on the basis of Choi et al. [42] who derived the exact matching conditions with respect to two box beams-joint structures. More detailed procedures will be given after the

fundamentals of higher-order beam theory for straight thin-walled box beams are presented. In order to verify the validity of the proposed joint matching conditions, two case studies including T-joint problems will be examined. The accuracy of the proposed analysis method will be checked by comparison with the results of ABAQUS shell analysis [44].

3.2 Higher-Order Beam Theory for Straight Thin-Walled Box Beams

First, a higher-order beam theory for straight thin-walled box beams, which is required if we are to interpret three or more box beams-joint structures, is introduced (see Refs. [6, 39] for more details).

In this study, it is assumed that the box beams-joint structures are subjected to out-of-plane bending or torsion, so five functions of the axial coordinate z are considered for one-dimensional field variables of the higher-order beam theory: vertical bending deflection $U_y(z)$, bending/shear rotation $\theta_x(z)$, torsional rotation $\theta_z(z)$, warping $W(z)$, and distortion $\chi(z)$ [39, 42]. Rigid-body motions of the box beam cross-section represented by $U_y(z)$, $\theta_x(z)$, and $\theta_z(z)$ or cross-sectional deformations represented by $W(z)$ and $\chi(z)$ are illustrated in Figs. 3.3(a) and 3.3(b), respectively.

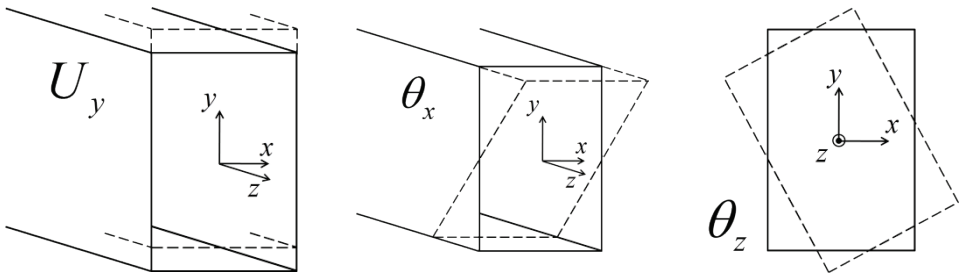

(a)

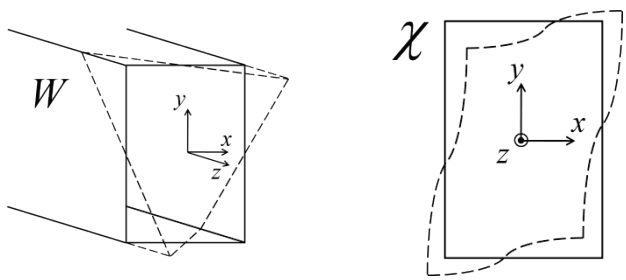

(b)

Fig. 3.3 (*a*) Rigid-body motions of the box beam cross-section represented by the field variables: vertical bending deflection U_y, bending/shear rotation θ_x, and torsional rotation θ_z, (*b*) deformations of cross-section represented by the field variables: warping W and distortion χ.

In the higher-order beam theory, three-dimensional displacements of a point located on the contour line of the box beam cross-section can be expressed as follows, by using one-dimensional field variables $\mathbf{U} = \{U_y, \theta_x, \theta_z, W, \chi\}^{\mathrm{T}}$ [6]:

$$u_n(s, z) = \psi_n^{U_y}(s) \cdot U_y(z) + \psi_n^{\theta_x}(s) \cdot \theta_x(z) + \psi_n^{\theta_z}(s) \cdot \theta_z(z) + \psi_n^{W}(s) \cdot W(z) + \psi_n^{\chi}(s) \cdot \chi(z) \tag{3.1a}$$

$$u_s(s, z) = \psi_s^{U_y}(s) \cdot U_y(z) + \psi_s^{\theta_x}(s) \cdot \theta_x(z) + \psi_s^{\theta_z}(s) \cdot \theta_z(z) + \psi_s^{W}(s) \cdot W(z) + \psi_s^{\chi}(s) \cdot \chi(z)$$

(3.1b)

$$u_z(s,\, z) = \psi_z^{U_y}(s)\cdot U_y(z) + \psi_z^{\theta_x}(s)\cdot \theta_x(z) + \psi_z^{\theta_z}(s)\cdot \theta_z(z) + \psi_z^{W}(s)\cdot W(z) + \psi_z^{\chi}(s)\cdot \chi(z)$$

(3.1c)

where n and s represent a normal coordinate and a tangential coordinate defined on the contour line, respectively (see Fig. 3.2(a) for the positive directions of n and s).

In Eq. (3.1), $\psi_p^{\alpha}(s)$ ($p = n,\, s,\, z;\ \alpha = U_y,\, \theta_x,\, \theta_z,\, W,\, \chi$), which are shape functions of s, are introduced to describe the displacement or deformation of the cross-section. Therefore, $\psi_p^{\alpha}(s)$ represent the displacement in the p direction generated on the cross-section with respect to the unit magnitude of field variable α [39]. The explicit expressions of $\psi_p^{\alpha}(s)$ are given in Appendix A.

Considering the Kirchhoff-Love plate theory [45], the three-dimensional displacements ($\tilde{u}_n,\, \tilde{u}_s,\, \tilde{u}_z$) of a generic point located away from the contour line by n can be expressed as follows, by using ($u_n,\, u_s,\, u_z$) in Eq. (3.1):

$$\tilde{u}_n(n,\, s,\, z) = u_n, \quad \tilde{u}_s(n,\, s,\, z) = u_s - n\frac{\partial u_n}{\partial s}, \quad \tilde{u}_z(n,\, s,\, z) = u_z - n\frac{\partial u_n}{\partial z} \qquad (3.2)$$

where $-n\cdot(\partial u_n / \partial s)$ and $-n\cdot(\partial u_n / \partial z)$ represent displacements in the s direction and the z direction respectively, occurring as the normal to the contour line is rotated. Dominant or non-vanishing strains ($\varepsilon_{ss},\, \varepsilon_{zz},\, \gamma_{sz}$) at a generic point can be derived from ($\tilde{u}_n,\, \tilde{u}_s,\, \tilde{u}_z$) in Eq. (3.2), and dominant or non-vanishing stresses ($\sigma_{ss},\, \sigma_{zz},\, \sigma_{sz}$) can be determined by applying the derived strains ($\varepsilon_{ss},\, \varepsilon_{zz},\, \gamma_{sz}$) to

the stress-strain relations.

In this study, the following two equations are used as the stress-strain relations in order to define the dominant stresses (σ_{ss}, σ_{zz}, σ_{sz}) precisely; either

$$\sigma_{ss} = \frac{E}{1-v^2}(\varepsilon_{ss} + v\varepsilon_{zz}), \qquad \sigma_{zz} = \frac{E}{1-v^2}(\varepsilon_{zz} + v\varepsilon_{ss}), \qquad \sigma_{sz} = G\gamma_{sz} \tag{3.3a}$$

or

$$\sigma_{ss} = E\varepsilon_{ss}, \qquad \sigma_{zz} = E\varepsilon_{zz}, \qquad \sigma_{sz} = G\gamma_{sz} \tag{3.3b}$$

where $E, G,$ and, v represent Young's modulus, shear modulus, and Poisson's ratio, respectively.

According to Kim and Kim [6], the dominant stresses derived from (θ_z, W, χ) that represent torsion of the box beam are defined by using the stress-strain relations in Eq. (3.3a). According to the Timoshenko beam theory (see e.g. [2]) the dominant stresses derived from (U_y, θ_x) that represent bending of the box beams are defined by using the stress-strain relations in Eq. (3.3b). Deriving the dominant strain associated with (U_y, θ_x), only (ε_{zz}, γ_{sz}) have non-zero values and $\varepsilon_{ss} = 0$. Therefore, only (σ_{zz}, σ_{sz}) are defined as dominant bending stresses, as with the Timoshenko beam theory, through the relations in Eq. (3.3b).

Using the displacements, strains, and stresses defined at a generic point, the three-dimensional total potential energy for the straight thin-walled box beam can be defined. Then, carrying out the surface integral for the cross-section S and applying the principle of minimum total potential energy, one can derive the one-

dimensional higher-order beam theory for the straight thin-walled box beam (see Refs. [6, 39] for the detailed procedures).

The derived higher-order beam theory is expressed by the relationship between the one-dimensional field variables $\mathbf{U}$ and generalized forces $\mathbf{F} = \{F_y, M_x, M_z, B, Q\}^{\mathrm{T}}$ which are work conjugates of $\mathbf{U}$. The generalized forces $\mathbf{F}$ are defined as:

$$\begin{aligned} F_y &= \iint_S (\sigma_{zs}\psi_s^{U_y})\, dsdn, \quad M_x = \iint_S (\sigma_{zz}\psi_z^{\theta_x})\, dsdn, \quad M_z = \iint_S (\sigma_{zs}\psi_s^{\theta_z})\, dsdn, \\ B &= \iint_S (\sigma_{zz}\psi_z^{W})\, dsdn, \qquad Q = \iint_S (\sigma_{zs}\psi_s^{\chi})\, dsdn \end{aligned} \tag{3.4}$$

where F_y, M_x, M_z, B, and Q denote one-dimensional force measures representing vertical force, bending moment, twisting moment, longitudinal bimoment, and transverse bimoment, respectively.

3.3 Derivation of the Exact Joint Matching Conditions

With respect to analysis of three or more box beams-joint structures by using the higher-order beam theory introduced in the previous section, the key is to define the exact joint matching conditions among the field variables which represent the behavior of the joint correctly.

After explaining the difficulties whereby the stiffness of the joint is overestimated when the matching conditions proposed in Refs. [39, 42] are directly

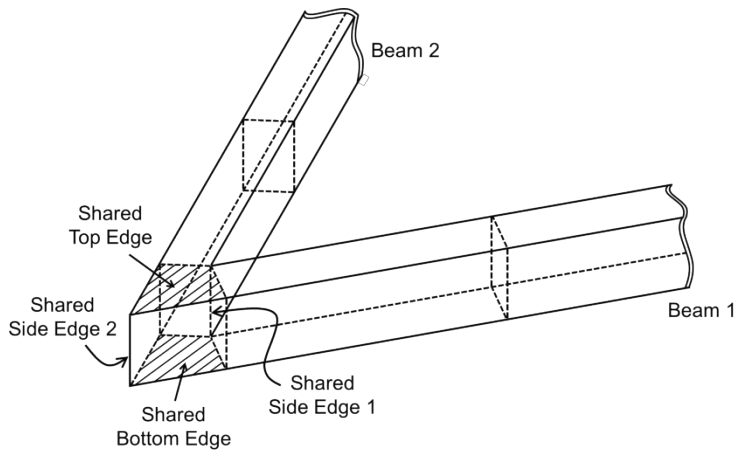

Fig. 3.4 Two thin-walled box beams-joint structures.

extended to three or more box beams-joint structures, we will propose and derive the exact joint matching conditions, which are applicable to three or more box beams-joint structures [46].

Concerning the two box beams-joint structure depicted in Fig. 3.4, the field variables of Beam k ($k = 1, 2$) are represented as,

$$\mathbf{U}_k = \{(U_y)_k, (\theta_x)_k, (\theta_z)_k, W_k, \chi_k\}^{\mathrm{T}} \tag{3.5}$$

In Choi et al. [42], joint matching conditions between $\mathbf{U}_1$ and $\mathbf{U}_2$ are exactly defined by introducing joint matrix $\mathbf{T}$. Through the various box beams-joint examples, it was shown that the matching conditions can describe the response of the joint precisely as interpreted by the shell elements.

When a two box beams-joint structure is modeled as shown in Fig. 3.5 by adopting the same procedure as the modeling in Fig. 3.2, the matching conditions

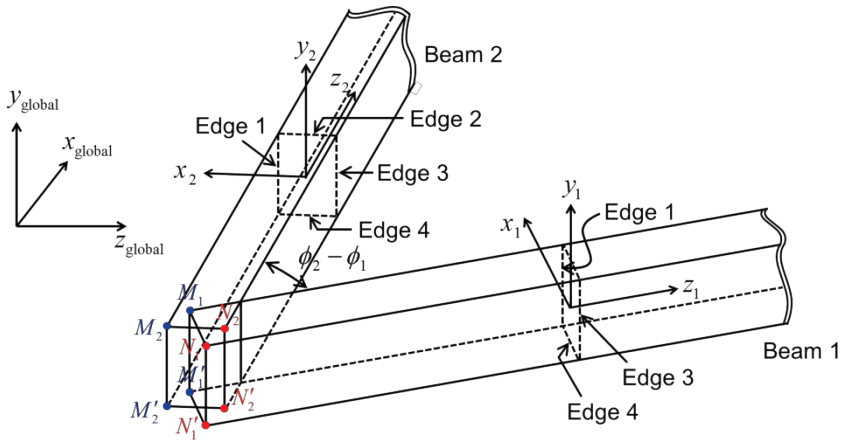

(a)

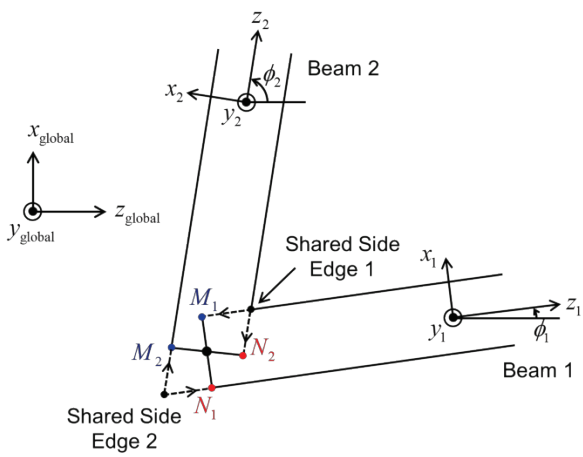

Fig. 3.5 (*a*) Beam Modeling for the two box beams-joint structures (Edge $M_1M'_1$ of Beam 1 and Edge N_2N_2' of Beam 2 are considered as if they were connected rigidly to each other (by an imaginary rigid body), and Edge N_1N_1' of Beam 1 and Edge $M_2M'_2$ of Beam 2 are also considered as if being connected rigidly to each other (by an imaginary rigid body).), (*b*) the top view of beam modeling (Shared Side Edge 1 in Fig. 4 is extended and represented by Edge $M_1M'_1$ of Beam 1 and Edge N_2N_2' of Beam 2 separately, and Share Side Edge 2 in Fig 4 is also extended and represented by Edge N_1N_1' of Beam 1 and Edge $M_2M'_2$ of Beam 2 separately.).

between $\mathbf{U}_1$ and $\mathbf{U}_2$ can be expressed as follows by using the joint matrix $\mathbf{T}$

proposed in Choi et al. [42]: (However, concerning the modeling in Fig. 3.5, the constraint conditions between Edge M_1M_1' and Edge N_2N_2' or between Edge M_2M_2' and Edge N_1N_1' were not considered when the following matching conditions are defined.)

$$\mathbf{U}_2 = \mathbf{T}(\phi_2 - \phi_1) \cdot \mathbf{U}_1 \tag{3.6a}$$

or

$$\begin{Bmatrix} (U_y)_2 \\ (\theta_x)_2 \\ (\theta_z)_2 \\ W_2 \\ \chi_2 \end{Bmatrix} = \begin{bmatrix} \overset{\mathbf{A}}{\begin{matrix} 1 & 0 & 0 \\ 0 & \cos(\phi_2-\phi_1) & -\sin(\phi_2-\phi_1) \\ 0 & \sin(\phi_2-\phi_1) & \cos(\phi_2-\phi_1) \end{matrix}} & \overset{\mathbf{B}}{\begin{matrix} 0 & 0 \\ 0 & (\frac{2b}{b+h})\cdot\{\sin(\phi_2-\phi_1)\} \\ 0 & -(\frac{2b}{b+h})\cdot\{1+\cos(\phi_2-\phi_1)\} \end{matrix}} \\ \begin{matrix} 0 & 0 & 0 \\ 0 & 0 & 0 \end{matrix} & \underset{\mathbf{C}}{\begin{matrix} 1 & 0 \\ 0 & -1 \end{matrix}} \end{bmatrix} \begin{Bmatrix} (U_y)_1 \\ (\theta_x)_1 \\ (\theta_z)_1 \\ W_1 \\ \chi_1 \end{Bmatrix} \tag{3.6b}$$

where ϕ_k ($k = 1, 2$) represents the angle between the axial coordinate z_k of Beam k and z_{global} in Fig. 3.5 (see Fig. 3.5(b) for the positive directions), and $(\phi_2 - \phi_1)$ in Eq. (3.6) denotes the joint angle of the two box beams-joint structure. Observing the joint matrix $\mathbf{T}(\phi_2 - \phi_1)$, its submatrix **A** represents the matching conditions among rigid-body motions. Submatrix **B** represents additional rigid-body motions ($(\theta_x)_2$, $(\theta_z)_2$) of Beam 2 generated by the higher-order deformations (W_1, χ_1) of Beam 1, and submatrix **C** represents the matching conditions among higher-order deformations (W, χ).

If one wishes to directly extend the matching conditions in Eq. (3.6) for the three or more box beams-joint structure in Fig. 3.2, it could be written as:

$$\mathbf{U}_i = \mathbf{T}(\phi_i - \phi_{i-1}) \cdot \mathbf{U}_{i-1}, \quad \mathbf{U}_{i+1} = \mathbf{T}(\phi_{i+1} - \phi_{i-1}) \cdot \mathbf{U}_{i-1}, \quad \mathbf{U}_{i+1} = \mathbf{T}(\phi_{i+1} - \phi_i) \cdot \mathbf{U}_i \quad (3.7)$$

where ϕ_k $(k = i-1, i, i+1;\ i \geq 2)$ refers to the angle between the axial coordinate z_k of Beam k and z_{global}, and $\mathbf{U}_k$ refers to the field variables of Beam k as defined with respect to the two box beams-joint structure. If the matching conditions in Eq. (3.7) are applied, the relations among χ_{i-1}, χ_i, and, χ_{i+1}, which are distortional deformation measures of Beam i-1, Beam i, and Beam i+1, respectively, will be expressed as (see submatrix **C** of joint matrix $\mathbf{T}$):

$$\chi_i = -\chi_{i-1}, \quad \chi_{i+1} = -\chi_{i-1}, \quad \chi_{i+1} = -\chi_i \quad (3.8)$$

Because the relations in Eq. (3.8) should be satisfied for arbitrary χ_{i-1}, χ_i, and, χ_{i+1}, the relations eventually represent $\chi_{i-1} = \chi_i = \chi_{i+1} = 0$.

Observing submatrix **B** in joint matrix $\mathbf{T}$, on the other hand, it can be seen that rigid-body motions (U_y, θ_x, θ_z) of a beam connected to the joint are additionally induced by distortional deformation χ as well as rigid-body motions of adjacent beams. Therefore, when the matching relations such as Eq. (3.8) (i.e. $\chi_{i-1} = \chi_i = \chi_{i+1} = 0$) are applied to the three or more box beams-joint structure, those relations overestimate the stiffness of the joint, and it is not possible to obtain an accurate result. For the same reason, when the matching conditions proposed in Jang et al. [39] are extended to the three or more box beams-joint structure, the stiffness of the joint again tends to be overestimated (see Ref. [43] for more details). Therefore, the joint matching conditions proposed in Refs. [39, 42] cannot be

directly extended to the three or more box beams-joint structure, and a new approach that is different from the existing methods should be developed, to deal with the three or more box beams-joint structure.

The matching conditions among field variables that contain higher-order deformations (W, χ) were determined mostly on the basis of the continuity among the three-dimensional displacements occurring at the joint [39-41, 43]. Since the higher-order deformations (W, χ) represent highly complex three-dimensional displacements which are very different for each edge, as depicted in Fig. 3.3(b), the continuity among the three-dimensional displacements occurring at the joint of the three or more box beams-joint structure cannot be satisfied precisely when they are treated at a single joint point (or line) within the scope of the higher-order beam theory. Therefore, rather than considering the continuity among three-dimensional displacements directly, we propose in this study a method to derive the matching conditions by first deriving equilibrium conditions among the generalized forces (F_y, M_x, M_z, B, Q) of each beam at the joint. Using the generalized force matching conditions, we then derive the continuity conditions for the generalized displacements (or field variables), which are energy conjugates of those forces.

If the joint is considered simply as a point, the terms (F_y, M_x, M_z) producing resultants can be expressed as a resultant force or moment, as shown in Fig. 3.6. But (B, Q), which do not produce any resultant, cannot be expressed as a resultant force or moment acting on a point. In order to overcome this difficulty, we propose

to express (B, Q), which are defined on the section, as so-called edge resultants as depicted in Fig. 3.7(a). Note that (B, Q) can produce non-zero resultants on each edge of the section, those resultants will be called edge resultants. This new approach is proposed in this study for the first time, and is an important step towards the derivation of the matching conditions for the generalized displacements at the joint.

As (B, Q) are represented by the edge resultants, (F_y, M_x, M_z) having net resultants over the section can be also represented by edge resultants defined on each edge, as demonstrated in Fig. 3.7(b). In the subsequent discussions, the non-vanishing resultants defined over the section will be referred to as "sectional" resultants. After all, a new method to represent (F_y, M_x, M_z, B, Q) by edge resultants and to additionally consider equilibriums among edge resultants at the

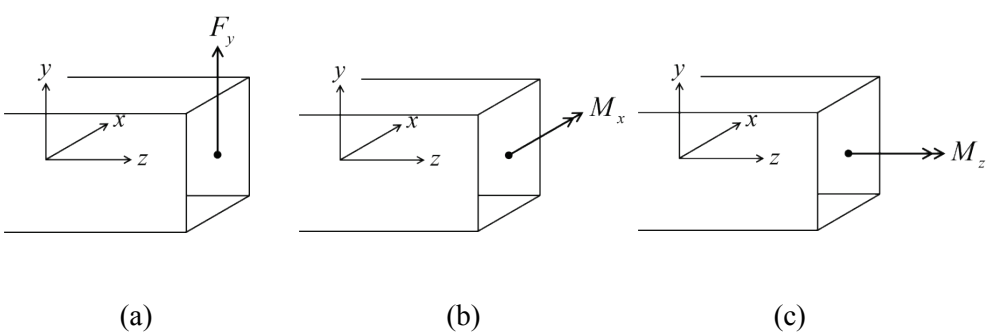

Fig. 3.6 Resultants (or sectional resultants) acting on the entire cross-section that are produced by the generalized forces: vertical force F_y, bending moment M_x, and twisting moment M_z.

edges shared by adjacent beams such as Edge $M_{i-1}M'_{i-1}$, Edge $N_iN'_i$, etc. will be employed to derive the joint equilibrium conditions among generalized forces. It is worth emphasizing once again that this method is the key in a derivation of the joint matching conditions among generalized displacements (or field variables) at the joint where three or more box beams meet.

3.3.1 Sectional and Edge Resultants Produced by Generalized Forces

Prior to dealing with the generalized forces equilibriums, the stresses which generalized forces induce on the section will be introduced, and from those stresses, sectional or edge resultants will be derived. According to the higher-order beam theory, the stresses on the section vary linearly in the normal direction to the contour. However, the variance of the stresses along the normal direction is quite small, and the small amount of the variance is also eliminated through the surface integral, so the sectional or edge resultants will be defined by using the stresses on the contour.

According to the higher-order beam theory, dominant stresses ($\sigma_{zz}, \sigma_{ss}, \sigma_{zs}$) on the contour can be related to the displacements as

$$\sigma_{zz}(s, z) = E\psi_z^{\theta_x}(s)\cdot\theta_x'(z) + \frac{E}{1-\nu^2}\psi_z^W(s)\cdot W'(z) \tag{3.9a}$$

$$\sigma_{ss}(s, z) = 0 \tag{3.9b}$$

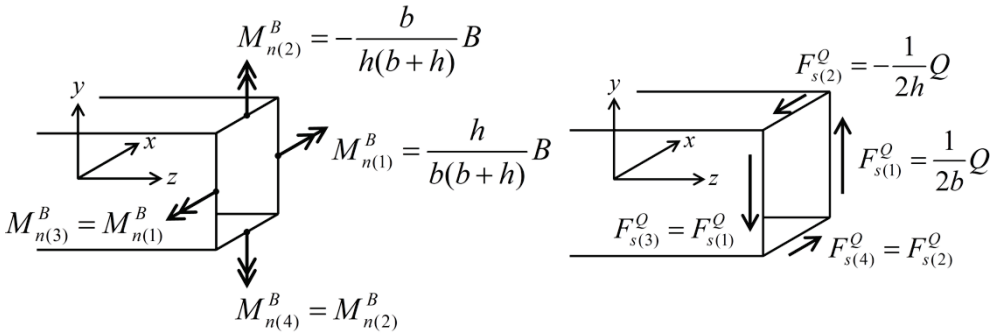

(a)

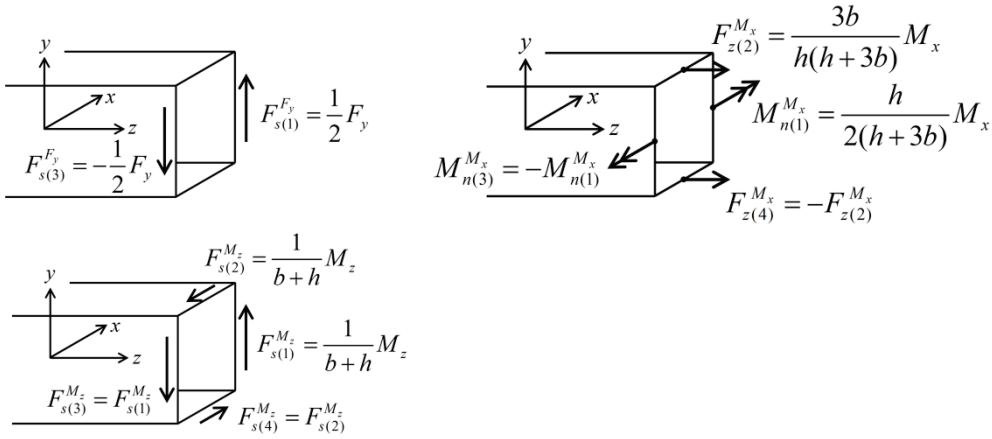

(b)

Fig. 3.7 (*a*) Edge resultants acting on each edge of the cross-section that are produced by the self-equilibrated generalized forces: longitudinal bimoment B and transverse bimoment Q, (*b*) edge resultants acting on each edge of the cross-section that are produced by the generalized forces having nonzero resultants: vertical force F_y, bending moment M_x, and twisting moment M_z

$$\begin{aligned}\sigma_{zs}(s,z) = G\{&\psi_s^{U_y}(s)\cdot U_y{}'(z) + \dot{\psi}_z^{\theta_x}(s)\cdot\theta_x(z) + \psi_s^{\theta_z}(s)\cdot\theta_z{}'(z)\\ &+\dot{\psi}_z^{W}(s)\cdot W(z) + \psi_s^{\chi}(s)\cdot\chi'(z)\}\end{aligned} \tag{3.9c}$$

where $(\dot{\ }) = \dfrac{\partial()}{\partial s}$ and $()' = \dfrac{\partial()}{\partial z}$. Whereas ($\psi_s^{U_y}, \psi_s^{\theta_z}, \psi_s^{\chi}$) in Eq. (3.9c) are orthogonal to each other, ($\dot{\psi}_z^{\theta_x}, \dot{\psi}_z^{W}$) can be expressed in terms of ($\psi_s^{U_y}, \psi_s^{\theta_z}, \psi_s^{\chi}$) because $\dot{\psi}_z^{\theta_x} = \psi_s^{U_y}, \dot{\psi}_z^{W} = \dfrac{b-h}{b+h}\psi_s^{\theta_z} + \psi_s^{\chi}$ (see the explicit expressions of ψ's in Appendix A). Therefore, $\sigma_{zs}(s, z)$ in Eq. (3.9c) can be written as a function of only ($\psi_s^{U_y}, \psi_s^{\theta_z}, \psi_s^{\chi}$) as:

$$\begin{aligned}\sigma_{zs}(s, z) = G[&\psi_s^{U_y}(s)\cdot\{U_y'(z) + \theta_x(z)\} + \psi_s^{\theta_z}(s)\cdot\{\theta_z'(z) + \frac{b-h}{b+h}W(z)\} \\ &+ \psi_s^{\chi}(s)\cdot\{\chi'(z) + W(z)\}]\end{aligned} \tag{3.10}$$

By applying σ_{zz} in Eq. (3.9a) and σ_{zs} in Eq. (3.10) to the definitions of the generalized forces in Eq. (3.4) and carrying out the surface integral for the cross-section *S*, they can be expressed in terms of generalized displacements as

$$\begin{aligned}F_y(z) &= \iint_S \sigma_{zs}(s, z)\cdot\psi_s^{U_y}(s)\, dsdn \\ &= \iint_S G[\psi_s^{U_y}\cdot\psi_s^{U_y}\cdot\{U_y' + \theta_x\} + \psi_s^{\theta_z}\cdot\psi_s^{U_y}\cdot\{\theta_z' + \frac{b-h}{b+h}W\} \\ &\qquad + \psi_s^{\chi}\cdot\psi_s^{U_y}\cdot\{\chi' + W\}]\, dsdn \\ &= \iint_S G[\psi_s^{U_y}\cdot\psi_s^{U_y}\cdot\{U_y' + \theta_x\}]\, dsdn \\ &= GJ_{F_y}\{U_y'(z) + \theta_x(z)\}\end{aligned} \tag{3.11a}$$

The second line in Eq. (3.11a) can be reduced to the third line because of the orthogonality conditions such that $\iint_S \psi_s^{\theta_z}\cdot\psi_s^{U_y}\, dsdn = 0$, $\iint_S \psi_s^{\chi}\cdot\psi_s^{U_y}\, dsdn = 0$ (see Appendix A). In addition, the orthogonality condition between ($\psi_z^{\theta_x}, \psi_z^{W}$) is

also satisfied as given in Appendix A. When those orthogonality conditions are used, the expressions for the remaining generalized forces can be simplified as

$$M_x(z) = \iint_S \sigma_{zz}(s,\, z) \cdot \psi_z^{\theta_x}(s)\; dsdn = EJ_{M_x}\theta_x{}'(z) \tag{3.11b}$$

$$M_z(z) = \iint_S \sigma_{zs}(s,\, z) \cdot \psi_s^{\theta_z}(s)\; dsdn = GJ_{M_z}\{\theta_z{}'(z) + \frac{b-h}{b+h}W(z)\} \tag{3.11c}$$

$$B(z) = \iint_S \sigma_{zz}(s,\, z) \cdot \psi_z^{W}(s)\; dsdn = \frac{E}{1-\nu^2}J_B W'(z) \tag{3.11d}$$

$$Q(z) = \iint_S \sigma_{zs}(s,\, z) \cdot \psi_s^{\chi}(s)\; dsdn = GJ_Q\{\chi'(z) + W(z)\} \tag{3.11e}$$

where J_β $(\beta = F_y, M_x, M_z, B, Q)$ denoting the moment of inertia for the generalized force β is defined as

$$\begin{aligned} &J_{F_y} = \iint_S (\psi_s^{U_y})^2\, dsdn,\; J_{M_x} = \iint_S (\psi_z^{\theta_x})^2\, dsdn,\; J_{M_z} = \iint_S (\psi_s^{\theta_z})^2\, dsdn, \\ &J_B = \iint_S (\psi_z^{W})^2\, dsdn,\quad J_Q = \iint_S (\psi_s^{\chi})^2\, dsdn \end{aligned} \tag{3.12}$$

Considering the relations between generalized forces and field variables that are given in Eq. (3.11), σ_{zz} in Eq. (3.9a) and σ_{zs} in Eq. (3.10) can be written in terms of generalized forces as

$$\sigma_{zz}(s,\, z) = \sigma_{zz}^{M_x} + \sigma_{zz}^{B} = \{\frac{M_x(z)}{J_{M_x}}\psi_z^{\theta_x}(s)\} + \{\frac{B(z)}{J_B}\psi_z^{W}(s)\} \tag{3.13a}$$

$$\sigma_{zs}(s,\, z) = \sigma_{zs}^{F_y} + \sigma_{zs}^{M_z} + \sigma_{zs}^{Q} = \{\frac{F_y(z)}{J_{F_y}}\psi_s^{U_y}(s)\} + \{\frac{M_z(z)}{J_{M_z}}\psi_s^{\theta_z}(s)\} + \{\frac{Q(z)}{J_Q}\psi_s^{\chi}(s)\} \tag{3.13b}$$

where (σ_{zz}, σ_{zs}) in Eq. (3.13) represent the stresses on the contour that generalized forces produce, and especially σ^{β} ($\beta = F_y, M_x, M_z, B, Q$) represents the stress produced by the generalized force β. Therefore, employing the stresses at arbitrary coordinates (*s*, *z*) that are given in Eq. (3.13), edge resultants produced by the generalized forces can be obtained.

If one obtains first the sectional resultants from Eqs. (3.13a, b) through surface integral, non-zero resultants obtained from Eqs. (3.13a, b) are represented obviously by (F_y, M_x, M_z) only. Note that the contribution of the stresses (σ_{zz}^{B}, σ_{zs}^{Q}), which are generated by (B, Q), to (F_y, M_x, M_z) is zero. Since (B, Q) do not produce any net resultants on the section as observed above, (B, Q) will be expressed by using edge resultants.

Now, it will be shown how to obtain the edge resultants that generalized force β ($\beta = F_y, M_x, M_z, B, Q$) produces. Stresses on (*s*, *z*) induced by those forces are given in Eq. (3.13), so edge resultants can be obtained by integrating stresses on each edge. The non-zero edge resultants determined from the stresses in Eq. (3.13) are axial force $F_{z(j)}^{\beta}$, tangential force $F_{s(j)}^{\beta}$, and normal moment $M_{n(j)}^{\beta}$ ($\beta = F_y, M_x, M_z, B, Q$), and are defined as

$$F_{z(j)}^{\beta} = \iint_{Edge\ j} \sigma_{zz}^{\beta}\ dsdn, \quad F_{s(j)}^{\beta} = \iint_{Edge\ j} \sigma_{zs}^{\beta}\ dsdn, \quad M_{n(j)}^{\beta} = \iint_{Edge\ j} s \cdot \sigma_{zz}^{\beta}\ dsdn \qquad (3.14)$$

Therefore, the edge resultants by the generalized force β can be determined by

using Eq. (3.14). For example, the edge resultants acting on Edge 1 (see Fig. 3.2) are determined as, by carrying out the integration in Eq. (3.14),

$$F_{z(1)}^{F_y} = 0, \qquad F_{s(1)}^{F_y} = \frac{1}{2}F_y, \qquad M_{n(1)}^{F_y} = 0 \tag{3.15a}$$

$$F_{z(1)}^{M_x} = 0, \qquad F_{s(1)}^{M_x} = 0, \qquad M_{n(1)}^{M_x} = \frac{h}{2(h+3b)}M_x \tag{3.15b}$$

$$F_{z(1)}^{M_z} = 0, \qquad F_{s(1)}^{M_z} = \frac{1}{b+h}M_z, \qquad M_{n(1)}^{M_z} = 0 \tag{3.15c}$$

$$F_{z(1)}^{B} = 0, \qquad F_{s(1)}^{B} = 0, \qquad M_{n(1)}^{B} = \frac{h}{b(b+h)}B \tag{3.15d}$$

$$F_{z(1)}^{Q} = 0, \qquad F_{s(1)}^{Q} = \frac{1}{2b}Q, \qquad M_{n(1)}^{Q} = 0 \tag{3.15e}$$

where b and h denote the width and the height of the box beam cross-section respectively, as mentioned in Introduction. The edge resultants above can be expressed schematically by forces or moments on each edge, as depicted in Fig. 3.7.

3.3.2 Generalized Forces Equilibrium Conditions

Now, the exact equilibrium conditions among generalized forces at the joint will be derived by considering the equilibriums of the edge resultants given in Fig. 3.7 in addition to those of the sectional resultants given in Fig. 3.6. To this end, the results given in Choi et al. [42] will be utilized. Because those results in Choi et al. [42] were derived without considering the concept of edge resultants proposed in this study, we will first interpret the results from the viewpoint of equilibrium

conditions of the sectional and edge resultants; this step is crucial to extend the results by Choi et al. [42] to joint structures involving more than two box beams.

Concerning the two box beams-joint structure depicted in Fig. 3.5, the equilibrium conditions between the generalized forces of Beams 1 and 2, $\mathbf{F}_1$ and $\mathbf{F}_2$, can be written as

$$\mathbf{T}^{-\mathrm{T}}(\phi_2 - \phi_1) \cdot \mathbf{F}_1 + \mathbf{F}_2 = \mathbf{0} \tag{3.16}$$

where $\mathbf{T}$ is the joint matrix given in Eq. (3.6) and $\mathbf{F}_k$ ($k = 1, 2$) is defined as

$$\mathbf{F}_k = \{(F_y)_k, (M_x)_k, (M_z)_k, B_k, Q_k\}^{\mathrm{T}} \tag{3.17}$$

The matrix $\mathbf{T}^{-\mathrm{T}}(\phi_2 - \phi_1)$, the transpose of the inverse of $\mathbf{T}(\phi_2 - \phi_1)$, transforms the generalized force $\mathbf{F}_1$ into the force based on the local coordinate system of Beam 2 (x_2, y_2, z_2). Because the equation given in Eq. (3.16) is derived from the displacement continuity and other geometrical conditions without considering the concepts of sectional and edge resultants, the result will be now interpreted in terms of the sectional and edge resultants.

If we write Eq. (3.16) explicitly as

$$(M_x)_1 \cos(\phi_2 - \phi_1) - (M_z)_1 \sin(\phi_2 - \phi_1) + (M_x)_2 = 0 \tag{3.18a}$$

$$(M_x)_1 \sin(\phi_2 - \phi_1) + (M_z)_1 \cos(\phi_2 - \phi_1) + (M_z)_2 = 0 \tag{3.18b}$$

$$B_1 + B_2 = 0 \tag{3.18c}$$

$$(F_y)_1 + (F_y)_2 = 0 \tag{3.18d}$$

$$-\frac{2b}{b+h}(M_x)_1 \sin(\phi_2-\phi_1)-\frac{2b}{b+h}(M_z)_1\{1+\cos(\phi_2-\phi_1)\}-Q_1+Q_2=0 \quad (3.18e)$$

one can rewrite Eqs. (3.18a-e) as, in terms of the sectional and edge resultants,

$$(M_x)_1 \cos(\phi_2-\phi_1)-(M_z)_1 \sin(\phi_2-\phi_1)+(M_x)_2=0 \quad (3.19a)$$

$$(M_x)_1 \sin(\phi_2-\phi_1)+(M_z)_1 \cos(\phi_2-\phi_1)+(M_z)_2=0 \quad (3.19b)$$

$$\{-\frac{b}{h(b+h)}B_1\}+\{-\frac{b}{h(b+h)}B_2\}=0 \quad (3.19c)$$

$$\{\frac{1}{2}(F_y)_1+\frac{1}{b+h}(M_z)_1+\frac{1}{2b}Q_1\}+\{\frac{1}{2}(F_y)_2-\frac{1}{b+h}(M_z)_2-\frac{1}{2b}Q_2\}=0 \quad (3.19d)$$

$$\{\frac{1}{2}(F_y)_1-\frac{1}{b+h}(M_z)_1-\frac{1}{2b}Q_1\}+\{\frac{1}{2}(F_y)_2+\frac{1}{b+h}(M_z)_2+\frac{1}{2b}Q_2\}=0 \quad (3.19e)$$

Note that Eqs. (3.19a, b) are equal to Eqs. (3.18a, b), and that Eq. (3.19c) can be obtained through multiplying Eq. (3.18c) by $-b/\{h(b+h)\}$. Meanwhile, Eq. (3.18e) can be simplified to

$$\{-\frac{2b}{b+h}(M_z)_1-Q_1\}+\{\frac{2b}{b+h}(M_z)_2+Q_2\}=0 \quad (3.20)$$

because $-\frac{2b}{b+h}\{(M_x)_1 \sin(\phi_2-\phi_1)+(M_z)_1 \cos(\phi_2-\phi_1)\}$ in Eq. (3.18e) is equal to $\frac{2b}{b+h}(M_z)_2$ according to Eq. (3.18b). Therefore, Eqs. (3.19d, e) can be obtained, first by multiplying Eqs. (3.18d) and (3.20) by $1/2$ and $1/(2b)$ respectively, and then adding or subtracting those two expressions.

Let us interpret Eq. (3.19) in terms of the sectional and edge resultants. First,

Eqs. (3.19a, b) represent equilibrium conditions in terms of the sectional resultants (M_x, M_z); Eq. (3.19a) represents the moment equilibrium in the x_2 direction, and Eq. (3.19b) represents the moment equilibrium in the z_2 direction (see Fig. 3.5 for the positive directions of x_2 and z_2). Therefore, it can be found from Eqs. (3.19a, b) that the resultant moment equilibriums should be satisfied at the joint depicted in Fig. 3.5. For our later extension to the case when more than two box beams meet at a joint, the equilibrium conditions in Eqs. (3.19a, b) can be expressed as, based on the global coordinate system (x_{global}, y_{global}, z_{global}):

$$(M_{x_{\text{global}}})_1 + (M_{x_{\text{global}}})_2 = 0 \tag{3.21a}$$

$$(M_{z_{\text{global}}})_1 + (M_{z_{\text{global}}})_2 = 0 \tag{3.21b}$$

where $(M_{x_{\text{global}}})_k$ and $(M_{z_{\text{global}}})_k$ $(k = 1, 2)$ are defined as

$$(M_{x_{\text{global}}})_k = (M_x)_k \cos\phi_k + (M_z)_k \sin\phi_k \tag{3.22a}$$

$$(M_{z_{\text{global}}})_k = -(M_x)_k \sin\phi_k + (M_z)_k \cos\phi_k \tag{3.22b}$$

The symbols $(M_{x_{\text{global}}})_k$ and $(M_{z_{\text{global}}})_k$ represent the resultant moments of Beam k in the x_{global} direction and in the z_{global} direction, respectively.

Examining Eqs. (3.19c-e), one can see that they represent equilibrium conditions in terms of edge resultants depicted in Fig. 3.7. In order to interpret the meaning of the equilibrium conditions given in Eqs. (3.19c-e), the connectivity between the edges of Beam 1 and those of Beam 2 at the joint shown in Fig. 3.5

should be investigated first because, unlike the sectional resultants defined for the entire cross-section, the edge resultants are defined for each edge of the section. In Fig. 3.5, Edge M_1N_1 and Edge M_2N_2 that represent Edge 2 of Beam 1 and Beam 2 respectively meet at the joint. Similarly, Edge $M_1'N_1'$ and Edge $M_2'N_2'$ that are Edge 4 of Beam 1 and Beam 2 respectively meet at the joint. Therefore, the equilibrium conditions can be considered among the edge resultants acting on Edge 2 of Beam 1 and Beam 2 or among those acting on Edge 4 of Beam 1 and Beam 2.

Because the remaining edges (Edge 1 and Edge 3 of Beam 1 and Beam 2) are not connected to each other in the model introduced to interpret the two box beams-joint structure shown in Fig. 3.5, it is necessary to define how those edges are connected. In this study, the connectivity among those edges is determined based on the actual joint connectivity depicted in Fig. 3.4. Edge M_1M_1' and Edge N_2N_2' in Fig. 3.5 representing Edge 1 of Beam 1 and Edge 3 of Beam 2 respectively are extended and expressed separately from Shared Side Edge 1 in Fig 3.4. Therefore, Edge M_1M_1' and Edge N_2N_2' can be considered as if they were connected rigidly to each other (by an imaginary rigid body) although they are separated. Likewise, because Edge N_1N_1' and Edge M_2M_2' in Fig. 3.5 representing Edge 3 of Beam 1 and Edge 1 of Beam 2 respectively are extended and separated from Shared Side Edge 2 in Fig. 3.4, they can be also considered as if they were connected rigidly to each other. Considering such rigid connections, the equilibrium among the edge resultants defined on Edge 1 of Beam 1 and on

Edge 3 of Beam 2 can be considered, and the equilibrium among those on Edge 3 of Beam 1 and on Edge 1 of Beam 2 can also be considered.

Based on the edge connectivities explained above, Eq. (19c) can be written as the normal moment equilibrium on Edge 2 or Edge 4 as:

$$(M_{n(2)})_1 + (M_{n(2)})_2 = 0 \tag{3.23a}$$

$$(M_{n(4)})_1 + (M_{n(4)})_2 = 0 \tag{3.23b}$$

where $(M_{n(2)})_k$ and $(M_{n(4)})_k$ $(k = 1, 2)$ are defined as

$$(M_{n(2)})_k = -\frac{b}{h(b+h)} B_k \,; \quad (M_{n(4)})_k = -\frac{b}{h(b+h)} B_k \tag{3.24a, b}$$

The symbols $(M_{n(2)})_k$ and $(M_{n(4)})_k$ represent the normal moment components of Beam k on Edge 2 and Edge 4, respectively (see the edge resultants given in Fig. 3.7). Therefore, it can be found from Eq. (3.19c) that the equilibrium for the normal moments defined on Edge j_1 ($j_1 = 2, 4$) should be satisfied at the joint in Fig. 3.5.

Equations (3.19d, e) can be written as the equilibrium among tangential edge forces defined on Edge 1 and Edge 3 of two beams:

$$(F_{s(1)})_1 - (F_{s(3)})_2 = 0 \tag{3.25a}$$

$$-(F_{s(3)})_1 + (F_{s(1)})_2 = 0 \tag{3.25b}$$

where $(F_{s(1)})_k$ and $(F_{s(3)})_k$ $(k = 1, 2)$ are given by

$$(F_{s(1)})_k = \frac{1}{2}(F_y)_k + \frac{1}{b+h}(M_z)_k + \frac{1}{2b} Q_k \tag{3.26a}$$

$$(F_{s(3)})_k = -\frac{1}{2}(F_y)_1 + \frac{1}{b+h}(M_z)_1 + \frac{1}{2b}Q_1 \tag{3.26b}$$

The symbols $(F_{s(1)})_k$ and $(F_{s(3)})_k$ represent the tangential forces of Beam k on Edge 1 and Edge 3, respectively (see the edge resultants given in Fig. 3.7). In deriving Eqs. (3.25a, b), care should be taken over the sign, because the positive tangential directions of Edge 1 and Edge 3 are opposite (see Fig. 3.2). Equations (3.25a, b) represent equilibriums in the y_{global} direction, which is the same as the tangential direction of Edge 1.

The analysis thus far reveals that the five equations in Eq. (3.18) taken from Choi et al. [42] correspond to two equilibrium conditions involving sectional resultants and three equilibrium conditions involving edge resultants. For a later extension to three or more box beams-joint structures, they are rewritten in terms of sectional and edge resultants as

$$(M_{x_{\text{global}}})_1 + (M_{x_{\text{global}}})_2 = 0 \tag{3.27a}$$

$$(M_{z_{\text{global}}})_1 + (M_{z_{\text{global}}})_2 = 0 \tag{3.27b}$$

$$(M_{n(2)})_1 + (M_{n(2)})_2 = (M_{n(4)})_1 + (M_{n(4)})_2 = 0 \tag{3.27c}$$

$$(F_{s(1)})_1 - (F_{s(3)})_2 = 0 \tag{3.27d}$$

$$-(F_{s(3)})_1 + (F_{s(1)})_2 = 0 \tag{3.27e}$$

Let us now consider the extension of Eq. (3.27) to the structure that N ($N \geq 3$) box beams are connected at the joint shown in Fig. 3.2. Because Eq.

(3.27) is defined as the equilibrium conditions for sectional and edge resultants, Eq. (3.27) is easy to be extended for the joint where three or more box beams meet.

In order to determine the equilibrium conditions for edge resultants, connectivity among the edges of N box beams at the joint should be investigated. Since Edge j_1 ($j_1 = 2, 4$) of N box beams meet at the joint (see Fig. 3.2), equilibrium among ($M_{n(j_1)}$) of N box beams can be considered. Connectivity among the remaining edges can be determined by considering the actual joint depicted in Fig. 3.1. For two adjacent box beams (Beam k ($k = 1, 2, \cdots, N$) and Beam k+1; Beam N+1 refers to Beam 1), Edge 1 of Beam k and Edge 3 of Beam k+1 can be considered as if they were connected rigidly to each other. Therefore, the equilibrium between $(F_{s(1)})_k$ and $(F_{s(3)})_{k+1}$ can be now considered.

Based on the connectivity among edges of box beams explained above, the generalized forces equilibrium conditions at the joint of N ($N \geq 3$) box beams-joint structure can be written as follows by extending the equilibrium conditions for sectional resultants or edge resultants given in Eq. (3.27):

$$\sum_{k=1}^{N} (M_{x_{\text{global}}})_k = 0 \tag{3.28a}$$

$$\sum_{k=1}^{N} (M_{z_{\text{global}}})_k = 0 \tag{3.28b}$$

$$\sum_{k=1}^{N} (M_{n(2)})_k = \sum_{k=1}^{N} (M_{n(4)})_k = 0 \tag{3.28c}$$

$$(F_{s(1)})_i - (F_{s(3)})_{i+1} = 0$$

$$(3.28d)$$

$$(\ i : \text{Natural number}, 1 \le i \le N\ )$$

where Eqs. (3.28a-c) express the equilibrium conditions in which all ($(M_{x_{\text{global}}})$, $(M_{z_{\text{global}}})$, $(M_{n(j_1)})$ ($j_1 = 2, 4$)) defined in N box beams participate, regardless of the number of box beams meeting at the joint, and Eq. (3.28d) represents the equilibrium condition between F_s acting on the edges of the adjacent two beams Beam i and Beam i+1 ($1 \le i \le N$). Therefore, Eq. (3.28d) consequently represents N number of equations, and Eqs. (3.28a-d) are expressed by N+3 number of equations for the case that N box beams meet at the joint. In case of $N = 2$, Eq. (3.28d) recovers Eqs. (3.27d, e).

3.3.3 Field Variables Joint Matching Conditions

Using the generalized forces equilibrium conditions defined above, let us now derive the joint matching conditions among field displacement variables ($U_y, \theta_x, \theta_z, W, \chi$). Because the field variables are the work conjugates of the generalized forces, one can associate them with the generalized forces by considering the principle of virtual work that the sum of virtual works is zero. In what follows, we will theoretically derive the matching conditions among field variables from the generalized forces equilibrium conditions.

For the derivation, the joint matching conditions among field variables of

Beam 1 and Beam 2 shown in Fig. 3.5 will be examined first by using the equilibrium conditions in Eq. (3.27) derived for two-beam joints. Then the conditions will be extended for the three or more box beams-joint structures. (In theory, the field variables matching conditions may be derived directly from Eq. (3.28), but the derivation is found to be too complex to employ.)

Referring to the two box beams-joint structure depicted in Fig. 3.5, consider $\mathbf{F}_k$ and $\mathbf{U}_k$ ($k = 1, 2$) denoting the generalized forces and field variables of Beam *k*, respectively. In terms of $\mathbf{F}_k$ and $\mathbf{U}_k$ ($k = 1, 2$), the principle of virtual work at the joint can be expressed as

$$\sum_{k=1}^{2} (\delta W'|_{\text{Beam } k}) = (\delta \mathbf{F}_1)^{\mathrm{T}} \mathbf{U}_1 + (\delta \mathbf{F}_2)^{\mathrm{T}} \mathbf{U}_2 = 0 \tag{3.29}$$

Equation (3.29) shows the sum of $(\delta W'|_{\text{Beam } k})$, which is complementary virtual work of Beam *k*, is zero [47], where $\delta \mathbf{F}_k$ refers to the admissible virtual force of Beam *k*. Because $\delta \mathbf{F}_1$ and $\delta \mathbf{F}_2$ comply with the equilibrium conditions in Eq. (3.27), $\delta \mathbf{F}_1$ and $\delta \mathbf{F}_2$ must satisfy the following relation:

$$\mathbf{M}_{\mathbf{F}_1} \cdot \delta \mathbf{F}_1 + \mathbf{M}_{\mathbf{F}_2} \cdot \delta \mathbf{F}_2 = 0 \tag{3.30a}$$

or

$$
\begin{bmatrix} 0 & \cos\phi_1 & \sin\phi_1 & 0 & 0 \\ 0 & -\sin\phi_1 & \cos\phi_1 & 0 & 0 \\ 0 & 0 & 0 & -\frac{b}{h(b+h)} & 0 \\ \frac{1}{2} & 0 & \frac{1}{b+h} & 0 & \frac{1}{2b} \\ \frac{1}{2} & 0 & -\frac{1}{b+h} & 0 & -\frac{1}{2b} \end{bmatrix} \begin{Bmatrix} \delta(F_y)_1 \\ \delta(M_x)_1 \\ \delta(M_z)_1 \\ \delta B_1 \\ \delta Q_1 \end{Bmatrix} +
$$

$$
\begin{bmatrix} 0 & \cos\phi_2 & \sin\phi_2 & 0 & 0 \\ 0 & -\sin\phi_2 & \cos\phi_2 & 0 & 0 \\ 0 & 0 & 0 & -\frac{b}{h(b+h)} & 0 \\ \frac{1}{2} & 0 & -\frac{1}{b+h} & 0 & -\frac{1}{2b} \\ \frac{1}{2} & 0 & \frac{1}{b+h} & 0 & \frac{1}{2b} \end{bmatrix} \begin{Bmatrix} \delta(F_y)_2 \\ \delta(M_x)_2 \\ \delta(M_z)_2 \\ \delta B_2 \\ \delta Q_2 \end{Bmatrix} = \begin{Bmatrix} 0 \\ 0 \\ 0 \\ 0 \\ 0 \end{Bmatrix} \tag{3.30b}
$$

where the matrices $\mathbf{M}_{\mathbf{F}_1}$ and $\mathbf{M}_{\mathbf{F}_2}$ are invertible because Eq. (3.30) represent five independent equilibrium conditions.

In order to apply the equilibrium conditions of $\delta\mathbf{F}_1$ and $\delta\mathbf{F}_2$ given in Eq. (3.30) to Eq. (3.29), let us first express $(\delta\mathbf{F}_k)^{\mathrm{T}}\mathbf{U}_k$ $(k=1,2)$ in Eq. (3.29) as, by using the matrix $\mathbf{M}_{\mathbf{F}_k}$ in Eq. (30):

$$
\begin{aligned}
\sum_{k=1}^{2}(\delta W'|_{\text{Beam } k}) &= (\delta\mathbf{F}_1)^{\mathrm{T}}(\mathbf{M}_{\mathbf{F}_1}^{\mathrm{T}}\cdot\mathbf{M}_{\mathbf{F}_1}^{-\mathrm{T}})\cdot\mathbf{U}_1 + (\delta\mathbf{F}_2)^{\mathrm{T}}(\mathbf{M}_{\mathbf{F}_2}^{\mathrm{T}}\cdot\mathbf{M}_{\mathbf{F}_2}^{-\mathrm{T}})\cdot\mathbf{U}_2 \\
&= (\mathbf{M}_{\mathbf{F}_1}\cdot\delta\mathbf{F}_1)^{\mathrm{T}}(\mathbf{M}_{\mathbf{F}_1}^{-\mathrm{T}}\cdot\mathbf{U}_1) + (\mathbf{M}_{\mathbf{F}_2}\cdot\delta\mathbf{F}_2)^{\mathrm{T}}(\mathbf{M}_{\mathbf{F}_2}^{-\mathrm{T}}\cdot\mathbf{U}_2) = 0
\end{aligned} \tag{3.31}
$$

According to Eq. (3.30), the relation between ($\mathbf{M}_{\mathbf{F}_1}\cdot\delta\mathbf{F}_1$) and ($\mathbf{M}_{\mathbf{F}_2}\cdot\delta\mathbf{F}_2$) in Eq. (3.31) is expressed as $(\mathbf{M}_{\mathbf{F}_2}\cdot\delta\mathbf{F}_2) = -(\mathbf{M}_{\mathbf{F}_1}\cdot\delta\mathbf{F}_1)$. Thus, applying this relation to Eq. (3.31) yields

$$
\begin{aligned}
\sum_{k=1}^{2}(\delta W'|_{\text{Beam } k}) &= (\mathbf{M}_{\mathbf{F}_1}\cdot\delta\mathbf{F}_1)^{\mathrm{T}}(\mathbf{M}_{\mathbf{F}_1}^{-\mathrm{T}}\cdot\mathbf{U}_1 - \mathbf{M}_{\mathbf{F}_2}^{-\mathrm{T}}\cdot\mathbf{U}_2) \\
&= (\delta\mathbf{F}_1)^{\mathrm{T}}\{\mathbf{M}_{\mathbf{F}_1}^{\mathrm{T}}\cdot(\mathbf{M}_{\mathbf{F}_1}^{-\mathrm{T}}\cdot\mathbf{U}_1 - \mathbf{M}_{\mathbf{F}_2}^{-\mathrm{T}}\cdot\mathbf{U}_2)\} = 0
\end{aligned} \tag{3.32}
$$

Because Eq. (3.32) should be satisfied for arbitrary $\delta\mathbf{F}_1$, it can be found that $\{\mathbf{M}_{\mathbf{F}_1}^{\mathrm{T}} \cdot (\mathbf{M}_{\mathbf{F}_1}^{-\mathrm{T}} \cdot \mathbf{U}_1 - \mathbf{M}_{\mathbf{F}_2}^{-\mathrm{T}} \cdot \mathbf{U}_2)\}$ in Eq. (3.32) should be zero. Note that the matrix $\mathbf{M}_{\mathbf{F}_1}^{\mathrm{T}}$ is invertible as mentioned above. Therefore, the following relation must hold:

$$\mathbf{M}_{\mathbf{F}_1}^{-\mathrm{T}} \cdot \mathbf{U}_1 = \mathbf{M}_{\mathbf{F}_2}^{-\mathrm{T}} \cdot \mathbf{U}_2 \tag{3.33}$$

Equation (3.33) represents the matching conditions to be met among the field variables when the equilibrium conditions in Eq. (3.27) are satisfied at the joint in Fig. 3.5. Based on the definitions of $\mathbf{M}_{\mathbf{F}_1}$ and $\mathbf{M}_{\mathbf{F}_2}$ in Eq. (3.30), Eq. (3.33) can be explicitly written as

$$(\Theta_x)_1 \cos\phi_1 + (\Theta_z)_1 \sin\phi_1 = (\Theta_x)_2 \cos\phi_2 + (\Theta_z)_2 \sin\phi_2 \tag{3.34a}$$

$$-(\Theta_x)_1 \sin\phi_1 + (\Theta_z)_1 \cos\phi_1 = -(\Theta_x)_2 \sin\phi_2 + (\Theta_z)_2 \cos\phi_2 \tag{3.34b}$$

$$(\Theta_{n(j_1)})_1 = (\Theta_{n(j_1)})_2 \qquad (j_1 = 2,\ 4) \tag{3.34c}$$

$$(U_{s(1)})_1 = -(U_{s(3)})_2 \tag{3.34d}$$

$$-(U_{s(3)})_1 = (U_{s(1)})_2 \tag{3.34e}$$

where Θ_x, Θ_z, $\Theta_{n(2)}$, $\Theta_{n(2)}$, $U_{s(1)}$, and $U_{s(3)}$ are defined as

$$\Theta_x = \theta_x;\quad \Theta_z = \theta_z - \frac{2b}{b+h}\chi \tag{3.35a, b}$$

$$\Theta_{n(2)} = \Theta_{n(4)} = -\frac{h(b+h)}{b}W \tag{3.35c, d}$$

$$U_{s(1)} = U_y + b\chi;\quad U_{s(3)} = -U_y + b\chi \tag{3.35e, f}$$

Although the expressions in Eq. (3.34) look different from the matching

conditions in Eq. (3.6) that Choi et al. [42] proposed, Eq. (3.34) represents the same relations among the field variables as those in Eq. (3.6); Eq. (3.6) can be derived directly from Eq. (3.34). While Eq. (3.6) was derived by taking directly into account the various conditions for the displacements, Eq. (3.34) derived in this study is obtained from the generalized forces equilibrium conditions and the principle of virtual work. The advantage of using Eq. (3.34) over Eq. (3.6) is that the specific formula by Eq. (3.34) can be directly extended to the case of three or more box beams-joint structures.

In order to extend the results in Eq. (3.34) for the joint where three or more box beams meet, the meaning of the matching conditions in Eq. (3.34) should be understood. Equations (3.34a, b) represent the continuity conditions among the work conjugates of the resultant moments considered in the equilibrium conditions in Eq. (3.27a, b). Therefore, $(\Theta_x)_k$ and $(\Theta_z)_k$ $(k = 1, 2)$ in Eqs. (3.34a, b) will be called the sectional effective rotation of Beam *k* at the joint in the x_k direction and in the z_k direction respectively, as depicted in Fig. 3.8(a, b). Based on this observation, it can be found that Eq. (3.34a) represents the continuity condition between $(\Theta_{x_{\text{global}}})_k = (\Theta_x)_k \cos\phi_k + (\Theta_z)_k \sin\phi_k$ ($k = 1, 2$), which denotes the sectional effective rotation of Beam *k* in the x_{global} direction. Likewise, Eq. (3.34b) represents the continuity condition between $(\Theta_{z_{\text{global}}})_k = -(\Theta_x)_k \sin\phi_k + (\Theta_z)_k$ $\cos\phi_k$

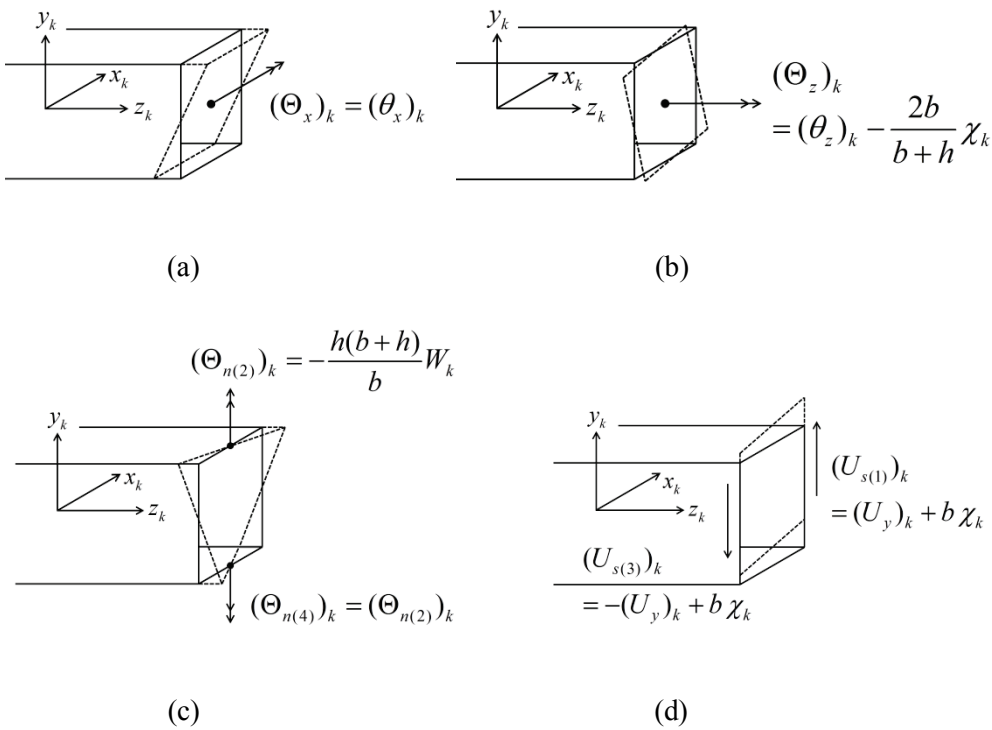

Fig. 3.8 Sectional displacements or edge displacements of Beam k (k=1, 2, …, N) associated with the generalized displacements (or field variables) joint matching conditions: (a) sectional effective rotation $(\Theta_x)_k$ in the x_k direction, (b) sectional effective rotation $(\Theta_z)_k$ in the z_k direction, (c) edge rotation $(\Theta_{n(2)})_k$ of Edge 2 in the y_k direction and edge rotation $(\Theta_{n(4)})_k$ of Edge 4 in the $-y_k$ direction, (d) edge displacement $(U_{s(1)})_k$ of Edge 1 in the y_k direction and edge displacement $(U_{s(3)})_k$ of Edge 3 in the $-y_k$ direction

$(k = 1, 2)$, which denotes the sectional effective rotation of Beam k in the z_{global} direction.

On the other hand, Eq. (3.34c) corresponds to the continuity condition between the work conjugates of the normal moments $M_{n(j_1)}$ $(j_1 = 2, 4)$ shown in Eq.

(3.27c). Therefore, Eq. (3.34c) is a statement of the continuity condition between $(\Theta_{n(j_1)})_k$ $(k=1, 2)$ which are the rotations of Edge j_1 of Beam k in the normal direction as depicted in Fig. 3.8(c).

Lastly, Eqs. (3.34d, e) represent the continuity conditions between the work conjugates of the tangential forces $F_{s(j_2)}$ $(j_2=1, 3)$ shown in Eqs. (3.27d, e). Therefore, $(U_{s(1)})_k$ and $(U_{s(3)})_k$ ($k=1, 2$) in Eqs. (3.34d, e) denote the displacements of Edge 1 and Edge 3, respectively, in the tangential direction as depicted in Fig. 3.8(d). Because the positive tangential directions of Edge 1 and Edge 3 are along $+y_k=+y_{\text{global}}$ and $-y_k=-y_{\text{global}}$, respectively (see Fig. 3.2), care should be taken over the sign. Thus, it can be found that Eq. (3.34d, e) express the continuity conditions with respect to the y_{global} axis.

Let us now derive the desired joint matching conditions at the joint where N ($N \geq 3$) box beams are connected, as shown in Fig. 3.2. As argued in the derivation of the generalized forces equilibrium conditions at the joint, Edge j_1 ($j_1=2, 4$) of Beam k ($k=1, 2, \cdots, N$) all meet each other at the joint, so continuity among $(\Theta_{n(j_1)})_k$ $(k=1, 2, \cdots, N)$ can be considered. The continuity conditions between $(U_{s(1)})_k$ and $(U_{s(3)})_{k+3}$ can also be considered because Edge 1 of Beam k ($k=1, 2, \cdots, N$) and Edge 3 of Beam k+1 (Beam N+1 refers to Beam 1) are regarded as being connected rigidly.

Using the edge connectivities just explained above and generalizing the

displacement continuity conditions (34) for $N = 2$ to the case of $N \geq 3$, the following relations can be obtained:

$$(\Theta_{x_{\text{global}}})_1 = (\Theta_{x_{\text{global}}})_2 = \cdots = (\Theta_{x_{\text{global}}})_N \tag{3.36a}$$

$$(\Theta_{z_{\text{global}}})_1 = (\Theta_{z_{\text{global}}})_2 = \cdots = (\Theta_{z_{\text{global}}})_N \tag{3.36b}$$

$$(\Theta_{n(j_1)})_1 = (\Theta_{n(j_1)})_2 = \cdots = (\Theta_{n(j_1)})_N \qquad (j_1 = 2, 4) \tag{3.36c}$$

$$(U_{s(1)})_k = -(U_{s(3)})_{k+1} \qquad (1 \leq k \leq N) \tag{3.36d}$$

Equations (3.36a, b) represent the continuity conditions for the sectional effective rotations of N box beams in the x_{global} direction and in the z_{global} direction, respectively. Equation (3.36c) is the continuity condition for the edge rotations in the normal direction on Edge j_1 ($j_1 = 2, 4$) of N box beams. On the other hand, Eq. (3.36d) is the continuity condition between the edge displacements in the y_{global} direction on Edge 1 of Beam k and Edge 3 of Beam k+1 ($1 \leq k \leq N$). Therefore, the independent number of equations from Eq. (36) becomes $3 \times (N-1) + N = 4N - 3$. The consistency between the force equilibrium equations, Eqs. (3.28a-d) and the displacement continuity equations, Eqs. (3.36a-d) at the joint is demonstrated in Appendix B.

3.4 Numerical Analysis

For the N ($N \geq 3$) box beams-joint structure under out-of-plane bending or torsion, the numerical method to analyze the response of the structure using the higher-

order beam theory and the exact matching conditions given in Eq. (3.36) will now be introduced. Then, some numerical examples will be analyzed by using the proposed analysis method. By comparing the present results with those obtained by ABAQUS shell analyses or by Timoshenko beam analyses, the validity and accuracy of the proposed method will be demonstrated.

3.4.1 Finite Element Equations

The finite element equations for Beam k ($k = 1, 2, \cdots, N$) among N box beams connected at the joint will be presented by using the stiffness matrix for the box beam element given in Appendix C. The stiffness matrix for the beam element can be derived on the basis of Refs. [6, 26], and piecewise linear interpolation will be employed to interpolate displacement variables (see Appendix C). The resulting finite element equation becomes

$$\mathbf{K}_k \cdot \mathbf{d}_k = \mathbf{f}_k \tag{3.37}$$

where $\mathbf{K}_k$, $\mathbf{d}_k$, and $\mathbf{f}_k$ in Eq. (3.37) refer to the stiffness matrix, the nodal displacement vector, and the nodal force vector for Beam k, respectively. Assembling all finite element equations for N box beams in numerical order, the finite element equations for the N box beams-joint structure can be determined:

$$\mathbf{K}_{\text{total}} \cdot \mathbf{d}_{\text{total}} = \mathbf{f}_{\text{total}} \tag{3.38}$$

If n number of nodes are used to model the N box beams-joint structure, $\mathbf{K}_{\text{total}}$, $\mathbf{d}_{\text{total}}$, and $\mathbf{f}_{\text{total}}$ in Eq. (3.38) denote $5n \times 5n$ total stiffness matrix, $5n \times 1$

total nodal displacement vector, and $5n \times 1$ total nodal force vector, respectively. The next step is to impose the matching conditions for nodal displacements of N box beams at the joint.

The proposed exact matching conditions of Eq. (3.36) can be applied to the finite element equations by using the method of Lagrange multipliers [48], an optimization method to find the maximum or minimum value of a function subject to equality constraints. Associated with this study, a problem to minimize the total potential energy of the N box beams-joint structure subject to the joint matching conditions in Eq. (3.36) is solved by employing the method of Lagrange multipliers.

To facilitate subsequent analysis, the matching conditions in Eq. (3.36) are expressed as equality constraints for $\mathbf{d}_{\text{total}}$ as

$$\mathbf{S} \cdot \mathbf{d}_{\text{total}} = \mathbf{0} \tag{3.39}$$

where $\mathbf{S}$ is a $(4N-3) \times (5n)$ matrix and Eq. (3.39) yields $(4N-3)$ independent equations. By introducing the Lagrange multiplier $\boldsymbol{\lambda}$, the following Lagrangian $\boldsymbol{\Pi}_L$ can be defined:

$$\boldsymbol{\Pi}_L(\mathbf{d}_{total}, \boldsymbol{\lambda}) = \frac{1}{2}\mathbf{d}_{\text{total}}^{\text{T}}\mathbf{K}_{\text{total}}\mathbf{d}_{\text{total}} - \mathbf{d}_{\text{total}}^{\text{T}}\mathbf{f}_{\text{total}} + \boldsymbol{\lambda}^{\text{T}}(\mathbf{S} \cdot \mathbf{d}_{\text{total}}) \tag{3.40}$$

According to the method of Lagrange multipliers, the stationary conditions of $\boldsymbol{\Pi}_L$ yields

$$\frac{\partial \boldsymbol{\Pi}_L}{\partial \mathbf{d}_{\text{total}}} = 0; \ \mathbf{K}_{\text{total}}\mathbf{d}_{\text{total}} - \mathbf{f}_{\text{total}} + \boldsymbol{\lambda}^{\text{T}}\mathbf{S} = \mathbf{0} \tag{3.41a}$$

$$\frac{\partial \mathbf{\Pi}_L}{\partial \boldsymbol{\lambda}} = 0; \ \mathbf{S} \cdot \mathbf{d}_{\text{total}} = \mathbf{0} \tag{3.41b}$$

The nodal displacement vector in Eqs. (3.41a, b), $\mathbf{d}_{\text{total}}$, satisfies the matching conditions in Eq. (3.36) and minimizes the potential energy of the *N* box beams-joint structure. Therefore, Eqs. (3.41a, b) represent the finite element equations for the *N* box beams-joint structure that include the matching conditions in Eq. (3.36). Finally, Eqs. (3.41a, b) can be expressed as a matrix equation as

$$\begin{bmatrix} \mathbf{k}_{\text{total}} & \mathbf{S}^{\text{T}} \\ \mathbf{S} & \mathbf{0} \end{bmatrix} \begin{Bmatrix} \mathbf{d}_{\text{total}} \\ \boldsymbol{\lambda} \end{Bmatrix} = \begin{Bmatrix} \mathbf{f}_{\text{total}} \\ \mathbf{0} \end{Bmatrix} \tag{3.42}$$

If proper boundary and loading conditions are prescribed, $\mathbf{d}_{\text{total}}$ (and $\boldsymbol{\lambda}$) can be determined from Eq. (3.42). Because the solution procedure is a standard one, no further discussion on numerical analysis will be necessary.

3.4.2 Numerical Examples

Several examples will be analyzed by using the finite element equations given in Eq. (3.42). The validity of the proposed approach will be demonstrated by comparing the results with those obtained from ABAQUS shell elements or Timoshenko beam elements. Because the joint flexibility is highly dependent upon the number of box beams connected at the joint, the joint angles among those beams, and the width and height (or aspect ratio) of the box beam cross-section, we will examine their effects on the solutions or the mechanical behavior of three or more box beams-joint structures.

Although box beam sections of different widths b and heights h are considered within a range $50\,\text{mm} \le b,\ h \le 200\,\text{mm}$, converged analysis results can be obtained with 40 beam elements regardless of those changes. Meanwhile, in two-dimensional ABAQUS shell analysis, $12.5\,\text{mm} \times 12.5\,\text{mm}$ square shell elements are mainly used to obtain converged analysis results. For example, if the dimensions of each box beam are width $b = 50\,\text{mm}$, height $h = 100\,\text{mm}$, and length $L = 1000\,\text{mm}$, it was found that the converged results were obtained if $(4+8+4+8)\times 80 = 1920$ shell elements were used to model the box beam in consideration.

Case Study 1: T-Joint Structure. A T-joint structure as depicted in Fig. 3.9(a) is considered in the first case study. The T-joint structure is a special case of three box beams-joint structures in that the influence of the cross-sectional deformations on the behavior of the joint is significantly displayed. Therefore, it is difficult to predict the behavior of that structure correctly by a classical beam theory, and efforts to express the flexibility of the T-joint structure by introducing artificial joint elements were reported [11, 12, 16].

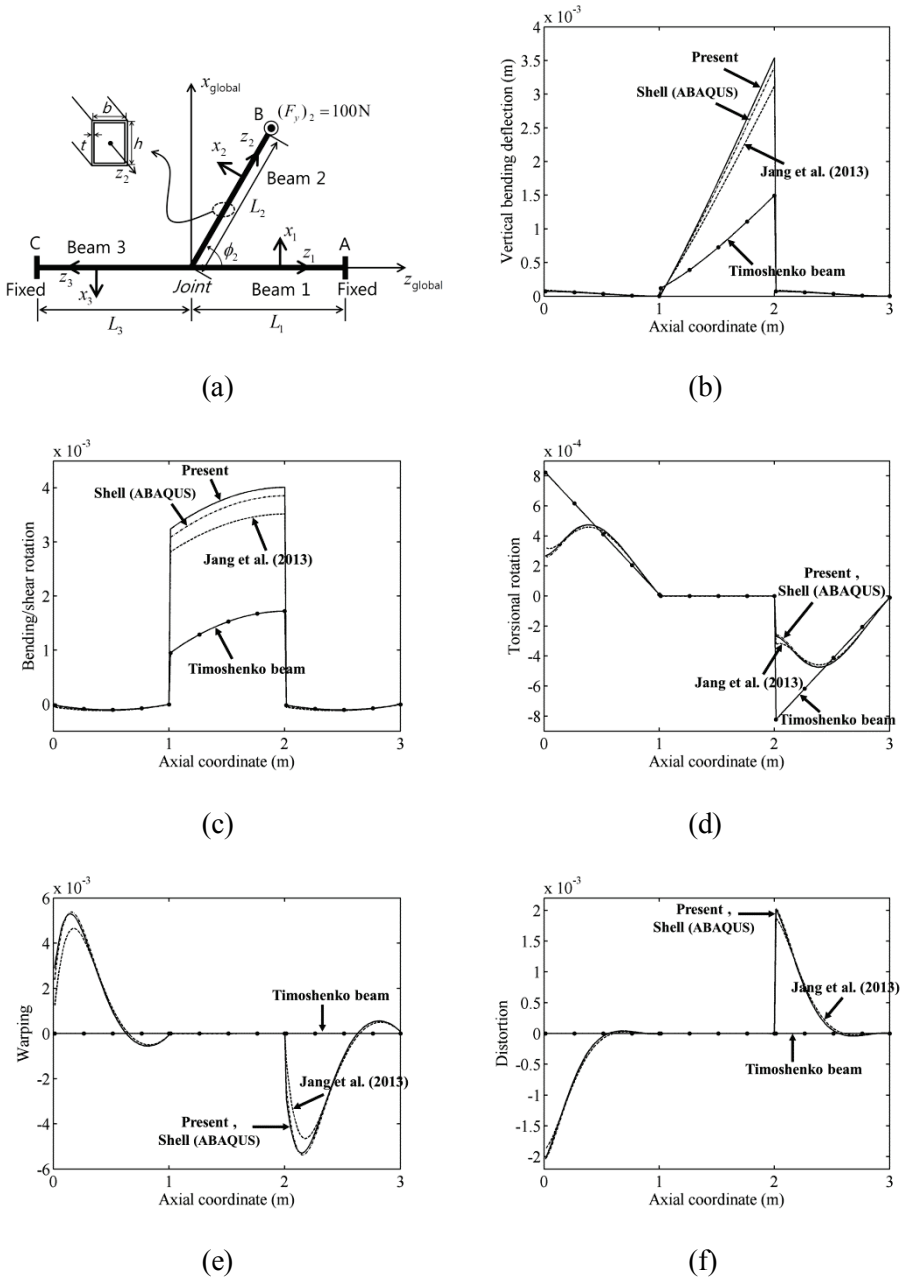

Fig. 3.9 Numerical results for the T-joint structure under vertical force F_y =100 N: (*a*) problem description (*L*=1000 mm, *b*=100 mm, *h*=50 mm, *t*=2 mm, ϕ_2= 90º), (*b*) vertical bending deflection U_y, (*c*) bending/shear rotation θ_x, (*d*) torsional rotation θ_z, (*e*) warping *W*, (*f*) distortion χ.

For the first example, the T-joint problem introduced in Jang et al. [43] is used. Beam 1 and Beam 3 are placed parallel to z_{global}, and the joint angle of Beam 2, ϕ_2, is 90°. All the box beams that make up the T-joint structure are identical. The length of those beams is $L = 1000$ mm, and the width (b), height (h) and thickness (t) of those beams are $b = 100$ mm, $h = 50$ mm, and $t = 2$ mm, respectively. The material properties of those beams are Young's modulus $E = 200$ Gpa and Poisson's ratio $\nu = 0.3$. The ends of Beam 1 and Beam 3 denoted by A and C are fixed, and the end of Beam 2 denoted by B is subjected to a vertical force $(F_y)_2 = 100$ N. The loaded end B is assumed to be rigid.

The results are given in Figs. 3.9(b-f) (the results include those by the approach in Jang et al. [43]). In the plot, the range of the axial coordinates, ($k-1, k$; $k = 1, 2, 3$), corresponds to Beam k. Observing the results based on those from the shell analysis, one can find that the analysis using the Timoshenko beam theory overestimates the stiffness of the T-joint structure, as mentioned in Introduction. In contrast, one can find that the approaches from this study or from Jang et al. [43] provide more precise results because the influence of the cross-sectional deformations are considered in those approaches. Especially, it can be seen that the approach proposed in this study, which employs the theoretically derived joint matching conditions, can predict the behavior of the T-joint structure as accurately as predicted by the shell analysis.

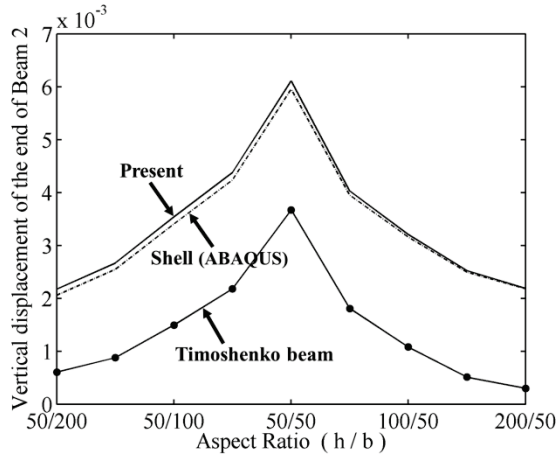

(a)

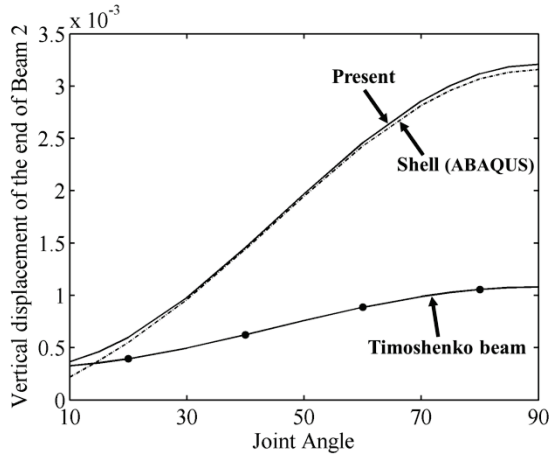

(b)

Fig. 3.10 (*a*) Numerical results for the T-joint structures shown in Fig. 9(a) with various widths (*b*) and heights (*h*) of the cross-section (or aspect ratios *h*/*b*) raging from *b*=200 mm, *h*=50 mm (*h*/*b*=50/200) to *b*=50 mm, *h*=200 mm (*h*/*b*=200/50), (*b*) numerical results for the T-joint structures shown in Fig. 9(a) with various joint angles ϕ_2 of Beam 2 ranging $10^o \leq \phi_2 \leq 90^o$.

Next, we check whether or not accurate results can still be provided by the

proposed approach when either b or h of the cross-section or ϕ_2 (which is the joint angle of Beam 2) is changed for the T-joint structure given in Fig. 3.9(a). Problems defined by changing b and h of the previous T-joint problem in a range from $b = 200\,\text{mm}, h = 50\,\text{mm}$ $(h/b = 50/200)$ to $b = 50\,\text{mm}, h = 200\,\text{mm}$ $(h/b = 200/50)$ are first solved, and the results are given in Fig. 3.10(a). The graph in Fig. 3.10(a) represents the variation in the vertical bending deflection $(U_y)_2$ of the end B when the aspect ratio (h/b) of the cross-section is varied. From the results, it can be found that the proposed approach can provide accurate results for the box beams-joint structures with sections of various widths or heights.

Problems defined from the first T-joint example by replacing b and h of the section as $b = 50\,\text{mm}, h = 100\,\text{mm}$ and changing ϕ_2 in a range from 10° to 90° are also solved, and the results are given in Fig. 3.10(b). The graph in Fig. 3.10(b) represents the variation in the vertical bending deflection $(U_y)_2$ of the end B when ϕ_2 is increased. From the results, it can be found that the proposed approach can also provide accurate and reliable results for the box beams-joint structure with various joint angles.

Case Study 2: N Thin-Walled Box Beams-Joint Structure. Box beams-joint structures involving several box beams are considered; see Fig. 3.11(a). To date, a beam theory-based analysis method applicable to complex box beams-joint structures, such as the one shown in Fig. 3.11(a), has not been proposed.

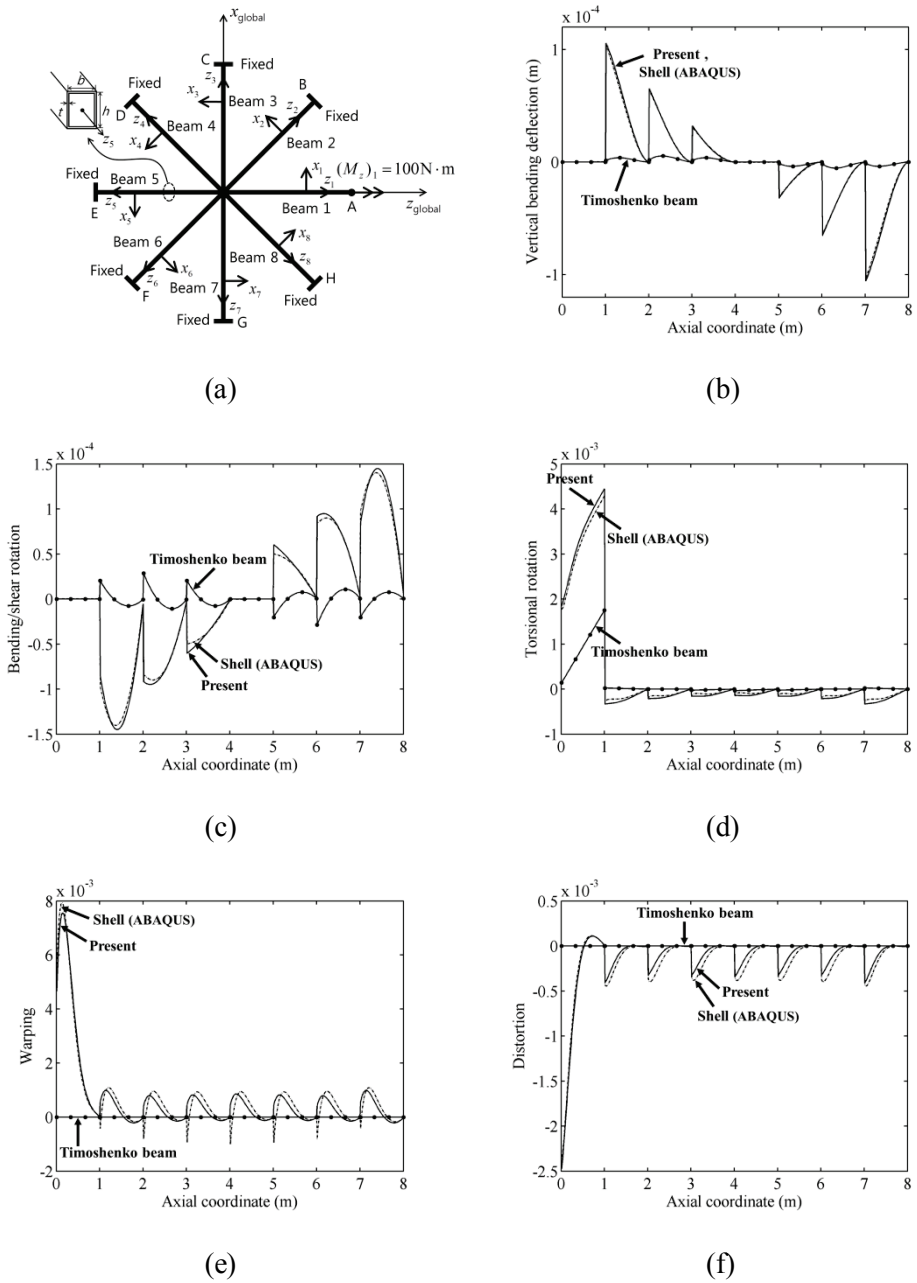

Fig. Numerical results for the eight box beams-joint structure under torsional moment M_z =100 N·m: (*a*) problem description (*L*=1000 mm, *b*=100 mm, *h*=50 mm, *t*=2 mm, ϕ_k= 45º (*k*=1, 2, …, 8)), (*b*) vertical bending deflecttion U_y. (*c*) bending/shear rotation θ_x, (*d*) torsional rotation θ_z, (*e*) warping *W*, (*f*) distortion χ.

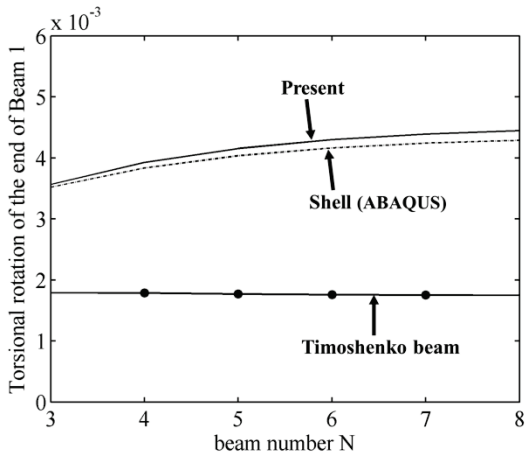

Fig. 3.11 Numerical results for the box beams-joint structures with various numbers of box beams (N) ranging $3 \leq N \leq 8$.

The joint angle of Beam k ($k = 1, 2, \cdots, 8$) in the beams-joint structure of Fig. 3.11(a) is $\phi_k = (\frac{360}{8}) \times (k-1)$, so the angle between two adjacent beams is uniformly 45°. All box beams constituting the structure are identical. The length of those beams is $L = 1000$ mm, and the dimensions of the beam cross-sections are $b = 100$ mm, $h = 50$ mm, and $t = 2$ mm, respectively. The material properties of those beams are Young's modulus $E = 200$ Gpa and Poisson's ratio $\nu = 0.3$. The end of Beam 1 denoted by A is subjected to a twisting moment $(M_z)_1 = 100\ \mathrm{N \cdot m}$, and is assumed to be rigid. The ends of the other box beams (B-H) are all fixed.

The results are given in Figs. 3.11(b-f). As in Fig. 3.9, the range of the axial coordinates, ($k-1, k$; $k = 1, 2, \cdots, 8$), corresponds to Beam k. Examing the results

on the basis of those from the shell analysis, the analysis using the Timoshenko beam theory highly overestimates the stiffness of the structure, as observed in the previous result. However, the proposed method can predict the response of the structure almost as accurately as those from the shell analysis, even though the number of box beams connected at the joint is significantly increased.

We now investigate if accurate results can be still obtained by the proposed method when the number of box beams connected at the joint is changed. To do this, problems that are defined based on the first example in Case study 2 are varied by changing the number of box beams connected at the joint, i.e. N is in a range $3 \le N \le 8$. The joint angle of Beam k ($k = 1, 2, \cdots, N$) is $\phi_k = (\frac{360}{N}) \times (k-1)$, and the angle between the two adjacent beams is uniformly $(\frac{360}{N})^\circ$.

The results are given in Fig. 3.12. The graph in Fig. 3.12 represents the variation of torsional rotation $(\theta_z)_1$ at the end A of Beam 1 when N is increased. From the results, it can be found that the proposed approach can provide accurate results for a box beams-joint structure composed of various numbers of box beams. Lastly, the problem with more complicated boundary conditions as depicted in Fig. 3.13(a) is considered; the structure shown in Fig. 3.13(a) is equal to the structure in the first example of case study 2. Observing the result given in Figs. 3.13(b-f), it can be found that the proposed approach can provide the correct result even where complicated boundary conditions are considered.

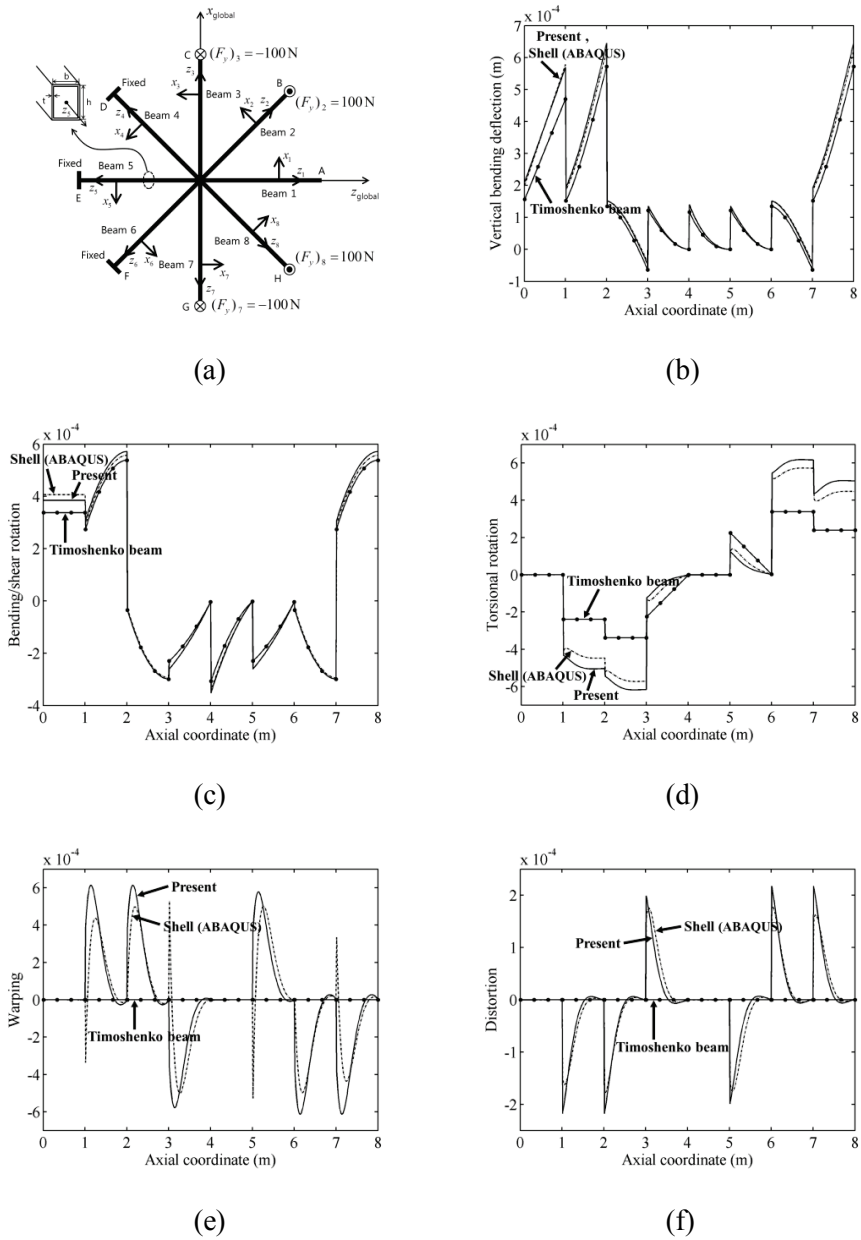

Figure 3.13 Numerical results for the eight box beams-joint structure with more complicated boundary conditions: (*a*) problem description (L=1000 mm, b=100 mm, h=50 mm, t=2 mm, ϕ_k= 45º (k=1, 2, …, 8)), (*b*) vertical bending deflecttion U_y, (*c*) bending/shear rotation θ_x, (*d*) torsional rotation θ_z, (*e*) warping W, (*f*) distortion χ.

3.5 Conclusions

When a three or more box beams-joint structure is subjected to out-of-plane bending or torsion, an analysis method based on the one-dimensional beam theory that is capable of analyzing the response of the structure is established. To take into account the influence of cross-sectional deformations on the behavior of the box beams-joint structure, the one-dimensional higher-order beam theory considering the warping and distortional deformations of the section as independent degrees of freedom is employed. The key in developing the one-dimensional analysis method for the box beams-joint structures is to determine the joint matching conditions among the field variables of the higher-order beam theory in which the warping and distortional deformations are included. In order to determine the exact joint matching conditions, joint equilibrium conditions of the generalized forces that are work conjugates of the field variables were first derived. Summarizing the process briefly, the generalized forces were expressed by the sectional resultants acting on the entire cross-section or the edge resultants acting on the edge of the section. Then, joint equilibrium conditions for the sectional resultants or edge resultants were determined based on the results in Choi et al. [42], and extending those conditions, the joint equilibrium conditions for the generalized forces that can be applied to the three or more box beams-joint structures were derived. Thereafter, considering the principle of virtual work at the joint in addition to the determined joint equilibrium conditions, the joint matching conditions for the field variables that are applicable to the three or more box beams-joint structures were exactly

derived.

Several numerical examples were solved by using the method proposed in this study, and the results were compared with those obtained by ABAQUS shell elements. For those examples, it was demonstrated that the proposed method can predict the behavior of the three or more box beams-joint structures as accurately as the shell finite element method, regardless of the number of box beams connected at the joint, the joint angle among the box beams, and the width or height of the section of the box beams. Comparing with a shell based method, the proposed analysis method has advantages such as convenience for modeling, the ease of modeling changes, and significantly fast analysis. Therefore, introducing the proposed analysis method in the initial design stage of a vehicle, the initial design model of the vehicle that meets the design criteria can be determined quickly, and a better initial design model can be expected when employing an analysis method with optimization design techniques. In addition, the methodology for deriving the joint matching conditions can be expected to be an important foundation for expanding the scope of structures that can be interpreted by using the higher-order beam theory-based approach to a three-dimensional box beams-joint structure.

Appendix A

The explicit expressions of the shape functions $\psi_p^{\alpha}(s)$ ($p = n, s, z$; $\alpha = U_y, \theta_x, \theta_z, W, \chi$) that are introduced in the higher-order beam theory to describe the displacements or deformations of the cross-section are given. The shape functions $\psi_p^{\alpha}(s)$ are separately defined on each edge for convenience; $\psi_p^{\alpha}(s_j)$ ($j = 1, 2, 3, 4$) denotes the shape function defined on Edge *j*. The coordinate s_j is based on the center of Edge *j* and is measured along the contour of Edge *j*.

$$\begin{aligned}
&\psi_n^{U_y}(s_j) = 0 && \text{(for } j = 1,\ 3) \text{ and } (-1)^{(j-2)/2} \text{ (for } j = 2,\ 4) \\
&\psi_s^{U_y}(s_j) = (-1)^{(j-1)/2} && \text{(for } j = 1,\ 3) \text{ and } 0 \text{ (for } j = 2,\ 4) \\
&\psi_z^{U_y}(s_j) = 0 && \text{(for } j = 1,\ 2, 3, 4)
\end{aligned} \tag{3.A1}$$

$$\begin{aligned}
&\psi_n^{\theta_x}(s_j) = 0 && \text{(for } j = 1,\ 2, 3, 4) \\
&\psi_s^{\theta_x}(s_j) = 0 && \text{(for } j = 1,\ 2, 3, 4) \\
&\psi_z^{\theta_x}(s_j) = (-1)^{(j-1)/2} s_j && \text{(for } j = 1,\ 3) \text{ and } (-1)^{(j-2)/2}\frac{h}{2} \text{ (for } j = 2,\ 4)
\end{aligned} \tag{3.A2}$$

$$\begin{aligned}
&\psi_n^{\theta_z}(s_j) = -s_j && \text{(for } j = 1,\ 2, 3, 4) \\
&\psi_s^{\theta_z}(s_j) = \frac{b}{2} && \text{(for } j = 1,\ 3) \text{ and } \frac{h}{2} \text{ (for } j = 2,\ 4) \\
&\psi_z^{\theta_z}(s_j) = 0 && \text{(for } j = 1,\ 2, 3, 4)
\end{aligned} \tag{3.A3}$$

$$\begin{aligned}
&\psi_n^{W}(s_j) = 0 && \text{(for } j = 1,\ 2, 3, 4) \\
&\psi_s^{W}(s_j) = 0 && \text{(for } j = 1,\ 2, 3, 4) \\
&\psi_z^{W}(s_j) = \frac{b}{2} s_j && \text{(for } j = 1,\ 3) \text{ and } -\frac{h}{2} s_j \text{ (for } j = 2,\ 4)
\end{aligned} \tag{3.A4}$$

$$\psi_n^{\chi}(s_j) = -\frac{4}{h(b+h)}s_j^3 + \frac{2b+h}{b+h}s_j \quad (\text{for } j=1,\ 3)$$

$$\frac{4}{b(b+h)}s_j^3 - \frac{b+2h}{b+h}s_j \quad (\text{for } j=2,\ 4) \tag{3.A5}$$

$$\psi_s^{\chi}(s_j) = \frac{bh}{b+h} \quad (\text{for } j=1,\ 3) \quad \text{and} \quad -\frac{bh}{b+h} \quad (\text{for } j=2,\ 4)$$

$$\psi_z^{\chi}(s_j) = 0 \quad (\text{for } j=1,\ 2,\ 3,\ 4)$$

where s_j ($j=1, 2, 3, 4$) are in the range of $-\frac{h}{2} \le s_1,\ s_3 \le \frac{h}{2}$ and $-\frac{b}{2} \le s_2,\ s_4 \le \frac{b}{2}$.

One can show the following orthogonality relation between ($\psi_z^{\theta_x}$, ψ_z^{W}):

$$\iint_S \psi_z^{\theta_x}(s)\cdot\psi_z^{W}(s)\ dsdn = \sum_{j=1}^{4}\{\iint_{Edge\ j} \psi_z^{\theta_x}(s_j)\cdot\psi_z^{W}(s_j)\ dsdn\} = 0 \tag{3.A6}$$

Likewise, one can also show the orthogonality conditions among ($\psi_s^{U_y}$, $\psi_s^{\theta_z}$, ψ_s^{χ}):

$$\iint_S \psi_s^{\alpha_1}(s)\cdot\psi_s^{\alpha_2}(s)\ dsdn = \sum_{j=1}^{4}\{\iint_{Edge\ j} \psi_s^{\alpha_1}(s_j)\cdot\psi_s^{\alpha_2}(s_j)\ dsdn\} = 0$$

$$(\alpha_1 = U_y,\ \theta_z,\ \chi;\ \alpha_2 = U_y,\ \theta_z,\ \chi;\ \alpha_1 \ne \alpha_2) \tag{3.A7}$$

Appendix B

In Appendix B, it will be shown that the sum of the virtual works for N ($N \ge 3$) box beams is zero at the joint in Fig. 3.2 when both the equilibrium conditions in Eq. (3.28) and the matching conditions in Eq. (3.36) are satisfied among N box beams at the joint.

If multiplying each condition in Eq. (3.28) by the admissible virtual

displacement associated with Eq. (3.36) ($\delta\Theta_{x_{\text{global}}}, \delta\Theta_{z_{\text{global}}}, \delta\Theta_{n(j_1)}, \delta U_{s(1)}$) and adding those products, the resulting equation should be always zero regardless of the virtual displacements

$$\begin{aligned}
&\delta(\Theta_{x_{\text{global}}})_p \times \{\sum_{k=1}^{N} (M_{x_{\text{global}}})_k\} + \delta(\Theta_{z_{\text{global}}})_p \times \{\sum_{k=1}^{N} (M_{z_{\text{global}}})_k\} \\
&+ \delta(\Theta_{n(j_1)})_p \times \{\sum_{k=1}^{N} (M_{n(j_1)})_k\} \\
&+ \sum_{k=1}^{N} [\delta(U_{s(1)})_k \times \{(F_{s(1)})_k - (F_{s(3)})_{k+1}\}] = 0
\end{aligned} \tag{3.B1}$$

where $\delta(\Theta_{x_{\text{global}}})_p$, $\delta(\Theta_{z_{\text{global}}})_p$, and $\delta(\Theta_{n(j_1)})_p$ represent the virtual displacements of an arbitrary box beam, Beam p $(1 \le p \le N)$. Because the virtual displacements introduced in Eq. (3.B1) satisfy the matching conditions in Eq. (3.36), Eq. (3.B1) can be expressed as

$$\begin{aligned}
&\sum_{k=1}^{N} \delta(\Theta_{x_{\text{global}}})_k \times (M_{x_{\text{global}}})_k + \sum_{k=1}^{N} \delta(\Theta_{z_{\text{global}}})_p \times (M_{z_{\text{global}}})_k \\
&+ \sum_{k=1}^{N} \delta(\Theta_{n(j_1)})_k \times (M_{n(j_1)})_k \\
&+ \sum_{k=1}^{N} [\delta(U_{s(1)})_k \times (F_{s(1)})_k + \delta(U_{s(3)})_{k+1} \times (F_{s(3)})_{k+1}\}] = 0
\end{aligned} \tag{3.B2}$$

When $\delta(U_{s(3)})_{k+1} \times (F_{s(3)})_{k+1}$ in Eq. (3.B2) is replaced by $\delta(U_{s(3)})_k \times (F_{s(3)})_k$, Eq. (3.B2) becomes (because Beam N+1 denotes Beam 1)

$$\sum_{k=1}^{N} \delta(\Theta_{x_{\text{global}}})_k \times (M_{x_{\text{global}}})_k + \sum_{k=1}^{N} \delta(\Theta_{z_{\text{global}}})_p \times (M_{z_{\text{global}}})_k$$
$$+ \sum_{k=1}^{N} \delta(\Theta_{n(j_1)})_k \times (M_{n(j_1)})_k \tag{3.B3}$$
$$+ \sum_{k=1}^{N} [\delta(U_{s(1)})_k \times (F_{s(1)})_k + \delta(U_{s(3)})_k \times (F_{s(3)})_k \}] = 0$$

Because the virtual displacements and the generalized forces in Eq. (3.B3) are the same as the expressions in Eq. (3.34) and in Eq. (3.27), respectively, Eq. (3.B3) can be rewritten in matrix form as, by employing the matrix $\mathbf{M}_{\mathrm{F}_k}$ $(k = 1, 2, \cdots, N)$,

$$\sum_{k=1}^{N} (\mathbf{M}_{\mathrm{F}_k}^{-\mathrm{T}} \cdot \delta \mathbf{U}_k)^{\mathrm{T}} (\mathbf{M}_{\mathrm{F}_k} \cdot \mathbf{F}_k) = \sum_{k=1}^{N} (\delta \mathbf{U}_k)^{\mathrm{T}} (\mathbf{M}_{\mathrm{F}_k}^{-1} \cdot \mathbf{M}_{\mathrm{F}_k}) \cdot \mathbf{F}_k = \sum_{k=1}^{N} (\delta \mathbf{U}_k)^{\mathrm{T}} \mathbf{F}_k = 0 \tag{3.B4}$$

Consequently, it can be found from Eq. (3.B4) that the sum of $(\delta \mathbf{U}_k)^{\mathrm{T}} \mathbf{F}_k$ $(k = 1, 2, \cdots, N)$, representing the virtual work of Beam *k*, vanishes at the joint when the conditions in Eq. (3.28) and Eq. (3.36) are satisfied at the joint.

Appendix C

The total potential energy of the box beam ($z_1 < z < z_2$) can be defined as

$$\begin{aligned}
\mathbf{\Pi} &= \frac{1}{2} \int_{z_1}^{z_2} \int_S \sigma_{ij} \varepsilon_{ij} \, dA \, dz - \int_S (\sigma_{zz} \tilde{u}_z + \sigma_{zs} \tilde{u}_s)_{z_1}^{z_2} \, dA \\
&= \frac{1}{2} \int_{z_1}^{z_2} \{ E J_{M_x} (\theta_x')^2 + G J_{F_y} (U_y' + \theta_x)^2 + E_1 C_1 (\chi)^2 + E_1 J_B (W')^2 \\
&\quad + G J_{M_z} (\theta_z' + \frac{b-h}{b+h} W)^2 + G J_Q (W + \chi')^2 + G C_2 (\chi')^2 \} \, dz \\
&\quad - [F_y U_y + M_x \theta_x + M_z \theta_z + B W + Q \chi]_{z_1}^{z_2}
\end{aligned} \tag{3.C1}$$

where J_β ($\beta = F_y, M_x, M_z, B, Q$) represents the moment of inertia for the generalized force β as defined in Section 3. 1, and the expressions of $J_{F_y}, J_{M_x}, J_{M_z}, J_B, J_Q, C_1$, and C_2 in Eq. (3.C1) are given by

$$
\begin{aligned}
&J_{F_y} = \iint_S (\psi_s^{U_y})^2\, dsdn = 2ht, \qquad J_{M_x} = \iint_S (\psi_z^{\theta_x})^2\, dsdn = \frac{h^2 t(3b+h)}{6}, \\
&J_{M_z} = \iint_S (\psi_s^{\theta_z})^2\, dsdn = \frac{bht(b+h)}{2}, \quad J_B = \iint_S (\psi_z^{W})^2\, dsdn = \frac{b^2h^2t(b+h)}{24}, \\
&J_Q = \iint_S (\psi_s^{\chi})^2\, dsdn = \frac{2b^2h^2t}{b+h}, \qquad C_1 = \iint_S (n\cdot\ddot{\psi}_n^{\chi})^2\, dsdn = \frac{8t^3}{b+h} \\
&C_2 = \iint_S (2n\cdot\dot{\psi}_n^{\chi})^2\, dsdn = \frac{2t^3(b^2+4bh+h^2)}{15(b+h)}
\end{aligned}
\tag{3.C2}
$$

According to Refs. [6, 26], the field variables $\mathbf{U}(z)$ of the one-dimensional box beam finite element ($z_1 < z < z_2$) can be expressed in terms of the nodal displacement vector $\mathbf{d}$ and the linear shape function $\mathbf{N}$ (ξ is a nondimensional coordinate in axial direction, and $-1 \le \xi \le 1$ in the box beam element).

$$\mathbf{U}(z) = \mathbf{N}\cdot\mathbf{d};$$

$$
\begin{Bmatrix} U_y(z) \\ \theta_x(z) \\ \theta_z(z) \\ W(z) \\ \chi(z) \end{Bmatrix}
=
\begin{bmatrix}
\frac{1-\xi}{2} & 0 & 0 & 0 & 0 & \frac{1+\xi}{2} & 0 & 0 & 0 & 0 \\
0 & \frac{1-\xi}{2} & 0 & 0 & 0 & 0 & \frac{1+\xi}{2} & 0 & 0 & 0 \\
0 & 0 & \frac{1-\xi}{2} & 0 & 0 & 0 & 0 & \frac{1+\xi}{2} & 0 & 0 \\
0 & 0 & 0 & \frac{1-\xi}{2} & 0 & 0 & 0 & 0 & \frac{1+\xi}{2} & 0 \\
0 & 0 & 0 & 0 & \frac{1-\xi}{2} & 0 & 0 & 0 & 0 & \frac{1+\xi}{2}
\end{bmatrix}
\begin{Bmatrix} U_y(z_1) \\ \theta_x(z_1) \\ \theta_z(z_1) \\ W(z_1) \\ \chi(z_1) \\ U_y(z_2) \\ \theta_x(z_2) \\ \theta_z(z_2) \\ W(z_2) \\ \chi(z_2) \end{Bmatrix}
$$

(3.C3)

Deriving the one-dimensional finite element equation for the box beam element by applying the principle of minimum total potential energy, the resulting matrix equation is of the following form:

$$\mathbf{f} = \mathbf{K} \cdot \mathbf{d} \tag{3.C4}$$

where $\mathbf{f}$ refers to the nodal force vector, as follows.

$$\mathbf{f} = \{F_y(z_1),\ M_x(z_1),\ M_z(z_1),\ B(z_1),\ Q(z_1),\ F_y(z_2),\ M_x(z_2),\ M_z(z_2),\ B(z_2),\ Q(z_2)\}^{\mathrm{T}}$$

(3.C5)

The stiffness matrix $\mathbf{K}$ defined from the procedure above is as:

$$\mathbf{K} = \begin{bmatrix} \mathbf{K}_{11} & \mathbf{K}_{12} \\ sym & \mathbf{K}_{22} \end{bmatrix} \tag{3.C6}$$

where the definitions of submatrix $\mathbf{K}_{11}$, $\mathbf{K}_{12}$ and $\mathbf{K}_{22}$ are as

$$\mathbf{K}_{11} = \begin{bmatrix} \frac{GJ_{F_y}}{l} & -\frac{GJ_{F_y}}{2} & 0 & 0 & 0 \\ & \frac{GlJ_{F_y}}{3} + \frac{EJ_{M_x}}{l} & 0 & 0 & 0 \\ & & \frac{GJ_{M_z}}{l} & -\frac{(b-h)GJ_{M_z}}{2(b+h)} & 0 \\ \text{sym} & & & \frac{(b-h)^2 GlJ_{M_z}}{3(b+h)^2} + \frac{GlJ_Q}{3} + \frac{E_1 J_B}{l} & -\frac{GJ_Q}{2} \\ & & & & \frac{E_1 lC_1}{3} + \frac{G(J_Q + C_2)}{l} \end{bmatrix} \tag{3.C7a}$$

$$\mathbf{K}_{12} = \begin{bmatrix} -\frac{GJ_{F_y}}{l} & -\frac{GJ_{F_y}}{2} & 0 & 0 & 0 \\ \frac{GJ_{F_y}}{2} & \frac{GlJ_{F_y}}{6} - \frac{EJ_{M_x}}{l} & 0 & 0 & 0 \\ 0 & 0 & -\frac{GJ_{M_z}}{l} & -\frac{(b-h)GJ_{M_z}}{2(b+h)} & 0 \\ 0 & 0 & & \frac{(b-h)^2 GlJ_{M_z}}{6(b+h)^2} + \frac{GlJ_Q}{6} - \frac{E_1 J_B}{l} & \frac{GJ_Q}{2} \\ 0 & 0 & & -\frac{GJ_Q}{2} & \frac{E_1 lC_1}{6} - \frac{G(J_Q + C_2)}{l} \end{bmatrix} \tag{3.C7b}$$

$$\mathbf{K}_{22} = \begin{bmatrix} \frac{GJ_{F_y}}{l} & \frac{GJ_{F_y}}{2} & 0 & 0 & 0 \\ & \frac{GlJ_{F_y}}{3} + \frac{EJ_{M_x}}{l} & 0 & 0 & 0 \\ & & \frac{GJ_{M_z}}{l} & \frac{(b-h)GJ_{M_z}}{2(b+h)} & 0 \\ \text{sym} & & & \frac{(b-h)^2 GlJ_{M_z}}{3(b+h)^2} + \frac{GlJ_Q}{3} + \frac{E_1 J_B}{l} & \frac{GJ_Q}{2} \\ & & & & \frac{E_1 lC_1}{3} + \frac{G(J_Q + C_2)}{l} \end{bmatrix} \quad (3.C7c)$$

l refers to the length of the box beam element ($l = z_2 - z_1$), and $E_1 = \dfrac{E}{1-\nu^2}$.

References

[1] Gere JM, Timoshenko SP. Mechanics of materials. 4th ed. Boston: PWS Pub. Co.; 1997.

[2] Timoshenko SP, Goodier JN. Theory of elasticity. 3rd ed. New York: McGraw-Hill Pub. Co.; 1970.

[3] Vlasov VZ. Thin-walled elastic beams. Jerusalem: Israel Program for Scientific Translations; 1961.

[4] Boswell LF, Zhang SH. A box beam finite element for the elastic analysis of thin-walled structures. Thin-Walled Struct 1983;1:353-83.

[5] Boswell LF, Zhang SH. The effect of distortion in thin-walled box-spine beams. Int J Solids Struct 1984;20:845-62.

[6] Kim JH, Kim YY. Analysis of thin-walled closed beams with general quadrilateral cross sections. J Appl Mech-Trans ASME 1999;66:904-12.

[7] Gonçalves R, Dinis PB, Camotim D. GBT formulation to analyse the first-order and buckling behaviour of thin-walled members with arbitrary cross-sections. Thin-Walled Struct 2009;47:583-600.

[8] Genoese A, Genoese A, Bilotta A, Garcea G. A mixed beam model with non-uniform warpings derived from the Saint Venànt rod. Comput Struct 2013;121:87-98.

[9] Ferradi MK, Cespedes X. A new beam element with transversal and warping eigenmodes. Comput Struct 2014;131:12-33.

[10] Vieira RF, Virtuoso FBE, Pereira EBR. A higher order beam model for thin-walled structures with in-plane rigid cross-sections. Eng Struct 2015;84:1-18.

[11] El-Sayed MEM. Calculation of joint spring rates using finite element formulation. Comput Struct 1989;33:977-81.

[12] Lee K, Nikolaidis E. A two-dimensional model for joints in vehicle structures. Comput Struct 1992;45:775-84.
[13] Al-Bermani FGA, Li B, Zhu K, Kitipornchai S. Cyclic and seismic response of flexibly jointed frames. Eng Struct 1994;16:249-55.
[14] Becker PJW, Wynn Jr RH, Berger EJ, Blough JR. Using rigid-body dynamics to measure joint stiffness. Mech Syst Signal Proc 1999;13:789-801.
[15] Donders S, Takahashi Y, Hadjit R, Van Langenhove T, Brughmans M, Van Genechten B et al. A reduced beam and joint concept modeling approach to optimize global vehicle body dynamics. Finite Elem Anal Des 2009;45:439-55.
[16] De Gaetano G, Mundo D, Cosco FI, Maletta C, Donders S. Concept Modelling of Vehicle Joints and Beam-Like Structures through Dynamic FE-Based Methods. Shock Vib 2014;2014:9. http://dx.doi.org/10.1155/2014/303567.
[17] Bauchau OA. A beam theory for anisotropic materials. J Appl Mech-Trans ASME 1985;52:416-22.
[18] Petrolo AS, Casciaro R. 3D beam element based on Saint Venànt's rod theory. Comput Struct 2004;82:2471-81.
[19] Cesnik CES, Hodges DH. VABS: A New Concept for Composite Rotor Blade Cross-Sectional Modeling. J Am Helicopter Soc 1997;42:27-38.
[20] Volovoi VV, Hodges DH. Theory of anisotropic thin-walled beams. J Appl Mech-Trans ASME 2000;67:453-9.
[21] Kim J-S, Cho M, Smith EC. An asymptotic analysis of composite beams with kinematically corrected end effects. Int J Solids Struct. 2008;45:1954-77.
[22] Carrera E. Theories and finite elements for multilayered plates and shells: a unified compact formulation with numerical assessment and benchmarking. Arch Comput Method Eng 2003;10:215-96.
[23] Carrera E, Giunta G, Nali P, Petrolo M. Refined beam elements with arbitrary cross-section geometries. Comput Struct 2010;88:283-93.
[24] Schardt R. Generalized beam theory—an adequate method for coupled stability problems. Thin-Walled Struct 1994;19:161-80.
[25] Silvestre N, Camotim D. First-order generalised beam theory for arbitrary orthotropic materials. Thin-Walled Struct 2002;40:755-89.
[26] Kim YY, Kim JH. Thin-walled closed box beam element for static and dynamic analysis. Int J Numer Methods Eng 1999;45:473-90.
[27] Kim JH, Kim YY. One-dimensional analysis of thin-walled closed beams having general cross-sections. Int J Numer Methods Eng 2000;49:653-68.
[28] Kim JH, Kim YY. Thin-walled multicell beam analysis for coupled torsion, distortion, and warping deformations. J Appl Mech-Trans ASME 2001;68:260-9.
[29] Jang G-W, Kim M-J, Kim YY. Analysis of thin-walled straight beams with

generally shaped closed sections using numerically determined sectional deformation functions. J Struct Eng 2012;138:1427-35.
[30] Genoese A, Genoese A, Bilotta A, Garcea G. A geometrically exact beam model with non-uniform warping coherently derived from the Saint Venant rod. Eng Struct 2014;68:33-46.
[31] Ferradi MK, Cespedes X, Arquier M. A higher order beam finite element with warping eigenmodes. Eng Struct 2013;46:748-62.
[32] Vieira RF, Virtuoso FBE, Pereira EBR. Definition of warping modes within the context of a higher order thin-walled beam model. Comput Struct 2015;147:68-78.
[33] Vacharajittiphan P, Trahair NS. Warping and distortion at I-section joints. J Struct Div 1974;100:547-64.
[34] Baigent AH, Hancock GJ. Structural analysis of assemblages of thin-walled members. Eng Struct 1982;4:207-16.
[35] Morrell PJB, Riddington JR, Ali FA, Hamid HA. Influence of joint detail on the flexural/torsional interaction of thin-walled structures. Thin-walled struct 1996;24:97-111.
[36] Trahair NS, Bradford MA, Nethercot D, Gardner L. The behaviour and design of steel structures to EC3. 4th ed. London: Taylor and Francis; 2008.
[37] Basaglia C, Camotim D, Silvestre N. Global buckling analysis of plane and space thin-walled frames in the context of GBT. Thin-Walled Struct 2008;46:79-101.
[38] Camotim D, Basaglia C. Buckling analysis of thin-walled steel structures using generalized beam theory (GBT): state-of-the-art report. Steel Constr 2013;6:117-31.
[39] Jang G-W, Kim KJ, Kim YY. Higher-order beam analysis of box beams connected at angled joints subject to out-of-plane bending and torsion. Int J Numer Methods Eng 2008;75:1361-84.
[40] Jang G-W, Kim YY. Higher-order in-plane bending analysis of box beams connected at an angled joint considering cross-sectional bending warping and distortion. Thin-Walled Struct 2009;47:1478-89.
[41] Jang G-W, Kim YY. Vibration analysis of piecewise straight thin-walled box beams without using artificial joint springs. J Sound Vibr 2009;326:647-70.
[42] Choi S, Jang G-W, Kim YY. Exact matching condition at a joint of thin-walled box beams under out-of-plane bending and torsion. J Appl Mech-Trans ASME 2012;79:051018.
[43] Jang G-W, Choi S, Kim YY. Analysis of Three Thin-Walled Box Beams Connected at a Joint under Out-of-Plane Bending Loads. J Eng Mech 2013;139:1350-61.
[44] Hibbett HD, Karlsson BI, Sorensen EP. ABAQUS/standard: User's Manual. 1998.
[45] Reddy JN. Theory and analysis of elastic plates. Philadelphia (PA): Taylor and Francis; 1999.

[46] Choi S, Kim YY. Exact Matching at a Joint of Multiply-Connected Box Beams under Out-of-Plane Bending and Torsion. Eng Struct (under review).
[47] Bauchau OA, Craig JI. Structural analysis: with applications to aerospace structures. New York: Springer; 2009.
[48] Babuška I. The finite element method with Lagrangian multipliers. Numer Math 1973;20:179-92.

CHAPTER 4.
Higher-Order Beam Analysis for Two Box Beams-Joint Systems Subjected to In-Plane Bending and Axial Loads

4.1 Introduction

Inconsistent with the hypothesis introduced in the classical Euler and Timoshenko beam theories (see e.g. Refs [1, 2]) is the fact that cross-sectional deformations are easily found in thin-walled box beams. Thus thin-walled box beams show much more flexible behavior than the analysis results from use of the classical beam theories would suggest. Especially, when two box beams are connected at an angled joint as depicted in Fig. 4.1, highly flexible behavior is observed near the joint region [3, 4]. This is because the cross-sectional deformations of the two box beams are further amplified at the joint, and the actual behavior of the two box beams-joint system in Fig. 4.1 is considerably different from that predicted by the classical beam analysis due to joint flexibility.

Because the classical beam theories inevitably overestimate the stiffness of thin-walled box beam structures (or members), one-dimensional higher-order beam theories have been developed that include additional degrees of

freedom accounting for flexibility of thin-walled box beams caused by cross-sectional deformations [5-13]. In higher-order beam theory, however, defining matching conditions among the degrees of freedom at the joint is difficult because the cross-sectional deformations that do not produce any non-zero resultants are also considered for the matching. Moreover, the fundamental cross-sectional deformations of the box beam members that cause the flexibility of the joint are not clearly identified for the in-plane loading boundary conditions. For these reasons, no one-dimensional analysis method based on the higher-order beam theory has yet been proposed that can interpret the exact behavior of the two box beams-joint system shown in Fig. 4.1 when in-plane loads are applied. Given these circumstances, we propose a new higher-order beam analysis method that is

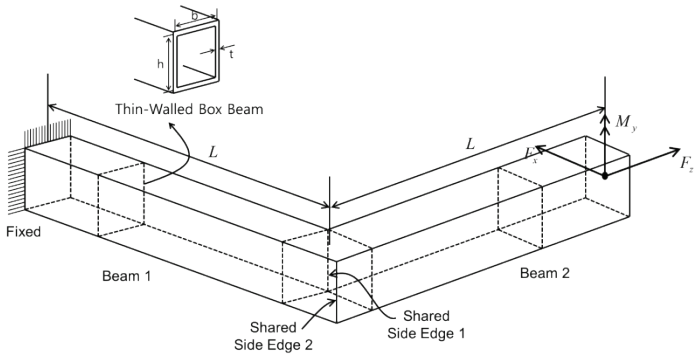

Fig. 4.1 Two thin-walled box beams-joint structure subjected to in-plane bending and tensile loads.

capable of capturing the responses of the two box beams-joint system under in-plane loads accurately.

First, let us review some previous approaches that tried to express the joint flexibility of thin-walled beam systems correctly by using the one-dimensional beam theory. Initial studies that were based on the classical beam theories regarded the connectivity among thin-walled beam members at a joint to be semi-rigid and proposed some artificial joint spring models to reflect the joint flexibility [14, 15]. Chang [14] introduced a joint model using a rotational spring to relate the in-plane bending moment with the bending rotation at the joint. Lee and Nikolaidis [15] proposed a joint model consisting of some rotational springs and a rigid section based on their assumption that the rotation center of each beam member should be located away from the joint. Meanwhile, Bylund [16] proposed a dynamic joint method which evaluates the stiffness of the joint by using eigenvalues and eigenmodes. Refs. [17, 18] suggested approaches to represent the stiffness of the joint with a super element; according to their approaches, the super element can be obtained by applying the static or dynamic reduction techniques to a joint model based on shell elements. However, because joint flexibility of a thin-walled beams-joint system is largely dependent on joint angles among beam members and the aspect ratios of beam cross-sections at

the joint, it is difficult to define an artificial joint model that would be consistently applicable to the systems of various joints.

Because a beam theory that can theoretically deal with the additional flexibility of thin-walled beam members or structures without using artificial concepts is needed for accurate, consistent analysis, higher-order beam theories that consider the cross-sectional deformations in addition to the rigid-body motions as independent degrees of freedom have been proposed. Based on the fundamental theory of thin-walled beams established by Vlasov [5], several analytic or semi-analytic methods that calculate the higher-order deformation modes of various thin-walled members have been proposed such as an approach based on Saint Venant's theory [19, 20], the variational asymptotic method [21-23], Carrera's unified formulation [24, 25], and the GBT cross-section analysis [26, 27]. Especially for thin-walled members of closed sections including thin-walled box beams, Kim and Kim [7, 28, 29] developed a higher-order beam theory (HoBT) which can interpret the responses of those beam members under a twisting moment as correctly as the shell analysis. Based on the HoBT, Kim and Kim [30] and Heo et al. [31] proposed topology and shape optimization approaches of thin-walled closed beam sections. Kim and Kim [8, 32] extended the scope of the higher-order beam analysis to thin-walled curved box beams. In

particular, they introduced a bending distortion of an hourglass shape to represent the additional flexibility that is observed in thin-walled curved box beams under in-plane loads [8]. Several higher-order beam models have been developed in recent years to analyze the stress field or nonlinear behavior of thin-walled box beam members. A mixed beam model with the independent description of stress and displacement fields was proposed by Genoese et al. [11, 33] who took into account the warping modes derived from their approach based on Saint Venant's theory. Ferradi et al. [12, 34] proposed a higher-order beam elements that incorporates distortion modes calculated by the modal analysis of beam cross-section decomposed with one-dimensional elements along with warping modes derived by their proposed equilibrium scheme. A higher-order beam model for the analysis of prismatic thin-walled members was suggested by Vieira et al. [13, 35] who considered uncoupled warping and distortion modes derived by their proposed eigenvalue problem.

As higher-order beam theories capable of capturing the flexible responses of thin-walled beam members accurately are available, efforts to theoretically represent the joint flexibility of thin-walled beam systems have been followed. Especially for the joint of thin-walled open section members, many researches defining the compatibility conditions among kinematic

variables have been proposed [36-40]. Vacharajittiphan and Trahair [36] studied the warping transmission/restraint as well as the influence of distortion on the warping transmission at the joint of two doubly symmetric I-section members. For the joint of two asymmetric open section members, Baigent and Hancock [37] derived the matching relations among the kinematic variables including warping from the equilibrium conditions determined by transforming force terms acting on the shear center and the centroid onto the member origin axes. Moreover, they suggested modeling techniques for the systems with various joint types and eccentric restraints. Based on the aforementioned results, Basaglia et al. [39] have recently derived the extended matching relations including the warping transmission for the joint of multiple open section beams. Thereafter, a Generalized Beam Theory (GBT) based one-dimensional approach for the analysis of various buckling behavior of thin-walled open section beam systems has been established by employing some additional displacement constraints at specific points of the joint Camotim and Basaglia [40].

In the case of thin-walled closed section beam systems, on the other hand, the distortional deformation, not significant in open section beams, is also responsible for flexible responses observed near joints. Thus, an investigation for the effects of distortion as well as warping on the joint

flexibility should be conducted. Moreover, the mechanical principles of the joint flexibility observed in two box beams-joint systems subjected to in-plane loads are different from those associated with the torsional warping (or warping transmission) which has been mainly investigated by the earlier works introduced above. For these reasons, no existing higher-order beam analysis has predicted the structural responses of two box beams-joint systems comparable with the plate/ shell analysis results when in-plane loads are applied. Recently, Jang and Kim [41] have proposed an analysis method based on a HoBT for two box beams-joint systems under in-plane loads. They established a HoBT that incorporates the bending warping representing the shear deformation of box beam section under transverse shear force [19] as well as the bending distortion proposed in [8] and developed approximate joint matching conditions among the kinematic variables. In their work, the three-dimensional displacements of two box beams were matched on the virtual joint section and then an optimization problem that minimizes the differences among those three-dimensional displacements was solved. The limitation of this approach is that the mechanical behavior of the joint cannot be accurately captured because the matching conditions were not exact. The section shape of the bending warping was also approximate one, so it should be further elaborated.

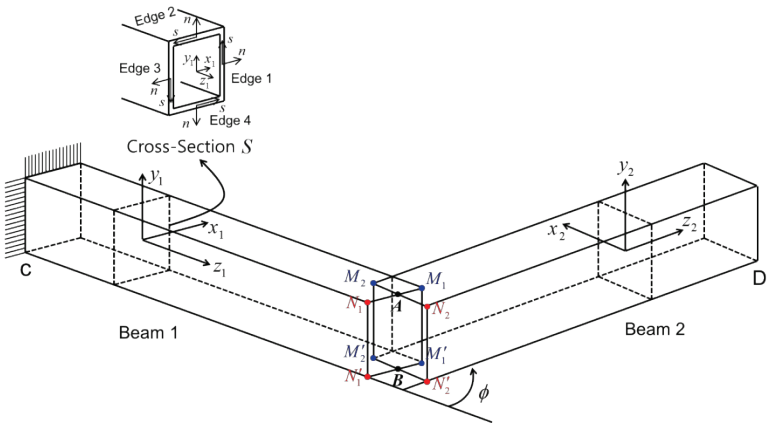

(a)

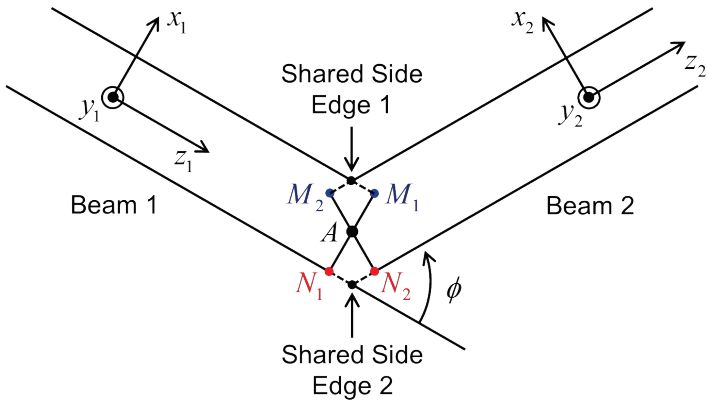

(b)

Fig. 4.2 (*a*) Beam modeling for the two box beams-joint structure (Edge $M_1M'_1$ of Beam 1 and Edge $M_2M'_2$ of Beam 2 are considered as if they were rigidly connected to each other by an imaginary rigid body, and Edge N_1N_1' of Beam 1 and Edge N_2N_2' of Beam 2 are also considered as if being rigidly connected to each other by an imaginary rigid body.), (*b*) the top view of beam modeling (Shared Side Edge 1 in Fig. 4.1 is extended and separated as Edge $M_1M'_1$ of Beam 1 and Edge $M_2M'_2$ of Beam 2, and Shared Side Edge 2 in Fig. 4.1 is also extended and separated as Edge N_1N_1' of Beam1 and Edge N_2N_2' of Beam 2.).

Therefore, in order to precisely predict the behavior of two box beams-joint systems under in-plane loads using a higher-order beam theory, a new HoBT employing correctly-defined sectional shapes corresponding to higher-order degrees of freedom is required. Also, we need to derive the exact joint matching conditions among the kinematic variables.

In this study, we aim to develop a new HoBT and derive exact joint matching conditions to precisely analyze the structural response of a two box beams-joint system under axial force F_z, transverse force F_x, and in-plane bending moment M_y, as depicted in Fig. 4.1. Beam 1 and Beam 2 are located on the same plane, and their widths, heights, and thicknesses are equal to *b*, *h*, and *t* respectively. For analyses based on the HoBT, we model the joint connectivity between Beam 1 and Beam 2 as shown in Fig. 4.2. As with classical beam theories, Jang and Kim [41], and Choi et al. [42], two beams converge to one point, and the point is defined as a joint (strictly, the joint refers to the point where the central axes of the two beams meet). Special efforts are made to establish the exact the joint matching conditions in which the continuity along the shared edges of the two beams meeting a joint should be considered. The details will be be presented in Section 4.4.

The key contributions of this study are i) the establishment of a new higher-order beam theory that considers sufficient higher-order deformation

degrees to express the flexible responses of the two box beams-joint systems under in-plane loads correctly, and ii) the theoretical derivation of the joint matching conditions among the field variables of the newly established HoBT. To do this, a HoBT incorporating the cross-sectional deformations of Fig. 4.3(b) in addition to the rigid-body motions of Fig. 4.3(a) will be established. The deformation shapes in Fig. 4.3(b) are theoretically derived by analyzing the mechanical responses of the box beam member when in-plane loads are applied. It is emphasized that the so-called bending distortion χ_1 is newly proposed here and that its importance in predicting correct structural behavior of box beams-joint systems is recognized for the first time.

Whereas Jang and Kim [41] employed some approximate techniques to define the joint matching conditions, the exact matching conditions to be derived for the present case considering in-plane bending and axial loads are inspired by the exact matching conditions derived for box beams-joint systems under out-of-plane loads [42]. In Choi et al. [42], a transformation matrix was introduced to represent the joint matching conditions, and a theoretical approach to derive the exact matching conditions was developed by considering some essential conditions that the transformation matrix must obey in addition to the equilibrium conditions and the continuity

conditions at the joint. Therefore, the approach proposed in Choi et al. [42] will be extended in this study to derive the joint matching conditions for the in-plane loading case. Following this strategy, the matching conditions between the six field variables ($U_z, U_x, \cdots, \chi_2$) of Beam 1 and Beam 2 in Fig. 4.1 will be newly derived in terms of a 6×6 transformation matrix $\mathbf{T}(\phi)$ (ϕ: the joint angle (see Fig. 4.2)). The construction of the transformation matrix for the present case dealing with in-plane bending and axial loads is much more difficult than that for the earlier case dealing with out-of-plane loads because the number of cross-sectional deformations for this case is larger and their shapes are much more complicated. In particular, contrary to the result in Choi et al. [42], the higher-order deformation degrees of Beam 1 and Beam 2 are coupled at the joint when in-plane loads are applied, and mechanical behavior of the higher-order deformations should be fully analyzed to determine those coupling relations. In this study, those relations are exactly derived within the developed HoBT by considering edge-wise equilibrium conditions with the concept of so-called "edge resultants" [43]. The details about the derivation of $\mathbf{T}(\phi)$ will be given in Section 4.4.

To check the validity of the higher-order beam theory that is newly established in this study, a case study will be examined first, in which straight thin-walled box beams with various aspect ratios of their cross-

sections are considered. To demonstrate the accuracy and the effectiveness of the proposed analysis approach using the theoretically derived joint matching conditions, two case studies will be investigated by using box beams-joint systems having various joint angles and cross-section aspect ratios. In each case study, the accuracy of the proposed approach will be checked by comparison with the ABAQUS shell analysis results [44].

4.2 Higher-Order Beam Theory for Straight Thin-Walled Box Beams

In order to interpret the two thin-walled box beams-joint structure shown in Fig. 4.1 precisely without using any artificial concepts, a higher-order beam theory which considers the primary cross-sectional deformations associated with the joint flexibility as the independent field variables and represents their mechanical behavior correctly is required.

To analyze the structure mentioned above, Jang and Kim [41] suggested the higher-order beam theory which includes the bending warping observed in the straight thin-walled box beams under in-plane bending loads (F_x, M_y) in addition to the bending distortion proposed in Kim and Kim [8], and they proved that the flexibility of the joint can be theoretically expressed by those cross-sectional deformations. However, the definition of the bending warping is mechanically incorrect because the shape of that is assumed by observation, and another primary

cross-sectional deformation (referred as bending distortion χ_1 in this study) that should be considered together in order to express the additional flexibility of thin-walled beam correctly in not involved. Consequently, the higher-order beam theory proposed by Jang and Kim [41] cannot precisely represent the behavior of the straight thin-walled box beams under (F_x, M_y), and that theory overestimates the bending rigidity of those box beams.

Therefore, a new higher-order beam theory considering six displacements or deformations of the box beams such as axial displacement U_z, transverse displacement U_x, in-plane bending/shear rotation θ_y, bending distortion χ_1, bending warping W_1, and bending distortion χ_2 as independent degrees of freedom will be established. Rigid-body motions of the box beam represented by (U_z, U_x, θ_y) are illustrated in Fig. 4.3(a), and cross-sectional deformations represented by (χ_1, W_1, χ_2) are illustrated in Fig. 4.3(b). χ_1 and W_1 represent the primary cross-sectional deformations associated with the additional flexibility of straight thin-walled box beams subjected to (F_x, M_y), and χ_2 represent the local deformation near the joint generated by the equilibrium at the joint.

In order to define those cross-sectional deformations as one-dimensional field variables of higher-order beam theory, shape functions representing their deformation patterns shown in Fig. 4.3(b) are employed. While the previous studies [16, 17] assumed the shape functions through observation, the shape functions will

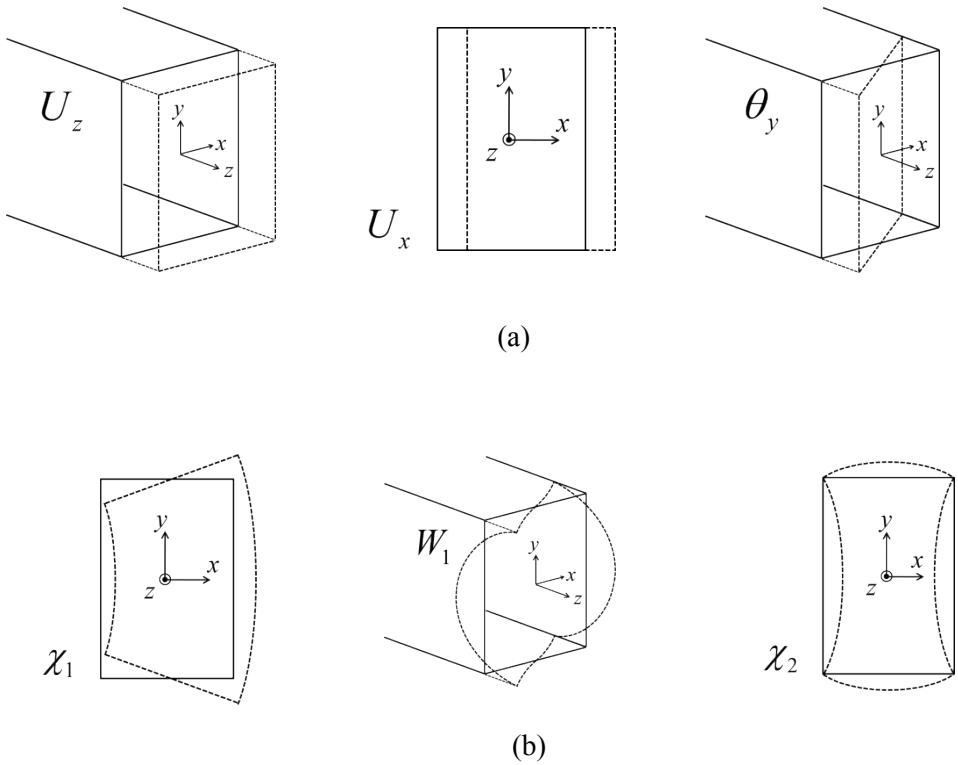

Fig. 4.3 (*a*) Rigid-body motions of the box beam cross-section represented by the field variables: axial displacement U_z, transverse displacement U_x and in-plane bending/shear rotation θ_y, (*b*) deformations of cross-section represented by the field variables: distortion χ_1, warping W_1 and distortion χ_2.

be theoretically derived in this study to define the higher-order beam theory precisely. In particular, χ_1 was not considered in the previous studies [8, 41], and χ_1 is first introduced in the higher-order beam theory to exactly describe the bending rigidity of thin-walled box beams and the additional flexibility represented by W_1.

Based on Refs. [7, 43], the one-dimensional higher-order beam theory considering the six rigid motions and cross-sectional deformations shown in Fig. 4.3(a, b) as the field variables will be defined in this section. The shape functions for (χ_1, W_1, χ_2) will be theoretically derived in the next section.

When one-dimensional field variables of the higher-order beam theory are expressed as the functions of axial coordinate z, $\mathbf{U}(z) = \{U_z(z), U_x(z), \theta_y(z), \chi_1(z), W_1(z), \chi_2(z)\}^{\mathrm{T}}$, three dimensional displacements of a point located on the contour line of the box beam cross-section can be written as follows by using $\mathbf{U}$ [7].

$$u_n(s, z) = \psi_n^{U_x}(s) \cdot U_x(z) + \psi_n^{\chi_1}(s) \cdot \chi_1(z) + \psi_n^{\chi_2}(s) \cdot \chi_2(z) \tag{4.1a}$$

$$u_s(s, z) = \psi_s^{U_x}(s) \cdot U_x(z) + \psi_s^{\chi_1}(s) \cdot \chi_1(z) + \psi_s^{\chi_2}(s) \cdot \chi_2(z) \tag{4.1b}$$

$$u_z(s, z) = \psi_z^{U_z}(s) \cdot U_z(z) + \psi_z^{\theta_y}(s) \cdot \theta_y(z) + \psi_z^{W_1}(s) \cdot W_1(z) \tag{4.1c}$$

Where n and s represent the coordinates in normal and tangential directions defined on the contour line respectively (the positive directions of coordinate n and s on each edge are given in Fig. 4.2(a)).

$u_p(s, z)$ ($p = n, s, z$) in Eq. (4.1) represent the displacement in p direction generated at the point (s, z) on the contour line. As shown in Fig. 4.3, (U_z, θ_y, W_1) represent the displacements or deformations on axial direction, and (U_x, χ_1, χ_2) represent those on the $x - y$ plane. Accordingly, u_z in Eq. (4.1c) is expressed by (U_z, θ_y, W_1), and (u_n, u_s) in Eqs. (4.1a, b) are expressed by (U_x, χ_1, χ_2).

$\psi_p^\alpha(s)$ ($p = n, s, z; \alpha = U_z, U_x, \theta_y, \chi_1, W_1, \chi_2$) in Eq. (4.1) are the shape functions which describe the deformation shape of field variable α shown in Fig. 4.3, and $\psi_p^\alpha(s)$ denote the displacement in p direction generated on the contour line by the unit magnitude of α. The explicit expressions of $\psi_p^\alpha(s)$ are given in Appendix A.

When the Kirchhoff-Love plate theory [45] is considered, three dimensional displacements at a generic point which is located away from the contour line by n can be written as follows by using (u_n, u_s, u_z) in Eq. (4.1).

$$\tilde{u}_n(n, s, z) = u_n(s, z) = \psi_n^{U_x} \cdot U_x + \psi_n^{\chi_1} \cdot \chi_1 + \psi_n^{\chi_2} \cdot \chi_2 \tag{4.2a}$$

$$\begin{aligned} \tilde{u}_s(n, s, z) &= u_s(s, z) - n\frac{\partial u_n(s,z)}{\partial s} \\ &= \psi_s^{U_x} \cdot U_x + \psi_s^{\chi_1} \cdot \chi_1 + \psi_s^{\chi_2} \cdot \chi_2 - n(\dot{\psi}_n^{U_x} \cdot U_x + \dot{\psi}_n^{\chi_1} \cdot \chi_1 + \dot{\psi}_n^{\chi_2} \cdot \chi_2) \end{aligned} \tag{4.2b}$$

$$\begin{aligned} \tilde{u}_z(n, s, z) &= u_z(s, z) - n\frac{\partial u_n(s,z)}{\partial z} \\ &= \psi_z^{U_z} \cdot U_z + \psi_z^{\theta_y} \cdot \theta_y + \psi_z^{W_1} \cdot W_1 - n(\psi_n^{U_x} \cdot U_x{}' + \psi_n^{\chi_1} \cdot \chi_1{}' + \psi_n^{\chi_2} \cdot \chi_2{}') \end{aligned} \tag{4.2c}$$

where $(\dot{\ })$ and $()'$ denote $(\dot{\ }) = \partial() / \partial s$ and $()' = \partial() / \partial z$ respectively. $-n \cdot (\partial u_n / \partial s)$ and $-n \cdot (\partial u_n / \partial z)$ in Eqs. (4.2b, c) represent the displacement in s and z directions respectively which arise from the rotation of the normal to the contour line.

According to the Kirchhoff-Love plate theory [45], the dominant strains ($\varepsilon_{ss}, \varepsilon_{zz}, \gamma_{sz}$) that occur at the same point can be defined from Eq. (4.2) as:

$$\varepsilon_{ss}(n,s,z)=\frac{\partial \tilde{u}_s}{\partial s}=\dot{\psi}_s^{\chi_1}\cdot\chi_1-n\{\ddot{\psi}_n^{\chi_1}\cdot\chi_1+\ddot{\psi}_n^{\chi_2}\cdot\chi_2\} \tag{4.3a}$$

$$\begin{aligned}\varepsilon_{zz}(n,s,z)=\frac{\partial \tilde{u}_z}{\partial z}&=\psi_z^{U_z}\cdot U_z{}'+\psi_z^{\theta_y}\cdot\theta_y{}'+\psi_z^{W_1}\cdot W_1'\\&\quad-n(\psi_n^{U_x}\cdot U_x{}''+\psi_n^{\chi_1}\cdot\chi_1{}''+\psi_n^{\chi_2}\cdot\chi_2{}'')\end{aligned} \tag{4.3b}$$

$$\begin{aligned}\gamma_{sz}(n,s,z)=\frac{\partial \tilde{u}_s}{\partial z}+\frac{\partial \tilde{u}_z}{\partial s}&=\psi_s^{U_x}\cdot U_x{}'+\psi_s^{\chi_1}\cdot\chi_1{}'+\dot{\psi}_z^{\theta_y}\cdot\theta_y\\&\quad+\dot{\psi}_z^{W_1}\cdot W_1-2n(\dot{\psi}_n^{\chi_1}\cdot\chi_1{}'+\dot{\psi}_n^{\chi_2}\cdot\chi_2{}')\end{aligned} \tag{4.3c}$$

where nonzero terms are given in Eq. (4.3) among the strains obtained from the displacements in Eq. (4.2). Subsequently, the dominant stresses ($\sigma_{ss}, \sigma_{zz}, \sigma_{sz}$) at the same point can be defined from ($\varepsilon_{ss}, \varepsilon_{zz}, \gamma_{sz}$) in Eq. (4.3) by employing the stress-strain relations as:

$$\begin{aligned}\sigma_{ss}(n,s,z)=\frac{E}{1-\nu^2}\{&(\dot{\psi}_s^{\chi_1}\cdot\chi_1+\nu\psi_z^{U_z}\cdot U_z{}'+\nu\psi_z^{\theta_y}\cdot\theta_y{}'+\nu\psi_z^{W_1}\cdot W_1')\\&-n(\ddot{\psi}_n^{\chi_1}\cdot\chi_1+\ddot{\psi}_n^{\chi_2}\cdot\chi_2+\nu\psi_n^{U_x}\cdot U_x{}''+\nu\psi_n^{\chi_1}\cdot\chi_1{}''+\nu\psi_n^{\chi_2}\cdot\chi_2{}'')\}\end{aligned} \tag{4a}$$

$$\begin{aligned}\sigma_{zz}(n,s,z)=E(\psi_z^{U_z}\cdot U_z{}')+\frac{E}{1-\nu^2}\{&(\psi_z^{\theta_y}\cdot\theta_y{}'+\psi_z^{W_1}\cdot W_1'+\nu\dot{\psi}_s^{\chi_1}\cdot\chi_1)\\&-n(\psi_n^{U_x}\cdot U_x{}''+\psi_n^{\chi_1}\cdot\chi_1{}''+\psi_n^{\chi_2}\cdot\chi_2{}''+\nu\ddot{\psi}_n^{\chi_1}\cdot\chi_1+\nu\ddot{\psi}_n^{\chi_2}\cdot\chi_2)\}\end{aligned} \tag{4b}$$

$$\sigma_{sz}(n,s,z)=G\{\psi_s^{U_x}\cdot U_x{}'+\psi_s^{\chi_1}\cdot\chi_1{}'+\dot{\psi}_z^{\theta_y}\cdot\theta_y+\dot{\psi}_z^{W_1}\cdot W_1-2n(\dot{\psi}_n^{\chi_1}\cdot\chi_1{}'+\dot{\psi}_n^{\chi_2}\cdot\chi_2{}')\} \tag{4c}$$

where E, G, ν represent Young's modulus, shear modulus, Poisson's ratio, respectively.

To define those stresses in Eq. (4.4) more precisely, two different stress-strain

relations given below are employed.

$$\sigma_{ss} = \frac{E}{1-\nu^2}(\varepsilon_{ss} + \nu\varepsilon_{zz}), \qquad \sigma_{zz} = \frac{E}{1-\nu^2}(\varepsilon_{zz} + \nu\varepsilon_{ss}), \qquad \sigma_{sz} = G\gamma_{sz} \tag{5a}$$

or

$$\sigma_{ss} = E\varepsilon_{ss}, \qquad \sigma_{zz} = E\varepsilon_{zz}, \qquad \sigma_{sz} = G\gamma_{sz} \tag{5b}$$

The dominant stresses generated by ($U_x, \theta_y, \chi_1, W_1, \chi_2$) which describe the bending behavior of box beam are defined by using the relations in Eq. (4.5a) because χ_1 represent the Poisson's effect [1] under the bending loads (F_x, M_y).

Meanwhile, only U_z is considered for the tensile or compressive behavior of box beam, and the cross-sectional deformation representing the Poisson's effect [1] under the axial load F_z is not included. Thus, the dominant stresses generated by U_z are defined by using the relations in Eq. (4.5b). As given in Eq. (4.3), the nonzero strain generated by U_z is only ε_{zz}, and the dominant stress σ_{zz} which is equal to the stress in the classical beam theory is defined through Eq. (4.5b) (see Eq. (4.4b)).

Using the displacements, strains, and stresses given in Eqs. (4.2-4), one can define the three dimensional total potential energy for the straight thin-walled box beam [7]. Subsequently, carrying out the surface integral for the cross-section S and applying the principle of minimum total potential energy, the exact higher-order beam theory employed in this study can be obtained (the detailed procedure is given in Appendix B). The newly established higher-order beam theory is

expressed as the relations between the field variables $\mathbf{U}$ and the generalized forces $\mathbf{F} = \{F_z, F_x, M_y, Q_1, B_1, Q_2\}^{\mathrm{T}}$, and $\mathbf{F}$ is defined as follows.

$$
\begin{aligned}
&F_z = \iint_S (\sigma_{zz}\psi_z^{U_z})\, dsdn, \quad F_x = \iint_S (\sigma_{zs}\psi_s^{U_x})\, dsdn, \quad M_y = \iint_S (\sigma_{zz}\psi_z^{\theta_y})\, dsdn, \\
&Q_1 = \iint_S (\sigma_{zs}\psi_s^{\chi_1})\, dsdn, \quad B_1 = \iint_S (\sigma_{zz}\psi_z^{W_1})\, dsdn, \quad Q_2 = \iint_S \sigma_{zs}(-n\dot{\psi}_n^{\chi_2})\, dsdn
\end{aligned}
\tag{4.6}
$$

where $F_z, F_x,$ and M_y represent resultant forces or moments such as axial force, transverse force, and in-plane bending moment respectively. On the contrary, the others denote self-equilibrated terms; B_1 represent longitudinal bimoment, and (Q_1, Q_2) represent transverse bimoments.

4.3 Derivation of Cross-Sectional Deformations (χ_1, W_1, χ_2)

The use of accurate shape functions $\psi(s)$ associated with the higher-order deformation degrees (χ_1, W_1, χ_2) is crucial in order to capture the flexible behavior of thin-walled box beams. Unlike earlier works [8, 41], we use a theoretical approach for accurate derivation of $\psi(s)$ for (χ_1, W_1, χ_2) and present newly-derived results [50].

4.3.1 Shape Function of χ_1

According to the classical beam theory [1, 2], the axial stress σ_{zz} generated at a point on the contour line by the in-plane bending moment M_y can be written as:

$$\sigma_{zz}(s,\, z) = \frac{M_y(z)}{I} \times \{-x(s)\} \tag{4.7}$$

where I represent the moment of inertia for M_y, and $x(s)$ denotes the x coordinate of the point at (s, z). By σ_{zz} given in Eq. (4.7), the strain ε_{zz} is generated, and simultaneously the strain ε_{ss} expressed as follows is also generated by the Poisson's effect [46].

$$\varepsilon_{ss}(s,\, z) = -\nu \frac{\sigma_{zz}}{E} = \frac{\nu M_y(z)}{EI} \times \{x(s)\} \tag{4.8}$$

According to Ref. [46], ε_{ss} given in Eq. (4.8) causes the cross-sectional deformation representing anticlastic curvature, and this deformation is considered in this study as the field variable χ_1.

When $u_s^{\chi_1}$ denotes the displacement associated with χ_1 in s direction on the contour line, $u_s^{\chi_1}$ generated from ε_{ss} given in Eq. (4.8) satisfies the following equation.

$$\frac{\partial u_s^{\chi_1}(s,\, z)}{\partial s} = \frac{\nu M_y(z)}{EI} \times \{x(s)\} \tag{4.9}$$

In addition, $u_s^{\chi_1}$ satisfies $u_s^{\chi_1}(s,\, z) = \psi_s^{\chi_1}(s) \cdot \chi_1(z)$ according to Eq. (4.1). When this relation is substituted into the Eq. (4.9), the following equation concerning $\psi_s^{\chi_1}(s)$ can be obtained.

$$\frac{\partial \psi_s^{\chi_1}(s)}{\partial s} = P_1^* \times \{x(s)\} \tag{4.10}$$

where P_1^* represents the proportional constant.

$\psi_s^{\chi_1}(s)$ will be exactly determined based on Eq. (4.10). When $x(s_j)$ represents the x coordinate of a point (s_j, z) on the Edge j ($j = 1, 2, 3, 4$) (see Fig. 4.2(a)), $x(s_j)$ can be expressed as:

$$x(s_1) = \frac{b}{2}, \qquad x(s_2) = -s_2, \qquad x(s_3) = -\frac{b}{2}, \qquad x(s_4) = s_4 \tag{4.11}$$

where b represents the width of cross-section as mentioned in Introduction (the height of cross-section is written by h). The coordinate s_j ($j = 1, 2, 3, 4$) is measured from the center of Edge j as shown in Fig. 4.2(a), and thus s_j has the following range: $-\frac{h}{2} \le s_1, s_3 \le \frac{h}{2}$ and $-\frac{b}{2} \le s_2, s_4 \le \frac{b}{2}$.

Substituting $x(s)$ in Eq. (4.11) into Eq. (4.10) and carrying out the integration for the coordinate s, $\psi_s^{\chi_1}(s_j)$ on Edge j ($j = 1, 2, 3, 4$) can be expressed as:

$$\begin{aligned} &\psi_s^{\chi_1}(s_1) = P_1^* \times \{\frac{b}{2}s_1 + C_1\}, \qquad &&\psi_s^{\chi_1}(s_2) = P_1^* \times \{-\frac{1}{2}s_2^{\,2} + C_2\}, \\ &\psi_s^{\chi_1}(s_3) = P_1^* \times \{-\frac{b}{2}s_3 + C_3\}, \qquad &&\psi_s^{\chi_1}(s_4) = P_1^* \times \{\frac{1}{2}s_4^{\,2} + C_4\} \end{aligned} \tag{4.12}$$

where C_1, C_2, C_3, and, C_4 represent the integration constants.

From the observation that σ_{zz} in Eq. (4.7) is symmetric with respect to the x-axis, one can find that the shape of χ_1 generated by σ_{zz} should be symmetric associated with the x-axis. To satisfy the x-axis symmetry,

therefore, $\psi_s^{\chi_1}(s_1)$ and $\psi_s^{\chi_1}(s_3)$ in Eq. (4.12) should meet the following odd function conditions, respectively.

$$\psi_s^{\chi_1}(s_1) = -\psi_s^{\chi_1}(-s_1), \qquad \psi_s^{\chi_1}(s_3) = -\psi_s^{\chi_1}(-s_3) \tag{4.13a}$$

In addition, the displacements in x direction on Edge 2 and Edge 4 represented by $\psi_s^{\chi_1}(s_2)$ and $\psi_s^{\chi_1}(s_4)$ respectively should be equal to meet the x-axis symmetry. Because the positive directions of s_2 and s_4 are $-x$ and $+x$ respectively (see Fig. 4.2(a)), the symmetry condition can be written as follows.

$$\psi_s^{\chi_1}(s_4 = s^*) = -\psi_s^{\chi_1}(s_2 = -s^*) \tag{4.13b}$$

where s^* represents an arbitrary constant within a range $-(b/2) \le s^* \le (b/2)$. The integral constants ($C_1 \sim C_4$) which satisfy the x-axis symmetry conditions given in Eqs. (4.13a, b) are as:

$$C_1 = C_3 = 0 \tag{4.14a}$$

$$C_4 = -C_2 \tag{4.14b}$$

Meanwhile, $\psi_s^{\chi_1}$ in Eq. (4.12) should satisfy the following orthogonality conditions with $\psi_s^{U_x}$ and $\psi_s^{\chi_2}$ so that the relation given in Eq. (4.1b) is defined correctly [5, 7].

$$\iint_S \psi_s^{\chi_1}(s) \cdot \psi_s^{U_x}(s)\, dA = 0 \tag{4.15a}$$

$$\iint_S \psi_s^{\chi_1}(s) \cdot \psi_s^{\chi_2}(s)\, dA = 0 \tag{4.15b}$$

Regardless of $\psi_s^{\chi_1}$, the condition in Eq. (4.15b) is satisfied by itself since

$\psi_s^{\chi_2}(s)=0$ as given in Appendix A. The orthogonality condition given in Eq. (4.15a) means that the cross-sectional deformation represented by χ_1 does not involve any rigid-body motion in *x* direction. (C_2, C_4) meeting the condition in Eq. (4.15a) are as follows.

$$C_2=\frac{b^2}{24}, \qquad C_4=-\frac{b^2}{24} \tag{4.16}$$

From the conditions for the *x*-axis symmetry and the orthogonality with U_x, all the constants ($C_1 \sim C_4$) in Eq. (4.12) are determined. The constant P_1^* in Eq. (4.12) determine the scale of cross-sectional deformation represented by the unit magnitude of χ_1, and $P_1^*=6/h^2$ will be used in this study.

When $u_s^{\chi_1}$ is generated on the contour line, $u_n^{\chi_1}$ is accompanied by the continuity at the corner *j* where Edge *j* and Edge *j*+1 ($j=1, 2, 3, 4$; Edge 5 denotes Edge 1) meet [6]; the $u_s^{\chi_1}$ generated on Edge 2 and Edge 4 are symmetric with respect to the *x*-axis as shown in Fig. 4.4(a), so the continuity at the corner *j* ($j=1, 2, 3, 4$) is satisfied by itself without having $u_n^{\chi_1}$ when $u_s^{\chi_1}$ are generated

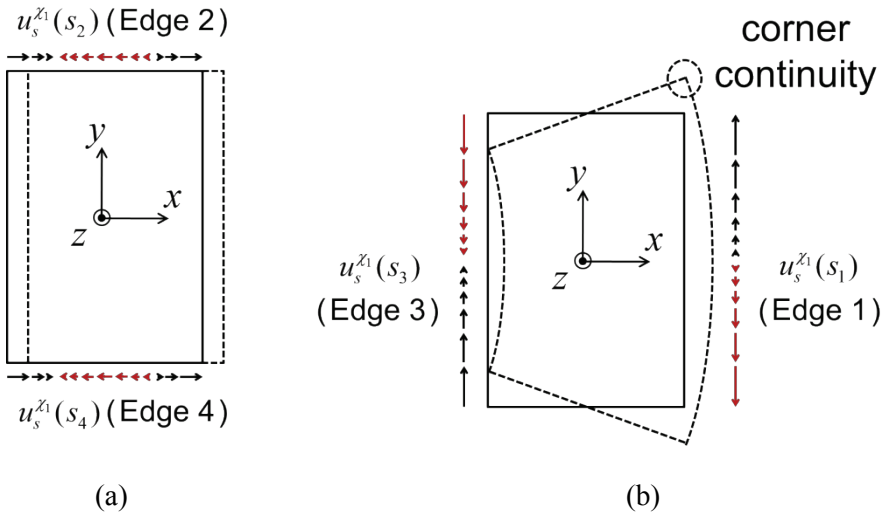

Fig. 4.4 (*a*) Displacements in *s* direction on Edge 2 and 4 represented by χ_1, (*b*) displacements in s direction on Edge 1 and Edge 3 represented by χ_1 and displacements in *n* direction on the entire cross-section accompanied by the continuity condition at each corner.

on Edge 2 and Edge 4. However, $u_s^{\chi_1}$ generated on Edge 1 and Edge 3 are anti-symmetric with respect to y-axis as shown in Fig. 4.4(b), so one can find that $u_n^{\chi_1}$ should be accompanied to meet the continuity at the corner *j* ($j = 1, 2, 3, 4$).

When $u_s^{\chi_1} = \psi_s^{\chi_1}(s) \cdot \chi_1(z)$ are generated on the contour line of Edge 1 and Edge 3, linear displacements $u_n^{\chi_1} = \psi_n^{\chi_1}(s) \cdot \chi_1(z)$ are generated on the contour line of Edge 2 and Edge 4 as shown in Fig. 4.4(b) to satisfy the following displacement continuity at the corner.

$$u_n^{\chi_1}(s_2 = -\frac{b}{2}) = u_s^{\chi_1}(s_1 = \frac{h}{2}), \qquad u_n^{\chi_1}(s_2 = \frac{b}{2}) = -u_s^{\chi_1}(s_3 = -\frac{h}{2}) \qquad (4.17a)$$

$$u_n^{\chi_1}(s_4=-\frac{b}{2})=u_s^{\chi_1}(s_3=\frac{h}{2}),\qquad u_n^{\chi_1}(s_4=\frac{b}{2})=-u_s^{\chi_1}(s_1=-\frac{h}{2})\tag{4.17b}$$

When $\psi_n^{\chi_1}(s_{j_1})$ at the Edge j_1 ($j_1=2,4$) are assumed as the following linear functions,

$$\psi_n^{\chi_1}(s_2)=a_{21}s_2+a_{22},\qquad \psi_n^{\chi_1}(s_4)=a_{41}s_4+a_{42}\tag{4.18}$$

those $\psi_n^{\chi_1}(s_{j_1})$ ($j_1=2,4$) can be determined by considering the displacement conditions given in Eq. (4.17), and consequently ($a_{21}, a_{22}, a_{41}, a_{42}$) in Eq. (4.18) are as follows.

$$a_{21}=-\frac{3}{h},\qquad a_{22}=0,\qquad a_{41}=\frac{3}{h},\qquad a_{42}=0\tag{4.19}$$

In addition to the displacement continuity, the following angle and moment continuities should also be satisfied at the corner according to Ref. [7]. For this reason, the parabolic displacements $u_n^{\chi_1}$ are accompanied on Edge 1 and Edge 3 as shown in Fig. 4.4(b).

$$\begin{aligned}&u_n^{\chi_1}(s_1=\frac{h}{2})=-u_s^{\chi_1}(s_2=-\frac{b}{2}),\qquad u_n^{\chi_1}(s_1=-\frac{h}{2})=u_s^{\chi_1}(s_4=\frac{b}{2}),\\&u_n^{\chi_1}(s_3=-\frac{h}{2})=u_s^{\chi_1}(s_2=\frac{b}{2}),\qquad u_n^{\chi_1}(s_3=\frac{h}{2})=-u_s^{\chi_1}(s_4=-\frac{b}{2})\end{aligned}\tag{4.20a}$$

$$\begin{aligned}&\beta_z^{\chi_1}(s_1=\frac{h}{2})=\beta_z^{\chi_1}(s_2=-\frac{b}{2}),\qquad \beta_z^{\chi_1}(s_1=-\frac{h}{2})=\beta_z^{\chi_1}(s_4=\frac{b}{2}),\\&\beta_z^{\chi_1}(s_3=-\frac{h}{2})=\beta_z^{\chi_1}(s_2=\frac{b}{2}),\qquad \beta_z^{\chi_1}(s_3=\frac{h}{2})=\beta_z^{\chi_1}(s_4=-\frac{b}{2})\end{aligned}\tag{4.20b}$$

$$\bar{M}_z^{\chi_1}(s_1=\frac{h}{2})=\bar{M}_z^{\chi_1}(s_2=-\frac{b}{2}),\qquad \bar{M}_z^{\chi_1}(s_1=-\frac{h}{2})=\bar{M}_z^{\chi_1}(s_4=\frac{b}{2}),$$
$$\bar{M}_z^{\chi_1}(s_3=-\frac{h}{2})=\bar{M}_z^{\chi_1}(s_2=\frac{b}{2}),\qquad \bar{M}_z^{\chi_1}(s_3=\frac{h}{2})=\bar{M}_z^{\chi_1}(s_4=-\frac{b}{2}) \tag{4.20c}$$

where $\beta_z^{\chi_1}(s_j)$ and $\bar{M}_z^{\chi_1}(s_j)$ at Edge j ($j=1, 2, 3, 4$) are defined as

$$\beta_z^{\chi_1}(s_j)=\frac{\partial u_n^{\chi_1}(s_j)}{\partial s};\qquad \bar{M}_z^{\chi_1}(s_j)=\frac{Et^3}{12}\times\frac{\partial^2 u_n^{\chi_1}(s_j)}{\partial s^2} \tag{4.21a, b}$$

The symbols $\beta_z^{\chi_1}(s_j)$ and $\bar{M}_z^{\chi_1}(s_j)$ represent the bending rotation and bending moment in z direction, respectively [7]. The moment $\bar{M}_z^{\chi_1}(s_j)$ in Eq. (4.21b) is approximately defined by the classical beam theory, and t in Eq. (4.21b) represents the thickness of Edge j.

When $\psi_n^{\chi_1}(s_{j_2})$ at the Edge j_2 ($j_2=1, 3$) are assumed as the following 4th order even functions which meet the x-axis symmetry condition,

$$\psi_n^{\chi_1}(s_1)=a_{11}s_1^{\ 4}+a_{12}s_1^{\ 2}+a_{13},\qquad \psi_n^{\chi_1}(s_3)=a_{31}s_3^{\ 4}+a_{32}s_3^{\ 2}+a_{33} \tag{4.22}$$

$\psi_n^{\chi_1}(s_{j_2})$ ($j_2=1, 3$) in Eq. (4.22) can be determined by employing those continuity conditions given in Eq. (4.21), and consequently (a_{11}, a_{12}, a_{13}, a_{31}, a_{32}, a_{33}) in Eq. (4.22) are as follows.

$$a_{11}=\frac{3}{h^4},\qquad a_{12}=-\frac{9}{2h^2},\qquad a_{13}=\frac{8b^2+15h^2}{16h^2},$$
$$a_{31}=-\frac{3}{h^4},\qquad a_{32}=\frac{9}{2h^2},\qquad a_{33}=-\frac{8b^2+15h^2}{16h^2} \tag{4.23}$$

4.3.2 Shape Function of W_1

The shape of the bending warping degree introduced in the earlier work [41] was only approximate so that there are cases where the analysis results are so accurate. For this reason, the shape function $\psi_z^{W_1}$ for the bending warping W_1 will be re-derived in this study from a theoretical approach [50].

When the transverse force F_x is applied to the thin-walled box beam, the in-plane bending moment M_y satisfying the equilibrium of is $\partial M_y / \partial z + F_x = 0$ accompanied, and thus σ_{zz} given in Eq. (4.7) is applied to the contour line of cross-section. However, σ_{zz} satisfies $(\partial \sigma_{zz} / \partial z) \neq 0$ in this case because $(\partial M_y / \partial z) \neq 0$.

Meanwhile, the following equilibrium condition always holds between the dominant stresses σ_{zz} and σ_{zs} according to Ref. [47] when any distributed loads are not applied.

$$\frac{\partial \sigma_{zz}}{\partial z} + \frac{\partial \sigma_{zs}}{\partial s} = 0 \tag{4.24}$$

Considering the equation above, one can find that σ_{zs} is generated on the contour line when F_x is applied, and the following condition to theoretically derive σ_{zs} can be obtained from Eq. (4.24).

$$\frac{\partial \sigma_{zs}}{\partial s} = -\frac{\partial \sigma_{zz}}{\partial z} = -\frac{1}{I}\left(\frac{\partial M_y(z)}{\partial z}\right) \times \{-x(s)\} = \frac{F_x(z)}{I} \times \{-x(s)\} \tag{4.25}$$

σ_{zs} meeting the condition in Eq. (4.25) produces the shear strain $\gamma_{sz} = \sigma_{zs} / G$

along the contour line, and consequently W_1 depicted in Fig. 4.3(b) occurs on the box beam by γ_{sz} [2, 19]. Therefore, σ_{zs} satisfying the condition in Eq. (4.25) will be theoretically derived first, and subsequently $\psi_z^{W_1}$ representing the shape of W_1 will be derived based on the obtained σ_{zs}.

When $\sigma_{zs}(s_j, z)$ represents σ_{zs} at Edge j ($j = 1, 2, 3, 4$), the following $\sigma_{zs}(s_j, z)$ satisfying Eq. (4.25) can be obtained through integration (see Eq. (4.11) for $x(s_j)$ at Edge j).

$$\begin{aligned} \sigma_{zs}(s_1, z) &= \frac{F_x(z)}{I} \times \{-\frac{b}{2} s_1 + \tilde{C}_1\}, & \sigma_{zs}(s_2, z) &= \frac{F_x(z)}{I} \times \{\frac{1}{2} s_2{}^2 + \tilde{C}_2\}, \\ \sigma_{zs}(s_3, z) &= \frac{F_x(z)}{I} \times \{\frac{b}{2} s_3 + \tilde{C}_3\}, & \sigma_{zs}(s_4, z) &= \frac{F_x(z)}{I} \times \{-\frac{1}{2} s_4{}^2 + \tilde{C}_4\} \end{aligned} \tag{4.26}$$

where ($\tilde{C}_1, \tilde{C}_2, \tilde{C}_3, \tilde{C}_4$) represent the integration constants. σ_{zs} in Eq. (4.26) is symmetric with respect to x-axis because F_x inducing σ_{zs} is applied along the x-axis. Considering this symmetry condition, the constant ($\tilde{C}_1 \sim \tilde{C}_4$) in Eq. (4.26) satisfy the following conditions (see Eq. (4.13) for the x-axis symmetry at each edge).

$$\tilde{C}_1 = \tilde{C}_3 = 0; \qquad \tilde{C}_4 = -\tilde{C}_2 \tag{4.27a, b}$$

In addition, σ_{zs} in Eq. (4.26) should meet the continuity condition $\sigma_{zs}(s_j, z)|_{\text{corner } j} = \sigma_{zs}(s_{j+1}, z)|_{\text{corner } j}$ at the corner j ($j = 1, 2, 3, 4$). This condition can be obtained from the consideration on the shear flow continuity between

$t \times \sigma_{zs}(s_j, z)$ at Edge j and $t \times \sigma_{zs}(s_{j+1}, z)$ at Edge j+1 (Edge 5 denotes Edge 1) at the corner j [22]. Although the shear stress at Edge j is linearly distributed in thickness direction, the effect is eliminated through the integration, and the shear flow at Edge j is expressed as $t \times \sigma_{zs}(s_j, z)$. The constants $\tilde{C}_2$ and $\tilde{C}_4$ which satisfy the continuity condition of σ_{zs} are as:

$$\tilde{C}_2 = -\frac{b^2 + 2bh}{8}, \qquad \tilde{C}_4 = \frac{b^2 + 2bh}{8} \tag{4.28}$$

As a result, $\sigma_{zs}(s_j, z)$ at Edge j produced by F_x can be given as follows.

$$\begin{aligned} \sigma_{zs}(s_1, z) &= \frac{F_x(z)}{I} \times \{-\frac{b}{2} s_1\}, & \sigma_{zs}(s_2, z) &= \frac{F_x(z)}{I} \times \{\frac{1}{2} s_2{}^2 - \frac{b^2 + 2bh}{8}\}, \\ \sigma_{zs}(s_3, z) &= \frac{F_x(z)}{I} \times \{\frac{b}{2} s_3\}, & \sigma_{zs}(s_4, z) &= \frac{F_x(z)}{I} \times \{-\frac{1}{2} s_4{}^2 + \frac{b^2 + 2bh}{8}\} \end{aligned} \tag{4.29}$$

In the higher-order beam theory, on the other hand, σ_{zs} on the contour line produced by F_x can be written as follows by using the field variables $\mathbf{U}(z)$ and the shape functions $\psi(s)$.

$$\sigma_{sz}(s, z) = G\{\psi_s^{U_x} \cdot U_x{}' + \dot{\psi}_z^{\theta_y} \cdot \theta_y + \psi_s^{\chi_1} \cdot \chi_1{}' + \dot{\psi}_z^{W_1} \cdot W_1\} \tag{4.30}$$

According to the higher-order beam theory, χ_1 by the Poisson's effect and W_1 by the shear strain are appeared in addition to the rigid-body motion (U_x, θ_y) in the box beam when F_x is applied, and referring to the Eq. (4.4c), one can fine that σ_{zs} on the contour line ($n = 0$) produced by ($U_x, \theta_y, \chi_1, W_1$) can be written as Eq. (4.30).

The shape functions ($\psi_s^{U_x}, \psi_z^{\theta_y}, \psi_s^{\chi_1}, \psi_z^{W_1}$) in Eq. (4.30) represent the distribution of σ_{zs}, and those functions except $\psi_z^{W_1}$ are previously determined (although the procedures to define ($\psi_s^{U_x}, \psi_z^{\theta_y}$) are not given, their definitions are so obvious since they represent the rigid-body motions). Considering the additional condition that σ_{zs} in Eq. (4.30) is equal to the previously determined σ_{zs} in Eq. (4.29), therefore, $\psi_z^{W_1}(s)$ can be precisely derived.

From the equality condition between σ_{zs} in Eqs. (4.29) and (4.30) at Edge j ($j = 1, 2, 3, 4$), the following conditions which $\dot{\psi}_z^{W_1}(s_j) \cdot W_1(z)$ should meet at the Edge j can be obtained (see Appendix A for the explicit expressions of ($\psi_s^{U_x}, \psi_z^{\theta_y}, \psi_s^{\chi_1}$)).

$$\dot{\psi}_z^{W_1}(s_1) \cdot W_1(z) = (-\frac{b}{2} s_1) \cdot \{\frac{1}{GI} F_x(z) + \frac{6}{h^2} \chi_1'(z)\} \tag{4.31a}$$

$$\begin{aligned} \dot{\psi}_z^{W_1}(s_2) \cdot W_1(z) = & (\frac{1}{2} s_2^{\,2}) \cdot \{\frac{1}{GI} F_x(z) + \frac{6}{h^2} \chi_1'(z)\} \\ & + \{-\frac{b^2 + 2bh}{8} \frac{1}{GI} F_x(z) + U_x'(z) - \theta_y(z) - \frac{b^2}{4h^2} \chi_1'(z)\} \end{aligned} \tag{4.31b}$$

$$\dot{\psi}_z^{W_1}(s_3) \cdot W_1(z) = (\frac{b}{2} s_3) \cdot \{\frac{1}{GI} F_x(z) + \frac{6}{h^2} \chi_1'(z)\} \tag{4.31c}$$

$$\begin{aligned} \dot{\psi}_z^{W_1}(s_4) \cdot W_1(z) = & (-\frac{1}{2} s_4^{\,2}) \cdot \{\frac{1}{GI} F_x(z) + \frac{6}{h^2} \chi_1'(z)\} \\ & - \{-\frac{b^2 + 2bh}{8} \frac{1}{GI} F_x(z) + U_x'(z) - \theta_y(z) - \frac{b^2}{4h^2} \chi_1'(z)\} \end{aligned} \tag{4.31d}$$

The conditions in Eq. (4.31) should hold for arbitrary coordinate (s, z), and the

functions of s and z given in Eq. (4.31) are independent each other. Thus, the conditions with respect to $\psi_z^{W_1}(s)$ can be obtained through the comparison among the functions of s.

First, comparing those functions of s_1 given in Eq. (4.31a), one can find that $\psi_z^{W_1}(s_1)$ should meet the following condition at Edge 1.

$$\dot{\psi}_z^{W_1}(s_1) = P_2^* \times (-\frac{b}{2} s_1) \tag{4.32a}$$

where P_2^* represents the proportional constant, and substituting the condition in Eq. (4.32a) into Eq. (4.31a), the following relation among the functions of z can be obtained.

$$P_2^* W_1(z) = \frac{1}{GI} F_x(z) + \frac{6}{h^2} \chi_1'(z) \tag{4.32b}$$

In sequence, substituting the relation in Eq. (4.32b) into Eq. (4.31b) (i.e., substituting $P_2^* W_1(z)$ into $\{\frac{1}{GI} F_x(z) + \frac{6}{h^2} \chi_1'(z)\}$ in Eq. (4.31b)) and then comparing those functions of s_2, one can find that $\psi_z^{W_1}(s_2)$ at Edge 2 should meet the following relation.

$$\dot{\psi}_z^{W_1}(s_2) - P_2^* \times (\frac{1}{2} s_2^{\,2}) = P_3^* \tag{4.33a}$$

where P_3^* represent the proportional constant. Likewise, it can be seen through substituting the relation in Eq. (4.33a) into Eq. (4.31b) that the following relation among those functions of z must hold.

$$P_3^* W_1(z) = \{-\frac{b^2+2bh}{8}\frac{1}{GI}F_x(z) + U_x'(z) - \theta_y(z) - \frac{b^2}{4h^2}\chi_1'(z)\} \qquad (4.33b)$$

Lastly, when those functions of z given in Eqs. (4.32b) and (4.33b) are substituted into Eqs. (4.31c) and (4.31d) respectively, the following relations for $\psi_z^{W_1}(s_3)$ and $\psi_z^{W_1}(s_4)$ can be obtained.

$$\dot{\psi}_z^{W_1}(s_3) = P_2^* \times (\frac{b}{2}s_3), \qquad \dot{\psi}_z^{W_1}(s_4) - P_2^* \times (-\frac{1}{2}s_4{}^2) = -P_3^* \qquad (4.34)$$

$\psi_z^{W_1}(s_j)$ at Edge j ($j = 1, 2, 3, 4$) which satisfy the relations derived above can be expressed as:

$$\begin{aligned} &\psi_z^{W_1}(s_1) = P_2^* \times \{-\frac{b}{4}s_1{}^2 + \tilde{a}_{11}\}, \qquad \psi_z^{W_1}(s_2) = P_2^* \times \{\frac{1}{6}s_2{}^3 + \tilde{a}_{22}s_2 + \tilde{a}_{21}\}, \\ &\psi_z^{W_1}(s_3) = P_2^* \times \{\frac{b}{4}s_3{}^2 + \tilde{a}_{31}\}, \qquad \psi_z^{W_1}(s_4) = P_2^* \times \{-\frac{1}{6}s_4{}^3 - \tilde{a}_{22}s_4 + \tilde{a}_{41}\} \end{aligned} \qquad (4.35)$$

where $\tilde{a}_{22} = (P_3^* / P_2^*)$, and ($\tilde{a}_{11}, \tilde{a}_{21}, \tilde{a}_{31}, \tilde{a}_{41}$) represent the integration constants.

When $u_z^{W_1}(s, z) = \psi_z^{W_1}(s) \cdot W_1(z)$ denotes the axial displacement on the contour line represented by W_1, the displacement continuity condition $u_z^{W_1}(s_j, z)|_{\text{corner } j} = u_z^{W_1}(s_{j+1}, z)|_{\text{corner } j}$ between $u_z^{W_1}(s_j, z)$ on Edge j and $u_z^{W_1}(s_{j+1}, z)$ on Edge j+1 at the corner j ($j = 1, 2, 3, 4$) must hold, and consequently the following conditions with respect to $\psi_z^{W_1}(s)$ given in Eq. (4.35) can be obtained.

$$\psi_z^{W_1}(s_1=\frac{h}{2})=\psi_z^{W_1}(s_2=-\frac{b}{2}),\qquad \psi_z^{W_1}(s_2=\frac{b}{2})=\psi_z^{W_1}(s_3=-\frac{h}{2}),$$
$$\psi_z^{W_1}(s_3=\frac{h}{2})=\psi_z^{W_1}(s_4=-\frac{b}{2}),\qquad \psi_z^{W_1}(s_4=\frac{b}{2})=\psi_z^{W_1}(s_1=-\frac{h}{2}) \tag{4.36}$$

Meanwhile, $\psi_z^{W_1}$ in Eq. (4.35) should meet the following orthogonality conditions with $\psi_z^{U_z}$ and $\psi_z^{\theta_y}$ so that the relation given in Eq. (4.1c) is defined correctly (see Appendix A for the explicit expression of ($\psi_z^{U_z}$, $\psi_z^{\theta_y}$)).

$$\iint_S \psi_z^{W_1}(s)\cdot\psi_z^{U_z}(s)\,dA=0\,;\qquad \iint_S \psi_z^{W_1}(s)\cdot\psi_z^{\theta_y}(s)\,dA=0 \tag{4.37a, b}$$

where Eqs. (4.37a) and (4.37b) mean that the cross-sectional deformation represented by W_1 does not include any rigid-body translation in z direction and any rigid-body rotation in y direction, respectively.

Considering those conditions given in Eqs. (4.36) and (4.37), the constants ($\tilde{a}_{11}$, $\tilde{a}_{21}$, $\tilde{a}_{22}$, $\tilde{a}_{31}$, $\tilde{a}_{41}$) in Eq. (4.35) which meet those conditions are obtained as follows.

$$\tilde{a}_{11}=-\tilde{a}_{31}=\frac{b(-2b^3+15bh^2+15h^3)}{240(b+3h)},\qquad \tilde{a}_{21}=0,$$
$$\tilde{a}_{22}=\frac{-b^3-5b^2h+10h^3}{40(b+3h)},\qquad \tilde{a}_{41}=0 \tag{4.38}$$

The constant P_2^* in Eq. (4.35) determine the scale of cross-sectional deformation represented by the unit magnitude of W_1, and $P_2^*=16/bh^2$ will be used in this study.

4.3.3 Shape Function of χ_2

Kim and Kim [8] established a HoBT incorporating χ_2 in order to express the flexibility of curved box beams, and later Jang and Kim [41] also used the same form of χ_2 proposed by Kim and Kim [8]. Because the form of χ_2 in Kim and Kim [8] involved some approximation ignoring the exact mechanics, there is a need to derive the exact form of χ_2 especially for accurate analysis of box beams meeting at a joint. A new derivation will be presented below [50].

First of all, we note that unlike χ_1 and W_1 considered above, χ_2 does not appear in a straight box beam subjected to (F_x, M_y). In other words, the sectional deformation associated with χ_2 shown in Fig. 4.3(b) only appears if two or more box beams meet at a joint with nonzero joint angles. In fact, χ_2 represents the local deformation observed near the joint of a two box beams-joint system under in-plane loads [41]. The shape function of χ_2 can be theoretically derived by considering the deformation patterns developed to satisfy the equilibrium state at the joint of two box beams. We will show later that in addition to the equilibrium conditions among sectional (or common) resultant forces or moments, the equilibrium conditions among the so-called edge resultants on Edge 1 and Edge 3 produced by (M_y, B_1, Q_2) can be considered at the joint. The detailed accounts of the edge resultants will be given in Section 4.4.4. Here, we simply remark that the edge resultants are the resultants evaluated separately for each edge. Therefore,

four sets of edge resultants can be defined for a given generalized force. Figure 4.8 suggests that M_y and B_1 all produce edge resultant forces $F_{z(j)}^{\beta}$ ($j = 1, 3$; $\beta = M_y, B_1$) parallel to the axial direction on Edge 1 and Edge 3. (For instance, $F_{z(3)}^{M_y}$ denotes the force resultant along the axial direction *z* defined on Edge 3 by the sectional resultant moment M_y.) Therefore, the sectional deformation associated with χ_2 can be generated in the process of achieving the equilibrium with respect to those edge resultants if a box beam meets another box beam at a joint with a non-zero joint angle.

Due to the edgewise equilibrium condition stated above, uniformly distributed loads on Edges 1 and 3, as depicted in Fig. 4.5(a), can be developed, which in turn induce χ_2. Figure 4.5(a) suggests that the edge resultants inducing χ_2 are in the $-x$ and $+x$ directions on Edge 1 and Edge 3 respectively. Therefore, the shape function $\psi_n^{\chi_2}(s)$ of χ_2 can be determined as the deformed shapes due to the uniformly-distributed external loads depicted in Fig. 4.5(a). Although the displacements in the *s* direction can be accompanied on Edge 2 and Edge 4 due to compression, $\psi_s^{\chi_2}(s) = 0$ is assumed in this study because the scale of displacements in the *s* direction is relatively very small compared to the scale of displacements in the *n* direction.

Using the symmetry of the applied loads with respect to both *x* and *y* axes in Fig. 4.5(a), one can define a bending problem depicted in Fig. 4.5(b). It models

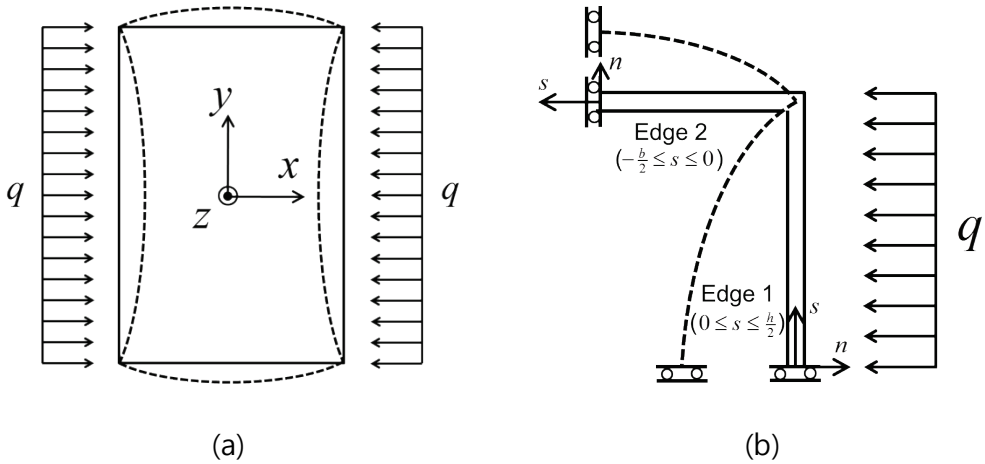

Fig. 4.5 (*a*) Distributed loads boundary condition and accompanied cross-sectional deformation χ_2 at the joint, (*b*) proposed equivalent problem to determine the deformation of χ_2 on the portion (the first quadrant) of the cross-section theoretically

only a portion of the cross-section (the first quadrant) with roller support conditions at its both ends. In the model, Edge 1 and Edge 2 are assumed to behave as beams, and their mechanics responses can be analyzed by using the classical Euler beam theory [1] as

$$u_n^{\chi_2}(s_1, z) = \{-\frac{1}{24}(s_1)^4 + \frac{h^2(3b+h)}{48(b+h)}(s_1)^2 - \frac{h^4(5b+h)}{384(b+h)}\} \cdot \{\frac{12}{Et^3}q(z)\} \quad (4.39a)$$

$$u_n^{\chi_2}(s_2, z) = \{-\frac{h^3}{24(b+h)}(s_2)^2 + \frac{b^2h^3}{96(b+h)}\} \cdot \{\frac{12}{Et^3}q(z)\} \quad (4.39b)$$

where $u_n^{\chi_2}(s_j, z)$ represents the displacement in the n direction generated on Edge j under the boundary conditions depicted in Fig. 4.5(b) and the ranges of the

coordinate s_j on Edge j ($j=1, 2$) are $0 \le s_1 \le (h/2)$ and $-(b/2) \le s_2 \le 0$, respectively.

When the external loads depicted in Fig. 4.5(a) are applied on the cross-section at a joint of two box beams, the displacement $u_n^{\chi_2}$ generated on the whole cross-section of a box beam meeting at a joint can be determined by using Eqs. (4.39a, b) and the symmetry conditions with respect to $s_1 = 0$ and $s_2 = 0$. Due to the symmetry, $u_n^{\chi_2}$ generated on Edge 1 for $-h/2 \le s_1 \le h/2$ and Edge 2 for $-b/2 \le s_2 \le b/2$ are expressed by even functions of s_i (i=1, 2), and thus $u_n^{\chi_2}$ on the entire range of Edge 1 and Edge 2 are exactly the same as $u_n^{\chi_2}$ given in Eqs. (4.39a, b). Moreover, $u_n^{\chi_2}$ on Edge 3 is equal to $u_n^{\chi_2}$ on Edge 1 by the y-axis symmetry, and $u_n^{\chi_2}$ on Edge 4 is equal to $u_n^{\chi_2}$ on Edge 2 by the x-axis symmetry. Using the expression $u_n^{\chi_2}(s_j, z) = \psi_n^{\chi_2}(s_j) \cdot \chi_2(z)$ ($j=1, 2, 3, 4$) for Edge j, the shape function $\psi_n^{\chi_2}(s_j)$ can be now written as follows:

$$\psi_n^{\chi_2}(s_1) = P_4^* \times \{-\frac{1}{24}(s_1)^4 + \frac{h^2(3b+h)}{48(b+h)}(s_1)^2 - \frac{h^4(5b+h)}{384(b+h)}\} \tag{4.40a}$$

$$\psi_n^{\chi_2}(s_2) = P_4^* \times \{-\frac{h^3}{24(b+h)}(s_2)^2 + \frac{b^2h^3}{96(b+h)}\} \tag{4.40b}$$

$$\psi_n^{\chi_2}(s_3) = P_4^* \times \{-\frac{1}{24}(s_3)^4 + \frac{h^2(3b+h)}{48(b+h)}(s_3)^2 - \frac{h^4(5b+h)}{384(b+h)}\} \tag{4.40c}$$

$$\psi_n^{\chi_2}(s_4) = P_4^* \times \{-\frac{h^3}{24(b+h)}(s_4)^2 + \frac{b^2h^3}{96(b+h)}\} \tag{4.40d}$$

The constant P_4^* in Eq. (4.40) determines the scale of cross-sectional deformation represented by the unit magnitude of χ_2, and $P_4^* = \{384(b+h)\} / \{h^4(5b+h)\}$ will be used in this study.

4.4 Derivation of Joint Matching Conditions

In the previous section, a new HoBT was proposed in which the shape functions are newly defined compared with earlier works [8, 41] and $\chi_1(z)$ is included as an additional degree of freedom for the analysis of box beams-joint systems. We will now establish a method analyze the structural behavior of two box beams-joint systems under in-plane loads (F_z, F_x, M_y) by using the newly-derived HoBT. The key for the joint analysis is how to derive the exact matching conditions among the field variables ($U_z, U_x, \cdots, \chi_2$) of Beam 1 and those Beam 2 at a beam joint. Because coupling phenomena at a joint are very complicated and also because no HoBT capable of handling mechanical behavior of thin-walled box beams at a joint, no theoretical method to exactly determine those joint matching conditions has been proposed. In this respect, the exact matching conditions will be derived in this study for the first time [50]. The present derivation is inspired by the exact matching method developed by Choi et al. [42] for box beams-joint systems under out-of-plane loads. However, additional considerations must be made to derive the exact joint matching conditions for box beams-joint systems under in-plane bending and axial loads because the required degrees of freedom (χ_1, W_1, χ_2)

involve much more complicated deformations than those involved in the problems considered by Choi et al. [42]. The detailed explanations for those additional considerations will be given below.

When the field variables of Beam k ($k = 1, 2$) are expressed as follows,

$$\mathbf{U}_k = \{(U_z)_k, (U_x)_k, (\theta_y)_k, (\chi_1)_k, (W_1)_k, (\chi_2)_k\}^{\mathrm{T}} \tag{4.41}$$

the matching conditions between $\mathbf{U}_1$ and $\mathbf{U}_2$ at the joint shown in Fig. 4.2 can be expressed as follows.

$$\mathbf{U}_2 = \mathbf{T}(\phi) \cdot \mathbf{U}_1 \tag{4.42a}$$

or

$$\begin{Bmatrix} (U_z)_2 \\ (U_x)_2 \\ (\theta_y)_2 \\ (\chi_1)_2 \\ (W_1)_2 \\ (\chi_2)_2 \end{Bmatrix} = \begin{bmatrix} t_{11} & t_{12} & t_{13} & t_{14} & t_{15} & t_{16} \\ t_{21} & t_{22} & t_{23} & t_{24} & t_{25} & t_{26} \\ t_{31} & t_{32} & t_{33} & t_{34} & t_{35} & t_{36} \\ t_{41} & t_{42} & t_{43} & t_{44} & t_{45} & t_{46} \\ t_{51} & t_{52} & t_{53} & t_{54} & t_{55} & t_{56} \\ t_{61} & t_{62} & t_{63} & t_{64} & t_{65} & t_{66} \end{bmatrix} \begin{Bmatrix} (U_z)_1 \\ (U_x)_1 \\ (\theta_y)_1 \\ (\chi_1)_1 \\ (W_1)_1 \\ (\chi_2)_1 \end{Bmatrix} \tag{4.42b}$$

where ϕ represent the joint angle between Beam 1 and Beam 2 (see Fig. 4.2(b) for the positive direction of ϕ), and $\mathbf{T}(\phi)$ denotes the 6×6 joint matrix representing the joint matching conditions between $\mathbf{U}_1$ and $\mathbf{U}_2$. In this study, we will determine the joint matrix $\mathbf{T}(\phi)$ which is valid for arbitrary joint angle ϕ and express the joint flexibility exactly. To do this, the following four propositions which $\mathbf{T}(\phi)$ should meet are defined, and the closed form of $\mathbf{T}(\phi)$ will be derived based on those propositions.

4.4.1 Proposition 1: Consideration of Zero Resultant by (Q_1, B_1, Q_2)

Taking into account the joint matching conditions given in Eq. (4.42) and the principle of virtual work together, the equilibrium conditions among the generalized forces $\mathbf{F}$ which are the work conjugates of those field variables in Eq. (4.42) can be also expressed by using $\mathbf{T}(\phi)$. Therefore, the equilibrium conditions among the resultant forces or moments which must hold at the joint will be considered in Proposition 1, and some part of $\mathbf{T}(\phi)$ will be determined through this consideration.

When the generalized force of Beam k () is expressed as follows,

$$\mathbf{F}_k = \{(F_z)_k, (F_x)_k, (M_y)_k, (Q_1)_k, (B_1)_k, (Q_2)_k\}^{\mathrm{T}} \tag{4.43}$$

the following equation meaning that the sum of virtual works of Beam 1 and Beam 2 are zero at the joint can be obtained from the principle of virtual work.

$$(\delta\mathbf{U}_1)^{\mathrm{T}}\mathbf{F}_1 + (\delta\mathbf{U}_2)^{\mathrm{T}}\mathbf{F}_2 = 0 \tag{4.44}$$

where $\delta\mathbf{U}_1$ and $\delta\mathbf{U}_2$ represent the virtual displacements of Beam 1 and Beam 2, respectively. Expressing $\delta\mathbf{U}_1$ as $\mathbf{T}^{-1}(\phi)\cdot\delta\mathbf{U}_2$ by using Eq. (4.42) and then substituting that expression into Eq. (4.44), the following equation can be obtained.

$$(\delta\mathbf{U}_2)^{\mathrm{T}}(\mathbf{T}^{-\mathrm{T}}(\phi)\cdot\mathbf{F}_1 + \mathbf{F}_2) = 0 \tag{4.45}$$

Since Eq. (4.45) should be always satisfied for arbitrary virtual displacement $\delta\mathbf{U}_2$, one can eventually obtain the following equilibrium condition between $\mathbf{F}_1$ and $\mathbf{F}_2$ at the joint.

$$\mathbf{T}^{-\mathrm{T}}(\phi)\cdot\mathbf{F}_1+\mathbf{F}_2=\mathbf{0} \tag{4.46}$$

Let us consider now the resultant forces or moments equilibrium conditions between $\mathbf{F}_1$ and $\mathbf{F}_2$ at the joint. It is worth mentioning that (Q_1, B_1, Q_2) among the generalized forces $\mathbf{F}$ which are the work conjugates of (χ_1, W_1, χ_2) are the self-equilibrated forces not producing any resultant forces or moments. Based on such characteristics, one can find that $((Q_1)_1, (B_1)_1, (Q_2)_1)$ of Beam 1 calculated at the joint cannot affect on the equilibrium among the resultant forces or moments of Beam 1 and Beam 2 at the joint, and that $((F_z)_2, (F_x)_2, (M_y)_2)$ of Beam 2 are not generated by $((Q_1)_1, (B_1)_1, (Q_2)_1)$ [42]. Therefore, the resultant forces or moments equilibrium conditions between $\mathbf{F}_1$ and $\mathbf{F}_2$ are simply given as the vector relations using $(\cos\phi, \sin\phi, \text{etc.})$ among $((F_z)_k, (F_x)_k, (M_y)_k)$ $(k=1, 2)$ having nonzero resultants, and consequently Eq. (4.46) should be written as follows from the consideration above.

$$\begin{bmatrix} \cos\phi & \sin\phi & 0 & 0 & 0 & 0 \\ -\sin\phi & \cos\phi & 0 & 0 & 0 & 0 \\ 0 & 0 & 1 & 0 & 0 & 0 \\ \bullet & \bullet & \bullet & \bullet & \bullet & \bullet \\ \bullet & \bullet & \bullet & \bullet & \bullet & \bullet \\ \bullet & \bullet & \bullet & \bullet & \bullet & \bullet \end{bmatrix} \begin{Bmatrix} (F_z)_1 \\ (F_x)_1 \\ (M_y)_1 \\ (Q_1)_1 \\ (B_1)_1 \\ (Q_2)_1 \end{Bmatrix} + \begin{Bmatrix} (F_z)_2 \\ (F_x)_2 \\ (M_y)_2 \\ (Q_1)_2 \\ (B_1)_2 \\ (Q_2)_2 \end{Bmatrix} = \begin{Bmatrix} 0 \\ 0 \\ 0 \\ 0 \\ 0 \\ 0 \end{Bmatrix} \tag{4.47}$$

where the parts expressed by dot $(\bullet)$ represent the elements of $\mathbf{T}^{-\mathrm{T}}$ to be obtained, and the elements in the dotted box are zero since $((Q_1)_1, (B_1)_1, (Q_2)_1)$ cannot affect on the resultant forces or moments equilibrium.

Therefore, identifying the form of $\mathbf{T}^{-\mathrm{T}}$ from the relation between $\mathbf{F}_1$ and $\mathbf{F}_2$ given in Eq. (4.47) and then deriving $\mathbf{T}$ from $\mathbf{T}^{-\mathrm{T}}$, the matching relation between $\mathbf{U}_1$ and $\mathbf{U}_2$ can be written as:

$$\begin{Bmatrix} (U_z)_2 \\ (U_x)_2 \\ (\theta_y)_2 \\ (\chi_1)_2 \\ (W_1)_2 \\ (\chi_2)_2 \end{Bmatrix} = \begin{bmatrix} \cos\phi & \sin\phi & 0 & t_{14} & t_{15} & t_{16} \\ -\sin\phi & \cos\phi & 0 & t_{24} & t_{25} & t_{26} \\ 0 & 0 & 1 & t_{34} & t_{35} & t_{36} \\ 0 & 0 & 0 & t_{44} & t_{45} & t_{46} \\ 0 & 0 & 0 & t_{54} & t_{55} & t_{56} \\ 0 & 0 & 0 & t_{64} & t_{65} & t_{66} \end{bmatrix} \begin{Bmatrix} (U_z)_1 \\ (U_x)_1 \\ (\theta_y)_1 \\ (\chi_1)_1 \\ (W_1)_1 \\ (\chi_2)_1 \end{Bmatrix} \tag{4.48}$$

4.4.2 Proposition 2: Displacement Continuity at the Intersection Point A and B

From the modeling shown in Fig. 4.2, the appearance of connection between the cross-sections of Beam 1 and Beam 2 at the joint is described in more detail in Fig. 4.6. As shown in Fig. 4.2(a) or Fig. 4.6, Beam1 and Beam2 meet each other at the intersection points A and B which are located at the center of Edge 2 and Edge 4 of each beam respectively. Therefore, some of t_{mn} ($m = 1, 2, \cdots, 6; n = 4, 5, 6$) in Eq. (4.48) will be determined in Proposition 2 by using the continuity conditions for the displacements of two beams calculated at the points A and B. However, the displacement fields on Edge 2 and Edge 4 are very complicated in the higher-order beam theory because the shape functions of (χ_1, W_1, χ_2) are represented by high-order polynomial functions. Thus, ($\bar{u}_s, \bar{u}_z$) representing the average displacements

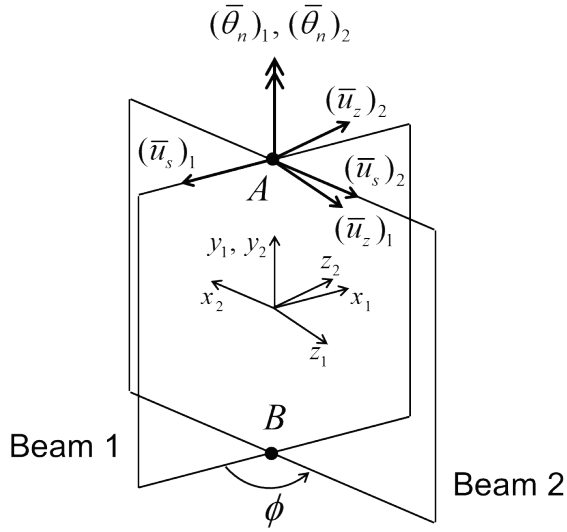

Fig. 4.6 Intersection points A and B at the joint between the cross-sections of Beam 1 and Beam 2 and the continuity conditions among displacements or rotations generated on those intersection points A and B

for the entire Edge 2 or Edge 4 will be used instead of (u_s, u_z) given in Eq. (4.1) to avoid defining the very localized displacement continuity conditions.

For example, the average displacements $(\overline{u}_s, \overline{u}_z)$ in s and z direction for the entire Edge 2 are as:

$$\overline{u}_s(z) = -U_x(z); \quad \overline{u}_z(z) = U_z(z) \tag{4.49a, b}$$

where $(\overline{u}_s, \overline{u}_z)$ can be obtained as follows from the displacements (u_s, u_z) on Edge 2 given in Eq. (4.1)

$$\overline{u}_s(z) = \int_{Edge2} u_s(s_2, z)\, ds_2 \Big/ \int_{Edge2} ds_2 \; ; \quad \overline{u}_z(z) = \int_{Edge2} u_z(s_2, z)\, ds_2 \Big/ \int_{Edge2} ds_2 \tag{4.50a, b}$$

The displacement continuity condition between $(\overline{u}_s, \overline{u}_z)$ of Beam 1 and Beam 2

at the point A can be written as:

$$(\overline{u}_s)_1(\boldsymbol{e}_s)_1 + (\overline{u}_z)_1(\boldsymbol{e}_z)_1 = (\overline{u}_s)_2(\boldsymbol{e}_s)_2 + (\overline{u}_z)_2(\boldsymbol{e}_z)_2 \tag{4.51}$$

where $(\overline{u}_p)_k$ and $(\boldsymbol{e}_p)_k$ ($p = s, z$; $k = 1, 2$) represent the average displacement and the unit vector in p direction defined on the point A of Beam k, respectively. The relations among $(\boldsymbol{e}_p)_k$ ($p = s, z$; $k = 1, 2$) at the point A can be written as (see Fig. 4.6):

$$(\boldsymbol{e}_z)_1 = (\boldsymbol{e}_z)_2 \cos\phi + (\boldsymbol{e}_s)_2 \sin\phi; \quad (\boldsymbol{e}_s)_1 = -(\boldsymbol{e}_z)_2 \sin\phi + (\boldsymbol{e}_s)_2 \cos\phi \tag{4.52a, b}$$

, and substituting the relations given in Eq. (4.52a, b) into the continuity condition in Eq. (4.51), one can obtain the following matching conditions between $\mathbf{U}_1$ and $\mathbf{U}_2$.

$$(U_z)_2 = (U_z)_1 \cos\phi + (U_x)_1 \sin\phi, \quad (U_x)_2 = -(U_z)_1 \sin\phi + (U_x)_1 \cos\phi \tag{4.53a, b}$$

All terms of $\mathbf{U}$ considered in this study are symmetric with respect to the x-axis (see Fig. 4.3(a, b)). Therefore, the continuity conditions among ($\overline{u}_s$, $\overline{u}_z$) defined on the point B are exactly equal to those conditions defined on the point A, and no additional conditions are obtained from the continuity conditions on the point B.

The continuity condition for the displacement u_n generated on the points A and B are additionally considered in Choi et al. [42] since they include the rigid-body motion in y direction as the field variable. On the other hand, the continuity condition for u_n will not be employed in this study because the displacement u_n on the points A and B are represented only by χ_2, and because the magnitude of

u_n is very small compared to that of (u_s, u_z). Instead, the continuity condition between the average rotation $\bar{\theta}_n$ in n direction generated on the points A and B of Beam 1 and Beam 2 will be employed together in this study because the rigid-body rotation in y direction is considered as the field variable θ_y.

For example, the average rotation $\bar{\theta}_n$ in n direction for the entire Edge 2 is as:

$$\bar{\theta}_n = \theta_y + \frac{4(5h^2 - b^2)}{5bh(b+3h)} W_1 \tag{4.54}$$

Through multiplying s_2 to the displacement $u_z(s_2, z)$ on Edge 2 given in Eq. (4.1) and then carrying out the line integration, the translation component of $u_z(s_2, z)$ can be eliminated, and the integration quantity with respect to the rotation of the entire Edge 2 are calculated as follows (see Appendix A for the explicit expressions of $\psi_z^{U_z}(s_2), \psi_z^{\theta_y}(s_2), \psi_z^{W_1}(s_2)$).

$$\begin{aligned}
&\int_{Edge2} s_2 \cdot u_z(s_2, z)\, ds_2 \\
&= U_z(z) \int_{Edge2} s_2 \cdot \psi_z^{U_z}(s_2)\, ds_2 + \theta_y(z) \int_{Edge2} s_2 \cdot \psi_z^{\theta_y}(s_2)\, ds_2 + W_1(z) \int_{Edge2} s_2 \cdot \psi_z^{W_1}(s_2)\, ds_2 \\
&= (\frac{b^3}{12}) \times \{\theta_y + \frac{4(5h^2 - b^2)}{5bh(b+3h)} W_1\}
\end{aligned} \tag{4.55a}$$

The average rotation $\bar{\theta}_n$ in n direction for the entire Edge 2 can be defined as follows by using the integration quantity calculated in Eq. (4.55a), and consequently $\bar{\theta}_n$ given in Eq. (4.54) can be obtained.

$$\int_{Edge\,2} s_2 \cdot u_z(s_2, z)\, ds_2 \equiv \int_{Edge\,2} s_2 \cdot (s_2 \cdot \bar{\theta}_n(z))\, ds_2 = (\frac{b^3}{12}) \times \bar{\theta}_n(z) \tag{4.55b}$$

Equation (54) shows that the effect W_1 by in addition to that by θ_y is appeared in the average rotation in *n* direction of Edge 2.

The continuity condition between $\bar{\theta}_n$ of Beam 1 and Beam 2 at the point A can be written as:

$$(\bar{\theta}_n)_1 (\boldsymbol{e}_n)_1 = (\bar{\theta}_n)_2 (\boldsymbol{e}_n)_2 \tag{4.56}$$

where $(\bar{\theta}_n)_k$ and $(\boldsymbol{e}_n)_k$ ($k = 1, 2$) represent the average rotation and the unit vector in *n* direction defined on the point A of Beam *k*. The following relation can be obtained from Eq. (4.56) because $(\boldsymbol{e}_n)_1 = (\boldsymbol{e}_n)_2$ at the point A (see Fig. 4.6).

$$(\theta_y)_2 + \frac{4(5h^2 - b^2)}{5bh(b+3h)}(W_1)_2 = (\theta_y)_1 + \frac{4(5h^2 - b^2)}{5bh(b+3h)}(W_1)_1 \tag{4.57}$$

Meanwhile, $(W_1)_2 = t_{54}(\chi_1)_1 + t_{55}(W_1)_1 + t_{56}(\chi_2)_1$ must hold from the relation given in Eq. (4.48), and substituting that relation into Eq. (4.57), $(\theta_y)_2$ can be expressed as:

$$(\theta_y)_2 = (\theta_y)_1 + \frac{4(5h^2 - b^2)}{5bh(b+3h)}\{-t_{54}(\chi_1)_1 + (1 - t_{55})(W_1)_1 - t_{56}(\chi_2)_1\} \tag{4.58}$$

When the continuity condition for $\bar{\theta}_n$ is considered at the point B, the same matching relation obtained from the continuity condition at the point A is derived.

Substituting the matching conditions given in Eqs. (4.53a, b) and Eq. (4.58) into Eq. (4.48), one can obtain the following matching conditions between $\mathbf{U}_1$

and $\mathbf{U}_2$ meeting the proposition 1 and 2.

$$\begin{Bmatrix} (U_z)_2 \\ (U_x)_2 \\ (\theta_y)_2 \\ (\chi_1)_2 \\ (W_1)_2 \\ (\chi_2)_2 \end{Bmatrix} = \begin{bmatrix} \cos\phi & \sin\phi & 0 & 0 & 0 & 0 \\ -\sin\phi & \cos\phi & 0 & 0 & 0 & 0 \\ 0 & 0 & 1 & -\frac{4(5h^2-b^2)}{5bh(b+3h)}t_{54} & \frac{4(5h^2-b^2)}{5bh(b+3h)}(1-t_{55}) & -\frac{4(5h^2-b^2)}{5bh(b+3h)}t_{56} \\ 0 & 0 & 0 & t_{44} & t_{45} & t_{46} \\ 0 & 0 & 0 & t_{54} & t_{55} & t_{56} \\ 0 & 0 & 0 & t_{64} & t_{65} & t_{66} \end{bmatrix} \begin{Bmatrix} (U_z)_1 \\ (U_x)_1 \\ (\theta_y)_1 \\ (\chi_1)_1 \\ (W_1)_1 \\ (\chi_2)_1 \end{Bmatrix} \tag{4.58}$$

4.4.3 Proposition 3: Use of the Relations $\mathbf{T}(\phi = 0^\circ) = \mathbf{I}$, $\mathbf{T}(\phi)\cdot\mathbf{T}(-\phi) = \mathbf{I}$, and $\mathbf{T}(\phi)\cdot\mathbf{T}(\phi) = \mathbf{T}(2\phi)$

To determine $\mathbf{T}(\phi)$ valid for arbitrary joint angle ϕ, the relation $\mathbf{T}(\phi_1)\cdot\mathbf{T}(\phi_2) = \mathbf{T}(\phi_1+\phi_2)$ should hold for arbitrary angles ϕ_1 and ϕ_2. Thus, employing $\mathbf{T}(\phi = 0^\circ) = \mathbf{I}$, $\mathbf{T}(\phi)\cdot\mathbf{T}(-\phi) = \mathbf{I}$, $\mathbf{T}(\phi)\cdot\mathbf{T}(\phi) = \mathbf{T}(2\phi)$ which are the special cases for the mentioned relation, some t_{mn} ($m = 4, 5, 6$; $n = 4, 5, 6$) in Eq. (4.59) will be determined in this study. In this regard, the relation $\mathbf{T}(\phi = 0^\circ) = \mathbf{I}$ represents that the structure shown in Fig. 4.2 is converged into the straight box beam when the joint angle $\phi = 0^\circ$.

Referring to Fig. 4.7, let us first determine the form of $\mathbf{T}(-\phi)$. Figure 4.7(a, b) represent the two thin-walled box beams-joint structures with joint angle $+\phi$ and $-\phi$, respectively. If the structure shown in Fig. 4.7(b) is rotated 180 degrees in z_1 direction, the structure can be regarded the structure having the joint angle $+\phi$

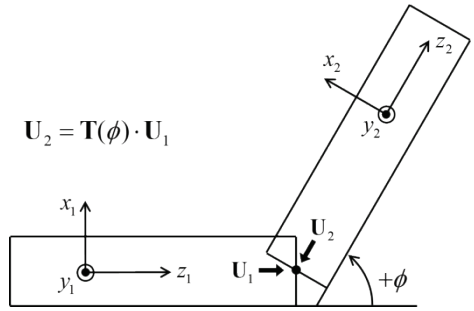

(a)

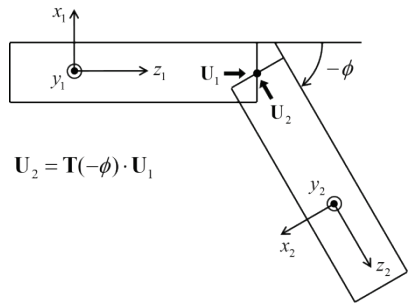

(b)

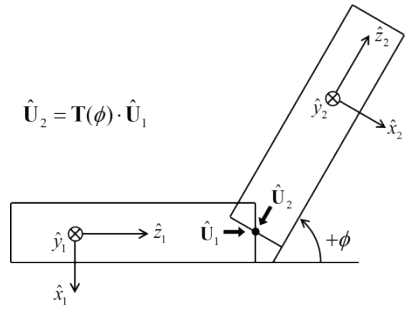

(c)

Fig. 4.7 Description of the procedure to determine the form of **T**(-ϕ): (*a*) matching conditions of **T**(ϕ) for a positive joint angle +ϕ, (*b*) **T**(-ϕ) defined for a negative joint angle $-\phi$, (*c*) **T**(ϕ) defined for the structure having a positive joint angle +ϕ and a different coordinate system ($\hat{x}$, $\hat{y}$, $\hat{z}$)

and the rotated local coordinates of Beam 1 and Beam 2 as depicted in Fig. 4.7(c). When $\hat{\mathbf{U}}_k$ ($k = 1, 2$) represents the field variables of Beam k defined by the local coordinate ($\hat{x}_k$, $\hat{y}_k$, $\hat{z}_k$) shown in Fig. 4.7(c), the matching condition between $\hat{\mathbf{U}}_1$ and $\hat{\mathbf{U}}_2$ at the joint can be written as:

$$\hat{\mathbf{U}}_2 = \mathbf{T}(\phi) \cdot \hat{\mathbf{U}}_1 \tag{4.60}$$

Meanwhile, the coordinate ($\hat{x}_k$, $\hat{y}_k$, $\hat{z}_k$) ($k = 1, 2$) shown in Fig. 4.7(c) can be related with the coordinate (x_k, y_k, z_k) in Fig. 4.7(a) as:

$$\hat{x}_k = -x_k, \quad \hat{y}_k = -\hat{y}_k, \quad \hat{z}_k = z_k \tag{4.61}$$

Considering those relations given in Eq. (4.61), one can also relate the field variables $\hat{\mathbf{U}}_k$ ($k = 1, 2$) with the field variables $\mathbf{U}_k$ (see the positive directions of those field variables shown in Fig. 4.3(a, b)).

$$\begin{aligned} &(\hat{U}_z)_k = (U_z)_k, \quad (\hat{U}_x)_k = -(U_x)_k, \quad (\hat{\theta}_y)_k = -(\theta_y)_k, \\ &(\hat{\chi}_1)_k = -(\chi_1)_k, \quad (\hat{W}_1)_k = -(W_1)_k, \quad (\hat{\chi}_2)_k = (\chi_2)_k \end{aligned} \tag{4.62}$$

Substituting Eq. (4.62) into Eq. (4.60) and then organizing the relations with respect to $\mathbf{U}_1$ and $\mathbf{U}_2$, one can obtain the matching relation $\mathbf{U}_2 = \mathbf{T}(-\phi) \cdot \mathbf{U}_1$ for the structure shown in Fig. 4.7(b). $\mathbf{T}(-\phi)$ obtained through this observation can be expressed as the following form.

$$\mathbf{T}(-\phi)=\begin{bmatrix} \cos\phi & -\sin\phi & 0 & 0 & 0 & 0 \\ \sin\phi & \cos\phi & 0 & 0 & 0 & 0 \\ 0 & 0 & 1 & -\frac{4(5h^2-b^2)}{5bh(b+3h)}t_{54} & \frac{4(5h^2-b^2)}{5bh(b+3h)}(1-t_{55}) & \frac{4(5h^2-b^2)}{5bh(b+3h)}t_{56} \\ 0 & 0 & 0 & t_{44} & t_{45} & -t_{46} \\ 0 & 0 & 0 & t_{54} & t_{55} & -t_{56} \\ 0 & 0 & 0 & -t_{64} & -t_{65} & t_{66} \end{bmatrix} \quad (4.63)$$

Comparing $\mathbf{T}(-\phi)$ given in Eq. (4.63) with $\mathbf{T}(\phi)$ given in Eq. (4.59), one can find that ($t_{44}, t_{45}, t_{54}, t_{55}, t_{66}$) are even functions, and that ($t_{46}, t_{56}, t_{64}, t_{65}$) are odd functions among the undetermined components t_{mn} ($m=4, 5, 6; n=4, 5, 6$) in $\mathbf{T}(\phi)$.

By the way, $\mathbf{T}(\phi)$ representing the so-called coordinate transformation matrix should meet the periodicity $\mathbf{T}(\phi+360^\circ)=\mathbf{T}(\phi)$, and thus it can be found that t_{mn} ($m=4, 5, 6; n=4, 5, 6$) in Eq. (4.59) should be expressed by the trigonometric functions ($\cos\phi, \sin\phi$) and constants. Moreover, the symmetry condition above and the condition $\mathbf{T}(\phi=0^\circ)=\mathbf{I}$ should be also satisfied. Therefore, $t_{44}\sim t_{66}$ can be written as follows from those considerations.

$$t_{44}(\phi)=1 \text{ or } \cos\phi,\quad t_{55}(\phi)=1 \text{ or } \cos\phi,\quad t_{66}(\phi)=1 \text{ or } \cos\phi \qquad (4.64a)$$

$$t_{45}(\phi)=t_{45}^*(1-\cos\phi),\quad t_{54}(\phi)=t_{54}^*(1-\cos\phi) \qquad (4.64b)$$

$$t_{46}(\phi)=t_{46}^*\sin\phi,\quad t_{56}(\phi)=t_{56}^*\sin\phi,\quad t_{64}(\phi)=t_{64}^*\sin\phi,\quad t_{65}(\phi)=t_{65}^*\sin\phi \qquad (4.64c)$$

The diagonal terms (t_{44}, t_{55}, t_{66}) of $\mathbf{T}(\phi)$ should be 1 or $\cos\phi$ as given in Eq. (4.64a) because those terms are even functions and should meet the condition $t_{mm}(\phi=0^\circ)=1$ ($m=4, 5, 6$). Among the off-diagonal terms of $\mathbf{T}(\phi)$, (t_{45}, t_{54})

should be the functions of ($1-\cos\phi$) as given in Eq. (4.64b) because they are even functions and should meet the condition $t_{mn}(\phi=0^\circ)=0$ ($m, n=4, 5; m \neq n$), and t_{45}^*, t_{54}^* in Eq. (4.64b) represent the proportional constants. The remained off-diagonal terms ($t_{46}, t_{56}, t_{64}, t_{65}$) of $\mathbf{T}(\phi)$ should be the functions of ($\sin\phi$) as given in Eq. (4.64c) because they are odd functions and should hold the condition $t_{m6}(\phi=0^\circ)= t_{6m}(\phi=0^\circ)=0$ ($m=4, 5$), and $t_{46}^*, t_{56}^*, t_{64}^*, t_{65}^*$ in Eq. (4.64c) represent the proportional constants either.

Considering Eq. (4.64), ($(\chi_1)_2, (W_1)_2, (\chi_2)_2$) of Beam 2 generated at the joint by ($(\chi_1)_1, (W_1)_1$, $(\chi_2)_1$) of Beam 1 can be written as:

$$\begin{Bmatrix} (\chi_1)_2 \\ (W_1)_2 \\ (\chi_2)_2 \end{Bmatrix} = \begin{bmatrix} t_{44} & t_{45}^*(1-\cos\phi) & t_{46}^*\sin\phi \\ t_{54}^*(1-\cos\phi) & t_{55} & t_{56}^*\sin\phi \\ t_{64}^*\sin\phi & t_{65}^*\sin\phi & t_{66} \end{bmatrix} \begin{Bmatrix} (\chi_1)_1 \\ (W_1)_1 \\ (\chi_2)_1 \end{Bmatrix} \tag{4.65}$$

where $(\chi_1)_k$ and $(\chi_2)_k$ ($k=1, 2$) represent the displacements on the $x_k - y_k$ plane of Beam k, and $(W_1)_k$ ($k=1, 2$) represent the axial displacements of Beam k (see Fig. 4.3(b)). Considering these displacement patterns of (χ_1, W_1, χ_2) in addition to the connectivity between the cross-sections of Beam 1 and Beam 2 shown in Fig. 4.6, one can find some contradictory relations between the displacements perpendicular to each other from Eq. (4.65). For example, the direction of displacements generated on Beam 2 by $(W_1)_1(1-\cos\phi)$ and of $(\chi_2)_1\sin\phi$ Beam 1 is perpendicular to the direction of $(\chi_1)_2$, and thus $(\chi_1)_2$

cannot be generated by the relations given in Eq. (4.65) with $((W_1)_1, (\chi_2)_1)$ of Beam1. Likewise, the directions of displacements generated on Beam 2 by $(\chi_1)_1(1-\cos\phi)$ and $(\chi_1)_1 \sin\phi$ of Beam 1 are perpendicular to the directions $(W_1)_2$ and $(\chi_2)_2$, respectively. Among those displacement relations given in Eq. (4.65), therefore, $(\chi_1)_2$ of Beam 2 should be decoupled with $(W_1)_1$ and $(\chi_2)_1$ of Beam 1, and $(W_1)_2$ and $(\chi_2)_2$ of Beam 2 should be decoupled with $(\chi_1)_1$ of Beam 1. Consequently, the following results can be obtained from this observation.

$$t_{45}^* = t_{46}^* = t_{54}^* = t_{64}^* = 0 \tag{4.66}$$

Subsequently, the conditions $\mathbf{T}(\phi)\cdot\mathbf{T}(-\phi)=\mathbf{I}$ and $\mathbf{T}(\phi)\cdot\mathbf{T}(\phi)=\mathbf{T}(2\phi)$ will be employed to obtain some of the undetermined t_{mn}. First, let us call the matrix given in Eq. (4.65) as $\mathbf{T}_{\text{sub}}(\phi)$ representing the submatrix of $\mathbf{T}(\phi)$. From the conditions $\mathbf{T}(\phi)\cdot\mathbf{T}(-\phi)=\mathbf{I}$ and $\mathbf{T}(\phi)\cdot\mathbf{T}(\phi)=\mathbf{T}(2\phi)$, it can be found that eventually $\mathbf{T}_{\text{sub}}(\phi)\cdot\mathbf{T}_{\text{sub}}(-\phi)=\mathbf{I}$ and $\mathbf{T}_{\text{sub}}(\phi)\cdot\mathbf{T}_{\text{sub}}(\phi)=\mathbf{T}_{\text{sub}}(2\phi)$ should be satisfied.

Using Eqs. (4.65) and (4.66), the condition $\mathbf{T}_{\text{sub}}(\phi)\cdot\mathbf{T}_{\text{sub}}(-\phi)=\mathbf{I}$ can be written as:

$$\begin{bmatrix} t_{44} & 0 & 0 \\ 0 & t_{55} & t_{56}^{*}\sin\phi \\ 0 & t_{65}^{*}\sin\phi & t_{66} \end{bmatrix}\begin{bmatrix} t_{44} & 0 & 0 \\ 0 & t_{55} & -t_{56}^{*}\sin\phi \\ 0 & -t_{65}^{*}\sin\phi & t_{66} \end{bmatrix}$$
$$= \begin{bmatrix} (t_{44})^2 & 0 & 0 \\ 0 & (t_{55})^2 - t_{56}^{*}t_{65}^{*}\sin^2\phi & -t_{56}^{*}\sin\phi(t_{55}-t_{66}) \\ 0 & t_{65}^{*}\sin\phi(t_{55}-t_{66}) & (t_{66})^2 - t_{56}^{*}t_{65}^{*}\sin^2\phi \end{bmatrix} = \begin{bmatrix} 1 & 0 & 0 \\ 0 & 1 & 0 \\ 0 & 0 & 1 \end{bmatrix} \tag{4.67}$$

, and considering the diagonal components in Eq. (4.67), one can find the following relations.

$$(t_{44})^2 = 1; \qquad (t_{55})^2 - (t_{66})^2 = 0 \tag{4.68a, b}$$

Since (t_{44}, t_{55}, t_{66}) satisfies Eq. (4.64a), (t_{44}, t_{55}, t_{66}) can be expressed as follows by considering Eq. (4.64a) together with Eqs. (4.68a, b).

$$t_{44} = 1; \qquad t_{55} = t_{66} \tag{4.69a, b}$$

When (t_{44}, t_{55}, t_{66}) meet the relations given in Eq. (69a, b), the relations for the off-diagonal components given in Eq. (4.67) are also satisfied.

Utilizing the results given in Eqs. (4.69a, b), $\mathbf{T}_{\text{sub}}(\phi)\cdot\mathbf{T}_{\text{sub}}(\phi) = \mathbf{T}_{\text{sub}}(2\phi)$ can be written as:

$$\begin{bmatrix} 1 & 0 & 0 \\ 0 & t_{55} & t_{56}^{*}\sin\phi \\ 0 & t_{65}^{*}\sin\phi & t_{55} \end{bmatrix}\begin{bmatrix} 1 & 0 & 0 \\ 0 & t_{55} & t_{56}^{*}\sin\phi \\ 0 & t_{65}^{*}\sin\phi & t_{55} \end{bmatrix}$$
$$= \begin{bmatrix} 1 & 0 & 0 \\ 0 & (t_{55})^2 + t_{56}^{*}t_{65}^{*}\sin^2\phi & 2t_{55}t_{56}^{*}\sin\phi \\ 0 & 2t_{55}t_{65}^{*}\sin\phi & (t_{55})^2 + t_{56}^{*}t_{65}^{*}\sin^2\phi \end{bmatrix} = \begin{bmatrix} 1 & 0 & 0 \\ 0 & t_{55}(2\phi) & 2t_{56}^{*}\cos\phi\sin\phi \\ 0 & 2t_{65}^{*}\cos\phi\sin\phi & t_{55}(2\phi) \end{bmatrix} \tag{4.70}$$

where t_{55} is 1 or $\cos\phi$ according to Eq. (4.64a). If t_{55} is assumed to be 1, the

following results are obtained from the relations between the components of (2, 3) or (3, 2) in Eq. (4.70).

$$2t_{56}^{*}\sin\phi(1-\cos\phi)=0, \qquad 2t_{65}^{*}\sin\phi(1-\cos\phi)=0 \tag{4.71}$$

Since Eq. (4.71) should be satisfied for arbitrary joint angle ϕ, $t_{56}^{*}=t_{65}^{*}=0$, and thus $\mathbf{T}_{\text{sub}}(\phi)=\mathbf{I}$. This represents the contradictory result that $((\chi_1)_1, (W_1)_1, (\chi_2)_1)$ of Beam1 are equal to $((\chi_1)_2, (W_1)_2, (\chi_2)_2)$ of Beam 2 regardless of the joint angle between two beams, and the flexibility of the joint appeared by the effects of cross-sectional deformations cannot be expressed through this matching conditions. Therefore, t_{55} should take the following form:

$$t_{55}=\cos\phi \tag{4.72}$$

, and when t_{55} in Eq. (4.72) is substituted for Eq. (4.70), the following relation between t_{56}^{*} and t_{65}^{*} can be obtained from the relation with respect to the components of (2, 2) or (3, 3) in the matrix.

$$t_{56}^{*}t_{65}^{*}=-1 \tag{4.73}$$

The matching conditions between $\mathbf{U}_1$ and $\mathbf{U}_2$ which satisfy all the conditions with respect to $\mathbf{T}(\phi)$ considered in Proposition 3 are as:

$$\begin{Bmatrix} (U_z)_2 \\ (U_x)_2 \\ (\theta_y)_2 \\ (\chi_1)_2 \\ (W_1)_2 \\ (\chi_2)_2 \end{Bmatrix} = \begin{bmatrix} \cos\phi & \sin\phi & 0 & 0 & 0 & 0 \\ -\sin\phi & \cos\phi & 0 & 0 & 0 & 0 \\ 0 & 0 & 1 & 0 & \frac{4(5h^2-b^2)}{5bh(b+3h)}(1-\cos\phi) & -\frac{4(5h^2-b^2)}{5bh(b+3h)}t_{56}^{*}\sin\phi \\ 0 & 0 & 0 & 1 & 0 & 0 \\ 0 & 0 & 0 & 0 & \cos\phi & t_{56}^{*}\sin\phi \\ 0 & 0 & 0 & 0 & -\dfrac{1}{t_{56}^{*}}\sin\phi & \cos\phi \end{bmatrix} \begin{Bmatrix} (U_z)_1 \\ (U_x)_1 \\ (\theta_y)_1 \\ (\chi_1)_1 \\ (W_1)_1 \\ (\chi_2)_1 \end{Bmatrix}$$

(4.74)

It can be seen that the matching conditions given in Eq. (4.74) are valid for any joint angle ϕ, because $\mathbf{T}(\phi)$ in Eq. (4.74) satisfies $\mathbf{T}(\phi_1)\cdot\mathbf{T}(\phi_2)=\mathbf{T}(\phi_1+\phi_2)$ for arbitrary ϕ_1 and ϕ_2,

4.4.4 Proposition 4: Equilibrium Condition on Edge 1 or Edge 3

When the matching conditions given in Eq. (4.74) are satisfied at the joint, the following equilibrium conditions between $\mathbf{F}_1$ and $\mathbf{F}_2$ should hold according to Eq. (4.46).

$$\begin{bmatrix} \cos\phi & \sin\phi & 0 & 0 & 0 & 0 \\ -\sin\phi & \cos\phi & 0 & 0 & 0 & 0 \\ 0 & 0 & 1 & 0 & 0 & 0 \\ 0 & 0 & 0 & 1 & 0 & 0 \\ 0 & 0 & \frac{4(5h^2-b^2)}{5bh(b+3h)}(1-\cos\phi) & 0 & \cos\phi & \dfrac{1}{t_{56}^{*}}\sin\phi \\ 0 & 0 & \frac{4(5h^2-b^2)}{5bh(b+3h)}t_{56}^{*}\sin\phi & 0 & -t_{56}^{*}\sin\phi & \cos\phi \end{bmatrix} \begin{Bmatrix} (F_z)_1 \\ (F_x)_1 \\ (M_y)_1 \\ (Q_1)_1 \\ (B_1)_1 \\ (Q_2)_1 \end{Bmatrix} + \begin{Bmatrix} (F_z)_2 \\ (F_x)_2 \\ (M_y)_2 \\ (Q_1)_2 \\ (B_1)_2 \\ (Q_2)_2 \end{Bmatrix} = \begin{Bmatrix} 0 \\ 0 \\ 0 \\ 0 \\ 0 \\ 0 \end{Bmatrix}$$

(4.75)

Subsequently, the equilibrium conditions given in the fifth and sixth rows in Eq.

(4.75) can be expressed as:

$$\{-\tfrac{4(5h^2-b^2)}{5bh(b+3h)}(M_y)_1+(B_1)_1\}\cos\phi+\frac{1}{t_{56}^*}(Q_2)_1\sin\phi+\{-\tfrac{4(5h^2-b^2)}{5bh(b+3h)}(M_y)_2+(B_1)_2\}=0$$

(4.76a)

$$-\{-\tfrac{4(5h^2-b^2)}{5bh(b+3h)}(M_y)_1+(B_1)_1\}\sin\phi+\frac{1}{t_{56}^*}(Q_2)_1\cos\phi+\frac{1}{t_{56}^*}(Q_2)_2=0 \qquad (4.76b)$$

where the relation $(M_y)_1+(M_y)_2=0$ obtained from the third row in Eq. (4.75) is employed in Eq. (4.76a).

Equations (76a, b) show that the additional equilibrium conditions among (M_y, B_1, Q_2) should be satisfied at the joint as well as two equilibrium conditions with respect to the resultant forces (F_z, F_x) and one equilibrium condition with respect to the resultant moment M_y. In this regard, (B_1, Q_2) produce the so-called edge resultants for each edge of the cross-section although they do not produce any resultant for the entire cross-section (this phenomenon has been found for the first time by Choi and Kim [43] dealing with the interpretation for the thin-walled beam structure subjected to out-of-plane loads).

Figure 4.8 shows the edge forces or the edge moments that are generated on each edge of the cross-section by M_y, B_1, and Q_2. For example, $M_{n(4)}^{M_y}$ represents the edge moment in *n* direction that is generated on Edge 4 by M_y (the detailed procedures in derivation of those edge resultants are given in Appendix C). Strictly speaking, Q_2 produces the edge moment $M_{z(j)}^{Q_2}$ ($j=1, 2, 3, 4$) in *z*

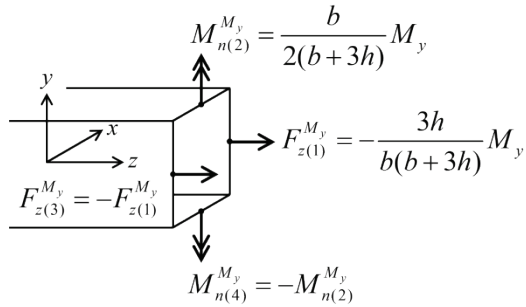

(a)

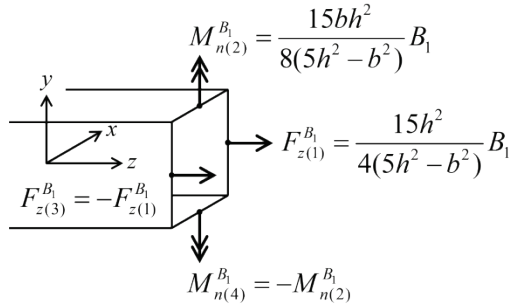

(b)

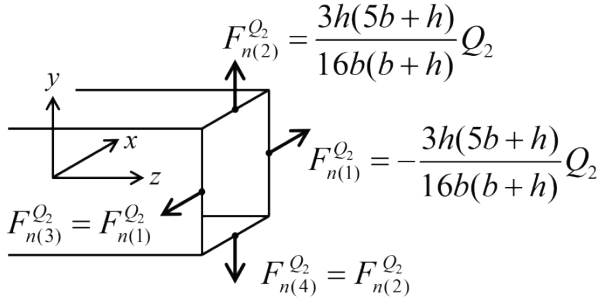

(c)

Fig. 4.8 Edge resultants acting on each edge of the cross-section that are produced by the generalized forces: in-plane bending moment M_y, longitudinal bimoment B_1 and transverse bimoment Q_2

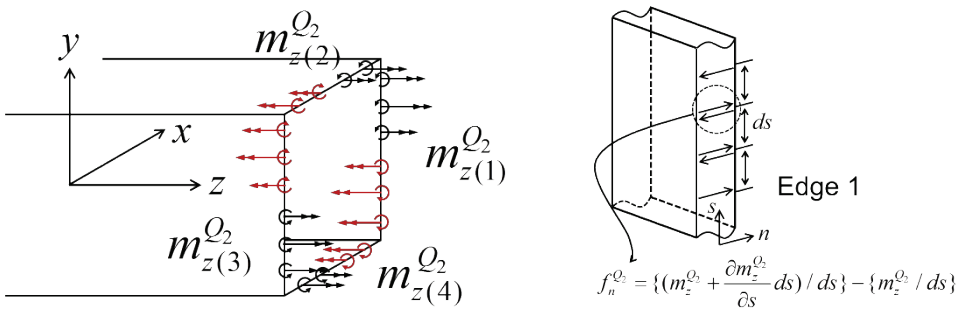

(a) (b)

Fig. 4.9 (*a*) Distributed axial moment $m_z^{Q_2}$ on the cross-section generated by the shear stress $\sigma_{sz}^{Q_2}$ of Q_2, (*b*) effective distributed normal force $f_n^{Q_2}$ acting on Edge 1 generated by the distributed moment $m_z^{Q_2}$

direction for each edge (Fig. 4.9(a)). According to the Kirchhoff-Love plate theory [45], however, $M_{z(j)}^{Q_2}$ eventually produces the effective edge forces $F_{n(j)}^{Q_2}$ ($j = 1, 2, 3, 4$) in n direction by the principle given in Fig. 4.9(b).

Considering Eqs. (4.76a, b), those forces represented by $\{-\frac{4(5h^2-b^2)}{5bh(b+3h)} M_y + B_1\}$ and $\{\frac{1}{t_{56}^*} Q_2\}$ should be placed on the same plane and should be perpendicular to each other. From this observation, one can find that Eqs. (4.76a, b) represent the equilibrium conditions among those edge resultants shown in Fig. 4.8 that are generated on Edge 1 or Edge 3. Although Edge 1 and Edge 3 of two beams are located apart from each other in Fig. 4.2, the connectivity among those edges can be defined by referring to Choi and Kim [43]. In other word, Shared Side Edge 1 at the actual joint shown in Fig. 4.1 is extended and divided into Edge $M_1 M_1'$ and

Edge M_2M_2' in the modeling shown in Fig. 4.2 which represent Edge 1 of Beam 1 and Beam 2, respectively, and thus Edge 1 of two beams at the joint can be regarded as if they are connected each other by a rigid body. Applying the same perspective to Shared Side Edge 2 shown in Fig. 4.1, Edge 3 of two beams at the joint can be also regarded as if they are rigidly connected each other. Therefore, the equilibrium conditions among the edge resultants generated on Edge j_2 ($j_2 = 1, 3$) of Beam 1 and Beam 2 can be considered at the joint.

The equilibrium conditions defined on Edge 1 and Edge 3 are equal to each other, and those conditions are expressed as:

$$\{-\tfrac{3h}{b(b+3h)}(M_y)_1 + \tfrac{15h^2}{4(5h^2-b^2)}(B_1)_1\}\cos\phi - \{\tfrac{3h(5b+h)}{16b(b+h)}(Q_2)_1\}\sin\phi + \{-\tfrac{3h}{b(b+3h)}(M_y)_2 + \tfrac{15h^2}{4(5h^2-b^2)}(B_1)_2\} = 0 \tag{4.77a}$$

$$-\{-\tfrac{3h}{b(b+3h)}(M_y)_1 + \tfrac{15h^2}{4(5h^2-b^2)}(B_1)_1\}\sin\phi - \{\tfrac{3h(5b+h)}{16b(b+h)}(Q_2)_1\}\cos\phi - \{\tfrac{3h(5b+h)}{16b(b+h)}(Q_2)_2\} = 0 \tag{4.77b}$$

It can be seen that Eqs. (4.77a, b) are equal to Eqs. (4.76a, b) multiplied by $\dfrac{15h^2}{4(5h^2-b^2)}$. Therefore, the constant t_{56}^* in Eqs. (4.76a, b) can be determined through the comparison with Eqs. (4.77a, b), and the value of t_{56}^* is as:

$$t_{56}^* = -\frac{20bh(b+h)}{(5b+h)(5h^2-b^2)} \tag{4.78}$$

, and the exact matching conditions between $\mathbf{U}_1$ and $\mathbf{U}_2$ can be obtained by substituting t_{56}^* in Eq. (4.78) into Eq. (4.74), and those conditions are as:

$$
\begin{Bmatrix} (U_z)_2 \\ (U_x)_2 \\ (\theta_y)_2 \\ (\chi_1)_2 \\ (W_1)_2 \\ (\chi_2)_2 \end{Bmatrix} = \begin{bmatrix} \cos\phi & \sin\phi & 0 & 0 & 0 & 0 \\ -\sin\phi & \cos\phi & 0 & 0 & 0 & 0 \\ 0 & 0 & 1 & 0 & \frac{4(5h^2-b^2)}{5bh(b+3h)}(1-\cos\phi) & \frac{16(b+h)}{(b+3h)(5b+h)}\sin\phi \\ 0 & 0 & 0 & 1 & 0 & 0 \\ 0 & 0 & 0 & 0 & \cos\phi & -\frac{20bh(b+h)}{(5b+h)(5h^2-b^2)}\sin\phi \\ 0 & 0 & 0 & 0 & \frac{(5b+h)(5h^2-b^2)}{20bh(b+h)}\sin\phi & \cos\phi \end{bmatrix} \begin{Bmatrix} (U_z)_1 \\ (U_x)_1 \\ (\theta_y)_1 \\ (\chi_1)_1 \\ (W_1)_1 \\ (\chi_2)_1 \end{Bmatrix}
\tag{4.79}
$$

4.5 Numerical Examples

The finite element equations of the HoBT for thin-walled box beams under in-plane bending and axial loads are given by Eqs. (4.B4-4.B6) in Appendix B and the exact joint matching equations are newly derived as Eq. (4.79). Because the procedure to analyze box beams-joint systems by using the higher-order beam theory and the joint matching conditions is exactly the same as the standard procedure using the finite element analysis based on the classical beam theories [48], the detailed descriptions for the analysis procedure will be omitted. The accuracy and effectiveness of the derived equations will be demonstrated in this section.

First, straight box beams with various aspect ratios of cross-sections will be analyzed. With this case study, we aim to examine if the proposed higher-order beam equations can capture correctly the additional flexibility of those straight box beams as well as the global responses. The second case study is concerned with the analysis of two box beams-joint systems with various joint angles and aspect ratios

of cross-sections. In this case study, the validity of the derived joint matching conditions of Eq. (4.79) will be mainly examined. It will test if the effects of the joint flexibility induced by higher-order deformations can be accurately captured by the proposed one-dimensional analysis approach.

All of the analysis results by the proposed approach are checked through comparing them with those of ABAQUS shell analysis, Timoshenko beam analysis, and also the analysis method by Jang and Kim [41] when applicable.

Case Study 1: Straight Thin-Walled Box Beams. In this case, we deal with the analysis of straight thin-walled box beams to check the accuracy of the newly derived HoBT. To this end, we ignore Beam 2 so that we can consider the situation where there is only Beam 1 in Fig. 4.2, a straight thin-walled box beam. For this case, the length (L) and the thickness (t) of Beam 1 are $L = 1000$ mm and $t = 2$ mm. The material properties of Beam 1 are Young's modulus $E = 200$ Gpa and Poisson's ratio $\nu = 0.3$. One end of Beam 1 is fixed as shown in Fig. 4.2, and the other end of Beam 1 is subjected to a transverse force $(F_x)_1 = 100$ N. The loaded end is assumed to be rigid. The examples with various cross-sections for this structure will be analyzed by using the finite element equations of one-dimensional higher-order beam theory given in Eq. (4.B4-4.B6), and the results will be compared with those by the mentioned other analysis approaches.

To obtain sufficiently converged results, 60 beam elements are used in one-dimensional beam analysis approaches for the modeling of Beam 1; although

various cross-sections with different widths and heights are considered, the converged results can be obtained by using 60 beam elements regardless of those changes. In two-dimensional shell analysis, $12.5\,\text{mm} \times 12.5\,\text{mm}$ square element is used for the modeling of Beam 1. The number of shell elements used is different depending on the dimensions of the cross-section, and to model Beam 1 with the width $b = 50$ mm and the height $h = 100$ mm, for example, $(4+8+4+8)\times 80 = 1920$ shell elements are used.

The analysis results for Beam 1 with $b = 50$ mm and $h = 100$ mm are given in Figs. 4.10(a-f). Each graph in Figs. 4.10(a-f) represents the magnitude of each field variable calculated along the z_1–axis. Only the results with respect to the rigid-body motion (U_z, U_x, θ_y) are considered among the results by Jang and Kim [41] because the shapes of the cross-sectional deformations considered in Jang and Kim [41] are somewhat different with (χ_1, W_1, χ_2) in this study. Observing the results based on those obtained by the shell analysis, one can find that the Timoshenko beam analysis cannot include the effects of the cross-sectional deformations although the bending rigidity of the box beam is correctly captured, and that the approach proposed by Jang and Kim [41] which includes the effects of the cross-sectional deformations cannot correctly express the bending rigidity of the box beam. Meanwhile, the proposed higher-order beam analysis can exactly

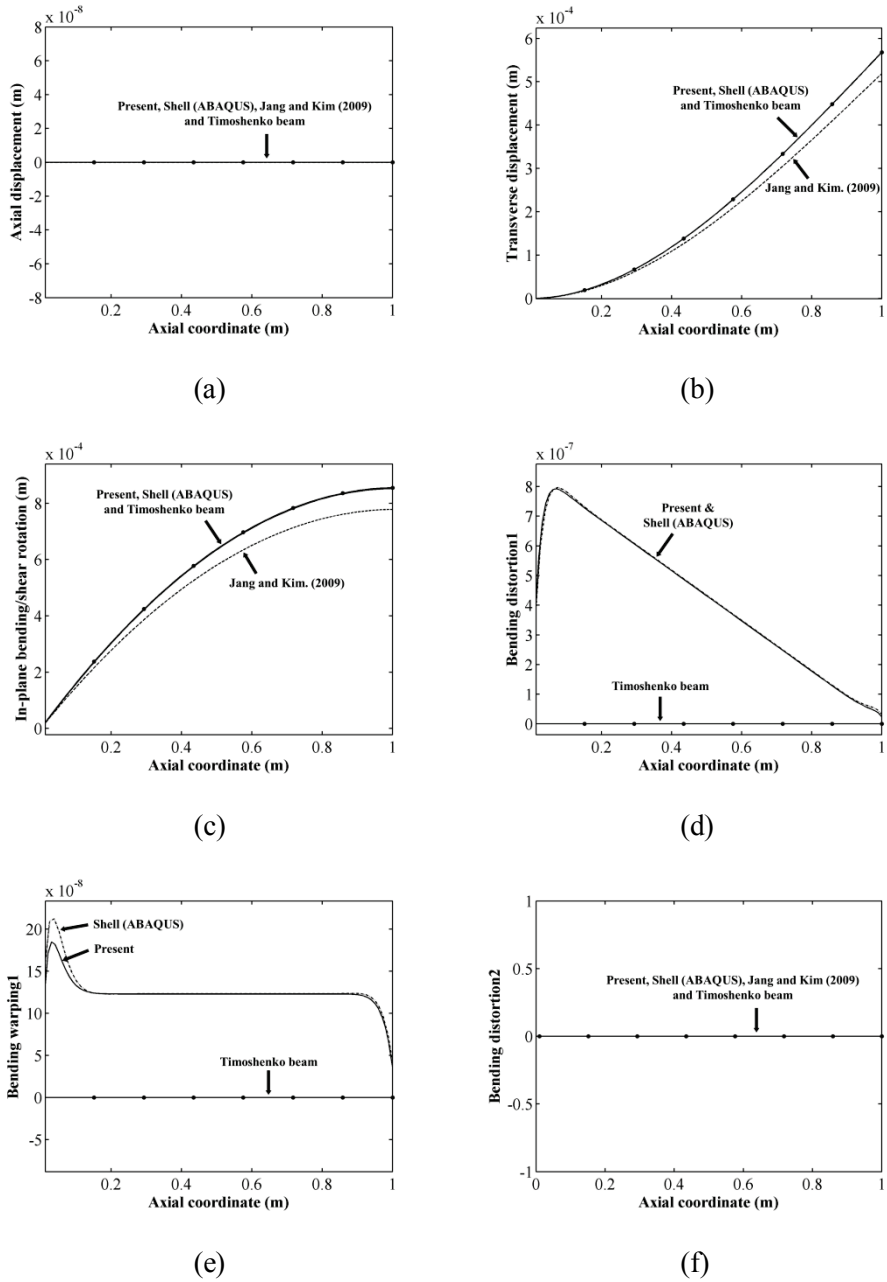

Fig. 4.10 Numerical results for the straight box beam (L=1000 mm, b=50 mm, h=100 mm, t=2 mm) under transverse force F_x =100 N: (a) axial displacement U_z, (b) transverse displacement U_x, (c) in-plane bending /shear rotation, (d) distortion χ_1, (e) warping W_1, (f) distortion χ_2.

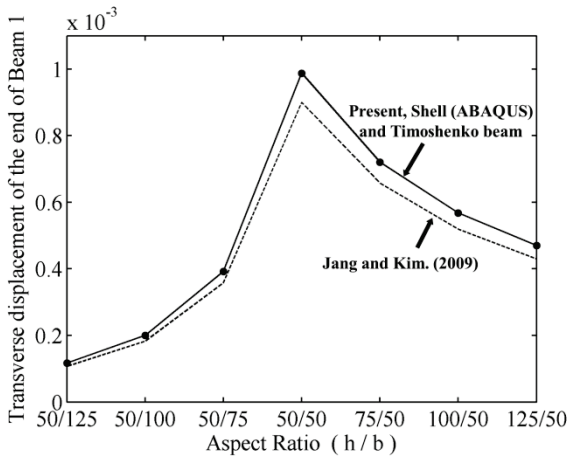

Fig. 4.11 Numerical results for the straight box beam (L=1000 mm, b=50 mm, h=100 mm, t=2 mm) under transverse force F_x =100 N: (a) axial displacement U_z, (b) transverse displacement U_x, (c) in-plane bending /shear rotation, (d) distortion χ_1, (e) warping W_1, (f) distortion χ_2

express not only the bending rigidity of the box beam but also the additional flexibility of the box beam by the cross-sectional deformations.

In sequence, the problems defined from the previous example by changing b and h of Beam 1 in a range from $b = 125$ mm, $h = 50$ mm ($h/b = 50/125$) to $b = 50$ mm, $h = 125$ mm ($h/b = 125/50$) are solved, and the results are given in Fig. 4.11. The graph in Fig. 4.11 represents the variation in the transverse displacement $(U_x)_1$ of the loaded end when the aspect ratio (h/b) of the cross-section is varied. From the results, one can find that the proposed higher-order beam analysis can provide the accurate bending behaviors for the box beams with cross-sections of various widths and heights.

Case Study 2: Two Box Beams-Joint Structures. The examples concerning the two thin-walled box beams-joint structures shown in Fig. 4.2 will be considered in the case study 2; the length (L) and thickness (t) of two beams are $L = 1000$ mm and $t = 2$ mm. The material properties of two beams are Young's modulus $E = 200$ Gpa and Poisson's ratio $\nu = 0.3$. One end of the structure is fixed as shown in Fig. 4.2, and the other end of the structure, denoted as D, is subjected to the in-plane bending moment $(M_y)_2 = 1\ \mathrm{N \cdot m}$. The loaded end is assumed to be rigid. The number of elements used to model the Beam k ($k = 1, 2$) is equal to that for Beam 1 in Case Study 1.

The problem with $b = 50$ mm, $h = 100$ mm for two beams and the joint angle $\phi = 90^\circ$ is considered for the first example, and the results are given in Fig. 4.12(a-f). The range of the axial coordinate ($k-1, k$) ($k = 1, 2$) in the each graph given in Fig. 4.12(a-f) represent the magnitude of each field variable for Beam k calculated along the axial direction. Likewise, the magnitudes of the rigid-body motions (U_z, U_x, θ_y) among the analysis results by Jang and Kim [41] are plotted in Fig. 4.12(a-c). Observing the results based on those from the shell analysis, it can be found that the Timoshenko beam analysis overestimates the stiffness of the structure as mentioned in Introduction. In contrast, one can find that the analysis methods proposed in this study and Jang and Kim [41] can express the flexibility of the structure more correctly because those methods consider the effects of the cross-sectional deformations. Especially it can be found that the accurate analysis

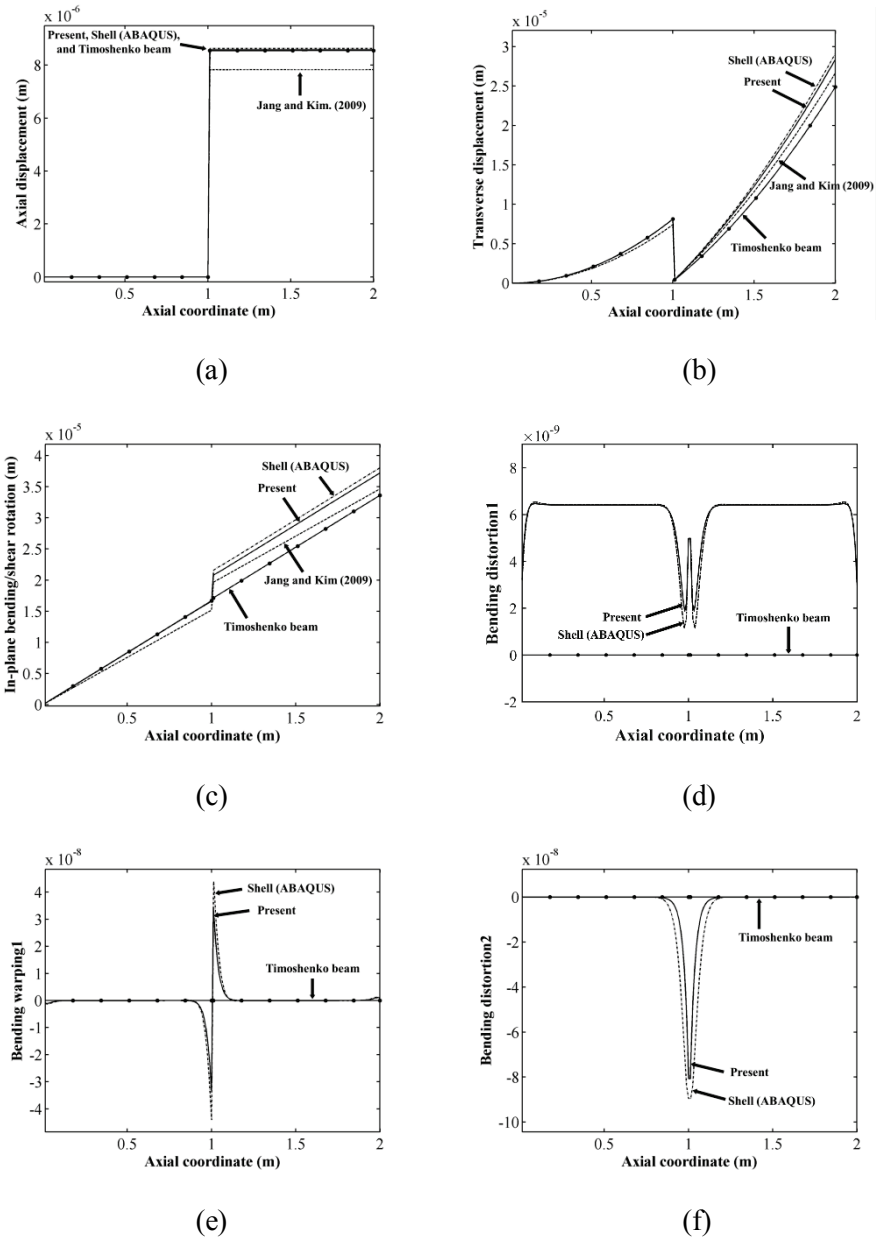

Fig. 4.12 Numerical results for the two thin-walled box beams-joint structure (L= 1000 mm, b=50 mm, h=100 mm, t=2 mm, ϕ=90º) under in-plane bending moment M_y =100 N·m: (a) axial displacement U_z, (b) transverse displacement U_x, (c) in-plane bending /shear rotation, (d) distortion χ_1, (e) warping W_1, (f) distortion χ_2.

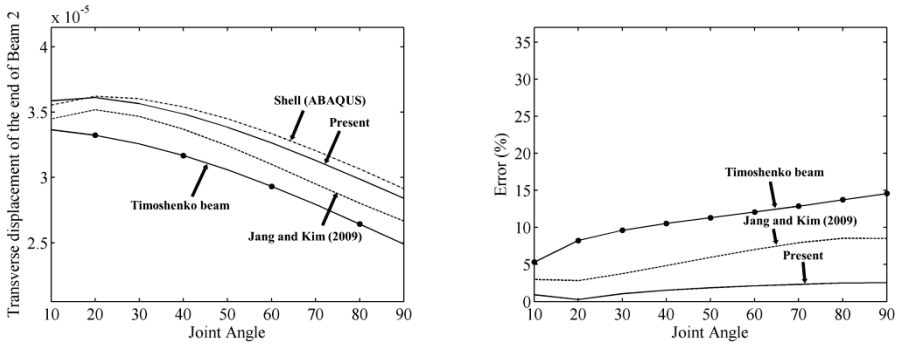

(a) (b)

Fig. 4.13 (*a*) Numerical results for the two box-beams-joint structures (L=1000 mm, b=50 mm, h=100 mm, t=2 mm) with various joint angles ϕ ranging 10° $\leq \phi \leq$90°, (*b*) percentage errors for the results of one-dimensional beam analyses given in Fig. 13(a) with respect to the result by the shell analysis

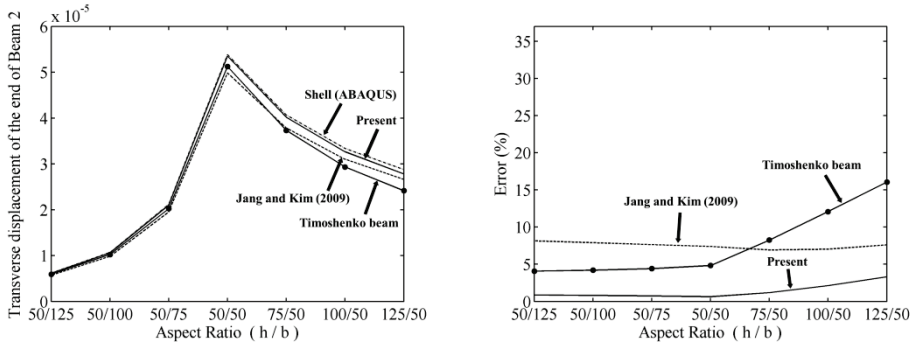

(a) (b)

Fig. 4.14 (*a*) Numerical results for the two box-beams-joint structures (L=1000 mm, t=2 mm, ϕ=90º) with various width (b) and heights (h) of the cross-secti on (or aspect ratios h/b) raging from b=125 mm, h=50 mm (h/b=50/125) to b=50 mm, h=125 mm (h/b=125/50), (*b*) percentage errors for the results of one-dimensional beam analyses given in Fig. 14(a) with respect to the result by the shell analysis

results which are almost equal to the results by the shell analysis can be obtained through the proposed approach.

Problems defined from the first example by changing ϕ in a range $10^\circ \le \phi \le 90^\circ$ are solved, and the results are given in Figs. 4.13(a, b). The graph in Fig. 4.13(a) represents the variation in the transverse displacement $(U_x)_2$ of the loaded end when the joint angle ϕ is varied. The percentage errors for the results of one-dimensional beam analyses are calculated based on the result by the shell analysis and are given in Fig. 4.13(b). From those results given in Figs. 4.13(a, b), it can be found that the proposed approach can provide the accurate results for the two box beams-joint structure with various joint angles.

Problems defined from the first example by changing the aspect ratio (*h*/*b*) in a range from $b = 125$ mm, $h = 50$ mm ($h/b = 50/125$) to $b = 50$ mm, $h =$ 125 mm ($h/b = 125/50$) are also considered and the results are given in Fig. 4.14(a, b). The graph in Fig. 4.14(a) represents the variation in the transverse displacement $(U_x)_2$ of the loaded end when the aspect ratio (*h*/*b*) is varied, and the graph given in Fig. 4.14(b) represents the percentage errors for the results of one-dimensional analyses with respect to the result by the shell analysis. From those results given in Figs. 4.14(a, b), one can also find that the proposed approach can give the accurate results for the two box beams-joint structure with various aspect ratios of the cross-section.

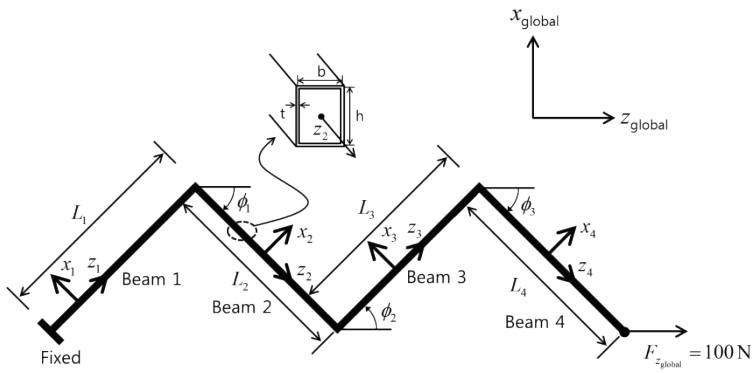

Fig. 4.15 Serially connected four box beams-joint structure (L=1000 mm, b=50 mm, h=100 mm, t=2 mm, ϕ_1= – 45º, ϕ_2=45º, ϕ_3= – 45º) subjected to in-plane force $F_{z_{\text{global}}} = 100\,\text{N}$

Case Study 3: Serially Connected Four Box Beams-Joint Structures. When several thin-walled box beams are serially connected in a zigzag form as shown in Fig. 4.15, the warping for Beam 2 and Beam 3 cannot be determined by Jang and Kim [41], and thus the structure given in Fig. 4.15 cannot be interpreted by Jang and Kim [41]. Therefore, it will be check whether the structure given in Fig. 4.15 can be interpreted by using the proposed approach. The length of those beams is $L = 1000$ mm, and the width (b), height (h), and thickness (t) of those beams are $b = 50$ mm, $h = 100$ mm, and $t = 2$ mm. The material properties of those beams are Young's modulus $E = 200$ Gpa and Poisson's ratio $\nu = 0.3$. The joint angles shown in Fig. 4.15 are $\phi_1 = -45^\circ$, $\phi_2 = 45^\circ$, $\phi_3 = -45^\circ$. One end of this structure is fixed, and the other end is subjected to the in-plane force $(F_z)_4 = (100/\sqrt{2})\,\text{N}$ and

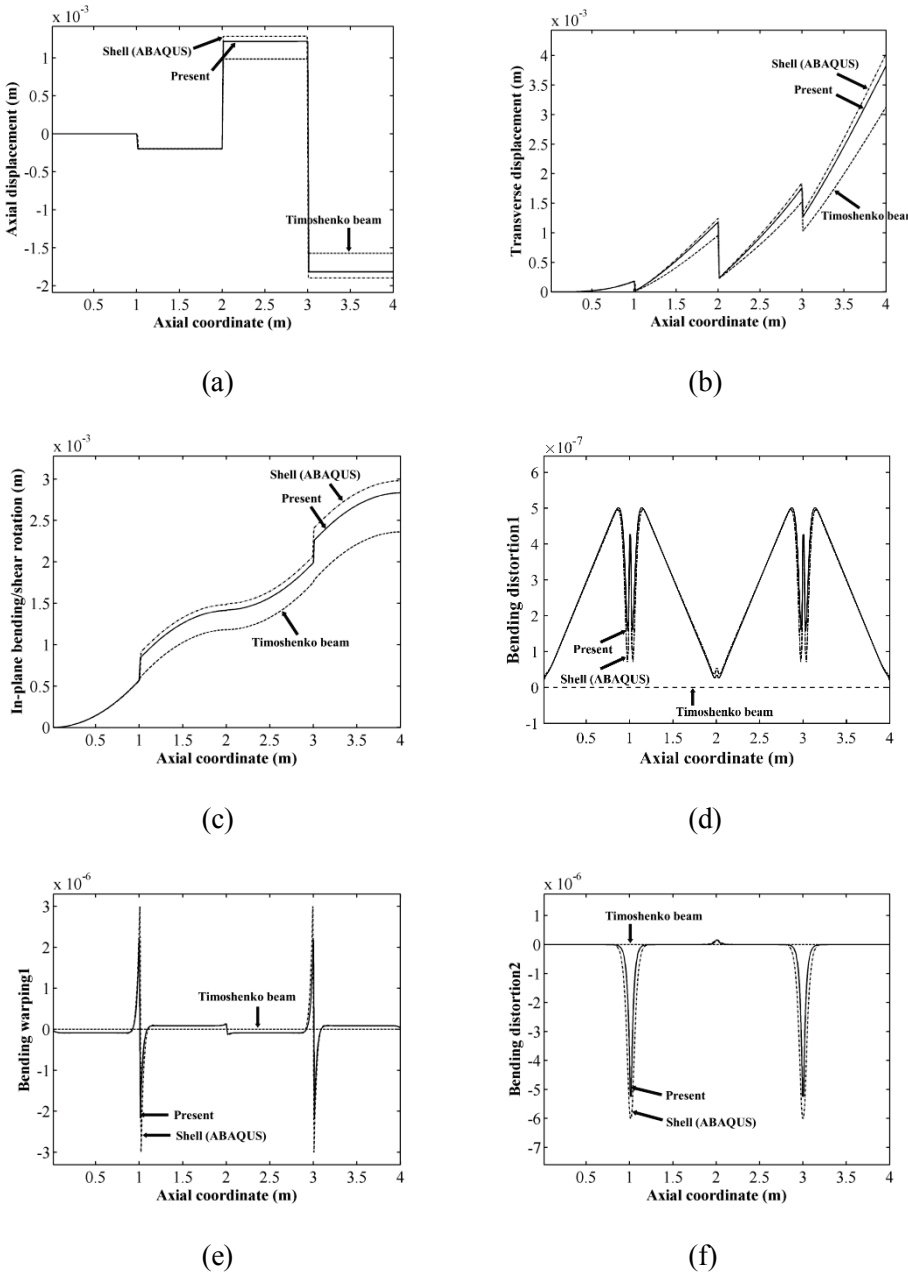

Fig. 4.16 Numerical results for the serially connected four box beams-joint structure given in Fig. 15: (*a*) axial displacement U_z, (*b*) transverse displacement U_x, (*c*) in-plane bending /shear rotation, (*d*) distortion χ_1, (*e*) warping W_1, (*f*) distortion χ_2.

$(F_x)_4 = (100/\sqrt{2})\,\mathrm{N}$. The loaded end is assumed to be rigid. The number of elements used to model the Beam k ($k = 1, 2, 3, 4$) is equal to that for Beam 1 in Case Study 1.

The results for the considered example are given in Fig. 4.16(a-f). The range of the axial coordinate ($k-1, k$) ($k = 1, 2, 3, 4$) in the each graph given in Fig. 4.16(a-f) represent the magnitude of each field variable for Beam k calculated along the axial direction. Observing the results based on those obtained by the shell analysis, it can be found that the proposed approach can provide the correct result even though more complicated structure is considered.

4.6 Conclusions

The exact one-dimensional beam analysis method applicable to the two thin-walled box beams-joint structures subjected to in-plane loads is established. To deal with the effects of the cross-sectional deformations on the flexibility of the box-beams joint structures, we first identified the dominant cross-sectional deformations and their shapes theoretically, and then we newly defined the higher-order beam theory employing those dominant cross-sectional deformations as the additional field variables. With respect to the development of the one-dimensional analysis method for the box beams-joint structures, the key is determining the mechanically correct joint matching conditions among the field variables. In this regard, the joint matrix $\mathbf{T}$ representing the joint matching conditions was employed in this study, and the

closed form of the matrix $\mathbf{T}$ was exactly derived by utilizing the essential conditions that $\mathbf{T}$ should hold. Various numerical examples were considered to check the validity of the higher-order beam theory and the joint matching conditions proposed in this study, and we demonstrated through these numerical examples that the proposed higher-order beam theory can express both the bending rigidity and the additional flexibility of the box beams accurately, and that the proposed joint matching conditions can consistently represent the exact flexibility of the joint of the box beams-joint structure with various aspect ratios of the beam cross-section and various joint angles. The theoretical approaches proposed in this study to determine the exact joint matching conditions for the exact shapes of the cross-sectional deformations are expected to serve as important building blocks in the expansion of the higher-order beam analyses for arbitrary shaped thin-walled beams-joint structures.

Appendix A

The explicit expressions of the shape functions $\psi_p^\alpha(s)$ ($p = n, s, z$; $\alpha = U_z, U_x, \theta_y, \chi_1, W_1, \chi_2$) are given below. As mentioned in Section 3, $\psi_p^\alpha(s_j)$ ($j = 1, 2, 3, 4$) represents the shape function defined on Edge j of the cross-section, and the coordinate s_j measured from the center of Edge j has the following range: $-\frac{h}{2} \le s_1, s_3 \le \frac{h}{2}$ and $-\frac{b}{2} \le s_2, s_4 \le \frac{b}{2}$.

$$\psi_z^{U_z}(s_j) = 1 \qquad \text{(for } j = 1,\ 2,\ 3,\ 4) \tag{4.A1}$$

$$\begin{aligned} &\psi_n^{U_x}(s_j) = (-1)^{(j-1)/2} \quad \text{(for } j = 1,\ 3) \quad \text{and} \quad 0 \qquad \text{(for } j = 2,\ 4) \\ &\psi_s^{U_x}(s_j) = 0 \qquad\qquad \text{(for } j = 1,\ 3) \quad \text{and} \quad (-1)^{(j)/2} \quad \text{(for } j = 2,\ 4) \end{aligned} \tag{4.A2}$$

$$\psi_z^{\theta_y}(s_j) = (-1)^{(j+1)/2}\frac{b}{2} \ \text{(for } j = 1,\ 3) \quad \text{and} \quad (-1)^{(j-2)/2} s_j \ \text{(for } j = 2,\ 4) \tag{4.A3}$$

$$\begin{aligned} \psi_n^{\chi_1}(s_j) &= (-1)^{(j-1)/2} \times \{\frac{3}{h^4}s_j^4 - \frac{9}{2h^2}s_j^2 + \frac{8b^2+15h^2}{16h^2}\} && \text{(for } j = 1,\ 3) \\ &= (-1)^{(j)/2} \times \{\frac{3}{h}s_j\} && \text{(for } j = 2,\ 4) \\ \psi_s^{\chi_1}(s_j) &= (-1)^{(j-1)/2} \times \{(\frac{6}{h^2}) \times (\frac{b}{2}s_j)\} && \text{(for } j = 1,\ 3) \\ &= (-1)^{(j)/2} \times \{(\frac{6}{h^2}) \times (\frac{1}{2}s_j^2 - \frac{b^2}{24})\} && \text{(for } j = 2,\ 4) \end{aligned} \tag{4.A4}$$

$$\begin{aligned} \psi_z^{W_1}(s_j) &= (-1)^{(j-1)/2} \times (\frac{16}{bh^2}) \times \{-\frac{b}{4}s_j^2 + \frac{b(-2b^3+15bh^2+15h^3)}{240(b+3h)}\} && \text{(for } j = 1,\ 3) \\ &= (-1)^{(j-2)/2} \times (\frac{16}{bh^2}) \times \{\frac{1}{6}s_j^3 + \frac{-b^3-5b^2h+10h^3}{40(b+3h)}s_j\} && \text{(for } j = 2,\ 4) \end{aligned}$$

(4.A5)

$$\begin{aligned} \psi_n^{\chi_2}(s_j) &= \frac{384(b+h)}{h^4(5b+h)} \times \{-\frac{1}{24}s_j^4 + \frac{h^2(3b+h)}{48(b+h)}s_j^2 - \frac{h^4(5b+h)}{384(b+h)}\} && \text{(for } j = 1,\ 3) \\ &= \frac{384(b+h)}{h^4(5b+h)} \times \{-\frac{h^3}{24(b+h)}s_j^2 + \frac{b^2h^3}{96(b+h)}\} && \text{(for } j = 2,\ 4) \\ \psi_s^{\chi_2}(s_j) &= 0 && \text{(for } j = 1,\ 2,\ 3,\ 4) \end{aligned}$$

(4.A6)

One can show the following orthogonality conditions among ($\psi_z^{U_z}$, $\psi_z^{\theta_y}$, $\psi_z^{W_1}$):

$$\iint_S \psi_z^{\theta_x}(s)\cdot\psi_z^{W}(s)\ dsdn = \sum_{j=1}^{4}\{\iint_{Edge\ j} \psi_z^{\theta_x}(s_j)\cdot\psi_z^{W}(s_j)\ dsdn\} = 0$$

$$\iint_S \psi_z^{\alpha_1}(s)\cdot\psi_z^{\alpha_2}(s)\ dsdn = \sum_{j=1}^{4}\{\iint_{Edge\ j} \psi_z^{\alpha_1}(s_j)\cdot\psi_z^{\alpha_2}(s_j)\ dsdn\} = 0 \qquad (4.A7)$$

$$(\alpha_1 = U_z,\ \theta_y,\ W_1;\ \alpha_2 = U_z,\ \theta_y,\ W_1;\ \alpha_1 \neq \alpha_2)$$

, and one can also show the following orthogonality conditions between ($\psi_s^{U_x}$, $\psi_s^{\chi_1}$):

$$\iint_S \psi_s^{U_x}(s)\cdot\psi_s^{\chi_1}(s)\ dsdn = \sum_{j=1}^{4}\{\iint_{Edge\ j} \psi_s^{U_x}(s_j)\cdot\psi_s^{\chi_1}(s_j)\ dsdn\} = 0 \qquad (4.A8)$$

Appendix B

Employing the displacement ($\tilde{u}_n, \tilde{u}_s, \tilde{u}_z$), the strain ($\varepsilon_{ss}, \varepsilon_{zz}, \gamma_{sz}$) and the stress ($\sigma_{ss}, \sigma_{zz}, \sigma_{sz}$) given in Eqs. (4.2-4), the total potential energy of the straight thin-walled box beam ($z_1 < z < z_2$) can be written as:

$$\begin{aligned}
\mathbf{\Pi} &= \frac{1}{2}\int_{z_1}^{z_2}\int_S \sigma_{ij}\varepsilon_{ij}\ dA\,dz - \int_S (\sigma_{zz}\tilde{u}_z + \sigma_{zs}\tilde{u}_s)_{z_1}^{z_2}\ dA \\
&= \frac{1}{2}\int_{z_1}^{z_2}\{EJ_{F_z}(U_z')^2 + E_1J_{M_y}\{(\theta_y')^2 - 2v(\theta_y')(\frac{6}{h^2}\chi_1) + (\frac{6}{h^2}\chi_1)^2\} \\
&\quad + E_1J_{B_1}(W_1')^2 + E_1C_1(\chi_1)^2 + E_1C_2(\chi_2)^2 \qquad (4.B1) \\
&\quad + GJ_{F_x}(U_x' - \theta_y - \frac{4(b^3+15h^3)}{15bh^2(b+3h)}W_1)^2 + GJ_{Q_1}(\chi_1' - \frac{8}{3b}W_1)^2 \\
&\quad + 4GC_3(\chi_1')^2 + 4GJ_{Q_2}(\chi_2')^2\}dz \\
&\quad - [F_zU_z + F_xU_x + M_y\theta_y + Q_1\chi_1 + B_1W_1 + Q_2\chi_2]_{z_1}^{z_2}
\end{aligned}$$

where the potential energy expressed by the second derivatives of the field

variables $\mathbf{U}$ such as (U_x'', χ_1'', χ_2'') are not considered since the linear shape function $\mathbf{N}$ will be employed (see Eq. (4.B2)), The relations $\dot{\psi}_z^{\theta_y} = -\psi_s^{U_x}$, $\dot{\psi}_s^{\chi_1} = -\frac{6}{h^2}\psi_z^{\theta_y}$ and $\dot{\psi}_z^{W_1} = -\frac{4(b^3+5h^3)}{15bh^2(b+3h)}\psi_s^{U_x} - \frac{16}{6b}\psi_s^{\chi_1}$ (see Appendix A) are considered in the derivation of the potential energy above. The symbol J_β ($\beta = F_z, F_x, M_y, Q_1, B_1, Q_2$) in Eq. (4.B1) represents the moment of inertia for the generalized force β, and the expressions of $J_{F_z}, J_{F_x}, J_{M_y}, J_{Q_1}, J_{B_1}, J_{Q_2}, C_1, C_2$ and C_3 are given as:

$$J_{F_z} = \iint_S (\psi_z^{U_z})^2\, dsdn = 2t(b+h), \qquad J_{F_x} = \iint_S (\psi_s^{U_x})^2\, dsdn = 2bt,$$

$$J_{M_y} = \iint_S (\psi_z^{\theta_y})^2\, dsdn = \frac{b^2t(b+3h)}{6}, \qquad J_{Q_1} = \iint_S (\psi_s^{\chi_1})^2\, dsdn = \frac{b^2t(b^3+15h^3)}{10h^4},$$

$$J_{B_1} = \iint_S (\psi_z^{W_1})^2\, dsdn = \frac{8t(b^6+10b^5h-70b^3h^3+210bh^5+105h^6)}{1575h^4(b+3h)},$$

$$J_{Q_2} = \iint_S (n\cdot\dot{\psi}_n^{\chi_2})^2\, dsdn = \frac{128t^3(2h^3+18bh^2+51b^2h+35b^3)}{315h^2(5b+h)^2}$$

$$C_1 = \iint_S (n\cdot\ddot{\psi}_n^{\chi_1})^2\, dsdn = \frac{36t^3}{5h^3}, \qquad C_2 = \iint_S (n\cdot\ddot{\psi}_n^{\chi_2})^2\, dsdn = \frac{512t^3(h^2+7bh+6b^2)}{15h^3(5b+h)^2}$$

$$C_3 = \iint_S (n\cdot\dot{\psi}_n^{\chi_1})^2\, dsdn = \frac{t^3(102h+210b)}{35h^2}$$

(4.B2)

According to Refs. [7, 49], the field variables $\mathbf{U}(z)$ of the one-dimensional box beam element ($z_1 < z < z_2$) can be written with respect to the nodal displacement vector $\mathbf{d}$ and the linear shape function $\mathbf{N}$ (ξ represent a non-dimensional coordinate in z direction, and has the range $-1 \le \xi \le 1$ in the box

beam element).

$$\mathbf{U}(z) = \mathbf{N} \cdot \mathbf{d};$$

$$\begin{Bmatrix} U_z(z) \\ U_x(z) \\ \theta_y(z) \\ \chi_1(z) \\ W_1(z) \\ \chi_2(z) \end{Bmatrix} = \begin{bmatrix} \frac{1-\xi}{2} & 0 & 0 & 0 & 0 & 0 & \frac{1+\xi}{2} & 0 & 0 & 0 & 0 & 0 \\ 0 & \frac{1-\xi}{2} & 0 & 0 & 0 & 0 & 0 & \frac{1+\xi}{2} & 0 & 0 & 0 & 0 \\ 0 & 0 & \frac{1-\xi}{2} & 0 & 0 & 0 & 0 & 0 & \frac{1+\xi}{2} & 0 & 0 & 0 \\ 0 & 0 & 0 & \frac{1-\xi}{2} & 0 & 0 & 0 & 0 & 0 & \frac{1+\xi}{2} & 0 & 0 \\ 0 & 0 & 0 & 0 & \frac{1-\xi}{2} & 0 & 0 & 0 & 0 & 0 & \frac{1+\xi}{2} & 0 \\ 0 & 0 & 0 & 0 & 0 & \frac{1-\xi}{2} & 0 & 0 & 0 & 0 & 0 & \frac{1+\xi}{2} \end{bmatrix} \begin{Bmatrix} U_z(z_1) \\ U_x(z_1) \\ \theta_y(z_1) \\ \chi_1(z_1) \\ W_1(z_1) \\ \chi_2(z_1) \\ U_z(z_2) \\ U_x(z_2) \\ \theta_y(z_2) \\ \chi_1(z_2) \\ W_1(z_2) \\ \chi_2(z_2) \end{Bmatrix} \tag{4.B3}$$

Deriving the one-dimensional finite element equation for the straight box beam element through the principle of minimum total potential energy, the resulting matrix equation is written in the following form:

$$\mathbf{f} = \mathbf{K} \cdot \mathbf{d} \tag{4.B4}$$

where $\mathbf{f}$ represent the nodal force vector, and is written as:

$$\begin{aligned} \mathbf{f} = \{ & F_z(z_1),\ F_x(z_1),\ M_y(z_1),\ Q_1(z_1),\ B_1(z_1),\ Q_2(z_1),\ F_z(z_2), \\ & F_x(z_2),\ M_y(z_2),\ Q_1(z_2),\ B_1(z_2),\ Q_2(z_2)\}^{\mathrm{T}} \end{aligned} \tag{4.B5}$$

, and the stiffness matrix $\mathbf{K}$ derived from the procedure above is written as:

$$\mathbf{K} = \begin{bmatrix} \mathbf{K}_{11} & \mathbf{K}_{12} \\ sym & \mathbf{K}_{22} \end{bmatrix} \tag{4.B6}$$

where the definitions of submatrix $\mathbf{K}_{11}$, $\mathbf{K}_{12}$ and $\mathbf{K}_{22}$ are as

$$
\mathbf{K}_{11} = \begin{bmatrix}
\frac{EJ_{F_z}}{l} & 0 & 0 & 0 & 0 & 0 \\
 & \frac{GJ_{F_x}}{l} & \frac{GJ_{F_x}}{2} & 0 & \frac{(b^3+15h^3)GJ_{F_x}}{15bh^2(b+3h)} & 0 \\
 & & \frac{lGJ_{F_x}}{3} + \frac{E_1J_{M_y}}{l} & \frac{3\nu E_1J_{M_y}}{h^2} & \frac{2(b^3+15h^3)lGJ_{F_x}}{45bh^2(b+3h)} & 0 \\
 & & & \frac{GJ_{Q_1}}{l} + \frac{lE_1C_1}{3} + \frac{12lE_1J_{M_y}}{h^4} + \frac{4GJ_{C_3}}{l} & \frac{2GJ_{Q_1}}{3b} & 0 \\
\text{sym} & & & & \frac{16(b^3+15h^3)^2 lGJ_{F_x}}{675b^2h^4(b+3h)^2} + \frac{64lGJ_{Q_1}}{27b^2} + \frac{E_1J_{B_1}}{l} & 0 \\
 & & & & & \frac{4GJ_{Q_2}}{l}
\end{bmatrix} \tag{4.B7a}
$$

$$
\mathbf{K}_{12} = \begin{bmatrix}
-\frac{EJ_{F_z}}{l} & 0 & 0 & 0 & 0 & 0 \\
0 & -\frac{GJ_{F_x}}{l} & \frac{GJ_{F_x}}{2} & 0 & \frac{(b^3+15h^3)GJ_{F_x}}{15bh^2(b+3h)} & 0 \\
0 & -\frac{GJ_{F_x}}{2} & \frac{lGJ_{F_x}}{6} - \frac{E_1J_{M_y}}{l} & \frac{3\nu E_1J_{M_y}}{h^2} & \frac{(b^3+15h^3)lGJ_{F_x}}{45bh^2(b+3h)} & 0 \\
0 & 0 & -\frac{3\nu E_1J_{M_y}}{h^2} & -\frac{GJ_{Q_1}}{l} + \frac{lE_1C_1}{6} + \frac{6lE_1J_{M_y}}{h^4} - \frac{4GJ_{C_3}}{l} & \frac{2GJ_{Q_1}}{3b} & 0 \\
-\frac{(b^3+15h^3)GJ_{F_x}}{15bh^2(b+3h)} & \frac{(b^3+15h^3)lGJ_{F_x}}{45bh^2(b+3h)} & & -\frac{2GJ_{Q_1}}{3b} & \frac{8(b^3+15h^3)^2 lGJ_{F_x}}{675b^2h^4(b+3h)^2} + \frac{32lGJ_{Q_1}}{27b^2} - \frac{E_1J_{B_1}}{l} & 0 \\
0 & 0 & 0 & 0 & 0 & -\frac{4GJ_{Q_2}}{l}
\end{bmatrix} \tag{4.B7b}
$$

$$
\mathbf{K}_{22} = \begin{bmatrix}
\frac{EJ_{F_z}}{l} & 0 & 0 & 0 & 0 & 0 \\
 & \frac{GJ_{F_x}}{l} & -\frac{GJ_{F_x}}{2} & 0 & -\frac{(b^3+15h^3)GJ_{F_x}}{15bh^2(b+3h)} & 0 \\
 & & \frac{lGJ_{F_x}}{3} + \frac{E_1J_{M_y}}{l} & -\frac{3\nu E_1J_{M_y}}{h^2} & \frac{2(b^3+15h^3)lGJ_{F_x}}{45bh^2(b+3h)} & 0 \\
 & & & \frac{GJ_{Q_1}}{l} + \frac{lE_1C_1}{3} + \frac{12lE_1J_{M_y}}{h^4} + \frac{4GJ_{C_3}}{l} & -\frac{2GJ_{Q_1}}{3b} & 0 \\
\text{sym} & & & & \frac{16(b^3+15h^3)^2 lGJ_{F_x}}{675b^2h^4(b+3h)^2} + \frac{64lGJ_{Q_1}}{27b^2} + \frac{E_1J_{B_1}}{l} & 0 \\
 & & & & & \frac{4GJ_{Q_2}}{l}
\end{bmatrix} \tag{4.B7c}
$$

where the symbol l represents the length of the box beam element ($l = z_2 - z_1$), and the symbol E_1 refers to $E_1 = \dfrac{E}{1-\nu^2}$.

Appendix C

According to the higher-order beam theory, the dominant stress (σ_{zz}, σ_{zs}) generated on the contour line ($n = 0$) of the cross-section can be written as:

$$\sigma_{zz}(s, z) = E(\psi_z^{U_z} \cdot U_z{}') + \frac{E}{1-\nu^2}(\psi_z^{\theta_y} \cdot \theta_y{}' + \psi_z^{W_1} \cdot W_1' + \nu\dot{\psi}_s^{\chi_1} \cdot \chi_1) \qquad (4.C1a)$$

$$\sigma_{sz}(s, z) = G(\ \psi_s^{U_x} \cdot U_x{}' + \psi_s^{\chi_1} \cdot \chi_1{}' + \dot{\psi}_z^{\theta_y} \cdot \theta_y + \dot{\psi}_z^{W_1} \cdot W_1\ ) \qquad (4.C1b)$$

The derivative terms ($\dot{\psi}_z^{\theta_y}, \dot{\psi}_s^{\chi_1}, \dot{\psi}_z^{W_1}$) in Eqs. (4.C1a, b) can be related with other shape functions ($\psi_s^{U_x}, \psi_z^{\theta_y}, \psi_s^{\chi_1}, \psi_z^{W_1}$) as $\dot{\psi}_z^{\theta_y} = -\psi_s^{U_x}$, $\dot{\psi}_s^{\chi_1} = -\frac{6}{h^2}\psi_z^{\theta_y}$, and $\dot{\psi}_z^{W_1} = -\frac{4(b^3+5h^3)}{15bh^2(b+3h)}\psi_s^{U_x} - \frac{16}{6b}\psi_s^{\chi_1}$ (See Appendix A), and thus Eqs. (4.C1a) and (C1b) can be rewritten as below.

$$\sigma_{zz}(s, z) = E(\psi_z^{U_z} \cdot U_z{}') + \frac{E}{1-\nu^2}\{\psi_z^{\theta_y} \cdot (\theta_y{}' - \nu\frac{6}{h^2}\chi_1) + \psi_z^{W_1} \cdot W_1'\} \qquad (4.C2a)$$

$$\sigma_{sz}(s, z) = G[\ \psi_s^{U_x} \cdot \{U_x{}' - \theta_y - \frac{4(b^3+5h^3)}{15bh^2(b+3h)}W_1\} + \psi_s^{\chi_1} \cdot \{\chi_1{}' - \frac{16}{6b}W_1\}] \qquad (4.C2b)$$

Substituting (σ_{zz}, σ_{zs}) in Eqs. (4.C2a, b) into the definitions of generalized forces $\mathbf{F}$ given in Eq. (4.6) and carrying out the surface integral for the cross-section *S*, one can obtain the following relations between the generalized forces $\mathbf{F}$ and the field variables $\mathbf{U}$.

$$
\begin{aligned}
F_z(z) &= \iint_S \sigma_{zz}(s,\, z)\cdot\psi_z^{U_z}(s)\; dsdn \\
&= \iint_S E[\psi_z^{U_z}\cdot\psi_z^{U_z}\cdot\{U_z{}'\}] + \frac{E}{1-\nu^2}[\,\psi_z^{\theta_y}\cdot\psi_z^{U_z}\cdot\{\theta_y{}' - \nu\frac{6}{h^2}\chi_1\} \\
&\qquad + \psi_z^{W_1}\cdot\psi_z^{U_z}\cdot\{W_1{}'\}]dsdn \qquad\qquad (4.C3a) \\
&= \iint_S E[\psi_z^{U_z}\cdot\psi_z^{U_z}\cdot\{U_z{}'\}]\; dsdn \\
&= EJ_{F_z}\{U_z{}'(z)\}
\end{aligned}
$$

The second line in Eq. (4.C3a) can be reduced as the third line by the orthogonality conditions such as $\iint_S \psi_z^{\theta_y}\cdot\psi_z^{U_z}\; dsdn = 0$ and $\iint_S \psi_z^{W_1}\cdot\psi_z^{U_z}\; dsdn = 0$ (See Appendix A). Moreover, the orthogonality condition between ($\psi_s^{U_x}, \psi_s^{\chi_1}$) can be also considered as given in Appendix A, and considering those orthogonality conditions, the remained generalized forces except Q_2 can be express as:

$$
F_x(z) = \iint_S \sigma_{zs}(s,\, z)\cdot\psi_s^{U_x}(s)\; dsdn = GJ_{F_x}\{U_x{}'(z) - \theta_y(z) - \frac{4(b^3+5h^3)}{15bh^2(b+3h)}W_1(z)\}
$$

(4.C3b)

$$
M_y(z) = \iint_S \sigma_{zz}(s,\, z)\cdot\psi_z^{\theta_y}(s)\; dsdn = \frac{E}{1-\nu^2}J_{M_y}\{\theta_y{}'(z) - \nu\frac{6}{h^2}\chi_1(z)\} \quad (4.C3c)
$$

$$
Q_1(z) = \iint_S \sigma_{zs}(s,\, z)\cdot\psi_s^{\chi_1}(s)\; dsdn = GJ_{Q_1}\{\chi_1{}'(z) - \frac{16}{6b}W_1(z)\} \qquad (4.C3d)
$$

$$
B_1(z) = \iint_S \sigma_{zz}(s,\, z)\cdot\psi_z^{W_1}(s)\; dsdn = \frac{E}{1-\nu^2}J_{B_1}\{W_1'(z)\} \qquad (4.C3e)
$$

where J_β ($\beta = F_z, F_x, M_y, Q_1, B_1$) represent the moment of inertia for the generalized force β, and the explicit expressions for J_β are given in Appendix

B.

Substituting those results given in Eq. (4.C3) into Eq. (4.C2), (σ_{zz}, σ_{zs}) on the contour line can be expressed in terms of the generalized forces as:

$$\sigma_{zz}(s,\, z) = \sigma_{zz}^{F_z} + \sigma_{zz}^{M_y} + \sigma_{zz}^{B_1} = \frac{F_z(z)}{J_{F_z}}\psi_z^{U_z}(s) + \frac{M_y(z)}{J_{M_y}}\psi_z^{\theta_y}(s) + \frac{B_1(z)}{J_{B_1}}\psi_z^{W_1}(s) \quad \text{(4.C4a)}$$

$$\sigma_{sz}(s,\, z) = \sigma_{zs}^{F_x} + \sigma_{zs}^{Q_1} = \frac{F_x(z)}{J_{F_x}}\psi_s^{U_x}(s) + \frac{Q_1(z)}{J_{Q_1}}\psi_s^{\chi_1}(s) \quad \text{(4.C4b)}$$

where σ^{β} ($\beta = F_z,\, F_x,\, M_y,\, Q_1,\, B_1$) represent the stress on the contour line produced by the generalized force β. Therefore, one can define the edge resultants of β generated on each edge by using σ^{β}.

Meanwhile, the definition of Q_2 given in Eq. (4.6) is different with those considered above because χ_2, the work conjugate of Q_2, represents the deformations only in n direction. Unlike the procedure introduced above, thus, $\sigma_{zs}(n,\, s,\, z)$ given in Eq. (4.4c) should be substituted into the definition of Q_2 in Eq. (4.6), and through that the following result can be obtained.

$$
\begin{aligned}
Q_2 &= \iint_S \sigma_{zs}(-n\dot{\psi}_n^{\chi_2})\ dsdn \\
&= \iint_S G\{\psi_s^{U_x}\cdot(-n\dot{\psi}_n^{\chi_2})\cdot U_x{}' + \psi_s^{\chi_1}\cdot(-n\dot{\psi}_n^{\chi_2})\cdot \chi_1{}' \\
&\qquad + \dot{\psi}_z^{\theta_y}\cdot(-n\dot{\psi}_n^{\chi_2})\cdot\theta_y + \dot{\psi}_z^{W_1}\cdot(-n\dot{\psi}_n^{\chi_2})\cdot W_1 \\
&\qquad + (-2n\dot{\psi}_n^{\chi_1})\cdot(-n\dot{\psi}_n^{\chi_2})\cdot\chi_1{}' + (-2n\dot{\psi}_n^{\chi_2})\cdot(-n\dot{\psi}_n^{\chi_2})\cdot\chi_2{}'\}\,dsdn \\
&= \iint_S G[(-2n\dot{\psi}_n^{\chi_2})\cdot(-n\dot{\psi}_n^{\chi_2})\cdot\{\chi_2{}'\}]\ dsdn \\
&= 2GJ_{Q_2}\{\chi_2{}'(z)\}
\end{aligned}
\tag{4.C5}
$$

The second line in Eq. (4.C5) can be reduced as the third line because most of the integral terms in the second line are eliminated through the integral in n direction or by the orthogonal condition such as $\iint_S (\dot{\psi}_n^{\chi_1})\cdot(\dot{\psi}_n^{\chi_2})\ dsdn = 0$. The symbol J_{Q_2} in Eq. (4.C5) represents the moment of inertia for Q_2 and the definition of J_{Q_2} is given in Appendix B. When the result given in Eq. (4.C5) is substituted into Eq. (4.6c), the stress $\sigma_{sz}^{Q_2}$ generated by Q_2 can be also obtained as:

$$
\sigma_{sz}^{Q_2}(n, s, z) = \frac{Q_2(z)}{J_{Q_2}}\{-n\dot{\psi}_n^{\chi_2}(s)\} \tag{4.C6}
$$

To investigate the meanings of the equilibrium conditions given in Eqs. (4.76a, b), the edge resultants generated by (M_y, B_1, Q_2) will be defined by utilizing ($\sigma_{zz}^{M_y}$, $\sigma_{zz}^{B_1}$, $\sigma_{sz}^{Q_2}$) in Eqs. (4.C4) and (4.C6). According to Choi and Kim [43], the non-zero resultants on Edge j ($j = 1, 2, 3, 4$) determined by σ^{β_1} ($\beta_1 = M_y, B_1$) are axial force $F_{z(j)}^{\beta}$, tangential force $F_{s(j)}^{\beta}$, and normal moment $M_{n(j)}^{\beta}$, and can be defined as below.

$$F_{z(j)}^{\beta} = \iint_{Edge\,j} \sigma_{zz}^{\beta}\, dsdn, \quad F_{s(j)}^{\beta} = \iint_{Edge\,j} \sigma_{zs}^{\beta}\, dsdn, \quad M_{n(j)}^{\beta} = \iint_{Edge\,j} s \cdot \sigma_{zz}^{\beta}\, dsdn \quad (4.C7)$$

As with Choi and Kim [43], the distribution of $\sigma_{zz}^{M_y}$ represented by $\psi_z^{\theta_y}$ is simply expressed in terms of the constant or the linear function on each edge as given in Appendix A, and thus the edge resultants of M_y shown in Fig. 4.8 can be obtained by substituting $\sigma_{zz}^{M_y}$ in Eq. (4.C4a) into Eq. (4.C7). On the contrary, the distribution of $\sigma_{zz}^{B_1}$ represented by $\psi_z^{W_1}$ is expressed by the highly complicated polynomial functions as given in Appendix A. For this reason, as in Session 4.2, care should be taken when the edge resultants of B_1 are determined; otherwise, underestimated edge resultants are calculated, and thus the incorrect equilibrium conditions concerning (M_y, B_1, Q_2) which is different with those given in Eqs. (4.76a, b) is derived.

To calculate the correct edge resultants of B_1, the following $\bar{\sigma}_{zz}^{B_1}$ is employed instead of $\sigma_{zz}^{B_1}$ given in Eq. (4.C4a).

$$\bar{\sigma}_{zz}^{B_1}(s, z) = \frac{B_1(z)}{\bar{J}_{B_1}} \bar{\psi}_z^{W_1}(s) \quad (4.C8a)$$

where $\bar{\psi}_z^{W_1}(s_j)$ ($j = 1, 2, 3, 4$) represents the average distribution of $\sigma_{zz}^{B_1}$ on Edge *j*, and is defined as:

$$\bar{\psi}_z^{W_1}(s_j) = (-1)^{(j-1)/2} \times \frac{2b(5h^2 - b^2)}{15h(b+3h)} \quad (\text{for } j = 1, 3) \quad (4.C8b)$$

$$\bar{\psi}_z^{W_1}(s_j) = (-1)^{(j-2)/2} \times \frac{4(5h^2 - b^2)}{5bh(b+3h)} s_j \qquad \text{(for } j = 2, 4) \tag{4.C8c}$$

The definition of $\bar{\psi}_z^{W_1}(s_j)$ given in Eqs. (4.C8b) and (4.C8c) are determined by employing the concepts introduced in Eqs. (4.50) and (4.55), respectively. The symbol $\bar{J}_{B_1}$ given in Eq. (4.C8a) can be defined by using $\bar{\psi}_z^{W_1}(s_j)$ as:

$$\bar{J}_{B_1} = \iint_S (\bar{\psi}_z^{W_1})^2 \, ds dn \tag{4.C8d}$$

The edge resultants of B_1 calculated by substituting $\bar{\sigma}_{zz}^{B_1}$ in Eq. (4.C8a) into Eq. (4.C7) are shown in Fig. 4.8, and one can find that those edge resultants are correctly determined because the equilibrium conditions concerning (M_y, B_1) shown in Fig. 4.8 are consistent with those given in Eqs. (4.76a, b).

Meanwhile, the following distributed axial moment $m_{z(j)}^{Q_2}(s_j)$ ($j = 1, 2, 3, 4$) is generated on Edge *j* by the stress $\sigma_{sz}^{Q_2}$ as shown in Fig. 4.9(a).

$$m_{z(j)}^{Q_2}(s_j) = \int_{Edge\ j} n \cdot \sigma_{zs}^{Q_2} \, dn = -\frac{t^3}{12} \frac{Q_2(z)}{J_{Q_2}} \{ \dot{\psi}_n^{\chi_2}(s_j) \} \tag{4.C9}$$

According to the Kirchhoff-Love plate theory [45], the effective distributed normal force $f_{n(j)}^{Q_2}(s_j)$ ($j = 1, 2, 3, 4$) is also generated on Edge *j* from the axial moment $m_{z(j)}^{Q_2}(s_j)$ by the principle shown in Fig. 4.9(b), and is defined as:

$$f_{n(j)}^{Q_2}(s_j) = \frac{\partial m_{z(j)}^{Q_2}(s_j)}{\partial s} = -\frac{t^3}{12} \frac{Q_2(z)}{J_{Q_2}} \{ \ddot{\psi}_n^{\chi_2}(s_j) \} \tag{4.C10}$$

Therefore, the non-zero edge resultants of Q_2 associated with the equilibrium

conditions given in Eqs. (4.76a, b) is the effective normal force $F_n^{Q_2}$, and $F_{n(j)}^{Q_2}$ on Edge j ($j = 1, 2, 3, 4$) can be defined by using $f_{n(j)}^{Q_2}(s_j)$ in Eq. (4.C10) as:

$$F_{n(j)}^{Q_2} = \int_{Edge\, j} f_{n(j)}^{Q_2}(s_j)\, ds_j \tag{4.C11}$$

However, underestimated edge resultants of Q_2 are also calculated when $f_n^{Q_2}$ given in Eq. (4.C10) is employed as with the case of edge resultants of B_1, and thus the following $\bar{f}_n^{Q_2}$ is used in place of $f_n^{Q_2}$.

$$\bar{f}_{n(j)}^{Q_2}(s_j) = -\frac{t^3}{12}\frac{Q_2(z)}{\bar{J}_{Q_2}}\{\bar{\ddot{\psi}}_n^{\chi_2}(s_j)\} \tag{4.C12a}$$

where $\bar{\ddot{\psi}}_n^{\chi_2}(s_j)$ ($j = 1, 2, 3, 4$) represents the average distribution of $f_n^{Q_2}$ on Edge j, and is defined as:

$$\bar{\ddot{\psi}}_n^{\chi_2}(s_j) = \frac{32b}{h^2(5b+h)} \qquad (\text{for } j = 1, 3) \tag{4.C12b}$$

$$\bar{\ddot{\psi}}_n^{\chi_2}(s_j) = -\frac{32}{h(5b+h)} \qquad (\text{for } j = 2, 4) \tag{4.C12c}$$

The definition of $\bar{\ddot{\psi}}_n^{\chi_2}(s_j)$ given in Eqs. (4.C12b, c) are determined through the concept introduced in Eq. (4.50). The symbol $\bar{J}_{Q_2}$ in Eq. (4.C12a) can be defined by using $\bar{\ddot{\psi}}_n^{\chi_2}(s_j)$ as:

$$\bar{J}_{Q_2} = \iint_S (n \cdot \bar{\ddot{\psi}}_n^{\chi_2})^2\, dsdn = \iint_S \{n \cdot (s \cdot \bar{\ddot{\psi}}_n^{\chi_2})\}^2\, dsdn \tag{4.C12d}$$

where $\bar{\ddot{\psi}}_n^{\chi_2}(s_j)$ ($j = 1, 2, 3, 4$) can be written as $\bar{\ddot{\psi}}_n^{\chi_2}(s_j) = s_j \cdot \bar{\ddot{\psi}}_n^{\chi_2}(s_j)$ because

$\bar{\psi}_n^{\chi_2}(s_j)$ represent the odd functions. The edge resultants of Q_2 calculated by substituting $\bar{f}_n^{Q_2}$ in Eq. (4.C12a) into Eq. (4.C11) are shown in Fig. 4.8.

References

[1] Gere JM, Timoshenko SP. Mechanics of materials. 4th ed. Boston: PWS Pub. Co.; 1997.

[2] Timoshenko SP, Goodier JN. Theory of elasticity. 3rd ed. New York: McGraw-Hill Pub. Co.; 1970.

[3] Malen DE. Fundamentals of automobile body structure design. Warrendale(PA): SAE International.; 2011.

[4] Sunami Y, Yugawa T, Yoshida Y. Analysis of joint rigidity in plane binding of plane joint structures. JSAE Review 1988; no.9.

[5] Vlasov VZ. Thin-walled elastic beams. Jerusalem: Israel Program for Scientific Translations; 1961.

[6] Boswell LF, Zhang SH. The effect of distortion in thin-walled box-spine beams. Int J Solids Struct 1984;20:845-62.

[7] Kim JH, Kim YY. Analysis of thin-walled closed beams with general quadrilateral cross sections. J Appl Mech-Trans ASME 1999;66:904-12.

[8] Kim Y, Kim YY. Analysis of thin-walled curved box beam under in-plane flexure. Int. J. Solids Struct 2003;40:6111-23.

[9] Pavazza R, Blagojević B. On the cross-section distortion of thin-walled beams with multi-cell cross-sections subjected to bending. Int. J. Solids Struct 2005;42:901-25.

[10] Gonçalves R, Dinis PB, Camotim D. GBT formulation to analyse the first-order and buckling behaviour of thin-walled members with arbitrary cross-sections. Thin-Walled Struct 2009;47:583-600.

[11] Genoese A, Genoese A, Bilotta A, Garcea G. A mixed beam model with non-uniform warpings derived from the Saint Venànt rod. Comput Struct 2013;121:87-98.

[12] Ferradi MK, Cespedes X. A new beam element with transversal and warping eigenmodes. Comput Struct 2014;131:12-33.

[13] Vieira RF, Virtuoso FBE, Pereira, EBR. A higher order model for thin-walled structures with deformable cross-sections. Int. J. Solids Struct 2014;51:575-98.

[14] Chang DC. Effects of flexible connections on body structural response. SAE Technical Paper 1974; No. 740041.

[15] Lee K, Nikolaidis E. A two-dimensional model for joints in vehicle structures. Comput Struct 1992;45:775-84.

[16] Bylund N. Fast and economic stiffness evaluation of mechanical joints. SAE Technical Paper 2003;1: No. 2751.
[17] Donders S, Takahashi Y, Hadjit R, Van Langenhove T, Brughmans M, Van Genechten B et al. A reduced beam and joint concept modeling approach to optimize global vehicle body dynamics. Finite Elem Anal Des 2009;45:439-55.
[18] De Gaetano G, Mundo D, Cosco FI, Maletta C, Donders S. Concept Modelling of Vehicle Joints and Beam-Like Structures through Dynamic FE-Based Methods. Shock Vib 2014;2014:9. http://dx.doi.org/10.1155/2014/303567.
[19] Bauchau OA. A beam theory for anisotropic materials. J Appl Mech-Trans ASME 1985;52:416-22.
[20] Petrolo AS, Casciaro R. 3D beam element based on Saint Venànt's rod theory. Comput Struct 2004;82:2471-81.
[21] Cesnik CES, Hodges DH. VABS: A New Concept for Composite Rotor Blade Cross-Sectional Modeling. J Am Helicopter Soc 1997;42:27-38.
[22] Volovoi VV, Hodges DH. Theory of anisotropic thin-walled beams. J Appl Mech-Trans ASME 2000;67:453-9.
[23] Kim J-S, Cho M, Smith EC. An asymptotic analysis of composite beams with kinematically corrected end effects. Int J Solids Struct. 2008;45:1954-77.
[24] Carrera E, Giunta G. Refined beam theories based on a unified formulation. Int. J. Appl. Mech. 2010; 2:117-43.
[25] Carrera E, Giunta G, Nali P, Petrolo M. Refined beam elements with arbitrary cross-section geometries. Comput Struct 2010;88:283-93.
[26] Schardt R. Generalized beam theory—an adequate method for coupled stability problems. Thin-Walled Struct 1994;19:161-80.
[27] Silvestre N, Camotim D. First-order generalised beam theory for arbitrary orthotropic materials. Thin-Walled Struct 2002;40:755-89.
[28] Kim JH, Kim YY. One-dimensional analysis of thin-walled closed beams having general cross-sections. Int. J. Numer. Methods Eng. 2000;49:653-68.
[29] Kim JH, Kim YY. Thin-walled multicell beam analysis for coupled torsion, distortion, and warping deformations. J Appl Mech-Trans ASME 2001;68:260-9.
[30] Kim YY, Kim TS. Topology optimization of beam cross sections. Int. J. Solids Struct. 2000;37:477-93.
[31] Heo S, Kim JH, Kim YY. Significance of distortion in thin-walled closed beam section design. Int. J. Solids Struct. 2003;40:633-48.
[32] Kim YY, Kim Y. A one-dimensional theory of thin-walled curved rectangular box beams under torsion and out-of-plane bending. Int. J. Numer. Methods Eng. 2002;53:1675-93.
[33] Genoese A, Genoese A, Bilotta A, Garcea G. A geometrically exact beam model with non-uniform warping coherently derived from the Saint Venant rod. Eng Struct 2014;68:33-46.

[34] Ferradi MK, Cespedes X, Arquier M. A higher order beam finite element with warping eigenmodes. Eng Struct 2013;46:748-62.
[35] Vieira RF, Virtuoso FBE, Pereira EBR. Definition of warping modes within the context of a higher order thin-walled beam model. Comput Struct 2015;147:68-78.
[36] Vacharajittiphan P, Trahair NS. Warping and distortion at I-section joints. J Struct Div 1974;100:547-64.
[37] Baigent AH, Hancock GJ. Structural analysis of assemblages of thin-walled members. Eng Struct 1982;4:207-16.
[38] Morrell PJB, Riddington JR, Ali FA, Hamid HA. Influence of joint detail on the flexural/torsional interaction of thin-walled structures. Thin-walled struct 1996;24:97-111.
[39] Basaglia C, Camotim D, Silvestre N. Global buckling analysis of plane and space thin-walled frames in the context of GBT. Thin-Walled Struct 2008;46:79-101.
[40] Camotim D, Basaglia C. Buckling analysis of thin-walled steel structures using generalized beam theory (GBT): state-of-the-art report. Steel Constr 2013;6:117-31.
[41] Jang G-W, Kim YY. Higher-order in-plane bending analysis of box beams connected at an angled joint considering cross-sectional bending warping and distortion. Thin-Walled Struct 2009;47:1478-89.
[42] Choi S, Jang G-W, Kim YY. Exact matching condition at a joint of thin-walled box beams under out-of-plane bending and torsion. J Appl Mech-Trans ASME 2012;79:051018.
[43] Choi S, Kim YY. Exact Matching at a Joint of Multiply-Connected Box Beams under Out-of-Plane Bending and Torsion. Eng Struct (under review).
[44] Hibbett HD, Karlsson BI, Sorensen EP. ABAQUS/standard: User's Manual. 1998.
[45] Reddy JN. Theory and analysis of elastic plates. Philadelphia (PA): Taylor and Francis; 1999.
[46] Love AEH. A treatise on the mathematical theory of elasticity. New York: Dover Publications; 2011.
[47] Bauchau OA, Craig JI. Structural analysis: with applications to aerospace structures. New York: Springer; 2009.
[48] Bathe, K.-J., 2006. Finite element procedures. Klaus-Jurgen Bathe.
[49] Kim YY, Kim JH. Thin-walled closed box beam element for static and dynamic analysis. Int J Numer Methods Eng 1999;45:473-90.
[50] Choi S, Kim YY. Analysis of two box beams-joint systems under in-plane bending and axial loads by one-dimensional higher-order beam theory. Int. J. Solids Struct. (Submitted)

CHAPTER 5.
Higher-Order Beam Analysis for Multiply-Connected Box Beams-Joint Systems Subjected to In-Plane Bending and Axial Loads

5.1 Introduction

The response of thin-walled beams is highly flexible than the analysis result obtained by classical Euler and Timoshenko beam theories (see, e.g. [1, 2]) since cross-sectional deformations not handled by those classical theories easily appear in thin-walled beams. Moreover, when thin-walled beams are connected at a joint, the magnitudes of cross-sectional deformations near the joint region are further amplified. For this reason, the joint region exhibits significant flexibilities, and the behavior of thin-walled beam structures having joints shows significant difference from the predicted result based on the classical beam theories. From the motivation that the classical beam theories overestimate stiffness of thin-walled beam structures, one-dimensional higher-order beam theories [3-9] considering the flexibilities of thin-walled beams caused by cross-sectional deformations have been developed. However, higher-order deformations which do not produce any resultants are considered together as additional degrees of freedom of the higher-order beam theories, and thus determination of the joint matching relations among all the degrees of freedom of the beams connected at the joint is a highly difficult

problem. Because of such difficulties, therefore, there is no exact analysis method using higher-order beam theories applicable to structures with three or more thin-walled beams meeting at a joint (referred to hereinafter in this paper as “three or more thin-walled beams”) subjected to in-plane loads. With this background, we propose an exact analysis approach for the first time, applicable to the mentioned three or more thin-walled beams-joint structures under in-plane loads.

First, we introduce some previous one-dimensional beam theory-based researches having been tried to interpret the flexible responses of the thin-walled beams-joint structures. Initial studies, which were based on the classical beam theories, regarded the connectivity among thin-walled beams at the joint as semi-rigid connection and proposed some artificial joint spring models to reflect the joint flexibility on their analysis approaches [10-12]. Chang [10] proposed a joint model employing a rotational spring which can be used to define the flexible relation between in-plane bending moment and its accompanied bending rotation at the joint, and Lee and Nikolaidis [12] proposed another joint model consisting of some rotational springs and a rigid section based on the assumption that the rotation center of each beam should be located away from the joint. Subsequently, Bylund [13] proposed the Dynamic Joint Method for determining the stiffness of the joint using eigenvalues and eigenmodes of the structure considered, and recently Donders et al. [14] suggested the method to represent the stiffness of the joint as the super element obtained by applying the Guyan reduction method to the detailed shell joint model. Because the flexibility of the joint is highly dependent upon the

aspect ratio of cross-section of the beams meeting at the joint and the joint angle among those beams, however, it is difficult to determine an approximate joint model consistently applicable to the thin walled beams-joint structures with various joints.

If there existed a beam theory including the effects arising from the cross-sectional deformations, then capturing the flexible responses of thin-walled beams-joint structure would be possible without employing artificial joint concepts. Therefore, there have been efforts to include some significant cross-sectional deformations as independent degrees of freedom in addition to conventional rigid-body motions of a beam cross-section, and consequently higher-order beam theories were proposed [3-9]. Vlasov [3] proposed a theoretical approach in determining the cross-sectional warping deformations of thin-walled beams subjected to twisting moment, and established the fundamental theories to include these sectional deformations as the additional degrees of freedom. Kim and Kim [6] developed the higher-order beam theory for thin-walled closed beams subjected to twisting moment which can interpret the responses of those beams as correctly as the shell analysis, and Kim and Kim [15, 16] extended the coverage of the higher-order beam theory to the thin-walled curved box beams.

Some efforts to theoretically represent the flexible responses of the joint appeared in the thin-walled box beams-joint structures without using artificial joint concepts have been followed based on the higher-order beam theories [17-23]. Especially, Choi and Kim [23] defined fundamental conditions regarding a higher-

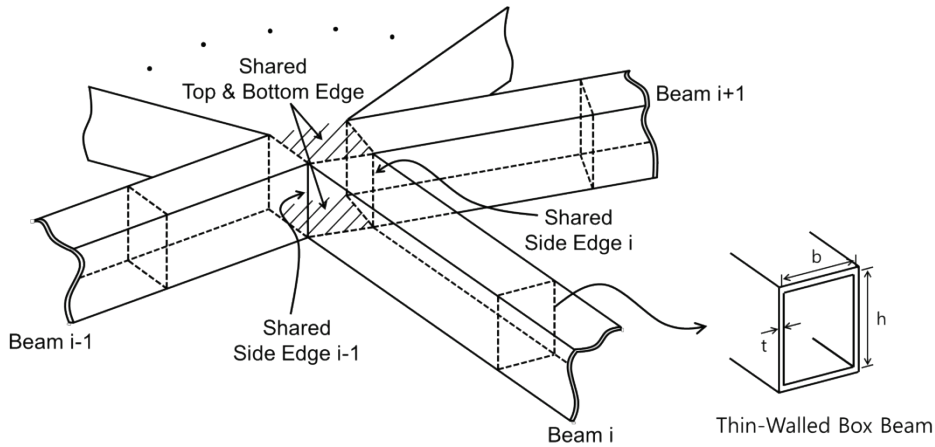

Fig. 5.1 Three or more thin-walled box beams-joint structures (only a portion of the structure such as Beam i-1, Beam i, and Beam i+1 ($i \geq 2$), is depicted, for convenience.).

order beam theory which must meet at a joint, and derived exact joint matching conditions applicable to the two box beams-joint structures under in-plane loads through a theoretical approach using those fundamental conditions. Moreover, Choi and Kim [23] demonstrated that analysis based on their proposed joint matching conditions can interpret responses of the joint as accurately as those by shell analysis. Although Choi and Kim [23] determined joint matching conditions with respect to two box beams-joint structures under in-plane loads and verified their results by obtaining meaningful analysis responses for various numerical examples, there still exists the difficulty that stiffness of the joints is overestimated when expanding their proposed matching conditions directly to three or more thin-walled box beams-joint structures. That is because those matching conditions excessively

constrain the joint to be deformed, and higher-order deformations cannot be properly generated at the joint. From the observations above, a new approach to theoretically determine joint matching conditions is required in order to establish exact higher-order beam theory-based analysis approach applicable to three or more thin-walled box beams-joint structures under in-plane loads.

Three or more box beams-joint structures under in-plane bending or longitudinal force will be analyzed in this study by using a higher-order beam theory. The unique contributions of this investigation are to newly establish a higher-order beam theory having 11 field variables which are all required in order to represent the flexibilities of the joint theoretically, and are to derive the exact matching relations among those 11 field variables of box beams meeting at the joint. Figure 5.1 shows a three or more box beams-joint structures. Only a portion of the structure, such as Beam i-1, Beam i, and Beam i+1 ($i \geq 2$) is depicted, for convenience. It is assumed that all the box beams in Fig. 5.1 are placed on the same plane, and also assumed that their width, height and thickness are equal to b, h and t, respectively. In order to interpret the box beams-joint structure shown in Fig. 5.1 using the higher-order beam theory, the joint connectivity between box beams is modeled as shown in Fig. 5.2. The joint where all the box beams converse is defined as the joint (strictly, the joint refers to the point where the central axes of box beams meet). As with Refs. [22, 23], in addition, Edge $M_{i-1}M'_{i-1}$ and Edge $N_iN'_i$ are considered as if they were attached rigidly to each other (by an

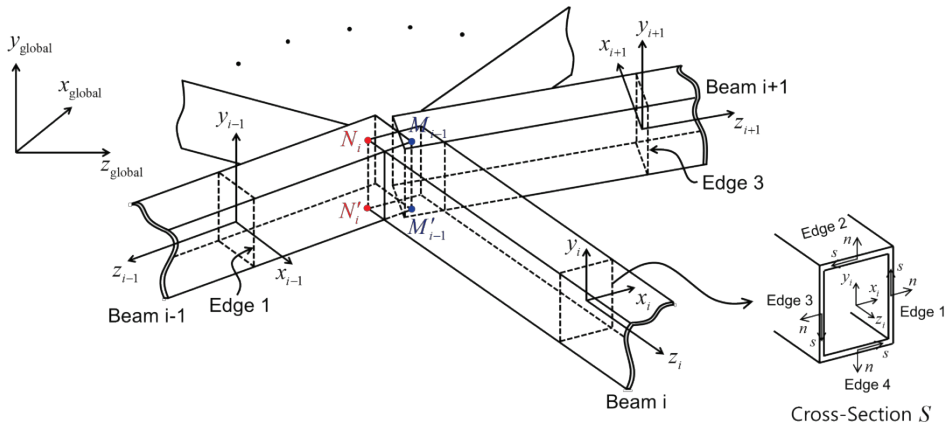

(a)

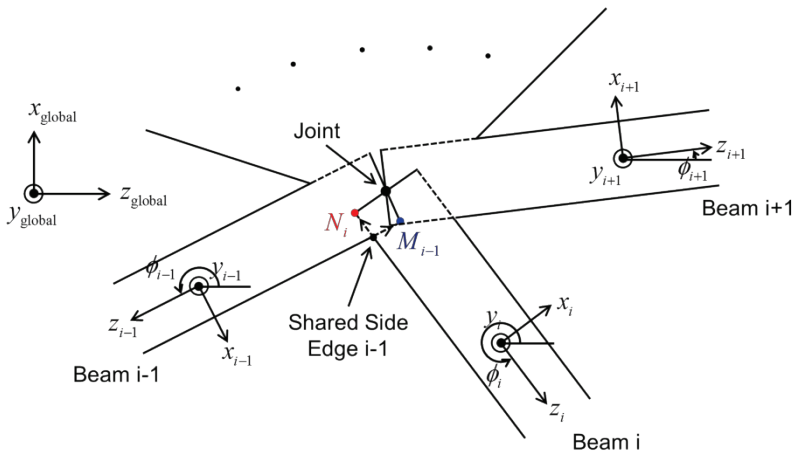

(b)

Fig. 5.2 (*a*) Beam modeling for the three or more box beams-joint structures (Edge $M_{i\text{-}1}M'_{i\text{-}1}$ of Beam *i*-1 and Edge N_iN_i' of Beam *i* ($i \geq 2$) are considered as if they were connected rigidly to each other (by an imaginary rigid body).), (*b*) the top view of beam modeling (Edge $M_{i\text{-}1}M'_{i\text{-}1}$ of Beam *i*-1 and Edge N_iN_i' of Beam *i* are extended and separated from Shared Side Edge *i*-1 ($i \geq 2$) in Fig. 5.1).

imaginary rigid body) because Shared Side Edge *i*-1 in Fig. 5.1, which is shared by

Beam i-1 and Beam i ($i \geq 2$), is extended and represented in Fig. 5.2 by Edge $M_{i-1}M'_{i-1}$ in Beam i-1 and Edge $N_iN'_i$ in Beam i separately. Therefore, both the equilibrium between the forces and the continuity between the displacements, which are generated at Edge $M_{i-1}M'_{i-1}$ and Edge $N_iN'_i$, can be considered although those edges are separated from each other.

To establish the higher-order beam theory applicable to the three or more box beams-joints structures under in-plane loads, we will introduce the higher-order deformations (χ_1^1, W_1^1, χ_1^2, W_1^2, χ_2, W_2, χ_3, χ_4) shown in Fig. 5.3(b) as the independent field variables in addition to the rigid-body motions shown in Fig. 5.3(a). Choi and Kim [23] theoretically defined the shape of the higher-order deformations (χ_1^g, W_1^g, χ_3) (see Fig. 5.3(c) for (χ_1^g, W_1^g)) and demonstrated that the higher-order beam theory including (χ_1^g, W_1^g, χ_3) are sufficient to interpret the flexible behavior of the two box beams-joint structure under in-plane loads. However, the matching conditions between Beam i and Beam i+1 ($i \geq 2$) should be independent with those between Beam i and Beam i-1 for three or more box beams-joint structures, and thus (χ_2, W_2, χ_4) should be additionally included in the higher-order beam theory. Moreover, (χ_1^1, W_1^1, χ_1^2, W_1^2), which represent more detailed field variables set regarding to the cross-sectional deformations (χ_1^g, W_1^g) describe, are considered instead of (χ_1^g, W_1^g) in order to develop more accurate one-dimensional analysis approach for three or more box beams-joint structures.

To derive exact joint matching conditions among those 11 field variables applicable to three or more box beams-joint structures, joint equilibrium conditions among generalized forces, which are the work conjugates of the field displacement variables, will be precisely defined first. Then, taking into account the defined equilibrium conditions and the principle of virtual work together, the desired joint matching conditions among field variables will be theoretically derived. Note that the work conjugates of the field variables representing the higher-order deformations do not generate any resultant forces or moments acting on the cross-section, but do generate resultant stresses acting on each of the edges as demonstrated in Choi and Kim [22]. If the equilibrium conditions on the edges (Edge $M_{i-1}M'_{i-1}$, Edge $N_iN'_i$, etc.) are considered in addition to the resultant forces and moments equilibrium conditions, therefore, generalized forces equilibrium conditions which are consistently valid for the three or more box beams-joint structures can be determined. Although the purpose of this study is to derive equilibrium conditions or matching conditions applicable to the three or more box beams-joint structures, the derived conditions should also be valid for the two box beams-joint structures in order for this approach to be reasonable. According to this observation, we derive more generalized matching conditions on the basis of Choi and Kim [23] who derive the exact matching conditions regarding to the two box beams-joint structures. In order to verify the validity of the proposed joint matching conditions, two case studies will be examined. The accuracy of the proposed analysis method will be checked by comparison with the results of

ABAQUS shell analysis [24].

5.2 Higher-Order Beam Theory for Straight Thin-Walled Box Beams

In order to interpret the three or more box beams-joint structures under in-plane loads precisely without employing any artificial concepts, a higher-order beam theory which includes the significant higher-order deformations associated with the flexibilities of the joint as independent field variables is required. Choi and Kim [23] theoretically defined the higher-order deformations (χ_1^g, W_1^g, χ_3) shown in Fig. 5.3(b, c) and established the higher-order beam theory including (χ_1^g, W_1^g, χ_3) which are applicable to the two box beams-joint structures under in-plane loads. However, it can be found that the analysis approach proposed by Choi and Kim [23] underestimate the joint flexibility of the three or more box beams-joint structures under in-plane loads and that one of the reasons for that difficulty is a rack of the higher-order deformations such as (χ_2, W_2, χ_4) with respect to determination of the joint matching conditions between Beam *i* and Beam *i*+1 ($i \geq 2$) independently with those between Beam *i* and Beam *i*-1.

Therefore, we will newly establish a higher-order beam theory considering 11 displacements of deformations of the box beams such as axial displacement U_z, transverse displacement U_x, in-plane bending/shear rotation θ_y, distortions

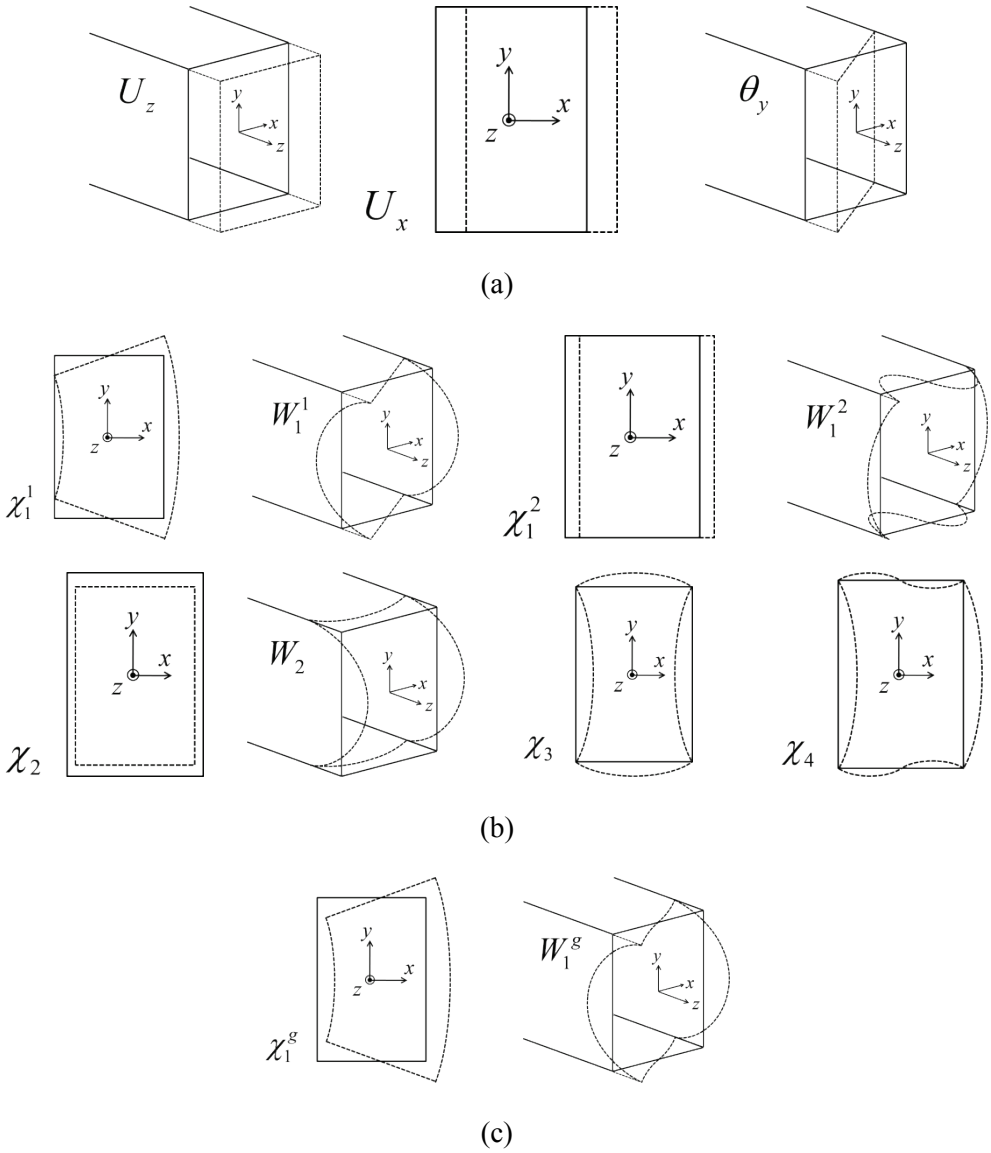

Fig. 5.3 (*a*) Rigid motions of the box beam cross-section represented by the field variables: axial displacement U_z , transverse displacement U_x and in-plane bending/shear rotation θ_y, (*b*) Deformations of cross-section represented by the field variables: distortions (χ_1^1, χ_1^2, χ_2, χ_3, χ_4) and warpings (W_1^1, W_1^2, W_2), (c) Deformations of cross-section represented by the field variables: distortion χ_1^g and warping W_1^g.

($\chi_1^1, \chi_1^2, \chi_2, \chi_3, \chi_4$) and warpings (W_1^1, W_1^2, W_2). Note that (χ_1^g, W_1^g) proposed by Choi and Kim [23] are divided into more detailed higher-order deformations ($\chi_1^1, W_1^1, \chi_1^2, W_1^2$) in this study to represent accurate flexible joint behavior although theoretically reasonable joint matching conditions can be determined using (χ_1^g, W_1^g).

In order to define those cross-sectional deformations as one-dimensional field variables of higher-order beam theory, shape functions representing the deformation patterns shown in Fig. 5.3(b) are employed, and thus the shape functions for (χ_2, W_2, χ_4) which are newly introduced as the independent field variables of the proposed higher-order beam theory will be theoretically derived in this study. Based on Refs. [6, 22, 23], the one-dimensional higher-order beam theory considering the 11 rigid motions and cross-sectional deformations shown in Fig. 5.3(a, b) as the field variables will be defined in this section, and subsequently the theoretical approach to derive the shape functions for (χ_2, W_2, χ_4) will introduced in the next section.

When one-dimensional field variables of the higher-order beam theory are expressed as the functions of axial coordinate z, $\mathbf{U}(z) = \{U_z(z), U_x(z), \theta_y(z), \chi_1^1(z), W_1^1(z), \chi_1^2(z), W_1^2(z), \chi_2(z), W_2(z), \chi_3(z), \chi_4(z)\}^{\mathrm{T}}$, the three-dimensional displacements of a point located on the contour line of the box beam cross-section can be written as follows by using $\mathbf{U}$ [23].

$$u_n(s,\,z)=\psi_n^{U_x}(s)\cdot U_x(z)+\psi_n^{\chi_1^1}(s)\cdot\chi_1^1(z)+\psi_n^{\chi_1^2}(s)\cdot\chi_1^2(z)$$
$$+\psi_n^{\chi_2}(s)\cdot\chi_2(z)+\psi_n^{\chi_3}(s)\cdot\chi_3(z)+\psi_n^{\chi_4}(s)\cdot\chi_4(z) \tag{5.1a}$$

$$u_s(s,\,z)=\psi_s^{U_x}(s)\cdot U_x(z)+\psi_s^{\chi_1^1}(s)\cdot\chi_1^1(z)+\psi_s^{\chi_1^2}(s)\cdot\chi_1^2(z)+\psi_s^{\chi_2}(s)\cdot\chi_2(z) \tag{5.1b}$$

$$u_z(s,\,z)=\psi_z^{U_z}(s)\cdot U_z(z)+\psi_z^{\theta_y}(s)\cdot\theta_y(z)+\psi_z^{W_1^1}(s)\cdot W_1^1(z)$$
$$+\psi_z^{W_1^2}(s)\cdot W_1^2(z)+\psi_z^{W_2}(s)\cdot W_2(z) \tag{5.1c}$$

where n and s represent a normal coordinate and a tangential coordinate defined on the contour line, respectively (see Fig. 5.2(a) for the positive directions of n and s).

The symbols $\psi_p^{\alpha}(s)$ ($p=n,\,s,\,z$; $\alpha=U_y,\,\theta_x,\,\theta_z,\,\chi_1^1,\,W_1^1,\,\chi_1^2,\,W_1^2,\,\chi_2,\,W_2,$ $\chi_3,\,\chi_4$), which are functions of s, are introduced in Eqs. (5.1a-c) to describe the displacements or deformations of the box beam cross-section. The meaning of the symbol $\psi_p^{\alpha}(s)$ is the displacement in the p direction generated on the cross-section with respect to the unit magnitude of the field variable α. The explicit expressions of the shape functions $\psi_p^{\alpha}(s)$ are given in Appendix A.

Considering the Kirchhoff-Love plate theory [25], the three dimensional displacements ($\tilde{u}_n,\,\tilde{u}_s,\,\tilde{u}_z$) of a generic point located away from the contour line by n can be expressed as, by using ($u_n,\,u_s,\,u_z$) given in Eqs. (5.1a-c):

$$\tilde{u}_n(n,\,s,\,z)=u_n(s,\,z)=\psi_n^{U_x}\cdot U_x+\psi_n^{\chi_1^1}\cdot\chi_1^1+\psi_n^{\chi_1^2}\cdot\chi_1^2+\psi_n^{\chi_2}\cdot\chi_2+\psi_n^{\chi_3}\cdot\chi_3+\psi_n^{\chi_4}\cdot\chi_4 \tag{5.2a}$$

$$\tilde{u}_s(n,\,s,\,z)=u_s(s,\,z)-n\frac{\partial u_n(s,z)}{\partial s}=\psi_s^{U_x}\cdot U_x+\psi_s^{\chi_1^1}\cdot\chi_1^1+\psi_s^{\chi_1^2}\cdot\chi_1^2+\psi_s^{\chi_2}\cdot\chi_2$$
$$-n(\dot{\psi}_n^{\chi_1^1}\cdot\chi_1^1+\dot{\psi}_n^{\chi_3}\cdot\chi_3+\dot{\psi}_n^{\chi_4}\cdot\chi_4) \tag{5.2b}$$

$$\tilde{u}_z(n,\, s,\, z) = u_z(s,\, z) - n\frac{\partial u_n(s,z)}{\partial z}$$
$$= \psi_z^{U_z} \cdot U_z + \psi_z^{\theta_y} \cdot \theta_y + \psi_z^{W_1^1} \cdot W_1^1 + \psi_z^{W_1^2} \cdot W_1^2 + \psi_z^{W_2} \cdot W_2$$
$$- n(\psi_n^{U_x} \cdot U_x{}' + \psi_n^{\chi_1^1} \cdot \chi_1^{1\prime} + \psi_n^{\chi_1^2} \cdot \chi_1^{2\prime} + \psi_n^{\chi_2} \cdot \chi_2{}' + \psi_n^{\chi_3} \cdot \chi_3{}' + \psi_n^{\chi_4} \cdot \chi_4{}')$$

(5.2c)

where the symbols $(\dot{\ })$ and $()'$ denote $(\dot{\ }) = \partial()/\partial s$ and $()' = \partial()/\partial z$, respectively. The displacement terms $-n \cdot (\partial u_n / \partial s)$ and $-n \cdot (\partial u_n / \partial z)$ given in Eqs. (5.2b, c) represent the displacement in s and z directions respectively which arise from the rotation of the normal to the contour line.

The dominant and nonzero strains ($\varepsilon_{ss}, \varepsilon_{zz}, \gamma_{sz}$) that occur at the same point can be derived from Eqs. (5.2b, c) as, according to the Kirchhoff-Love plate theory [25]:

$$\varepsilon_{ss}(n,\, s,\, z) = \frac{\partial \tilde{u}_s}{\partial s} = \dot{\psi}_s^{\chi_1^1} \cdot \chi_1^1 + \dot{\psi}_s^{\chi_1^2} \cdot \chi_1^2 + \dot{\psi}_s^{\chi_2} \cdot \chi_2 - n\{\ddot{\psi}_n^{\chi_1^1} \cdot \chi_1^1 + \ddot{\psi}_n^{\chi_3} \cdot \chi_3 + \ddot{\psi}_n^{\chi_4} \cdot \chi_4\}$$

(5.3a)

$$\varepsilon_{zz}(n,\, s,\, z) = \frac{\partial \tilde{u}_z}{\partial z} = \psi_z^{U_z} \cdot U_z{}' + \psi_z^{\theta_y} \cdot \theta_y{}' + \psi_z^{W_1^1} \cdot W_1^{1\prime} + \psi_z^{W_1^2} \cdot W_1^{2\prime} + \psi_z^{W_2} \cdot W_2{}' \quad (5.3b)$$

$$\gamma_{sz}(n,\, s,\, z) = \frac{\partial \tilde{u}_s}{\partial z} + \frac{\partial \tilde{u}_z}{\partial s} = \psi_s^{U_x} \cdot U_x{}' + \dot{\psi}_z^{\theta_y} \cdot \theta_y + \psi_s^{\chi_1^1} \cdot \chi_1^{1\prime} + \dot{\psi}_z^{W_1^1} \cdot W_1^1 + \psi_s^{\chi_1^2} \cdot \chi_1^{2\prime} + \dot{\psi}_z^{W_1^2} \cdot W_1^2$$
$$+ \psi_s^{\chi_2} \cdot \chi_2{}' + \dot{\psi}_z^{W_2} \cdot W_2 - 2n(\dot{\psi}_n^{\chi_1^1} \cdot \chi_1^{1\prime} + \dot{\psi}_n^{\chi_3} \cdot \chi_3{}' + \dot{\psi}_n^{\chi_4} \cdot \chi_4{}')$$

(5.3c)

Subsequently, the dominant and nonzero stresses ($\sigma_{ss}, \sigma_{zz}, \sigma_{sz}$) at the same point can be defined from ($\varepsilon_{ss}, \varepsilon_{zz}, \gamma_{sz}$) given in Eqs. (5.3a-c) by employing the stress-strain relations as:

$$\sigma_{ss}(n,s,z)=\frac{E}{1-\nu^2}[\{\dot{\psi}_s^{\chi_1}\cdot\chi_1^1+\dot{\psi}_s^{\chi_1^2}\cdot\chi_1^2+\dot{\psi}_s^{\chi_2}\cdot\chi_2+\nu(\psi_z^{U_z}\cdot U_z{}'+\psi_z^{\theta_y}\cdot\theta_y{}'$$
$$+\psi_z^{W_1^1}\cdot W_1^{1\prime}+\psi_z^{W_1^2}\cdot W_1^{2\prime}+\psi_z^{W_2}\cdot W_2{}')\}-n(\ddot{\psi}_n^{\chi_1^1}\cdot\chi_1^1+\ddot{\psi}_n^{\chi_3}\cdot\chi_3+\ddot{\psi}_n^{\chi_4}\cdot\chi_4)]$$

(5.4a)

$$\sigma_{zz}(n,s,z)=\frac{E}{1-\nu^2}[\{\psi_z^{U_z}\cdot U_z{}'+\psi_z^{\theta_y}\cdot\theta_y{}'+\psi_z^{W_1^1}\cdot W_1^{1\prime}+\psi_z^{W_1^2}\cdot W_1^{2\prime}+\psi_z^{W_2}\cdot W_2{}'$$
$$+\nu(\dot{\psi}_s^{\chi_1^1}\cdot\chi_1^1+\dot{\psi}_s^{\chi_1^2}\cdot\chi_1^2+\dot{\psi}_s^{\chi_2}\cdot\chi_2)\}-n(\ddot{\psi}_n^{\chi_1^1}\cdot\chi_1^1+\ddot{\psi}_n^{\chi_3}\cdot\chi_3+\ddot{\psi}_n^{\chi_4}\cdot\chi_4)]$$

(5.4b)

$$\sigma_{sz}(n,s,z)=G\{\psi_s^{U_x}\cdot U_x{}'+\dot{\psi}_z^{\theta_y}\cdot\theta_y+\psi_s^{\chi_1^1}\cdot\chi_1^{1\prime}+\dot{\psi}_z^{W_1^1}\cdot W_1^1+\psi_s^{\chi_1^2}\cdot\chi_1^{2\prime}+\dot{\psi}_z^{W_1^2}\cdot W_1^2$$
$$+\psi_s^{\chi_2}\cdot\chi_2{}'+\dot{\psi}_z^{W_2}\cdot W_2-2n(\dot{\psi}_n^{\chi_1^1}\cdot\chi_1^{1\prime}+\dot{\psi}_n^{\chi_3}\cdot\chi_3{}'+\dot{\psi}_n^{\chi_4}\cdot\chi_4{}')\}$$

(5.4c)

where E, G, ν represent Young's modulus, shear modulus, Poisson's ratio, respectively. The following stress-strain relations under the plane stress assumption are employed in derivation of those stresses above because each edge of the box beam cross-section is a thin plate.

$$\sigma_{ss}=\frac{E}{1-\nu^2}(\varepsilon_{ss}+\nu\varepsilon_{zz}),\qquad \sigma_{zz}=\frac{E}{1-\nu^2}(\varepsilon_{zz}+\nu\varepsilon_{ss}),\qquad \sigma_{sz}=G\gamma_{sz}\tag{5.5}$$

Using those displacements, strains and stresses defined at a generic point, three-dimensional total potential energy for the straight box beam can be defined, and then carrying out the surface integral for the cross-section S and applying the principle of minimum total potential energy, one can derive the one-dimensional higher-order beam theory for the straight box beam (see Refs. [6, 22, 23] for the detailed procedures).

The derived higher-order beam theory is expressed by the relation between the field variables $\mathbf{U}$ and generalized forces $\mathbf{F} = \{F_z, F_x, M_y, Q_1^1, B_1^1, Q_1^2, B_1^2, Q_2, B_2, Q_3, Q_4\}^{\mathrm{T}}$ which are work conjugates of $\mathbf{U}$. The generalized forces $\mathbf{F}$ are defined as:

$$
\begin{aligned}
&F_z = \iint_S (\sigma_{zz}\psi_z^{U_z})\, dsdn, && F_x = \iint_S (\sigma_{zs}\psi_s^{U_x})\, dsdn, && M_y = \iint_S (\sigma_{zz}\psi_z^{\theta_y})\, dsdn,\\
&Q_1^1 = \iint_S (\sigma_{zs}\psi_s^{\chi_1^1})\, dsdn, && B_1^1 = \iint_S (\sigma_{zz}\psi_z^{W_1^1})\, dsdn, && Q_1^2 = \iint_S (\sigma_{zs}\psi_s^{\chi_1^2})\, dsdn,\\
&B_1^2 = \iint_S (\sigma_{zz}\psi_z^{W_1^2})\, dsdn, && Q_2 = \iint_S (\sigma_{zs}\psi_s^{\chi_2})\, dsdn, && B_2 = \iint_S (\sigma_{zz}\psi_z^{W_2})\, dsdn,\\
&Q_3 = \iint_S \sigma_{zs}(n\cdot\dot{\psi}_n^{\chi_3})\, dsdn, && Q_4 = \iint_S \sigma_{zs}(n\cdot\dot{\psi}_n^{\chi_4})\, dsdn
\end{aligned}
\tag{5.6}
$$

where (F_z, F_x, M_y) represent resultant forces or moments such as axial force, transverse force, and in-plane bending moment, respectively. On the contrary, the other forces represent self-equilibrated terms; ($Q_1^1, Q_1^2, Q_2, Q_3, Q_4$) represent transverse bimoments, and (B_1^1, B_1^2, B_2) represent longitudinal bimoments.

5.3 Derivation of Cross-Sectional Deformations (χ_2, W_2, χ_4)

To represent the flexible responses of thin-walled box beams-joint structure correctly, theoretically reasonable shape functions $\psi(s)$ for (χ_2, W_2, χ_4) are should be employed in the higher-order beam theory. For this reason, $\psi(s)$ for (χ_2, W_2, χ_4) used in this study are theoretically determined, and the derivations for

those shape functions will be introduced in this section.

5.3.1 Shape Function of χ_2

The axial stress σ_{zz} generated at a point on the contour line by the axial force F_z can be written as, according to the classical beam theory [1, 2],

$$\sigma_{zz}(s, z) = \frac{F_z(z)}{A} \tag{5.7}$$

where A represent the area of the box beam cross-section. From σ_{zz} given in Eq. (5.7), the strain ε_{zz} is generated, and simultaneously the strain ε_{ss} expressed as follows is also accompanied by the Poisson's effect [2].

$$\varepsilon_{ss}(s, z) = -\nu \frac{\sigma_{zz}}{E} = -\frac{\nu F_z(z)}{EA} \tag{5.8}$$

The strain ε_{ss} given in Eq. (5.8) causes the cross-sectional deformation representing Poisson's mode according to Ref. [2], and this deformation is considered in this study as the field variable χ_2.

When $u_s^{\chi_2}$ denotes the displacement associated with χ_2 in s direction on the contour line, $u_s^{\chi_2}$ generated from ε_{ss} given in Eq. (5.8) satisfies the following equation.

$$\frac{\partial u_s^{\chi_1}(s, z)}{\partial s} = -\frac{\nu F_z(z)}{EA} \tag{5.9}$$

In addition, $u_s^{\chi_2}$ satisfies $u_s^{\chi_2}(s, z) = \psi_s^{\chi_2}(s) \cdot \chi_2(z)$ according to Eq. (5.1), and thus substituting this relation into Eq. (5.9), the following equation regarding to

$\psi_s^{\chi_2}(s)$ can be obtained.

$$\frac{\partial \psi_s^{\chi_2}(s)}{\partial s} = P_1^* \tag{5.10}$$

where P_1^* represents the proportional constant. Carrying out the integration for coordinate s, consequently $\psi_s^{\chi_2}(s_j)$ on Edge j ($j = 1, 2, 3, 4$) can be expressed as:

$$\begin{aligned} &\psi_s^{\chi_2}(s_1) = P_1^* \times \{s_1 + C_1\}, \qquad \psi_s^{\chi_2}(s_2) = P_1^* \times \{s_2 + C_2\}, \\ &\psi_s^{\chi_2}(s_3) = P_1^* \times \{s_3 + C_3\}, \qquad \psi_s^{\chi_2}(s_4) = P_1^* \times \{s_4 + C_4\} \end{aligned} \tag{5.11}$$

where C_1, C_2, C_3, and, C_4 represent the integration constants.

From the observation that σ_{zz} in Eq. (5.7) is symmetric with respect to both x and y axes, one can find that the shape of χ_2 generated by σ_{zz} should be symmetric regarding to both x and y axes. To satisfy the mentioned symmetry condition, therefore, the constants ($C_1 \sim C_4$) should meet the following relations.

$$C_1 = C_3; \quad C_2 = C_4 \tag{5.12}$$

In addition, $\psi_s^{\chi_2}$ should satisfy the following orthogonality conditions with $\psi_s^{U_x}$ so that the relation given in Eq. (5.1b) is defined correctly [3, 22, 23].

$$\iint_S \psi_s^{\chi_2}(s) \cdot \psi_s^{U_x}(s)\, dA = 0 \tag{5.13}$$

The orthogonality condition above means that the higher-order deformation χ_2 does not involve any rigid-body motion in x direction, and the values for the constants (C_1, C_3) can be determined as, through the orthogonality conditions given in Eq. (5.13),

$$C_1 = C_3 = 0 \tag{5.14}$$

Likewise, one can also consider the following orthogonality condition of χ_2 with respect to the rigid-body translation in y direction

$$\iint_S \psi_s^{\chi_2}(s) \cdot \psi_s^{U_y}(s)\, dA = 0 \tag{5.15}$$

where the definition of $\psi_s^{U_y}(s_j)$ on Edge j ($j = 1, 2, 3, 4$) are as

$$\psi_s^{U_y}(s_1) = 1\,;\quad \psi_s^{U_y}(s_2) = 0\,;\quad \psi_s^{U_y}(s_3) = -1\,;\quad \psi_s^{U_y}(s_4) = 0 \tag{5.16}$$

The symbol $\psi_s^{U_y}(s_j)$ represents the displacement of Edge j when the cross-section is rigidly translated in y direction. Using the orthogonality condition given in Eq. (5.15), the values for the remained constants (C_2, C_4) are determined as:

$$C_2 = C_4 = 0 \tag{5.17}$$

From the symmetry conditions with respect to x and y axes and the orthogonality conditions with the rigid-body motions in x and y directions, all the constants ($C_1 \sim C_4$) in Eq. (5.11) are determined. The constant P_1^* in Eq. (5.12) determine the scale of the cross-sectional deformation represented by the unit magnitude of χ_2, and $P_1^* = -2/h$ will be used in this study.

When $u_s^{\chi_2}$ is generated on the contour line, $u_n^{\chi_2}$ is accompanied by the continuity at the corner j where Edge j and Edge j+1 ($j = 1, 2, 3, 4$; Edge 5 denotes Edge 1) meet. Because of that $u_s^{\chi_2}$ generated on Edge 1 and Edge 3 are identical, and that $u_s^{\chi_2}$ generated on Edge 2 and Edge 4 are also identical, each edge is

rigidly translated in $-n$ direction, and the shape functions $\psi_n^{\chi_2}(s_j)$ ($j = 1, 2, 3, 4$) describing the translation of Edge j are given in Appendix A.

5.3.2 Shape Function of W_2

According to the higher-order beam theory, Q_2 denoting the work conjugate of χ_2 generates the following shear stress $\sigma_{zs}^{Q_2}$ on the contour line (see Section 3. 1).

$$\sigma_{zs}^{Q_2}(s, z) = \frac{Q_2(z)}{J_{Q_2}} \psi_s^{\chi_2}(s) \tag{5.18}$$

The shear stress $\sigma_{zs}^{Q_2}$ given in Eq. (5.18) produces the shear strain $\gamma_{zs}^{Q_2} = \sigma_{zs}^{Q_2} / G$ along the contour line, and consequently W_2 shown in Fig. 5.3(b) occurs on the box beam by $\gamma_{zs}^{Q_2}$ [2]. When $u_z^{W_2}(s, z)$ represents the axial displacement on the contour line represented by W_2, the following condition which $u_z^{W_2}(s, z)$ should meet can be defined from Eq. (5.18).

$$\gamma_{zs}^{Q_2} = \frac{\partial u_z^{W_2}}{\partial s} = \frac{Q_2(z)}{GJ_{Q_2}} \psi_s^{\chi_2}(s) \tag{5.19}$$

Since $u_z^{W_2}(s, z) = \psi_z^{W_2}(s) \cdot W_2(z)$ as given in Eq. (5.1c), the following equation regarding to the shape function $\psi_z^{W_2}(s)$ of W_2 can be obtained from Eq. (5.19).

$$\frac{\partial \psi_z^{W_2}(s)}{\partial s} = P_2^* \times \psi_s^{\chi_2}(s) \tag{5.20}$$

where P_2^* represents the proportional constant. Carrying out the integration for coordinate s, consequently $\psi_z^{W_2}(s_j)$ on Edge j ($j = 1, 2, 3, 4$) can be expressed as:

$$\psi_z^{W_2}(s_1) = P_2^* \times \{-\frac{1}{h}s_1^{\,2} + C_1\}, \qquad \psi_z^{W_2}(s_2) = P_2^* \times \{-\frac{1}{h}s_2^{\,2} + C_2\},$$
$$\psi_z^{W_2}(s_3) = P_2^* \times \{-\frac{1}{h}s_3^{\,2} + C_3\}, \qquad \psi_z^{W_2}(s_4) = P_2^* \times \{-\frac{1}{h}s_4^{\,2} + C_4\} \tag{5.21}$$

where (C_1, C_2, C_3, C_4) represent the integration constants.

$\psi_z^{W_2}(s_j)$ ($j = 1, 2, 3, 4$) in Eq. (5.21) should be symmetric with respect to *x*-axis and *y*-axis because distribution of $\sigma_{zs}^{Q_2}$ along the contour line satisfy those symmetry conditions. Considering the mentioned symmetry conditions, one can find the following relations associated with the constants ($C_1 \sim C_4$) in Eq. (5.21).

$$C_1 = C_3; \qquad C_2 = C_4 \tag{5.22}$$

In addition, the displacement continuity condition $u_z^{W_2}(s_j, z)|_{\text{corner } j} = u_z^{W_2}(s_{j+1}, z)|_{\text{corner } j}$ between $u_z^{W_2}(s_j, z)$ on Edge *j* and $u_z^{W_2}(s_{j+1}, z)$ on Edge *j*+1 at the corner *j* ($j = 1, 2, 3, 4$) must hold, and consequently the following conditions with respect to $\psi_z^{W_2}(s)$ given in Eq. (5.21) can be obtained.

$$\psi_z^{W_2}(s_1 = \frac{h}{2}) = \psi_z^{W_2}(s_2 = -\frac{b}{2}), \qquad \psi_z^{W_2}(s_2 = \frac{b}{2}) = \psi_z^{W_2}(s_3 = -\frac{h}{2}),$$
$$\psi_z^{W_2}(s_3 = \frac{h}{2}) = \psi_z^{W_2}(s_4 = -\frac{b}{2}), \qquad \psi_z^{W_2}(s_4 = \frac{b}{2}) = \psi_z^{W_2}(s_1 = -\frac{h}{2}) \tag{5.23}$$

Meanwhile, $\psi_z^{W_2}$ in Eq. (5.35) should meet the following orthogonality condition with $\psi_z^{U_z}$ so that the relation given in Eq. (5.1c) is defined correctly.

$$\iint_S \psi_z^{W_2}(s) \cdot \psi_z^{U_z}(s)\, dA = 0 \tag{5.24}$$

where Eq. (5.24) means that the cross-sectional deformation represented by W_2

does not include any rigid-body translation in z.

Considering the conditions of $\psi_z^{W_2}$ given in Eqs. (5.22-24), the constants ($C_1 \sim C_4$) in Eq. (5.21) meeting those conditions can be determined as:

$$C_1 = C_3 = -\frac{2b^3 - 3bh^2 - h^3}{12h(b+h)}; \qquad C_2 = C_2 = -\frac{2h^3 - 3b^2h - b^3}{12h(b+h)} \tag{5.25}$$

The constant P_2^* in Eq. (5.21) determine the scale of cross-sectional deformation represented by the unit magnitude of W_2, and $P_2^* = 4/h$ will be used in this study.

5.3.3 Shape Function of χ_4

To define the edge forces in n direction on Edge 1 and Edge 3 independently, χ_4 representing antisymmetric deformation of the box beam cross-section with respect to y-axis as shown in Fig. 5.3(b) should be introduced in the higher-order beam theory. As with the field variable χ_3, deformation of the box beam cross-section in n direction is represented by χ_4, and one can assume the shape function $\psi_n^{\chi_4}(s_j)$ on Edge j ($j = 1, 2, 3, 4$) as follows.

$$\psi_n^{\chi_4}(s_1) = a_{11}(s_1)^4 + a_{12}(s_1)^2 + a_{13} \tag{5.26a}$$

$$\psi_n^{\chi_4}(s_2) = a_{21}(s_2)^3 + a_{22}(s_2) \tag{5.26b}$$

$$\psi_n^{\chi_4}(s_3) = -a_{11}(s_3)^4 - a_{12}(s_3)^2 - a_{13} \tag{5.26c}$$

$$\psi_n^{\chi_4}(s_3) = -a_{21}(s_3)^3 - a_{22}(s_3) \tag{5.26d}$$

where $\psi_n^{\chi_4}(s_j)$ ($j=1, 2, 3, 4$) satisfy both the symmetric and antisymmetric conditions with respect to x-axis and y-axis respectively. When $u_n^{\chi_4}(s, z)=\psi_n^{\chi_4}(s)\cdot\chi_4(z)$ refers to the displacement on the contour line in n direction represented by χ_4, one can consider the following displacement continuity conditions.

$$\begin{aligned} &u_n^{\chi_4}(s_1=\pm\frac{h}{2}, z)=0\,; \quad u_n^{\chi_4}(s_2=0 \text{ or } \pm\frac{b}{2}, z)=0\,; \\ &u_n^{\chi_4}(s_3=\pm\frac{h}{2}, z)=0\,; \quad u_n^{\chi_4}(s_4=0 \text{ or } \pm\frac{b}{2}, z)=0 \end{aligned} \tag{5.27}$$

In addition, the following angle and moment continuities should also be satisfied at the corner according to Ref. [6].

$$\begin{aligned} &\beta_z^{\chi_4}(s_1=\frac{h}{2})=\beta_z^{\chi_4}(s_2=-\frac{b}{2}), \qquad \beta_z^{\chi_4}(s_1=-\frac{h}{2})=\beta_z^{\chi_4}(s_4=\frac{b}{2}), \\ &\beta_z^{\chi_4}(s_3=-\frac{h}{2})=\beta_z^{\chi_4}(s_2=\frac{b}{2}), \qquad \beta_z^{\chi_4}(s_3=\frac{h}{2})=\beta_z^{\chi_4}(s_4=-\frac{b}{2}) \end{aligned} \tag{5.28a}$$

$$\begin{aligned} &\bar{M}_z^{\chi_4}(s_1=\frac{h}{2})=\bar{M}_z^{\chi_4}(s_2=-\frac{b}{2}), \qquad \bar{M}_z^{\chi_4}(s_1=-\frac{h}{2})=\bar{M}_z^{\chi_4}(s_4=\frac{b}{2}), \\ &\bar{M}_z^{\chi_4}(s_3=-\frac{h}{2})=\bar{M}_z^{\chi_4}(s_2=\frac{b}{2}), \qquad \bar{M}_z^{\chi_4}(s_3=\frac{h}{2})=\bar{M}_z^{\chi_4}(s_4=-\frac{b}{2}) \end{aligned} \tag{5.28b}$$

where $\beta_z^{\chi_4}(s_j)$ and $\bar{M}_z^{\chi_4}(s_j)$ at Edge j ($j=1, 2, 3, 4$) are defined as

$$\beta_z^{\chi_4}(s_j)=\frac{\partial u_n^{\chi_4}(s_j)}{\partial s}\,; \qquad \bar{M}_z^{\chi_4}(s_j)=\frac{Et^3}{12}\times\frac{\partial^2 u_n^{\chi_4}(s_j)}{\partial s^2} \tag{5.29a, b}$$

The symbols $\beta_z^{\chi_4}(s_j)$ and $\bar{M}_z^{\chi_4}(s_j)$ represent the bending rotation and bending moment in z direction, respectively [6] . The moment $\bar{M}_z^{\chi_4}(s_j)$ in Eq. (5.28b) is

approximately defined by the classical beam theory, and t in Eq. (5.28b) represents the thickness of Edge j.

$\psi_n^{\chi_4}(s_j)$ ($j = 1, 2, 3, 4$) given in Eq. (5.26) can be determined through those continuity conditions given in Eqs. (5.27-5.29) as:

$$\psi_n^{\chi_4}(s_1) = P_3^* \times \{-\frac{b(b+3h)}{2h^3}(s_1)^4 + \frac{3b(b+h)}{4h}(s_1)^2 + \frac{bh(-5b-3h)}{32}\} \quad (5.30a)$$

$$\psi_n^{\chi_4}(s_2) = P_3^* \times \{(s_2)^3 - \frac{b^2}{4}(s_2)\} \quad (5.30b)$$

$$\psi_n^{\chi_4}(s_3) = P_3^* \times \{\frac{b(b+3h)}{2h^3}(s_3)^4 - \frac{3b(b+h)}{4h}(s_3)^2 - \frac{bh(-5b-3h)}{32}\} \quad (5.30c)$$

$$\psi_n^{\chi_4}(s_4) = P_3^* \times \{-(s_4)^3 + \frac{b^2}{4}(s_4)\} \quad (5.30d)$$

The constant P_3^* in Eq. (5.30) determine the scale of cross-sectional deformation represented by the unit magnitude of χ_4, and $P_3^* = -\frac{32}{bh(5b+3h)}$ will be used in this study.

5.4 Derivation of the Exact Joint Matching Conditions

With respect to analysis of three or more box beams-joint structures by using the higher-order beam theory established in the previous section, the key is to define the exact joint matching conditions among the field variables which represent the behavior of the joint correctly.

After explaining the difficulties whereby the stiffness of the joint is

overestimated when the matching conditions proposed in Choi and Kim [23] are directly extended to three or more box beams-joint structures, we will propose and derive the exact joint matching conditions, which are applicable to three or more box beams-joint structures.

Concerning the two box beams-joint structure shown in Fig. 5.4, the field variables of Beam k ($k = 1, 2$) employed in Choi and Kim [23] are represented as,

$$\hat{\mathbf{U}}_k = \{(U_z)_k, (U_x)_k, (\theta_y)_k, (\chi_1^g)_k, (W_1^g)_k, (\chi_3)_k\}^{\mathrm{T}} \tag{5.31}$$

In Choi and Kim [23], joint matching conditions between $\hat{\mathbf{U}}_1$ and $\hat{\mathbf{U}}_2$ are exactly defined by introducing joint matrix $\mathbf{T}$. Through the various box beams-joint examples, it was shown that the matching conditions can describe the response of the joint precisely as interpreted by the shell elements.

When a two box beams-joint structure is modeled as shown in Fig. 5.5 by adopting the same procedure as the modeling in Fig. 5.2, the matching conditions between $\hat{\mathbf{U}}_1$ and $\hat{\mathbf{U}}_2$ can be expressed as follows by using the joint matrix $\mathbf{T}$ proposed in Choi and Kim [23]: (However, concerning the modeling in Fig. 5.5,

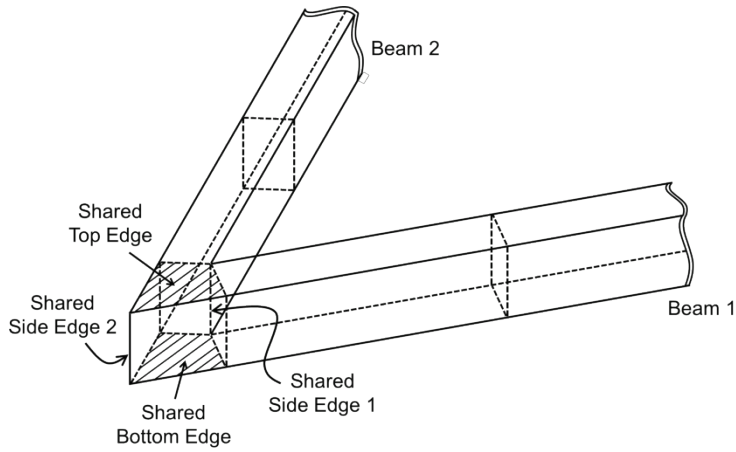

Fig. 5.4 Two thin-walled box beams-joint structures.

the constraint conditions between Edge M_1M_1' and Edge N_2N_2' or between Edge M_2M_2' and Edge N_1N_1' were not considered when the following matching conditions are defined.)

$$\hat{\mathbf{U}}_2 = \mathbf{T}(\phi_2 - \phi_1) \cdot \hat{\mathbf{U}}_1 \tag{5.32a}$$

or

$$\begin{Bmatrix} (U_z)_2 \\ (U_x)_2 \\ (\theta_y)_2 \\ (\chi_1^g)_2 \\ (W_1^g)_2 \\ (\chi_3)_2 \end{Bmatrix} = \begin{bmatrix} \mathbf{A} & \mathbf{B} \\ \mathbf{0} & \mathbf{C} \end{bmatrix} \begin{Bmatrix} (U_z)_1 \\ (U_x)_1 \\ (\theta_y)_1 \\ (\chi_1^g)_1 \\ (W_1^g)_1 \\ (\chi_3)_1 \end{Bmatrix} \tag{5.32b}$$

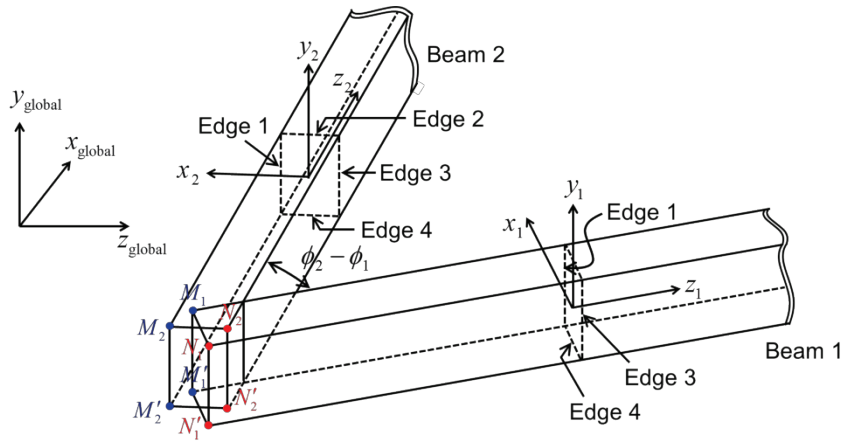

(a)

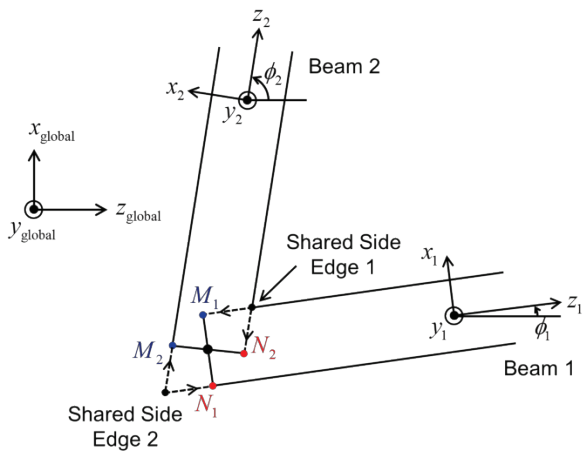

Fig. 5.5 (*a*) Beam Modeling for the two box beams-joint structures (Edge $M_1M'_1$ of Beam 1 and Edge N_2N_2' of Beam 2 are considered as if they were connected rigidly to each other (by an imaginary rigid body), and Edge N_1N_1' of Beam 1 and Edge $M_2M'_2$ of Beam 2 are also considered as if being connected rigidly to each other (by an imaginary rigid body).), (*b*) the top view of beam modeling (Shared Side Edge 1 in Fig. 5.4 is extended and represented by Edge $M_1M'_1$ of Beam 1 and Edge N_2N_2' of Beam 2 separately, and Share Side Edge 2 in Fig 5.4 is also extended and represented by Edge N_1N_1' of Beam 1 and Edge $M_2M'_2$ of Beam 2 separately.).

where the definitions of submatrix **A**, **B** and **C** are as

$$\mathbf{A}=\begin{bmatrix}\cos(\phi_2-\phi_1) & \sin(\phi_2-\phi_1) & 0\\ -\sin(\phi_2-\phi_1) & \cos(\phi_2-\phi_1) & 0\\ 0 & 0 & 1\end{bmatrix} \tag{5.32c}$$

$$\mathbf{B}=\begin{bmatrix}0 & 0 & 0\\ 0 & 0 & 0\\ 0 & \frac{4(5h^2-b^2)}{5bh(b+3h)}(1+\cos(\phi_2-\phi_1)) & -\frac{16(b+h)}{(b+3h)(5b+h)}\sin(\phi_2-\phi_1)\end{bmatrix} \tag{5.32d}$$

$$\mathbf{C}=\begin{bmatrix}-1 & 0 & 0\\ 0 & -\cos(\phi_2-\phi_1) & \frac{20bh(b+h)}{(5b+h)(5h^2-b^2)}\sin(\phi_2-\phi_1)\\ 0 & -\frac{(5b+h)(5h^2-b^2)}{20bh(b+h)}\sin(\phi_2-\phi_1) & -\cos(\phi_2-\phi_1)\end{bmatrix} \tag{5.32e}$$

where ϕ_k ($k=1, 2$) represents the angle between the axial coordinate z_k of Beam k and z_{global} in Fig. 5.5 (see Fig. 5.5(b) for the positive directions), and ($\phi_2-\phi_1$) in Eq. (5.32) denotes the joint angle of the two box beams-joint structure. Observing the joint matrix $\mathbf{T}(\phi_2-\phi_1)$, its submatrix **A** represents the matching conditions among rigid-body motions. Submatrix **B** represents additional rigid-body motion ($(\theta_y)_2$) of Beam 2 generated by the higher-order deformations ($(W_1^g)_1$, $(\chi_3)_1$) of Beam 1, and submatrix **C** represents the matching conditions among higher-order deformations (χ_1^g, W_1^g, χ_3).

If one wishes to directly extend the matching conditions in Eq. (5.32) for T-joint structure, for example, it could be written as:

$$\hat{\mathbf{U}}_2=\mathbf{T}(\phi_2-\phi_1)\cdot\hat{\mathbf{U}}_1,\quad \hat{\mathbf{U}}_3=\mathbf{T}(\phi_3-\phi_2)\cdot\hat{\mathbf{U}}_2,\quad \hat{\mathbf{U}}_1=\mathbf{T}(\phi_1-\phi_3)\cdot\hat{\mathbf{U}}_3 \tag{5.33}$$

where the joint angles (ϕ_1, ϕ_2, ϕ_3) in Eq. (5.33) are $\phi_1 = 0^\circ$, $\phi_2 = 90^\circ$, $\phi_3 = 180^\circ$ in T-joint structure. If the matching conditions in Eq. (5.32) are applied, the relations among $(\chi_1^g)_1, (\chi_1^g)_2$, and, $(\chi_1^g)_3$, will be expressed as:

$$(\chi_1^g)_2 = -(\chi_1^g)_1, \qquad (\chi_1^g)_3 = -(\chi_1^g)_2, \qquad (\chi_1^g)_1 = -(\chi_1^g)_3 \tag{5.34}$$

Because the relations in Eq. (5.34) should be satisfied for arbitrary $(\chi_1^g)_1, (\chi_1^g)_2$, and, $(\chi_1^g)_3$, the relations eventually represent $(\chi_1^g)_1 = (\chi_1^g)_2 = (\chi_1^g)_3 = 0$.

Likewise, the relations among (W_1^g, χ_3) of three box beams will be expressed as:

$$(W_1^g)_2 = \frac{20bh(b+h)}{(5b+h)(5h^2-b^2)}(\chi_3)_1 \; ; \qquad (\chi_3)_2 = -\frac{(5b+h)(5h^2-b^2)}{20bh(b+h)}(W_1^g)_1 \tag{5.35a}$$

$$(W_1^g)_3 = \frac{20bh(b+h)}{(5b+h)(5h^2-b^2)}(\chi_3)_2 \; ; \qquad (\chi_3)_3 = -\frac{(5b+h)(5h^2-b^2)}{20bh(b+h)}(W_1^g)_2 \tag{5.35b}$$

$$(W_1^g)_1 = (W_1^g)_3 \; ; \qquad (\chi_3)_1 = (\chi_3)_3 \tag{5.35c}$$

The relations given in Eqs. (5.35a-c) should also be satisfied for arbitrary ($(W_1^g)_k, (\chi_3)_k$) of Beam k ($k = 1, 2, 3$), the relations eventually represent $(W_1^g)_1 = (W_1^g)_2 = (W_1^g)_3 = 0$ and $(\chi_3)_1 = (\chi_3)_2 = (\chi_3)_3 = 0$.

Observing submatrix **B** in joint matrix **T**, on the other hand, it can be seen that rigid-body motions (θ_y) of the beams connected to the joint are additionally induced by higher-order deformations (W_1^g, χ_3) as well as rigid-body motions (θ_y) of adjacent beams. Therefore, when the matching relations such as Eqs. (5.34) and

(35) (i.e. all the higher-order deformations of three box beams are zero) are applied to the T-joint structure, those relations overestimate the stiffness of the joint, and it is not possible to obtain an accurate result.

Observing the results in Choi and Kim [23], the joint matching conditions defined on Edge 1 are equal to those defined on Edge 3 because the higher-order deformations (χ_1^g, W_1^g, χ_3) having y-axis antisymmetric deformation pattern are only employed. To define the joint matching conditions on Edge 1 and Edge 3 independently, therefore, the higher-order deformations (χ_2, W_2, χ_4) having y-axis symmetric deformation patterns should be employed together. From the same reason, when the matching conditions given in Eq. (5.32) are extended to the three or more box beams-joint structure, the stiffness of the joint again tends to be overestimated. Therefore, the joint matching conditions proposed by Choi and Kim [23] cannot be directly extended to the three or more box beams-joint structure, and a new approach that is different from the existing methods should be developed, to deal with the three or more box beams-joint structure under in-plane loads.

To develop a new analysis approach applicable to three or more box beams-joint structure under in-plane loads, we will first define the equilibrium conditions among the generalized forces (F_z, F_x, M_y, Q_1^g, B_1^g, Q_2, B_2, Q_3, Q_4) of each beam at the joint. Choi and Kim [22] demonstrated that the self-equilibrated forces (Q_1^g, B_1^g, Q_2, B_2, Q_3, Q_4) produce non-zero resultants on each edge of the box beam cross-section, and Choi and Kim [23] found the equilibrium conditions

among (F_z, F_x, M_y, Q_1^g, B_1^g, Q_3) of two beams at the angled joint. Based on Refs. [22, 23], therefore, we will derive for the first time the equilibrium conditions applicable to the three or more box beams-joint structures. Subsequently, applying the principle of virtual work to the equilibrium conditions we determined, we will derive the exact joint matching conditions for the generalized displacements (or field variables) which are energy conjugates of those generalized forces.

5.4.1 Sectional and Edge Resultants Produced by Generalized Forces

Prior to dealing with the generalized forces equilibriums, the stresses which generalized forces induce on the section will be introduced, and from those stresses, sectional or edge resultants will be derived.

According to Eq. (5.4), dominant stresses (σ_{zz}, σ_{zs}) on the contour ($n=0$) can be related to the displacements as:

$$\sigma_{zz}(s,z)=\frac{E}{1-\nu^2}(\psi_z^{U_z}\cdot U_z{}'+\psi_z^{\theta_y}\cdot\theta_y{}'+\psi_z^{W_1^g}\cdot W_1^{g\prime}+\psi_z^{W_2}\cdot W_2{}'+\nu\dot{\psi}_s^{\chi_1^g}\cdot\chi_1^g+\nu\dot{\psi}_s^{\chi_2}\cdot\chi_2) \tag{5.36a}$$

$$\sigma_{sz}(s,z)=G(\psi_s^{U_x}\cdot U_x{}'+\psi_s^{\chi_1^g}\cdot\chi_1^{g\prime}+\psi_s^{\chi_2}\cdot\chi_2{}'+\dot{\psi}_z^{\theta_y}\cdot\theta_y+\dot{\psi}_z^{W_1^g}\cdot W_1^g+\dot{\psi}_z^{W_2}\cdot W_2) \tag{5.36b}$$

The derivative terms ($\dot{\psi}_z^{\theta_y}$, $\dot{\psi}_s^{\chi_1^g}$, $\dot{\psi}_s^{\chi_2}$, $\dot{\psi}_z^{W_1^g}$, $\dot{\psi}_z^{W_2}$) in Eqs. (5.36a, b) can be related with other shape functions ($\psi_s^{U_x}$, $\psi_z^{\theta_y}$, $\psi_s^{\chi_1^g}$, $\psi_z^{W_1^g}$, $\psi_s^{\chi_2}$, $\psi_z^{W_2}$) as $\dot{\psi}_z^{\theta_y}=-\psi_s^{U_x}$, $\dot{\psi}_s^{\chi_1^g}=-\frac{6}{h^2}\psi_z^{\theta_y}$, $\dot{\psi}_s^{\chi_2}=-\frac{2}{h}\psi_z^{U_z}$, $\dot{\psi}_z^{W_1^g}=-\frac{4(b^3+5h^3)}{15bh^2(b+3h)}\psi_s^{U_x}-\frac{16}{6b}\psi_s^{\chi_1}$ and $\dot{\psi}_z^{W_2}=$

$\frac{4}{h}\psi_s^{\chi_2}$ (see the explicit expressions of ψ's in Appendix A), and thus Eqs. (5.36a, b) can be rewritten as:

$$\sigma_{zz}(s,z)=\frac{E}{1-\nu^2}\{\psi_z^{U_z}\cdot(U_z{}'-\nu\frac{2}{h}\chi_2)+\psi_z^{\theta_y}\cdot(\theta_y{}'-\nu\frac{6}{h^2}\chi_1^g)+\psi_z^{W_1^g}\cdot W_1^{g\prime}+\psi_z^{W_2}\cdot W_2{}'\} \tag{5.37a}$$

$$\begin{aligned}\sigma_{sz}(s,z)=G[\,&\psi_s^{U_x}\cdot\{U_x{}'-\theta_y-\frac{4(b^3+5h^3)}{15bh^2(b+3h)}W_1^g\}\\&+\psi_s^{\chi_1^g}\cdot\{\chi_1^{g\prime}-\frac{16}{6b}W_1^g\}+\psi_s^{\chi_2}\cdot\{\chi_2{}'+\frac{4}{h}W_2\}]\end{aligned} \tag{5.37b}$$

Substituting (σ_{zz},σ_{zs}) in Eqs. (5.37a, b) into the definitions of generalized forces $\mathbf{F}$ given in Eq. (5.6) and carrying out the surface integral for the cross-section *S*, one can obtain the following relations between the generalized forces $\mathbf{F}$ and the field variables $\mathbf{U}$.

$$\begin{aligned}F_z(z)&=\iint_S\sigma_{zz}(s,z)\cdot\psi_z^{U_z}(s)\,dsdn\\&=\iint_S\frac{E}{1-\nu^2}[\,\psi_z^{U_z}\cdot\psi_z^{U_z}\cdot\{U_z{}'-\nu\frac{2}{h}\chi_2\}+\psi_z^{\theta_y}\cdot\psi_z^{U_z}\cdot\{\theta_y{}'-\nu\frac{6}{h^2}\chi_1^g\}\\&\qquad+\psi_z^{W_1^g}\cdot\psi_z^{U_z}\cdot\{W_1^{g\prime}\}+\psi_z^{W_2}\cdot\psi_z^{U_z}\cdot\{W_2{}'\}]dsdn\\&=\iint_S\frac{E}{1-\nu^2}[\psi_z^{U_z}\cdot\psi_z^{U_z}\cdot\{U_z{}'-\nu\frac{2}{h}\chi_2\}]\,dsdn\\&=\frac{E}{1-\nu^2}J_{F_z}\{U_z{}'(z)-\nu\frac{2}{h}\chi_2(z)\}\end{aligned} \tag{5.38a}$$

The second line in Eq. (5.38a) can be reduced as the third line by the orthogonality conditions such as $\iint_S\psi_z^{\theta_y}\cdot\psi_z^{U_z}\,dsdn=0$, $\iint_S\psi_z^{W_1^g}\cdot\psi_z^{U_z}\,dsdn=0$ and $\iint_S\psi_z^{W_2}\cdot\psi_z^{U_z}\,dsdn=0$ (See Appendix A). Moreover, the orthogonality condition

among ($\psi_s^{U_x}, \psi_s^{\chi_1^g}, \psi_s^{\chi_2}$) can be also considered as given in Appendix A, and considering those orthogonality conditions, the remained generalized forces except (Q_3, Q_4) can be express as:

$$F_x(z) = \iint_S \sigma_{zs}(s, z) \cdot \psi_s^{U_x}(s)\, dsdn = GJ_{F_x}\{U_x'(z) - \theta_y(z) - \frac{4(b^3+5h^3)}{15bh^2(b+3h)} W_1^g(z)\}$$

(5.38b)

$$M_y(z) = \iint_S \sigma_{zz}(s, z) \cdot \psi_z^{\theta_y}(s)\, dsdn = \frac{E}{1-\nu^2} J_{M_y}\{\theta_y'(z) - \nu \frac{6}{h^2} \chi_1^g(z)\} \quad (5.38c)$$

$$Q_1^g(z) = \iint_S \sigma_{zs}(s, z) \cdot \psi_s^{\chi_1^g}(s)\, dsdn = GJ_{Q_1^g}\{\chi_1^{g\prime}(z) - \frac{16}{6b} W_1^g(z)\} \quad (5.38d)$$

$$B_1^g(z) = \iint_S \sigma_{zz}(s, z) \cdot \psi_z^{W_1^g}(s)\, dsdn = \frac{E}{1-\nu^2} J_{B_1^g}\{W_1^{g\prime}(z)\} \quad (5.38e)$$

$$Q_2(z) = \iint_S \sigma_{zs}(s, z) \cdot \psi_s^{\chi_2}(s)\, dsdn = GJ_{Q_2}\{\chi_2'(z) + \frac{4}{h} W_2(z)\} \quad (5.38f)$$

$$B_2(z) = \iint_S \sigma_{zz}(s, z) \cdot \psi_z^{W_2}(s)\, dsdn = \frac{E}{1-\nu^2} J_{B_2}\{W_2'(z)\} \quad (5.38g)$$

where J_β ($\beta = F_z, F_x, M_y, Q_1^g, B_1^g, Q_2, B_2$) represent the moment of inertia for the generalized force β, and the explicit expressions for J_β are given in Appendix A.

Substituting those results given in Eq. (5.38) into Eq. (5.37), (σ_{zz}, σ_{zs}) on the contour line can be expressed in terms of the generalized forces as:

$$\sigma_{zz}(s,z)=\sigma_{zz}^{F_z}+\sigma_{zz}^{M_y}+\sigma_{zz}^{B_1^g}+\sigma_{zz}^{B_2}=\frac{F_z(z)}{J_{F_z}}\psi_z^{U_z}(s)+\frac{M_y(z)}{J_{M_y}}\psi_z^{\theta_y}(s)+\frac{B_1^g(z)}{J_{B_1^g}}\psi_z^{W_1^g}(s)+\frac{B_2(z)}{J_{B_2}}\psi_z^{W_2}(s) \tag{5.39a}$$

$$\sigma_{sz}(s,z)=\sigma_{zs}^{F_x}+\sigma_{zs}^{Q_1^g}+\sigma_{zs}^{Q_2}=\frac{F_x(z)}{J_{F_x}}\psi_s^{U_x}(s)+\frac{Q_1^g(z)}{J_{Q_1^g}}\psi_s^{\chi_1^g}(s)+\frac{Q_2(z)}{J_{Q_2}}\psi_s^{\chi_2}(s) \tag{5.39b}$$

where σ^{β} ($\beta=F_z, F_x, M_y, Q_1^g, B_1^g, Q_2, B_2$) represent the stress on the contour line produced by the generalized force β. Therefore, one can define the edge resultants of β generated on each edge by using σ^{β}.

Meanwhile, the definitions of (Q_3, Q_4) given in Eq. (5.6) are different with those considered above because (χ_3, χ_4), the work conjugate of (Q_3, Q_4) respectively, represent the deformations only in n direction. Unlike the procedure introduced above, thus, $\sigma_{zs}(n,s,z)$ at a generic point located away from the contour line by n should be substituted into the definition of Q_3, Q_4 in Eq. (5.6), and through that the following result can be obtained.

$$\begin{aligned}
Q_3 &= \iint_S \sigma_{zs}(-n\dot{\psi}_n^{\chi_3})\ dsdn \\
&= \iint_S G\{\psi_s^{U_x}\cdot(-n\dot{\psi}_n^{\chi_3})\cdot U_x' + \dot{\psi}_z^{\theta_y}\cdot(-n\dot{\psi}_n^{\chi_3})\cdot\theta_y + \psi_s^{\chi_1^g}\cdot(-n\dot{\psi}_n^{\chi_3})\cdot\chi_1^{g\prime} \\
&\quad + \dot{\psi}_z^{W_1^g}\cdot(-n\dot{\psi}_n^{\chi_3})\cdot W_1^g + \psi_s^{\chi_2}\cdot(-n\dot{\psi}_n^{\chi_3})\cdot\chi_2' + \dot{\psi}_z^{W_2}\cdot(-n\dot{\psi}_n^{\chi_3})\cdot W \\
&\quad + (-2n\ \dot{\psi}_n^{\chi_1^g})\cdot(-n\dot{\psi}_n^{\chi_3})\cdot\chi_1^{g\prime} + (-2n\ \dot{\psi}_n^{\chi_3})\cdot(-n\dot{\psi}_n^{\chi_3})\cdot\chi_3' \\
&\quad + (-2n\dot{\psi}_n^{\chi_4})\cdot(-n\dot{\psi}_n^{\chi_3})\cdot\chi_4')\}\ dsdn \\
&= \iint_S G[(-2n\dot{\psi}_n^{\chi_3})\cdot(-n\dot{\psi}_n^{\chi_3})\cdot\{\chi_3'\}]\ dsdn \\
&= 2GJ_{Q_3}\{\chi_3'(z)\}
\end{aligned} \tag{5.40a}$$

The second line in Eq. (5.40a) can be reduced as the third line because most of the integral terms in the second line are eliminated through the integral in n direction or by the orthogonal conditions such as $\iint_S (\dot{\psi}_n^{\chi_1^g}) \cdot (\dot{\psi}_n^{\chi_3})\, dsdn = 0$ and $\iint_S (\dot{\psi}_n^{\chi_4}) \cdot (\dot{\psi}_n^{\chi_3})\, dsdn = 0$. In addition, the orthogonality conditions such as $\iint_S (\dot{\psi}_n^{\chi_1^g}) \cdot (\dot{\psi}_n^{\chi_4})\, dsdn = 0$ and $\iint_S (\dot{\psi}_n^{\chi_3}) \cdot (\dot{\psi}_n^{\chi_4})\, dsdn = 0$ can be also considered as given in Appendix A, and considering those orthogonality conditions, Q_4 can be expressed as:

$$
\begin{aligned}
Q_4 &= \iint_S \sigma_{zs}(-n\dot{\psi}_n^{\chi_4})\ dsdn \\
&= \iint_S G\{\psi_s^{U_x} \cdot (-n\dot{\psi}_n^{\chi_4}) \cdot U_x' + \dot{\psi}_z^{\theta_y} \cdot (-n\dot{\psi}_n^{\chi_4}) \cdot \theta_y + \psi_s^{\chi_1^g} \cdot (-n\dot{\psi}_n^{\chi_4}) \cdot \chi_1^{g\prime} \\
&+ \dot{\psi}_z^{W_1^g} \cdot (-n\dot{\psi}_n^{\chi_4}) \cdot W_1^g + \psi_s^{\chi_2} \cdot (-n\dot{\psi}_n^{\chi_4}) \cdot \chi_2' + \dot{\psi}_z^{W_2} \cdot (-n\dot{\psi}_n^{\chi_4}) \cdot W \\
&+ (-2n\, \dot{\psi}_n^{\chi_1^g}) \cdot (-n\dot{\psi}_n^{\chi_4}) \cdot \chi_1^{g\prime} + (-2n\, \dot{\psi}_n^{\chi_3}) \cdot (-n\dot{\psi}_n^{\chi_4}) \cdot \chi_3' \\
&+ (-2n\dot{\psi}_n^{\chi_4}) \cdot (-n\dot{\psi}_n^{\chi_4}) \cdot \chi_4')\}\, dsdn \\
&= \iint_S G[(-2n\dot{\psi}_n^{\chi_4}) \cdot (-n\dot{\psi}_n^{\chi_4}) \cdot \{\chi_4'\}]\, dsdn \\
&= 2GJ_{Q_4}\{\chi_4'(z)\}
\end{aligned}
\tag{5.40b}
$$

The symbols (J_{Q_3}, J_{Q_4}) in Eqs. (5.40a, b) represent the moment of inertia for Q_3, Q_4 respectively and the definitions of (J_{Q_3}, J_{Q_4}) are given in Appendix A. When the results given in Eqs. (5.40a, b) are substituted into Eq. (5.6c), the stresses ($\sigma_{sz}^{Q_3}$, $\sigma_{sz}^{Q_4}$) which are generated by (Q_3, Q_4) can be also obtained as:

$$\sigma_{sz}^{Q_3}(n, s, z) = \frac{Q_3(z)}{J_{Q_3}}\{-n\dot{\psi}_n^{\chi_3}(s)\} \tag{5.41a}$$

$$\sigma_{sz}^{Q_4}(n, s, z) = \frac{Q_4(z)}{J_{Q_4}}\{-n\dot{\psi}_n^{\chi_4}(s)\} \tag{5.41b}$$

First, it will be shown how to obtain the edge resultants of generalized force β_1 ($\beta_1 = F_z, F_x, M_y$) which have conventional or sectional resultants as shown in Fig. 5.6. Stresses on (s, z) induced by those forces are given in Eq. (5.39), and edge resultants of those forces can be obtained by integrating stresses on each edge according to Choi and Kim [22]. The non-zero edge resultants determined from the stresses in Eq. (5.39) are axial force $F_{z(j)}^{\beta_1}$, tangential force $F_{s(j)}^{\beta_1}$, and normal moment $M_{n(j)}^{\beta_1}$ ($\beta_1 = F_z, F_x, M_y$), and are defined as

$$F_{z(j)}^{\beta_1} = \iint_{Edge\ j} \sigma_{zz}^{\beta_1}\ dsdn, \quad F_{s(j)}^{\beta_1} = \iint_{Edge\ j} \sigma_{zs}^{\beta_1}\ dsdn, \quad M_{n(j)}^{\beta_1} = \iint_{Edge\ j} s \cdot \sigma_{zz}^{\beta_1}\ dsdn \tag{5.42}$$

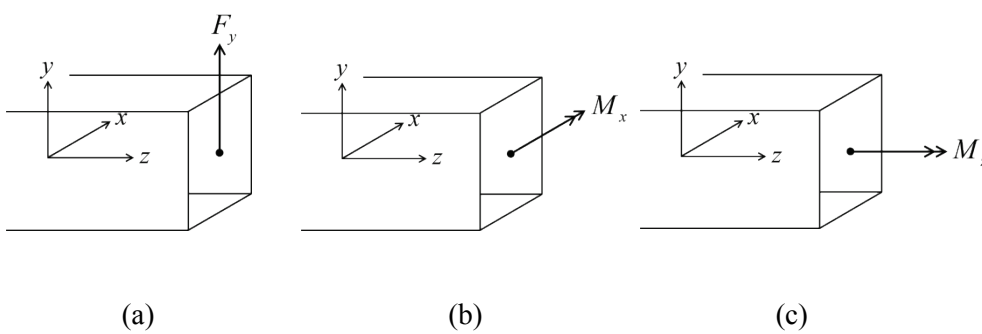

Fig. 5.6 Resultants (or sectional resultants) acting on the entire cross-section that are produced by the generalized forces: vertical force F_y, bending moment M_x, and twisting moment M_z.

On the contrary, the distribution of σ^{β_2} ($\beta_2 = Q_1^g, B_1^g, Q_2, B_2$) represented by the shape function ($\psi_s^{\alpha_2}$ or $\psi_z^{\alpha_2}$) of the work conjugate α_2 ($\alpha_2 = \chi_1^g, W_1^g, \chi_2, W_2$) is expressed by the highly complicated polynomial functions as given in Appendix A. For this reason, care should be taken when the edge resultants of β_2 are determined according to Choi and Kim [23]. To calculate the correct edge resultants of β_2 ($\beta_2 = Q_1^g, B_1^g, Q_2, B_2$), the following $\bar{\sigma}_{zz}^{\beta_2}$ or $\bar{\sigma}_{zs}^{\beta_2}$ is employed instead of $\sigma_{zz}^{\beta_2}$ or $\sigma_{zs}^{\beta_2}$ given in Eq. (5.39).

$$\bar{\sigma}_{zz}^{\beta_2}(s, z) = \frac{\beta_2(z)}{\bar{J}_{\beta_2}} \bar{\psi}_z^{\alpha_2}(s) \tag{5.43a}$$

$$\bar{\sigma}_{zs}^{\beta_2}(s, z) = \frac{\beta_2(z)}{\bar{J}_{\beta_2}} \bar{\psi}_s^{\alpha_2}(s) \tag{5.43b}$$

where $\bar{\psi}^{\alpha_2}(s_j)$ ($j = 1, 2, 3, 4$) represents the average distribution of σ^{β_2} on Edge j, and is defined as:

$$\begin{aligned} &\bar{\psi}_s^{\chi_1^g}(s_{j_1} \mid -\frac{h}{2} \le s_{j_1} \le 0) = (-1)^{(j_1+1)/2} \times \frac{3b}{4h}, \\ &\bar{\psi}_s^{\chi_1^g}(s_{j_1} \mid 0 \le s_{j_1} \le \frac{h}{2}) = (-1)^{(j_1-1)/2} \times \frac{3b}{4h} \qquad (j_1 = 1, 3) \\ &\bar{\psi}_s^{\chi_1^g}(s_{j_2}) = 0 \qquad (j_2 = 2, 4) \end{aligned} \tag{5.44a}$$

$$\begin{aligned} &\bar{\psi}_z^{W_1^g}(s_{j_1}) = (-1)^{(j-1)/2} \times \frac{2b(5h^2 - b^2)}{15h(b+3h)} \qquad (\text{for } j_1 = 1, 3) \\ &\bar{\psi}_z^{W_1^g}(s_{j_2}) = (-1)^{(j_2-2)/2} \times \frac{4(5h^2 - b^2)}{5bh(b+3h)} s_{j_2} \qquad (\text{for } j_2 = 2, 4) \end{aligned} \tag{5.44b}$$

$$\bar{\psi}_s^{\chi_2}(s_{j_1} \mid -\frac{h}{2} \le s_{j_1} \le 0) = \frac{1}{2}, \quad \bar{\psi}_s^{\chi_2}(s_{j_1} \mid 0 \le s_{j_1} \le \frac{h}{2}) = -\frac{1}{2} \qquad (j_1 = 1, 3)$$
$$\bar{\psi}_s^{\chi_2}(s_{j_2} \mid -\frac{b}{2} \le s_{j_2} \le 0) = \frac{b}{2h}, \quad \bar{\psi}_s^{\chi_2}(s_{j_2} \mid 0 \le s_{j_2} \le \frac{b}{2}) = -\frac{b}{2h} \quad (j_2 = 2, 4) \tag{5.44c}$$

$$\bar{\psi}_z^{W_2}(s_{j_1}) = \frac{2b(h-b)}{3h^2} \qquad (\text{for } j_1 = 1, 3)$$
$$\bar{\psi}_z^{W_2}(s_{j_2}) = -\frac{2(h-b)}{3h} \qquad (\text{for } j_2 = 2, 4) \tag{5.44d}$$

The definitions of $\bar{\psi}_s^{\alpha_2}(s_j)$ ($\alpha_2 = \chi_1^g, \chi_2$; $j = 1, 2, 3, 4$) given in Eqs. (5.44a, c) are as:

$$\bar{\psi}_s^{\alpha_2}(s_{j_1} \mid -\frac{h}{2} \le s_{j_1} \le 0) = \int_{-\frac{h}{2}}^{0} \psi_s^{\alpha_2}(s_{j_1})\, ds_{j_1} \Big/ \int_{-\frac{h}{2}}^{0} ds_{j_1},$$
$$\bar{\psi}_s^{\alpha_2}(s_{j_1} \mid 0 \le s_{j_1} \le \frac{h}{2}) = \int_{0}^{\frac{h}{2}} \psi_s^{\alpha_2}(s_{j_1})\, ds_{j_1} \Big/ \int_{0}^{\frac{h}{2}} ds_{j_1} \quad (j_1 = 1, 3) \tag{5.45a}$$

$$\bar{\psi}_s^{\alpha_2}(s_{j_2} \mid -\frac{b}{2} \le s_{j_2} \le 0) = \int_{-\frac{b}{2}}^{0} \psi_s^{\alpha_2}(s_{j_2})\, ds_{j_2} \Big/ \int_{-\frac{b}{2}}^{0} ds_{j_2}$$
$$\bar{\psi}_s^{\alpha_2}(s_{j_2} \mid 0 \le s_{j_2} \le \frac{b}{2}) = \int_{0}^{\frac{b}{2}} \psi_s^{\alpha_2}(s_{j_2})\, ds_{j_2} \Big/ \int_{0}^{\frac{b}{2}} ds_{j_2} \quad (j_2 = 2, 4) \tag{5.45b}$$

, and the definitions of $\bar{\psi}_z^{\alpha_2}(s_j)$ ($\alpha_2 = W_1^g, W_2$; $j = 1, 2, 3, 4$) given in Eqs. (5.44b, d) are as:

$$\bar{\psi}_s^{\alpha_2}(s_j) = \int \psi_s^{\alpha_2}(s_j)\, ds_j \Big/ \int ds_j \tag{5.46a}$$

or

$$\bar{\psi}_s^{\alpha_2}(s_j) = \{\int s_j \cdot \psi_s^{\alpha_2}(s_j)\, ds_j \Big/ \int (s_j)^2\, ds_j\} \cdot s_j \tag{5.46b}$$

where $\bar{\psi}_z^{\alpha_2}(s_j)$ is obtained through Eq. (5.46a) when $\psi_z^{\alpha_2}(s_j)$ is an even function. Otherwise, Eq. (5.46b) is employed to determine $\bar{\psi}_z^{\alpha_2}(s_j)$.

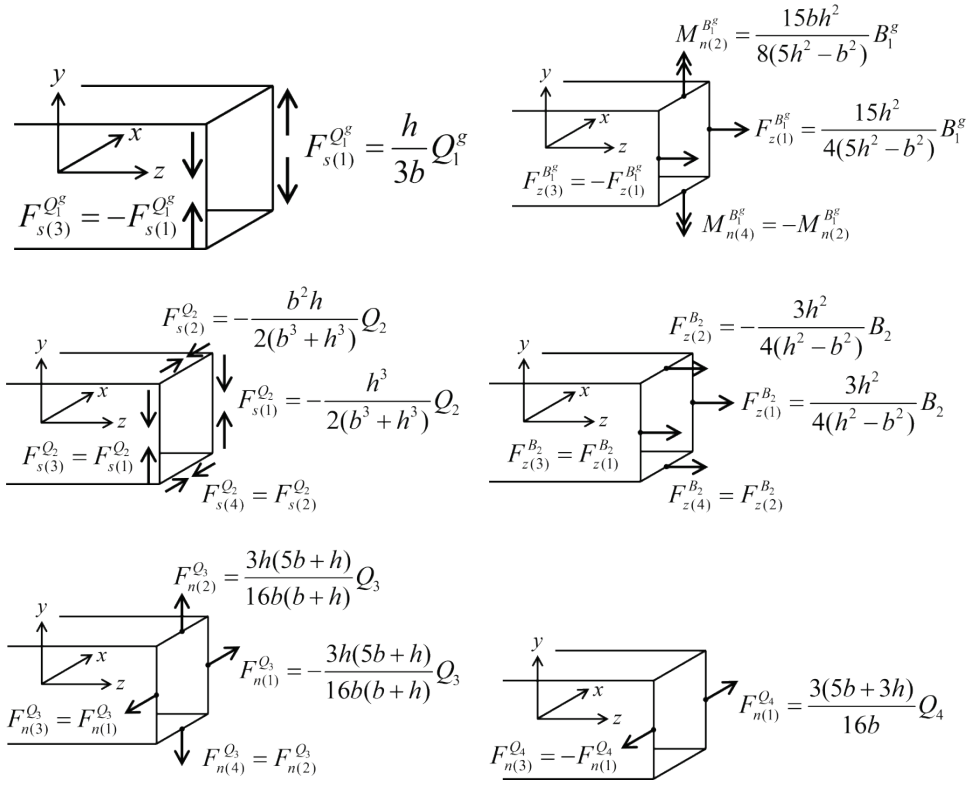
$F_{s(1)}^{Q_1^g} = \frac{h}{3b} Q_1^g$
$F_{s(3)}^{Q_1^g} = -F_{s(1)}^{Q_1^g}$
$M_{n(2)}^{B_1^g} = \frac{15bh^2}{8(5h^2 - b^2)} B_1^g$
$F_{z(1)}^{B_1^g} = \frac{15h^2}{4(5h^2 - b^2)} B_1^g$
$F_{z(3)}^{B_1^g} = -F_{z(1)}^{B_1^g}$
$M_{n(4)}^{B_1^g} = -M_{n(2)}^{B_1^g}$
$F_{s(2)}^{Q_2} = -\frac{b^2 h}{2(b^3 + h^3)} Q_2$
$F_{s(1)}^{Q_2} = -\frac{h^3}{2(b^3 + h^3)} Q_2$
$F_{s(3)}^{Q_2} = F_{s(1)}^{Q_2}$
$F_{s(4)}^{Q_2} = F_{s(2)}^{Q_2}$
$F_{z(2)}^{B_2} = -\frac{3h^2}{4(h^2 - b^2)} B_2$
$F_{z(1)}^{B_2} = \frac{3h^2}{4(h^2 - b^2)} B_2$
$F_{z(3)}^{B_2} = F_{z(1)}^{B_2}$
$F_{z(4)}^{B_2} = F_{z(2)}^{B_2}$
$F_{n(2)}^{Q_3} = \frac{3h(5b + h)}{16b(b + h)} Q_3$
$F_{n(1)}^{Q_3} = -\frac{3h(5b + h)}{16b(b + h)} Q_3$
$F_{n(3)}^{Q_3} = F_{n(1)}^{Q_3}$
$F_{n(4)}^{Q_3} = F_{n(2)}^{Q_3}$
$F_{n(1)}^{Q_4} = \frac{3(5b + 3h)}{16b} Q_4$
$F_{n(3)}^{Q_4} = -F_{n(1)}^{Q_4}$

(a)

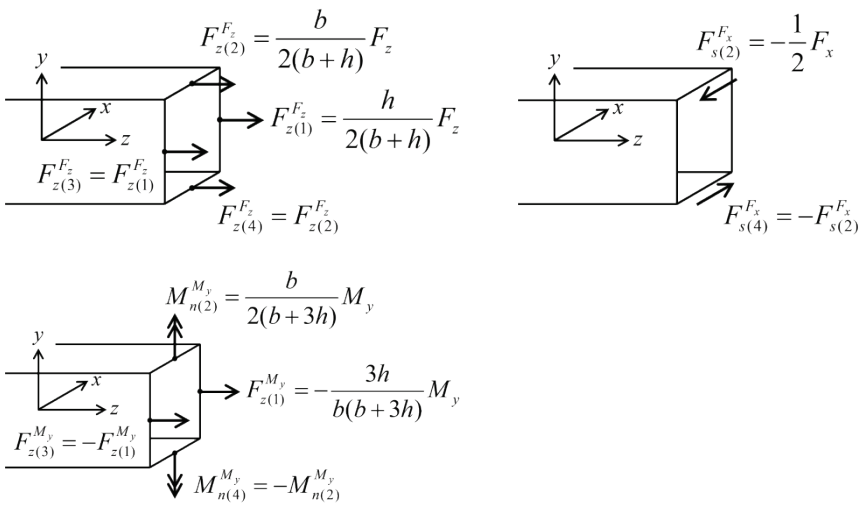
$F_{z(2)}^{F_z} = \frac{b}{2(b + h)} F_z$
$F_{z(1)}^{F_z} = \frac{h}{2(b + h)} F_z$
$F_{z(3)}^{F_z} = F_{z(1)}^{F_z}$
$F_{z(4)}^{F_z} = F_{z(2)}^{F_z}$
$F_{s(2)}^{F_x} = -\frac{1}{2} F_x$
$F_{s(4)}^{F_x} = -F_{s(2)}^{F_x}$
$M_{n(2)}^{M_y} = \frac{b}{2(b + 3h)} M_y$
$F_{z(1)}^{M_y} = -\frac{3h}{b(b + 3h)} M_y$
$F_{z(3)}^{M_y} = -F_{z(1)}^{M_y}$
$M_{n(4)}^{M_y} = -M_{n(2)}^{M_y}$

(b)

Fig. 5.7 (*a*) Edge resultants acting on each edge of the cross-section that are produced by the self-equilibrated generalized forces: transverse bimoment (Q_1^g, Q_2, Q_3, Q_4) and longitudinal bimoment (B_1^g, B_2), (*b*) Edge resultants acting on each edge of the cross-section that are produced by the generalized forces having nonzero resultants: longitudinal force F_z , transverse force F_x , in-plane bending moment M_y.

The symbol $\bar{J}_{\beta_2}$ ($\beta_2 = B_1^g, B_2$) given in Eq. (5.43a) can be defined by using $\bar{\psi}_z^{\alpha_2}(s_j)$ ($\alpha_2 = W_1^g, W_2$) as:

$$\bar{J}_{\beta_2} = \iint_S (\bar{\psi}_z^{\beta_2})^2 \, ds dn \tag{5.47a}$$

, and the symbol $\bar{J}_{\beta_2}$ ($\beta_2 = Q_1^g, Q_2$) given in Eq. (5.43b) can be defined by using $\bar{\psi}_s^{\alpha_2}(s_j)$ ($\alpha_2 = \chi_1^g, \chi_2$) as:

$$\bar{J}_{\beta_2} = \iint_S (\bar{\psi}_s^{\beta_2})^2 \, ds dn \tag{5.47b}$$

The edge resultants of β_2 ($\beta_2 = Q_1^g, B_1^g, Q_2, B_2$) calculated by substituting ($\bar{\sigma}_{zz}^{\beta_2}, \bar{\sigma}_{zs}^{\beta_2}$) in Eqs. (5.43a, b) into Eq. (5.42) are shown in Fig. 5.7(a).

On the other hand, the following distributed axial moment $m_{z(j)}^{\beta_3}(s_j)$ ($\beta_3 = Q_3, Q_4$; $j = 1, 2, 3, 4$) is generated on Edge *j* by the stress $\sigma_{sz}^{\beta_3}$ [23].

$$m_{z(j)}^{\beta_3}(s_j) = \int_{Edge\, j} n \cdot \sigma_{zs}^{\beta_3} \, dn = -\frac{t^3}{12} \frac{\beta_3(z)}{J_{\beta_3}} \{ \dot{\psi}_n^{\alpha_3}(s_j) \} \tag{5.48}$$

where $\alpha_3 = \chi_3, \chi_4$. According to the Kirchhoff-Love plate theory [25], the effective distributed normal force $f_{n(j)}^{\beta_3}(s_j)$ ($j = 1, 2, 3, 4$) is also generated on

Edge j from the axial moment $m_{z(j)}^{\beta_3}(s_j)$ by the principle given in Choi and Kim [23], and is defined as:

$$f_{n(j)}^{\beta_3}(s_j) = -\frac{\partial m_{z(j)}^{\beta_3}(s_j)}{\partial s} = \frac{t^3}{12}\frac{\beta_3(z)}{J_{\beta_3}}\{\ddot{\psi}_n^{\alpha_3}(s_j)\} \tag{5.49}$$

Therefore, the effective normal force $F_n^{\beta_3}$ concerning the joint equilibrium conditions can be defined as the non-zero edge resultant of β_3 according to Choi and Kim [23], and $F_{n(j)}^{\beta_3}$ on Edge j ($j = 1, 2, 3, 4$) can be defined by using $f_{n(j)}^{\beta_3}(s_j)$ in Eq. (5.49) as:

$$F_{n(j)}^{\beta_3} = \int_{Edge\ j} f_{n(j)}^{\beta_3}(s_j)\, ds_j \tag{5.50}$$

According to Choi and Kim [23], however, underestimated edge resultants of β_3 are calculated when $f_n^{\beta_3}$ given in Eq. (5.49) is employed, and thus the following $\overline{f}_n^{\beta_3}$ ($\beta_3 = Q_3, Q_4$) are used in place of $f_n^{\beta_3}$.

$$\overline{f}_{n(j)}^{\beta_3}(s_j) = \frac{t^3}{12}\frac{\beta_3(z)}{\overline{J}_{\beta_3}}\{\overline{\ddot{\psi}}_n^{\alpha_3}(s_j)\} \tag{5.51}$$

where $\overline{\ddot{\psi}}_n^{\alpha_3}(s_j)$ ($\alpha_3 = \chi_3, \chi_4$; $j = 1, 2, 3, 4$) represent the average distribution of $f_n^{\beta_3}$ on Edge j, and are defined as:

$$\begin{aligned} \overline{\ddot{\psi}}_n^{\chi_3}(s_j) &= \frac{32b}{h^2(5b+h)} && \text{(for } j = 1, 3) \\ \overline{\ddot{\psi}}_n^{\chi_3}(s_j) &= -\frac{32}{h(5b+h)} && \text{(for } j = 2, 4) \end{aligned} \tag{5.52a}$$

$$\bar{\ddot{\psi}}_n^{\chi_4}(s_j) = (-1)^{(j+1)/2} \times \frac{32b}{h^2(5b+3h)} \qquad \text{(for } j = 1, 3)$$
$$\bar{\ddot{\psi}}_n^{\chi_4}(s_j) = 0 \qquad \text{(for } j = 2, 4) \tag{5.52b}$$

The definitions of $\bar{\ddot{\psi}}_n^{\alpha_3}(s_j)$ ($\alpha_3 = \chi_3, \chi_4$; $j = 1, 2, 3, 4$) given in Eqs. (5.52a, b) are as:

$$\bar{\ddot{\psi}}_n^{\alpha_3}(s_j) = \int \ddot{\psi}_n^{\alpha_3}(s_j)\, ds_j \,/ \int ds_j \tag{5.53}$$

,and the symbol $\bar{J}_{\beta_3}$ in Eq. (5.51) can be defined by using $\bar{\ddot{\psi}}_n^{\alpha_3}(s_j)$ as:

$$\bar{J}_{\beta_3} = \iint_S (n \cdot \bar{\ddot{\psi}}_n^{\alpha_3})^2\, dsdn = \iint_S \{n \cdot (s \cdot \bar{\ddot{\psi}}_n^{\alpha_3})\}^2\, dsdn \tag{5.54}$$

where $\bar{\dot{\psi}}_n^{\alpha_3}(s_j)$ ($\alpha_3 = \chi_3, \chi_4$; $j = 1, 2, 3, 4$ $j = 1, 2, 3, 4$) can be written as $\bar{\dot{\psi}}_n^{\alpha_3}(s_j) = s_j \cdot \bar{\ddot{\psi}}_n^{\alpha_3}(s_j)$ because $\bar{\dot{\psi}}_n^{\alpha_3}(s_j)$ represent the odd functions. The edge resultants of β_3 ($\beta_3 = Q_3, Q_4$) calculated by substituting $\bar{f}_n^{\beta_3}$ in Eq. (5.51) into Eq. (5.50) are shown in Fig. 5.7.

5.4.2 Generalized Forces Equilibrium Conditions

The equilibrium conditions among generalized forces $\hat{\mathbf{F}} = \{F_z, F_x, M_y, Q_1^g, B_1^g, Q_2, B_2, Q_3, Q_4\}^{\mathrm{T}}$ at the joint will be derived by considering the equilibriums of the edge resultants given in Fig. 5.7 in addition to those of the sectional resultants given in Fig. 5.6. To this end, the joint equilibrium conditions among the generalized forces ($F_z, F_x, M_y, Q_1^g, B_1^g, Q_3$) proposed by Choi and Kim [23] will be utilized; we will first interpret those results from the viewpoint of

equilibrium conditions of the sectional and edge resultants, and then we will extend those results for the joint equilibrium conditions with respect to the generalized forces $\tilde{\mathbf{F}} = \{F_z, F_x, M_y, Q_1^g, B_1^g, Q_2, B_2, Q_3, Q_4\}^{\mathrm{T}}$.

Concerning the two box beams-joint structure depicted in Fig. 5.5, the joint equilibrium conditions proposed by Choi and Kim [23] can be written as:

$$(F_z)_1 \cos(\phi_2 - \phi_1) + (F_x)_1 \sin(\phi_2 - \phi_1) + (F_z)_2 = 0 \tag{5.55a}$$

$$-(F_z)_1 \sin(\phi_2 - \phi_1) + (F_x)_1 \cos(\phi_2 - \phi_1) + (F_x)_2 = 0 \tag{5.55b}$$

$$(M_y)_1 + (M_y)_2 = 0 \tag{5.55c}$$

$$(Q_1^g)_1 - (Q_1^g)_2 = 0 \tag{5.55d}$$

$$\begin{aligned} &\tfrac{4(5h^2-b^2)}{5bh(b+3h)}(M_y)_1\{-1-\cos(\phi_2-\phi_1)\} + (B_1^g)_1 \cos(\phi_2-\phi_1) \\ &\qquad - \tfrac{(5b+h)(5h^2-b^2)}{20bh(b+h)}(Q_3)_1 \sin(\phi_2-\phi_1) - (B_1^g)_2 = 0 \end{aligned} \tag{5.55e}$$

$$\begin{aligned} &-\tfrac{16(b+h)}{(b+3h)(5b+h)}(M_y)_1 \sin(\phi_2-\phi_1) + \tfrac{20bh(b+h)}{(5b+h)(5h^2-b^2)}(B_1^g)_1 \sin(\phi_2-\phi_1) \\ &\qquad + (Q_3)_1 \cos(\phi_2-\phi_1) - (Q_3)_2 = 0 \end{aligned} \tag{5.55f}$$

, and one can rewrite Eqs. (55a-f) as, in terms of the sectional and edge resultants shown in Fig. 5.6 and 5.7,

$$(F_z)_1 \cos\phi_1 - (F_x)_1 \sin\phi_1 + (F_z)_2 \cos\phi_2 - (F_x)_2 \sin\phi_2 = 0 \tag{5.56a}$$

$$(F_z)_1 \sin\phi_1 + (F_x)_1 \cos\phi_1 + (F_z)_2 \sin\phi_2 + (F_x)_2 \cos\phi_2 = 0 \tag{5.56b}$$

$$(M_y)_1 + (M_y)_2 = 0 \tag{5.56c}$$

$$\frac{h}{3b}(Q_1^g)_1 - \frac{h}{3b}(Q_1^g)_2 = 0 \tag{5.56d}$$

$$\{-\tfrac{3h}{b(b+3h)}(M_y)_1+\tfrac{15h^2}{4(5h^2-b^2)}(B_1^g)_1\}\cos\phi_1-\{-\tfrac{3h(5b+h)}{16b(b+h)}(Q_3)_1\}\sin\phi_1$$
$$+\{\tfrac{3h}{b(b+3h)}(M_y)_2-\tfrac{15h^2}{4(5h^2-b^2)}(B_1^g)_2\}\cos\phi_2-\{\tfrac{3h(5b+h)}{16b(b+h)}(Q_3)_2\}\sin\phi_2=0$$

(5.56e)

$$\{-\tfrac{3h}{b(b+3h)}(M_y)_1+\tfrac{15h^2}{4(5h^2-b^2)}(B_1^g)_1\}\sin\phi_1+\{-\tfrac{3h(5b+h)}{16b(b+h)}(Q_3)_1\}\cos\phi_1$$
$$+\{\tfrac{3h}{b(b+3h)}(M_y)_2-\tfrac{15h^2}{4(5h^2-b^2)}(B_1^g)_2\}\sin\phi_2+\{\tfrac{3h(5b+h)}{16b(b+h)}(Q_3)_2\}\cos\phi_2=0$$

(5.56f)

Equation (5.56a-c) can be obtained from Eqs. (5.55a-c) and represent the equilibrium conditions among the sectional resultants (F_z, F_x, M_y) shown in Fig. 5.6 defined with respect to the global coordinate system (x_{global}, y_{global}, z_{global}).

On the other hand, Eqs. (5.56d-f) represent the equilibrium conditions concerning the edge resultants (Q_1^g, B_1^g, Q_3) shown in Fig. 5.7. Equation (5.56d) can be obtained from Eq. (5.55d) by multiplying ($h/3b$), and one can find that Eq. (5.56d) represents the equilibrium condition between the edge resultant $F_{s(1)}^{Q_1^g}$ of Beam 1 and $F_{s(3)}^{Q_1^g}$ of Beam 2. Equations (5.56e, f) can be obtained from Eqs. (5.55e, f), and one can fine that Eq. (5.56e, f) represent the equilibrium conditions among ($F_{z(1)}^{M_y}$, $F_{z(1)}^{B_1^g}$, $F_{n(1)}^{Q_3}$) of Beam 1 and ($F_{z(3)}^{M_y}$, $F_{z(3)}^{B_1^g}$, $F_{n(3)}^{Q_3}$) of Beam 2 (Because the edge forces ($F_s^{Q_1^g}$, $F_z^{M_y}$, $F_z^{B_1^g}$, $F_n^{Q_3}$) in Eqs. (5.56d-f) are antisymmetric with respect to y-axis, Eq. (5.56d) can represents the equilibrium condition between $F_{s(3)}^{Q_1^g}$ of Beam 1 and $F_{s(1)}^{Q_1^g}$ of Beam 2, and Eqs. (5.56e, f) can represent the equilibrium

conditions among ($F_{z(3)}^{M_y}$, $F_{z(3)}^{B_1^g}$, $F_{n(3)}^{Q_3}$) of Beam 1 and ($F_{z(1)}^{M_y}$, $F_{z(1)}^{B_1^g}$, $F_{n(1)}^{Q_3}$) of Beam 2 as well).

Note that generalized forces (F_z, F_x, M_y, Q_1^g, B_1^g, Q_3) are sufficient to express equilibrium conditions for the two box beams-joint structure as demonstrated by Choi and Kim [23]. However, the equilibrium conditions among edge resultants defined on Edge 1 and Edge 3 are no more identical, and thus additional generalized forces (Q_2, B_2, Q_4) should be employed together in order to express the equilibrium conditions on Edge 1 and Edge 3 independently.

Based on the previous observation for Eqs. (5.56a-f), one can determine the following equilibrium conditions among (F_z, F_x, M_y, Q_1^g, B_1^g, Q_2, B_2, Q_3, Q_4) regarding to the two box beams-joint structure:

$$(F_{z_{\text{global}}})_1 + (F_{z_{\text{global}}})_2 = 0 \tag{5.57a}$$

$$(F_{x_{\text{global}}})_1 + (F_{x_{\text{global}}})_2 = 0 \tag{5.57b}$$

$$(M_{y_{\text{global}}})_1 + (M_{y_{\text{global}}})_2 = 0 \tag{5.57c}$$

$$(F_{s(1)})_1 - (F_{s(3)})_2 = 0 \tag{5.57d}$$

$$(F_{z_{\text{global}}(1)})_1 + (F_{z_{\text{global}}(3)})_2 = 0 \tag{5.57e}$$

$$(F_{x_{\text{global}}(1)})_1 + (F_{x_{\text{global}}(3)})_2 = 0 \tag{5.57f}$$

$$-(F_{s(3)})_1 + (F_{s(1)})_2 = 0 \tag{5.57g}$$

$$(F_{z_{\text{global}}(3)})_1 + (F_{z_{\text{global}}(1)})_2 = 0 \tag{5.57h}$$

$$(F_{x_{\text{global}}(3)})_1 + (F_{x_{\text{global}}(1)})_2 = 0 \tag{5.57i}$$

where $(F_{z_{\text{global}}})_k, (F_{x_{\text{global}}})_k, (M_{y_{\text{global}}})_k, (F_{s(1)})_k, (F_{z_{\text{global}}(1)})_k, (F_{x_{\text{global}}(1)})_k, (F_{s(3)})_k, (F_{z_{\text{global}}(3)})_k$ and $(F_{x_{\text{global}}(3)})_k$ for Beam k ($k = 1, 2$) are defined as

$$(F_{z_{\text{global}}})_k = (F_z)_k \cos\phi_k - (F_x)_k \sin\phi_k \tag{5.58a}$$

$$(F_{x_{\text{global}}})_k = (F_z)_k \sin\phi_k + (F_x)_k \cos\phi_k \tag{5.58b}$$

$$(M_{y_{\text{global}}})_k = (M_y)_k \tag{5.58c}$$

$$(F_{s(1)})_k = \frac{h}{3b}(Q_1^g)_k - \frac{h^3}{2(b^3+h^3)}(Q_2)_k \tag{5.58d}$$

$$\begin{aligned}(F_{z_{\text{global}}(1)})_k = &\{-\tfrac{3h}{b(b+3h)}(M_y)_k + \tfrac{15h^2}{4(5h^2-b^2)}(B_1^g)_k + \tfrac{3h^2}{4(h^2-b^2)}(B_2)_k\}\cos\phi_k \\ &-\{-\tfrac{3h(5b+h)}{16b(b+h)}(Q_3)_k + \tfrac{3(5b+3h)}{16b}(Q_4)_k\}\sin\phi_k\end{aligned} \tag{5.58e}$$

$$\begin{aligned}(F_{x_{\text{global}}(1)})_k = &\{-\tfrac{3h}{b(b+3h)}(M_y)_k + \tfrac{15h^2}{4(5h^2-b^2)}(B_1^g)_k + \tfrac{3h^2}{4(h^2-b^2)}(B_2)_k\}\sin\phi_k \\ &+\{-\tfrac{3h(5b+h)}{16b(b+h)}(Q_3)_k + \tfrac{3(5b+3h)}{16b}(Q_4)_k\}\cos\phi_k\end{aligned} \tag{5.58f}$$

$$(F_{s(3)})_k = -\frac{h}{3b}(Q_1^g)_k - \frac{h^3}{2(b^3+h^3)}(Q_2)_k \tag{5.58g}$$

$$\begin{aligned}(F_{z_{\text{global}}(3)})_k = &\{\tfrac{3h}{b(b+3h)}(M_y)_k - \tfrac{15h^2}{4(5h^2-b^2)}(B_1^g)_k + \tfrac{3h^2}{4(h^2-b^2)}(B_2)_k\}\cos\phi_k \\ &-\{\tfrac{3h(5b+h)}{16b(b+h)}(Q_3)_k + \tfrac{3(5b+3h)}{16b}(Q_4)_k\}\sin\phi_k\end{aligned} \tag{5.58h}$$

$$\begin{aligned}(F_{x_{\text{global}}(3)})_k = &\{\tfrac{3h}{b(b+3h)}(M_y)_k - \tfrac{15h^2}{4(5h^2-b^2)}(B_1^g)_k + \tfrac{3h^2}{4(h^2-b^2)}(B_2)_k\}\sin\phi_k \\ &+\{\tfrac{3h(5b+h)}{16b(b+h)}(Q_3)_k + \tfrac{3(5b+3h)}{16b}(Q_4)_k\}\cos\phi_k\end{aligned} \tag{5.58i}$$

The symbols $(F_{z_{\text{global}}})_k$ and $(F_{x_{\text{global}}})_k$ ($k = 1, 2$) represent the sectional resultant forces of Beam k in z_{global} direction and x_{global} direction, respectively, and the

symbol $(M_{y_{\text{global}}})_k$ represent the sectional resultant moment of Beam k in y_{global} direction. Meanwhile, the symbol $(F_{s(j)})_k$ ($j = 1, 3;\ k = 1, 2$) represents the edge resultant force on Edge j (especially $0 \le s_j \le \frac{h}{2}$) of Beam k in s direction, and the symbols $(F_{z_{\text{global}}(j)})_k$ and $(F_{x_{\text{global}}(j)})_k$ ($j = 1, 3;\ k = 1, 2$) represent the edge resultant forces on Edge j of Beam k in z_{global} direction and x_{global} direction, respectively.

Let us now consider the extension of Eq. (5.57) to the structure that N ($N \ge 3$) box beams are connected at the joint shown in Fig. 5.2. Because Eq. (5.57) is defined as the equilibrium conditions for sectional and edge resultants, Eq. (5.57) is easy to be extended for the joint where three or more box beams meet.

In order to determine the equilibrium conditions for the edge resultants ($F_{s(j)}$, $F_{z_{\text{global}}(j)}$ and $F_{x_{\text{global}}(j)}$) ($j = 1, 3$), connectivity among Edge 1 or Edge 3 of N box beams at the joint should be investigated. According to Choi and Kim [22], connectivity among those edges can be determined by considering the actual joint depicted in Fig. 5.1. For two adjacent box beams (Beam k ($k = 1, 2, \cdots, N$) and Beam k+1; Beam N+1 refers to Beam 1), Edge 1 of Beam k and Edge 3 of Beam k+1 can be considered as if they were connected rigidly to each other. Therefore, the equilibrium between ($(F_{s(1)})_k$, $(F_{z_{\text{global}}(1)})_k$ and $(F_{x_{\text{global}}(1)})_k$) and ($(F_{s(3)})_{k+1}$, $(F_{z_{\text{global}}(3)})_{k+1}$ and $(F_{x_{\text{global}}(3)})_{k+1}$) can be now considered.

Based on the connectivity among edges of box beams explained above, the

generalized forces equilibrium conditions at the joint of N ($N \geq 3$) box beams-joint structure can be written as follows by extending the equilibrium conditions for sectional resultants or edge resultants given in Eq. (5.57):

$$\sum_{k=1}^{N} (F_{z_{\text{global}}})_k = 0 \tag{5.59a}$$

$$\sum_{k=1}^{N} (F_{x_{\text{global}}})_k = 0 \tag{5.59b}$$

$$\sum_{k=1}^{N} (M_{y_{\text{global}}})_k = 0 \tag{5.59c}$$

$$(F_{s(1)})_i - (F_{s(3)})_{i+1} = 0 \tag{5.59d}$$

$$(F_{z_{\text{global}}(1)})_k + (F_{z_{\text{global}}(3)})_{k+1} = 0 \tag{5.59e}$$

$$(F_{x_{\text{global}}(1)})_k + (F_{x_{\text{global}}(3)})_{k+1} = 0 \tag{5.59f}$$

$$(\ i : \text{Natural number}, 1 \leq i \leq N\ )$$

where Eqs. (5.59a-c) express the equilibrium conditions in which all ($(F_{z_{\text{global}}})$, $(F_{x_{\text{global}}})$, $(M_{y_{\text{global}}})$ defined in N box beams participate, regardless of the number of box beams meeting at the joint. Meanwhile, Eq. (5.59d-f) represent the equilibrium conditions between the edge resultants of the adjacent two beams Beam i and Beam i+1 ($1 \leq i \leq N$). Therefore, Eq. (5.59d-f) consequently represent 3N number of equations, and Eqs. (5.59a-f) are expressed by 3N+3 number of equations for the case that N box beams meet at the joint. In case of $N = 2$, Eq. (5.59d-f) recovers Eqs. (5.57d-i).

5.4.3 Field Variables Joint Matching Conditions

Using the generalized forces equilibrium conditions defined above, let us now derive the joint matching conditions among field displacement variables $\tilde{\mathbf{U}} = \{ U_z, U_x, \theta_y, \chi_1^g, W_1^g, \chi_2, W_2, \chi_3, \chi_4 \}^{\mathrm{T}}$. Because the field variables are the work conjugates of the generalized forces, one can associate them with the generalized forces by considering the principle of virtual work that the sum of virtual works is zero. In what follows, we will theoretically derive the matching conditions among field variables from the generalized forces equilibrium conditions.

For the derivation, the joint matching conditions among field variables of Beam 1 and Beam 2 shown in Fig. 5.5 will be examined first by using the equilibrium conditions in Eq. (5.57) derived for two-beam joints. Then the conditions will be extended for the three or more box beams-joint structures. (In theory, the field variables matching conditions may be derived directly from Eq. (5.59), but the derivation is found to be too complex to employ.)

Referring to the two box beams-joint structure depicted in Fig. 5.5, consider $\tilde{\mathbf{F}}_k$ and $\tilde{\mathbf{U}}_k$ ($k = 1, 2$) denoting the generalized forces and field variables of Beam *k*, respectively. In terms of $\tilde{\mathbf{F}}_k$ and $\tilde{\mathbf{U}}_k$ ($k = 1, 2$), the principle of virtual work at the joint can be expressed as

$$\sum_{k=1}^{2}(\delta W'|_{\text{Beam } k}) = (\delta\tilde{\mathbf{F}}_1)^{\mathrm{T}}\tilde{\mathbf{U}}_1 + (\delta\tilde{\mathbf{F}}_2)^{\mathrm{T}}\tilde{\mathbf{U}}_2 = 0 \tag{5.60}$$

Equation (5.60) shows the sum of $(\delta W'|_{\text{Beam } k})$, which is complementary virtual work of Beam *k*, is zero [26], where $\delta\tilde{\mathbf{F}}_k$ refers to the admissible virtual force of Beam *k*. Because $\delta\tilde{\mathbf{F}}_1$ and $\delta\tilde{\mathbf{F}}_2$ comply with the equilibrium conditions in Eq. (5.28), $\delta\tilde{\mathbf{F}}_1$ and $\delta\tilde{\mathbf{F}}_2$ must satisfy the following relation:

$$\mathbf{M}_{\mathbf{F}_1}\cdot\delta\tilde{\mathbf{F}}_1 + \mathbf{M}_{\mathbf{F}_2}\cdot\delta\tilde{\mathbf{F}}_2 = 0 \tag{5.61}$$

where $\mathbf{M}_{\mathbf{F}_1}$ and $\mathbf{M}_{\mathbf{F}_2}$ are defined as

$$\mathbf{M}_{\mathbf{F}_1} = \begin{bmatrix}
\cos\phi_1 & -\sin\phi_1 & 0 & 0 & 0 & 0 & 0 & 0 & 0 \\
\sin\phi_1 & \cos\phi_1 & 0 & 0 & 0 & 0 & 0 & 0 & 0 \\
0 & 0 & 1 & 0 & 0 & 0 & 0 & 0 & 0 \\
0 & 0 & 0 & \frac{h}{3b} & 0 & -\frac{h^3}{2(b^3+h^3)} & 0 & 0 & 0 \\
0 & 0 & -\frac{3h}{b(b+3h)}\cos\phi_1 & 0 & \frac{15h^2}{4(5h^2-b^2)}\cos\phi_1 & 0 & \frac{3h^2}{4(h^2-b^2)}\cos\phi_1 & \frac{3h(5b+h)}{16b(b+h)}\sin\phi_1 & -\frac{3(5b+3h)}{16b}\sin\phi_1 \\
0 & 0 & -\frac{3h}{b(b+3h)}\sin\phi_1 & 0 & \frac{15h^2}{4(5h^2-b^2)}\sin\phi_1 & 0 & \frac{3h^2}{4(h^2-b^2)}\sin\phi_1 & -\frac{3h(5b+h)}{16b(b+h)}\cos\phi_1 & \frac{3(5b+3h)}{16b}\cos\phi_1 \\
0 & 0 & 0 & -\frac{h}{3b} & 0 & -\frac{h^3}{2(b^3+h^3)} & 0 & 0 & 0 \\
0 & 0 & \frac{3h}{b(b+3h)}\cos\phi_1 & 0 & -\frac{15h^2}{4(5h^2-b^2)}\cos\phi_1 & 0 & \frac{3h^2}{4(h^2-b^2)}\cos\phi_1 & -\frac{3h(5b+h)}{16b(b+h)}\sin\phi_1 & -\frac{3(5b+3h)}{16b}\sin\phi_1 \\
0 & 0 & \frac{3h}{b(b+3h)}\sin\phi_1 & 0 & -\frac{15h^2}{4(5h^2-b^2)}\sin\phi_1 & 0 & \frac{3h^2}{4(h^2-b^2)}\sin\phi_1 & \frac{3h(5b+h)}{16b(b+h)}\cos\phi_1 & \frac{3(5b+3h)}{16b}\cos\phi_1
\end{bmatrix} \tag{5.62a}$$

$\mathbf{M}_{\mathbf{F}_2} =$

$$\begin{bmatrix}
\cos\phi_2 & -\sin\phi_2 & 0 & 0 & 0 & 0 & 0 & 0 & 0 \\
\sin\phi_2 & \cos\phi_2 & 0 & 0 & 0 & 0 & 0 & 0 & 0 \\
0 & 0 & 1 & 0 & 0 & 0 & 0 & 0 & 0 \\
0 & 0 & 0 & -\frac{h}{3b} & 0 & -\frac{h^3}{2(b^3+h^3)} & 0 & 0 & 0 \\
0 & 0 & \frac{3h}{b(b+3h)}\cos\phi_2 & 0 & -\frac{15h^2}{4(5h^2-b^2)}\cos\phi_2 & 0 & \frac{3h^2}{4(h^2-b^2)}\cos\phi_2 & -\frac{3h(5b+h)}{16b(b+h)}\sin\phi_2 & -\frac{3(5b+3h)}{16b}\sin\phi_2 \\
0 & 0 & \frac{3h}{b(b+3h)}\sin\phi_2 & 0 & -\frac{15h^2}{4(5h^2-b^2)}\sin\phi_2 & 0 & \frac{3h^2}{4(h^2-b^2)}\sin\phi_2 & \frac{3h(5b+h)}{16b(b+h)}\cos\phi_2 & \frac{3(5b+3h)}{16b}\cos\phi_2 \\
0 & 0 & 0 & \frac{h}{3b} & 0 & -\frac{h^3}{2(b^3+h^3)} & 0 & 0 & 0 \\
0 & 0 & -\frac{3h}{b(b+3h)}\cos\phi_2 & 0 & \frac{15h^2}{4(5h^2-b^2)}\cos\phi_2 & 0 & \frac{3h^2}{4(h^2-b^2)}\cos\phi_2 & \frac{3h(5b+h)}{16b(b+h)}\sin\phi_2 & -\frac{3(5b+3h)}{16b}\sin\phi_2 \\
0 & 0 & -\frac{3h}{b(b+3h)}\sin\phi_2 & 0 & \frac{15h^2}{4(5h^2-b^2)}\sin\phi_2 & 0 & \frac{3h^2}{4(h^2-b^2)}\sin\phi_2 & -\frac{3h(5b+h)}{16b(b+h)}\cos\phi_2 & \frac{3(5b+3h)}{16b}\cos\phi_2
\end{bmatrix} \tag{5.62b}$$

The matrices $\mathbf{M}_{\mathbf{F}_1}$ and $\mathbf{M}_{\mathbf{F}_2}$ above are invertible because Eq. (5.61) represents nine independent equilibrium conditions.

In order to apply the equilibrium conditions of $\delta\tilde{\mathbf{F}}_1$ and $\delta\tilde{\mathbf{F}}_2$ given in Eq. (5.61) to Eq. (5.60), let us first express $(\delta\tilde{\mathbf{F}}_k)^{\mathrm{T}}\tilde{\mathbf{U}}_k$ $(k=1,2)$ in Eq. (5.60) as, by using the matrix $\mathbf{M}_{\mathbf{F}_k}$ in Eq. (5.62):

$$\begin{aligned}
\sum_{k=1}^{2}(\delta W'|_{\text{Beam } k}) &= (\delta\tilde{\mathbf{F}}_1)^{\mathrm{T}}(\mathbf{M}_{\mathbf{F}_1}^{\mathrm{T}}\cdot\mathbf{M}_{\mathbf{F}_1}^{-\mathrm{T}})\cdot\tilde{\mathbf{U}}_1 + (\delta\tilde{\mathbf{F}}_2)^{\mathrm{T}}(\mathbf{M}_{\mathbf{F}_2}^{\mathrm{T}}\cdot\mathbf{M}_{\mathbf{F}_2}^{-\mathrm{T}})\cdot\tilde{\mathbf{U}}_2 \\
&= (\mathbf{M}_{\mathbf{F}_1}\cdot\delta\tilde{\mathbf{F}}_1)^{\mathrm{T}}(\mathbf{M}_{\mathbf{F}_1}^{-\mathrm{T}}\cdot\tilde{\mathbf{U}}_1) + (\mathbf{M}_{\mathbf{F}_2}\cdot\delta\tilde{\mathbf{F}}_2)^{\mathrm{T}}(\mathbf{M}_{\mathbf{F}_2}^{-\mathrm{T}}\cdot\tilde{\mathbf{U}}_2) = 0
\end{aligned} \tag{5.63}$$

According to Eq. (5.61), the relation between $(\mathbf{M}_{\mathbf{F}_1}\cdot\delta\tilde{\mathbf{F}}_1)$ and $(\mathbf{M}_{\mathbf{F}_2}\cdot\delta\tilde{\mathbf{F}}_2)$ in Eq. (5.63) is expressed as $(\mathbf{M}_{\mathbf{F}_2}\cdot\delta\tilde{\mathbf{F}}_2) = -(\mathbf{M}_{\mathbf{F}_1}\cdot\delta\tilde{\mathbf{F}}_1)$. Thus, applying this relation to Eq. (5.63) yields

$$\sum_{k=1}^{2}(\delta W'|_{\text{Beam } k}) = (\mathbf{M}_{\mathbf{F}_1} \cdot \delta\tilde{\mathbf{F}}_1)^{\mathrm{T}}(\mathbf{M}_{\mathbf{F}_1}^{-\mathrm{T}} \cdot \tilde{\mathbf{U}}_1 - \mathbf{M}_{\mathbf{F}_2}^{-\mathrm{T}} \cdot \tilde{\mathbf{U}}_2)$$
$$= (\delta\tilde{\mathbf{F}}_1)^{\mathrm{T}}\{\mathbf{M}_{\mathbf{F}_1}^{\mathrm{T}} \cdot (\mathbf{M}_{\mathbf{F}_1}^{-\mathrm{T}} \cdot \tilde{\mathbf{U}}_1 - \mathbf{M}_{\mathbf{F}_2}^{-\mathrm{T}} \cdot \tilde{\mathbf{U}}_2)\} = 0 \tag{5.64}$$

Because Eq. (5.64) should be satisfied for arbitrary $\delta\tilde{\mathbf{F}}_1$, it can be found that $\{\mathbf{M}_{\mathbf{F}_1}^{\mathrm{T}} \cdot (\mathbf{M}_{\mathbf{F}_1}^{-\mathrm{T}} \cdot \tilde{\mathbf{U}}_1 - \mathbf{M}_{\mathbf{F}_2}^{-\mathrm{T}} \cdot \tilde{\mathbf{U}}_2)\}$ in Eq. (5.64) should be zero. Note that the matrix $\mathbf{M}_{\mathbf{F}_1}^{\mathrm{T}}$ is invertible as mentioned above. Therefore, the following relation must hold:

$$\mathbf{M}_{\mathbf{F}_1}^{-\mathrm{T}} \cdot \tilde{\mathbf{U}}_1 = \mathbf{M}_{\mathbf{F}_2}^{-\mathrm{T}} \cdot \tilde{\mathbf{U}}_2 \tag{5.65}$$

Equation (5.65) represents the matching conditions to be met among the field variables when the equilibrium conditions in Eq. (5.57) are satisfied at the joint in Fig. 5.5. Based on the definitions of $\mathbf{M}_{\mathbf{F}_1}$ and $\mathbf{M}_{\mathbf{F}_2}$ in Eqs. (5.62a, b), Eq. (5.65) can be explicitly written as

$$(U_z)_1 \cos\phi_1 - (U_x)_1 \sin\phi_1 = (U_z)_2 \cos\phi_2 - (U_x)_2 \sin\phi_2 \tag{5.66a}$$

$$(U_z)_1 \sin\phi_1 + (U_x)_1 \cos\phi_1 = (U_z)_2 \sin\phi_2 + (U_x)_2 \cos\phi_2 \tag{5.66b}$$

$$(\Theta_y)_1 = (\Theta_y)_2 \tag{5.66c}$$

$$(U_{s(1)})_1 = -(U_{s(3)})_2 \tag{5.66d}$$

$$(U_{z(1)})_1 \cos\phi_1 - (U_{x(1)})_1 \sin\phi_1 = (U_{z(3)})_2 \cos\phi_2 - (U_{x(3)})_2 \sin\phi_2 \tag{5.66e}$$

$$(U_{z(1)})_1 \sin\phi_1 + (U_{x(1)})_1 \cos\phi_1 = (U_{z(3)})_2 \sin\phi_2 + (U_{x(3)})_2 \cos\phi_2 \tag{5.66f}$$

$$-(U_{s(3)})_1 = (U_{s(1)})_2 \tag{5.66g}$$

$$(U_{z(3)})_1 \cos\phi_1 - (U_{x(3)})_1 \sin\phi_1 = (U_{z(1)})_2 \cos\phi_2 - (U_{x(1)})_2 \sin\phi_2 \tag{5.66h}$$

$$(U_{z(3)})_1 \sin\phi_1 + (U_{x(3)})_1 \cos\phi_1 = (U_{z(1)})_2 \sin\phi_2 + (U_{x(1)})_2 \cos\phi_2 \tag{5.66i}$$

where Θ_y, $U_{s(1)}$, $U_{z(1)}$, $U_{x(1)}$, $U_{s(3)}$, $U_{z(3)}$, and $U_{x(3)}$ are defined as

$$\Theta_y = \theta_y + \frac{4(5h^2 - b^2)}{5h(b^2 + 3bh)} W_1^g \tag{5.67a}$$

$$U_{s(1)} = \frac{3b}{2h}\chi_1^g - \frac{b^3 + h^3}{h^3}\chi_2; \quad U_{s(3)} = -\frac{3b}{2h}\chi_1^g - \frac{b^3 + h^3}{h^3}\chi_2 \tag{5.67b, c}$$

$$\begin{aligned} U_{z(1)} &= -\frac{2(b^2 - 5h^2)}{15h^2} W_1^g + \frac{2(h^2 - b^2)}{3h^2} W_2; \\ U_{z(3)} &= \frac{2(b^2 - 5h^2)}{15h^2} W_1^g + \frac{2(h^2 - b^2)}{3h^2} W_2 \end{aligned} \tag{5.67d}$$

$$\begin{aligned} U_{x(1)} &= -\frac{8b(b+h)}{3h(5b+h)}\chi_3 + \frac{8b}{3(5b+3h)}\chi_4; \\ U_{x(3)} &= \frac{8b(b+h)}{3h(5b+h)}\chi_3 + \frac{8b}{3(5b+3h)}\chi_4 \end{aligned} \tag{5.67e}$$

Although the expressions in Eq. (5.66) look different from the matching conditions that Choi and Kim [23] proposed, Eq. (5.66) represents the same relations among the field variables (U_z, U_x, θ_y, χ_1^g, W_1^g, χ_3) as those in Eq. (5.32); the joint matching conditions in Eq. (5.32) can be derived directly from Eq. (5.66). On the other hand, the advantage of using Eq. (5.66) is that the specific formula by Eq. (5.66) can be directly extended to the case of three or more box beams-joint structures.

In order to extend the results in Eq. (5.66) for the joint where three or more box beams meet, the meaning of the matching conditions in Eq. (5.66) should be

understood. Equations (5.66a, b) represent the continuity conditions among the rigid-body displacements U_z and U_x shown in Figs. 5.8 (a, b). It can be found that Eq. (5.66a) represents the continuity condition between $(U_{z_{global}})_k = (U_z)_k \cos\phi_k - (U_x)_k \sin\phi_k$ ($k = 1, 2$), which denotes the rigid-body motion of of Beam k in the z_{global} direction. Likewise, Eq. (5.66b) represents the continuity condition between $(U_{x_{global}})_k = (U_z)_k \sin\phi_k + (U_x)_k \cos\phi_k$ ($k = 1, 2$), which denotes the rigid-body motion of Beam k in the x_{global} direction. Equation (5.66c) represents the continuity condition among the work conjugates of the resultant moments considered in the equilibrium conditions in Eq. (5.57c). Therefore, $(\Theta_y)_k$ in Eq. (5.66c) will be called the sectional effective rotation of Beam k at the joint in the y_k direction, as depicted in Fig. 5.8(c), and it can be found that Eq. (5.66c) represents the continuity condition between $(\Theta_{y_{\text{global}}})_k = (\Theta_y)_k$ ($k = 1, 2$), which denotes the sectional effective rotation of Beam k in the y_{global} direction.

Meanwhile, Eqs. (5.66d, g) corresponds to the continuity conditions between the work conjugates of the tangential forces $F_{s(j)}$ ($j = 1, 3$) shown in Eqs. (5.57d, g). Therefore, $(U_{s(1)})_k$ and $(U_{s(3)})_k$ ($k = 1, 2$) in Eqs. (5.66d, g) denote the displacements of Edge 1 and Edge 3, respectively in the tangential direction as

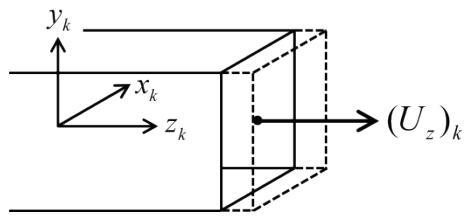
y_k
x_k
z_k
$(U_z)_k$

(a)

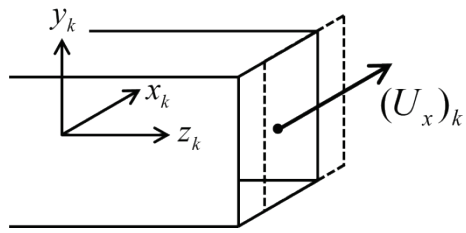
y_k
x_k
z_k
$(U_x)_k$

(b)

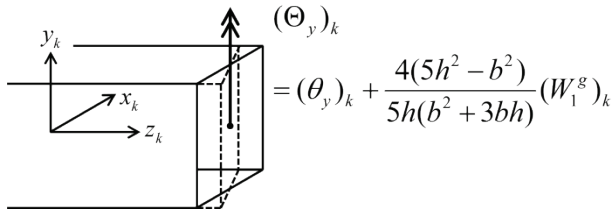
$(\Theta_y)_k$
y_k
x_k
z_k
$= (\theta_y)_k + \frac{4(5h^2 - b^2)}{5h(b^2 + 3bh)}(W_1^g)_k$

(c)

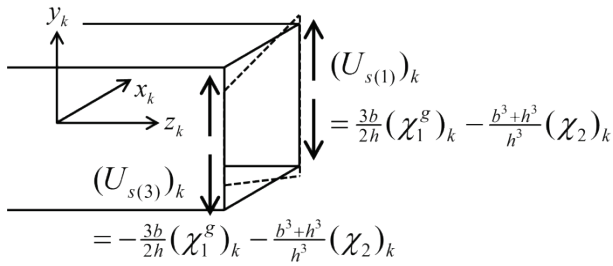
y_k
x_k
z_k
$(U_{s(1)})_k$
$= \frac{3b}{2h}(\chi_1^g)_k - \frac{b^3+h^3}{h^3}(\chi_2)_k$
$(U_{s(3)})_k$
$= -\frac{3b}{2h}(\chi_1^g)_k - \frac{b^3+h^3}{h^3}(\chi_2)_k$

(d)

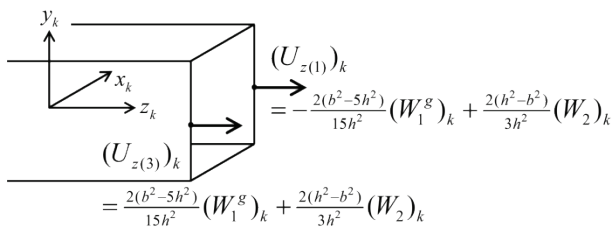

(e)

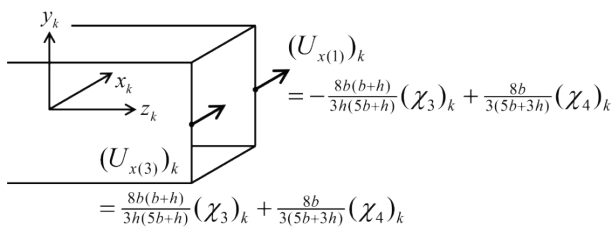

(f)

Fig. 5.8 Sectional displacements or edge displacements associated with the generalized displacements (or field variables) joint matching conditions: (a) sectional displacement $(U_z)_k$ in z_k direction, (b) sectional displacement $(U_x)_k$ in x_k direction, (c) sectional rotation $(\phi_z)_k$ in y_k direction (d) edge displacements $(U_{s(1)})_k$, $(U_{s(3)})_k$ of Edge 1 and Edge 3 in s direction (e) edge displacements $(U_{z(1)})_k$, $(U_{z(3)})_k$ of Edge 1 and Edge 3 in z_k direction and (f) edge displacements $(U_{x(1)})_k$, $(U_{x(3)})_k$ of Edge 1 and Edge 3 in x_k direction

depicted in Fig. 8(d). Because the positive tangential directions of Edge 1 and Edge 3 are along $+y_k = +y_{\text{global}}$ and $-y_k = -y_{\text{global}}$, respectively (see Fig. 5.2), care should be taken over the sign. Thus, it can be found that Eqs. (5.66d, g) express the continuity conditions with respect to the y_{global} axis.

Lastly, Eqs (5.66e, f, h, i) represent the continuity conditions between the work conjugates of the edge resultants shown in Eqs. (5.57e, f, h, i). Therefore,

$(U_{z(j)})_k$ and $(U_{x(j)})_k$ ($j=1, 3$; $k=1, 2$) in Eqs. (5.66e, f, h, i) denote the displacements of Edge j in z direction and x direction respectively direction as depicted in Figs. 5.8(e, f). It can be found that Eqs. (5.66e, h) represent the continuity conditions between $(U_{z_{global}(j)})_k = (U_{z(j)})_k \cos\phi_k - (U_{x(j)})_k \sin\phi_k$ ($j=1$, 3 ; $k=1, 2$), and that Eqs. (5.66f, i) represent the continuity conditions between $(U_{x_{global}(j)})_k = (U_{z(j)})_k \sin\phi_k + (U_{x(j)})_k \cos\phi_k$ ($j=1, 3$; $k=1, 2$).

Let us now derive the desired joint matching conditions at the joint where N ($N \geq 3$) box beams are connected, as shown in Fig. 5.2. As argued in the derivation of the generalized forces equilibrium conditions at the joint, the continuity conditions between ($(U_{s(1)})_k$, $(U_{z_{\text{global}}(1)})_k$, $(U_{x_{\text{global}}(1)})_k$) and ($(U_{s(3)})_{k+1}$, $(U_{z_{\text{global}}(3)})_{k+1}$, $(U_{x_{\text{global}}(3)})_{k+1}$) can be considered because Edge 1 of Beam k ($k=1, 2, \cdots, N$) and Edge 3 of Beam k+1 (Beam N+1 refers to Beam 1) are regarded as being connected rigidly.

Using the edge connectivity just explained above and generalizing the displacement continuity conditions given in Eq. (5.66) for $N=2$ to the case of $N \geq 3$, the following relations can be obtained:

$$(U_{z_{global}})_1 = (U_{z_{global}})_2 = \cdots = (U_{z_{global}})_N \tag{5.68a}$$

$$(U_{x_{global}})_1 = (U_{x_{global}})_2 = \cdots = (U_{x_{global}})_N \tag{5.68b}$$

$$(\Theta_{y_{\text{global}}})_1 = (\Theta_{y_{\text{global}}})_2 = \cdots = (\Theta_{y_{\text{global}}})_N \tag{5.68c}$$

$$(U_{s(1)})_k = -(U_{s(3)})_{k+1} \tag{5.68d}$$

$$(U_{z_{\text{global}}(1)})_k = (U_{z_{\text{global}}(3)})_k \tag{5.68e}$$

$$(U_{x_{\text{global}}(1)})_k = (U_{x_{\text{global}}(3)})_k \tag{5.68f}$$

Equations (5.68a, b) represent the continuity conditions for the rigid-body displacements of N box beams in the z_{global} direction and in the x_{global} direction, respectively, and Eq. (5.68c) represent the continuity condition for the sectional effective rotations of N box beams in the y_{global} direction. On the other hand, Eqs. (5.68d-f) are the continuity conditions between the edge displacements on Edge 1 of Beam k and Edge 3 of Beam k+1 $(1 \le k \le N)$. Therefore, the independent number of equations from Eq. (5.68) becomes $3 \times (N-1) + 3N = 6N - 3$.

5.4.4 Use of more precise field variables ($\chi_1^1, W_1^1, \chi_1^2, W_1^2$)

According to the joint matching conditions given in Eq. (5.68), the rigid-body rotations (θ_y) of the box beams connected at the joint are additionally generated by higher-order deformation (W_1^g) as well as rigid-body motions (θ_y) of adjacent beams. To interpret the exact joint flexibility, therefore, higher-order deformations (W_1^1, W_1^2) representing more accurate bending warping should be employed instead of (W_1^g). Meanwhile, it can be found that theoretically reasonable shape function $\psi_z^{W_1^g}$ of W_1^g is related with that of χ_1^g as $\psi_z^{W_1^g} = -\dfrac{4(b^3+5h^3)}{15bh^2(b+3h)}\psi_s^{U_x}$

$-\frac{16}{6b}\psi_s^{\chi_1}$. Therefore, bending distortions (χ_1^1, χ_1^2) should be also employed instead of (χ_1^g) in order to define theoretically valid (W_1^1, W_1^2).

As shown in Choi and Kim [23], the bending distortion χ_1^g represents the cross-sectional deformation generated by the Poisson's effect when in-plane bending moment M_y is applied. Thus, we introduce a new set of bending distortions (χ_1^1, χ_1^2) representing the cross-sectional deformations induced by the Poisson's effect on Edge 1, 3 and on Edge 2, 4, respectively. The shape functions $\psi_s^{\chi_1^1}(s_j), \psi_s^{\chi_1^2}(s_j)$ on Edge j ($j = 1, 2, 3, 4$) satisfy the following conditions:

$$\dot{\psi}_s^{\chi_1^1}(s_j) = (-1)^{(j+1)/2} \times \frac{b}{2} \quad (j = 1, 3)\,; \quad \dot{\psi}_s^{\chi_1^1}(s_j) = 0 \qquad (j = 2, 4) \qquad (5.69a)$$

$$\dot{\psi}_s^{\chi_1^2}(s_j) = 0 \quad (j = 1, 3)\,; \quad \dot{\psi}_s^{\chi_1^2}(s_j) = (-1)^{(j)/2} \times s_j \qquad (j = 2, 4) \qquad (5.69b)$$

Considering the symmetry conditions and the orthogonality conditions proposed in Choi and Kim [23], one can determine the shape functions $\psi_s^{\chi_1^1}, \psi_s^{\chi_1^2}$ (the explicit expressions of $\psi_s^{\chi_1^1}, \psi_s^{\chi_1^2}$ are given in Appendix A).

According to Choi and Kim [23], the bending warping W_1^g represents the cross-sectional deformation generated by the shear stress when transverse force F_x is applied. The following shear stress is defined when the field variables ($U_x, \theta_y, \chi_1^1, W_1^1$) are employed to represent the in-plane bending deformations

$$\sigma_{sz}(s,z)=\frac{F_x(z)}{J_{F_x}}\psi_s^{U_x}(s)+\frac{Q_1^1(z)}{J_{Q_1^1}}\psi_s^{\chi_1^1}(s) \tag{5.70}$$

, and the primary bending warping W_1^1 having the relation $\dot{\psi}_z^{W_1^1}=\frac{4h}{b(b+3h)}\psi_s^{U_x}-\frac{4}{h}\psi_s^{\chi_1^1}$ can be obtained (see Choi and Kim [23] for the detailed procedure). Subsequently, when the field variables (U_x, θ_y, χ_1^1, W_1^1, χ_1^2, W_1^2) are employed to represent the in-plane bending deformation, the following shear stress is defined

$$\sigma_{sz}(s,z)=\frac{F_x(z)}{J_{F_x}}\psi_s^{U_x}(s)+\frac{Q_1^1(z)}{J_{Q_1^1}}\psi_s^{\chi_1^1}(s)+\frac{Q_1^2(z)}{J_{Q_1^2}}\psi_s^{\chi_1^2}(s) \tag{5.71}$$

, and the secondary bending warping W_1^2, which represents the higher bending warping deformation, can be derived. The shape function $\psi_z^{W_1^2}$ of W_1^2 satisfies the relation $\dot{\psi}_z^{W_1^2}=\frac{8}{5b}\psi_s^{U_x}-\frac{4}{h}\psi_s^{\chi_1^1}-\frac{4(h+2b)}{b^2}\psi_s^{\chi_1^2}$ (see Choi and Kim [23] for the detailed procedure). The explicit expressions of $\psi_z^{W_1^1}$, $\psi_z^{W_1^2}$ are given in Appendix A.

When (χ_1^1, χ_1^2) are employed instead of (χ_1^g), it can be found that χ_1^1 represents the edge displacements of (χ_1^g) with respect to the joint matching relations, and thus the definitions of $U_{s(1)}, U_{s(3)}$ in Eqs. (5.66, 5.68) can be expressed in terms of (χ_1^1, χ_1^2) as:

$$U_{s(1)} = \chi_1^1 - \frac{b^3 + h^3}{h^3}\chi_2 ; \quad U_{s(3)} = -\chi_1^1 - \frac{b^3 + h^3}{h^3}\chi_2 \tag{5.72}$$

When (W_1^1, W_1^2) are employed instead of (W_1^g), one can see that both (W_1^1, W_1^2) represent the edge displacements of (W_1^g) with respect to the joint matching relations, and thus the definitions of $\Theta_y, U_{z(1)}, U_{z(3)}$ in Eqs. (5.66, 5.68) can be expressed in terms of (W_1^1, W_1^2) as:

$$\Theta_y = \theta_y + \frac{4h}{b(b+3h)}W_1^1 - \frac{4h}{5b^2}W_1^2 \tag{5.73a}$$

$$\begin{aligned} U_{z(1)} &= \frac{2}{3}W_1^1 - \frac{2(b+3h)}{15b}W_1^2 + \frac{2(h^2-b^2)}{3h^2}W_2 ; \\ U_{z(3)} &= -\frac{2}{3}W_1^1 + \frac{2(b+3h)}{15b}W_1^2 + \frac{2(h^2-b^2)}{3h^2}W_2 \end{aligned} \tag{5.73b, c}$$

5.5 Numerical Analysis

The finite element equations for Beam k ($k = 1, 2, \cdots, N$) among N box beams connected at the joint can be defined as, by using the stiffness matrix for the straight box beam element ($z_1 < z < z_2$) (see Refs. [7, 22, 23] for the detailed derivation),

$$\mathbf{K}_k \cdot \mathbf{d}_k = \mathbf{f}_k \tag{5.74}$$

where $\mathbf{K}_k, \mathbf{d}_k$, and $\mathbf{f}_k$ in Eq. (5.74) refer to the stiffness matrix, the nodal displacement vector, and the nodal force vector for Beam k, respectively. Assembling all finite element equations for N box beams in numerical order, the

finite element equations for the N box beams-joint structure can be determined:

$$\mathbf{K}_{\text{total}} \cdot \mathbf{d}_{\text{total}} = \mathbf{f}_{\text{total}} \tag{5.75}$$

If n number of nodes are used to model the N box beams-joint structure, $\mathbf{K}_{\text{total}}$, $\mathbf{d}_{\text{total}}$, and $\mathbf{f}_{\text{total}}$ in Eq. (5.75) denote $11n \times 11n$ total stiffness matrix, $11n \times 1$ total nodal displacement vector, and $11n \times 1$ total nodal force vector, respectively. The next step is to impose the matching conditions for nodal displacements of N box beams at the joint.

The proposed exact matching conditions of Eq. (5.68) can be applied to the finite element equations by using the method of Lagrange multipliers [27], an optimization method to find the maximum or minimum value of a function subject to equality constraints. Associated with this study, a problem to minimize the total potential energy of the N box beams-joint structure subject to the joint matching conditions in Eq. (5.68) is solved by employing the method of Lagrange multipliers.

To facilitate subsequent analysis, the matching conditions in Eq. (5.68) are expressed as equality constraints for $\mathbf{d}_{\text{total}}$ as

$$\mathbf{S} \cdot \mathbf{d}_{\text{total}} = \mathbf{0} \tag{5.76}$$

where $\mathbf{S}$ is a $(6N-3) \times (11n)$ matrix and Eq. (5.76) yields ($6N-3$) independent equations. By introducing the Lagrange multiplier $\boldsymbol{\lambda}$, the following Lagrangian $\boldsymbol{\Pi}_L$ can be defined:

$$\boldsymbol{\Pi}_L(\mathbf{d}_{total}, \boldsymbol{\lambda}) = \frac{1}{2}\mathbf{d}_{\text{total}}^{\text{T}}\mathbf{K}_{\text{total}}\mathbf{d}_{\text{total}} - \mathbf{d}_{\text{total}}^{\text{T}}\mathbf{f}_{\text{total}} + \boldsymbol{\lambda}^{\text{T}}(\mathbf{S} \cdot \mathbf{d}_{\text{total}}) \tag{5.77}$$

According to the method of Lagrange multipliers, the stationary conditions of $\mathbf{\Pi}_L$ yields

$$\frac{\partial \mathbf{\Pi}_L}{\partial \mathbf{d}_{\text{total}}} = 0; \ \mathbf{K}_{\text{total}}\mathbf{d}_{\text{total}} - \mathbf{f}_{\text{total}} + \boldsymbol{\lambda}^{\text{T}}\mathbf{S} = \mathbf{0} \tag{5.78a}$$

$$\frac{\partial \mathbf{\Pi}_L}{\partial \boldsymbol{\lambda}} = 0; \ \mathbf{S} \cdot \mathbf{d}_{\text{total}} = \mathbf{0} \tag{5.78b}$$

The nodal displacement vector in Eqs. (5.78a, b), $\mathbf{d}_{\text{total}}$, satisfies the matching conditions in Eq. (5.68) and minimizes the potential energy of the *N* box beams-joint structure. Therefore, Eqs. (5.78a, b) represent the finite element equations for the *N* box beams-joint structure that include the matching conditions in Eq. (5.68). Finally, Eqs. (5.78a, b) can be expressed as a matrix equation as

$$\begin{bmatrix} \mathbf{k}_{\text{total}} & \mathbf{S}^{\text{T}} \\ \mathbf{S} & \mathbf{0} \end{bmatrix} \begin{Bmatrix} \mathbf{d}_{\text{total}} \\ \boldsymbol{\lambda} \end{Bmatrix} = \begin{Bmatrix} \mathbf{f}_{\text{total}} \\ \mathbf{0} \end{Bmatrix} \tag{5.79}$$

If proper boundary and loading conditions are prescribed, $\mathbf{d}_{\text{total}}$ (and $\boldsymbol{\lambda}$) can be determined from Eq. (5.79). Because the solution procedure is a standard one, no further discussion on numerical analysis will be necessary.

5.5.1 Numerical Examples

Several examples will be analyzed by using the finite element equations given in Eq. (5.79). The validity of the proposed approach will be demonstrated by comparing the results with those obtained from ABAQUS shell elements or Timoshenko beam elements. Because the joint flexibility is highly dependent upon

the number of box beams connected at the joint, the joint angles among those beams, and the width and height (or aspect ratio) of the box beam cross-section, we will examine their effects on the solutions or the mechanical behavior of three or more box beams-joint structures.

Although box beam sections of different widths b and heights h are considered within a range $50\,\text{mm} \le b,\ h \le 150\,\text{mm}$, converged analysis results can be obtained with 40 beam elements regardless of those changes. Meanwhile, in two-dimensional ABAQUS shell analysis, $12.5\,\text{mm} \times 12.5\,\text{mm}$ square shell elements are mainly used to obtain converged analysis results. For example, if the dimensions of each box beam are width $b = 50\,\text{mm}$, height $h = 100\,\text{mm}$, and length $L = 1000\,\text{mm}$, it was found that the converged results were obtained if $(4+8+4+8)\times 80 = 1920$ shell elements were used to model the box beam in consideration.

Case Study 1: Three Box Beams-Joint Structure. A three box beams-joint structure as depicted in Fig. 5.9(a) is considered in the first case study.

For the first example, the three box beams-joint structure with the joint angles

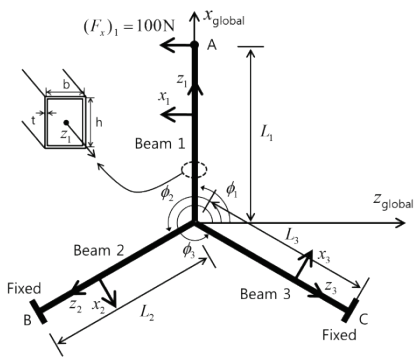
$(F_x)_1 = 100\text{N}$
x_{global}
A
z_1
x_1
b
t
h
z_1
Beam 1
L_1
ϕ_2
ϕ_1
z_{global}
L_3
x_3
Beam 2
ϕ_3
Fixed
z_2
x_2
L_2
Beam 3
z_3
B
C
Fixed

(a)

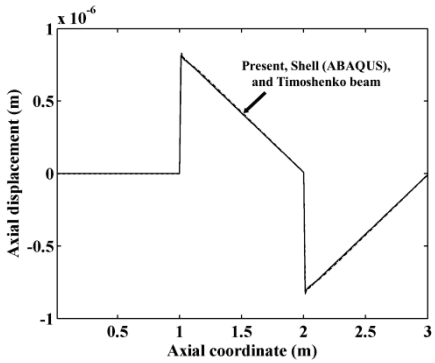
x 10^-6
Present, Shell (ABAQUS), and Timoshenko beam
Axial displacement (m)
Axial coordinate (m)

(b)

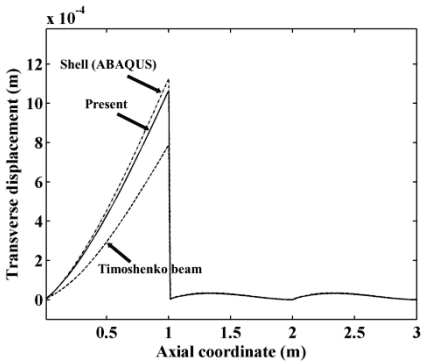
x 10^-4
Shell (ABAQUS)
Present
Timoshenko beam
Transverse displacement (m)
Axial coordinate (m)

(c)

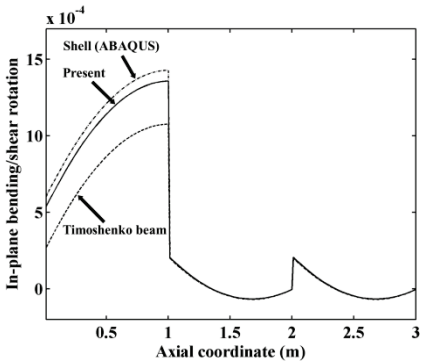
x 10^-4
Shell (ABAQUS)
Present
Timoshenko beam
In-plane bending/shear rotation
Axial coordinate (m)

(d)

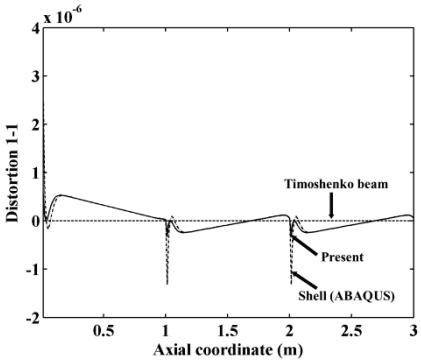
x 10^-6
Timoshenko beam
Present
Shell (ABAQUS)
Distortion 1-1
Axial coordinate (m)

(e)

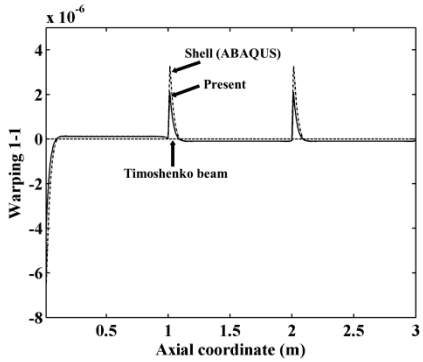
x 10^-6
Shell (ABAQUS)
Present
Timoshenko beam
Warping 1-1
Axial coordinate (m)

(f)

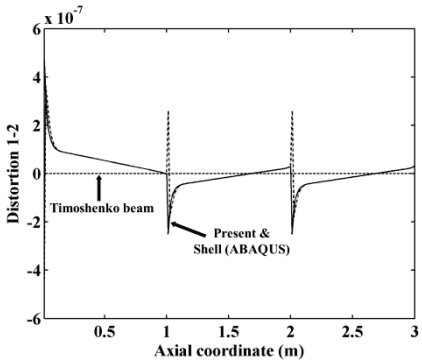

(g)

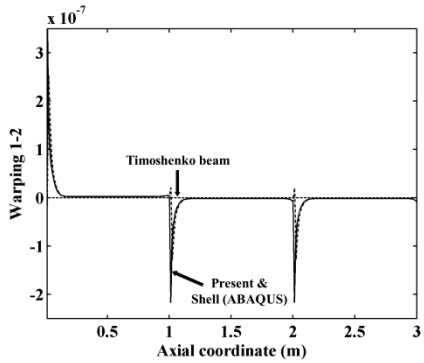

(h)

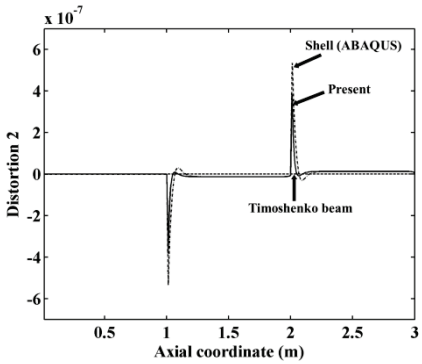

(e)

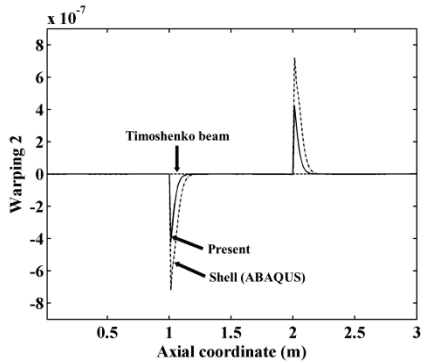

(f)

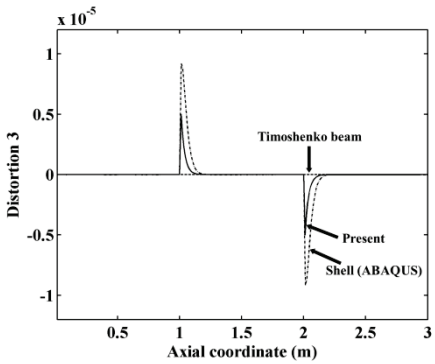

(e)

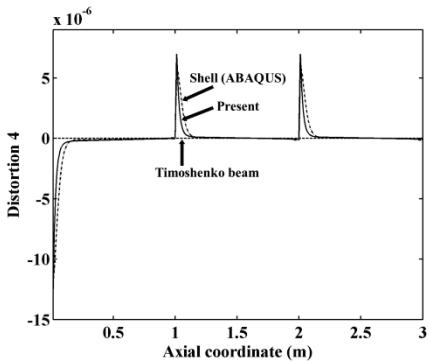

(f)

Fig. 5.9 Numerical results for the three box beams-joint structure under transverse force $(F_x)_1$=100 N: (a) problem description (L_1=L_2=L_3=1000 mm, b=50 mm,

h=100 mm, t=2 mm, ϕ_1= 90º , ϕ_2= 210º , ϕ_3= 330º), (b) axial displacement U_z, (c) transverse displacement U_x, (d) in-plane bending/shear rotation θ_y, (e) distortion 1-1 χ_1^1, (f) warping 1-1 W_1^1, (g) distortion 1-2 χ_1^2, (h) warping 1-2 W_1^2, (i) distortion 2 χ_2, (j) warping 2 W_2, (k) distortion 3 χ_3, (l) distortion 4 χ_4.

$\phi_1 = 90^\circ$, $\phi_2 = 210^\circ$ and $\phi_3 = 330^\circ$ as shown in Fig. 5.9(a) is considered. All the box beams that make up the mentioned structure are identical. The length of those beams is $L = 1000$ mm, and the width (b), height (h) and thickness (t) of those beams are $b = 50$ mm, $h = 100$ mm, and $t = 2$ mm, respectively. The material properties of those beams are Young's modulus $E = 200$ Gpa and Poisson's ratio $\nu = 0.3$. The ends of Beam 2 and Beam 3 denoted by B and C are fixed, and the end of Beam 1 denoted by A is subjected to a transverse force $(F_x)_1 = 100$ N. The loaded end A is assumed to be rigid.

The results are given in Figs. 5.9(b-l). In the plot, the range of the axial coordinates, ($k-1, k$; $k = 1, 2, 3$), corresponds to Beam k. Observing the results based on those from the shell analysis, one can find that the analysis using the Timoshenko beam theory overestimates the stiffness of the three box beams-joint structure, as mentioned in Introduction. In contrast, one can find that the proposed approaches employing the theoretically derived joint matching conditions can predict the behavior of the three box beams-joint structure as accurately as predicted by the shell analysis.

Next, we check whether or not accurate results can still be provided by the

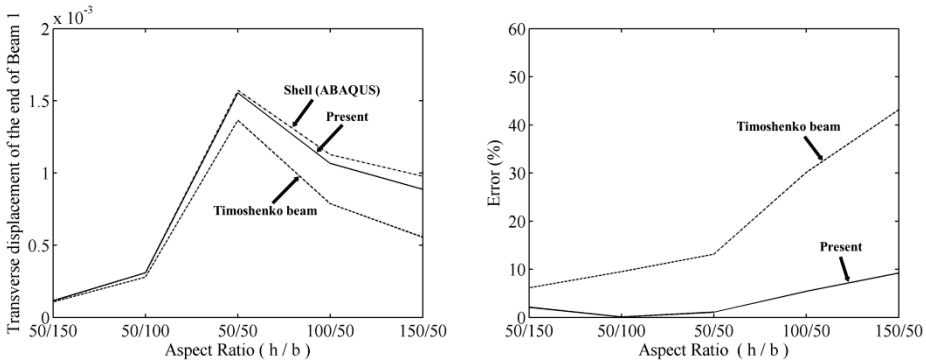

(a) (b)

Fig. 5.10 (a) Numerical results for the three box beams-joint structures shown in Fig. 5.9(a) with various widths (*b*) and heights (h) of the cross-section (or aspect ratios *h*/*b*) raging from *b*=150 mm, *h*=50 mm (*h*/*b*=50/150) to *b*=50 mm, *h*=150 mm (*h*/*b*=150/50), (b) percent errors for one-dimensional analyses with respect to the result from shell analysis.

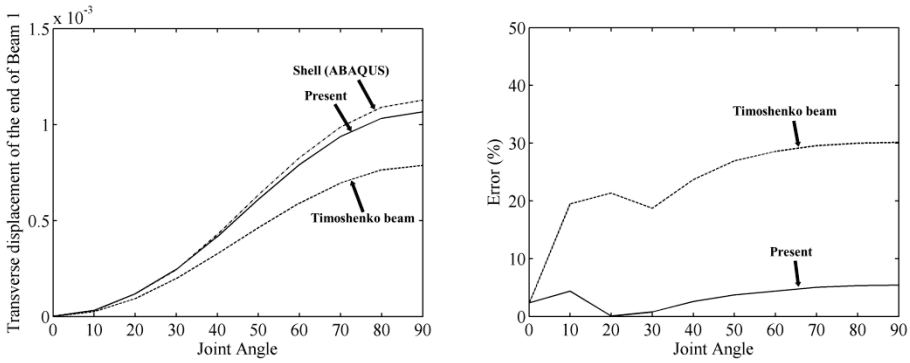

(a) (b)

Fig. 5.11 (a) Numerical results for the three box beams-joint structures shown in Fig. 5.9(a) with various joint angles ϕ_1 of Beam 1 ranging $0^o \leq \phi_1 \leq 90^o$, (b) percent errors for one-dimensional analyses with respect to the result from shell analysis.

proposed approach when either b or h of the cross-section or ϕ_1 (which is the joint angle of Beam 1) is changed for the three box beams-joint structure shown in Fig. 5.9(a). Problems defined by changing b and h of the previous problem in a range from $b = 150\,\text{mm}, h = 50\,\text{mm}$ $(h/b = 50/150)$ to $b = 50\,\text{mm}, h = 150\,\text{mm}$ $(h/b = 150/50)$ are first solved, and the results are given in Figs. 5.10(a, b). The graph in Fig. 5.10(a) represents the variation in the transverse displacement $(U_x)_1$ of the end A when the aspect ratio (h/b) of the cross-section is varied, and the graph in Fig. 5.10(b) represent the percent error of the one-dimensional analysis results with respect to the shell result. From those graphs, it can be found that the proposed approach can provide accurate results for the box beams-joint structures with sections of various widths or heights.

Problems defined from the first example by changing ϕ_1 in a range from 0° to 90° are also solved, and the results are given in Figs. 5.11(a, b). The graph in Fig. 5.11(a) represents the variation in the transverse displacement $(U_x)_1$ of the end A when ϕ_1 is increased, and the percent error of the one-dimensional analysis results with respect to the shell result is shown in Fig. 5.11(b). From those results, it can be found that the proposed approach can also provide accurate and reliable results for the box beams-joint structure with various joint angles.

Case Study 2: N Thin-Walled Box Beams-Joint Structure. Box beams-joint structures involving several box beams are considered; see Fig. 5.12(a).

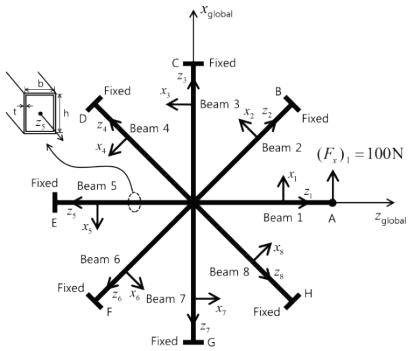
x_{global}
z_{global}
Fixed
Beam 1
Beam 2
Beam 3
Beam 4
Beam 5
Beam 6
Beam 7
Beam 8
$(F_x)_1 = 100\text{N}$
A
B
C
D
E
F
G
H

(a)

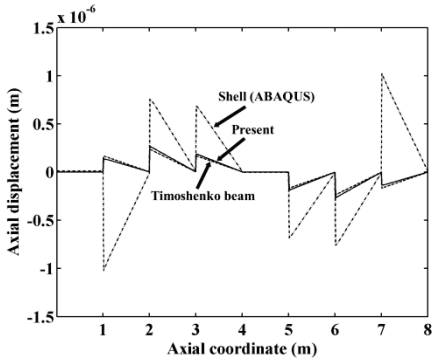
x 10^-6
Axial displacement (m)
Axial coordinate (m)
Shell (ABAQUS)
Present
Timoshenko beam

(b)

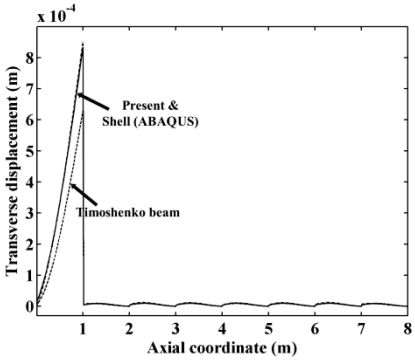
x 10^-4
Transverse displacement (m)
Axial coordinate (m)
Present &
Shell (ABAQUS)
Timoshenko beam

(c)

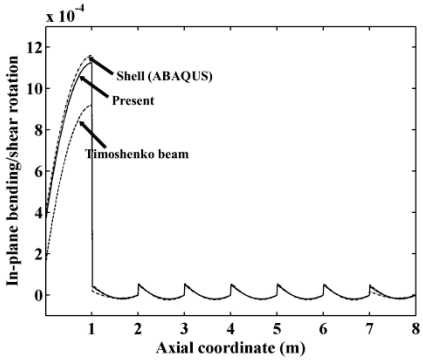
x 10^-4
In-plane bending/shear rotation
Axial coordinate (m)
Shell (ABAQUS)
Present
Timoshenko beam

(d)

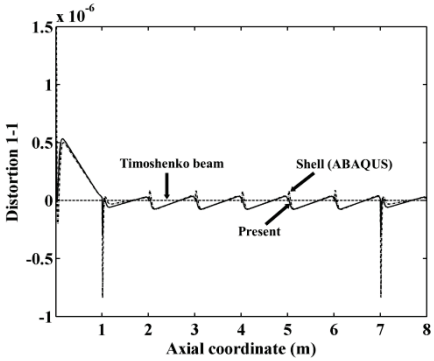
x 10^-6
Distortion 1-1
Axial coordinate (m)
Timoshenko beam
Shell (ABAQUS)
Present

(e)

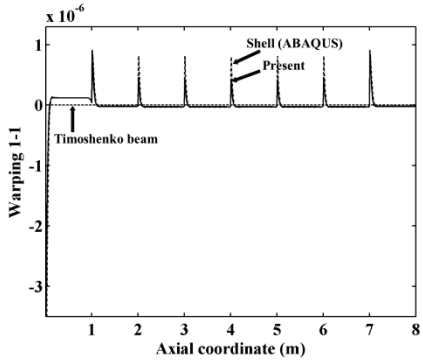
x 10^-6
Warping 1-1
Axial coordinate (m)
Shell (ABAQUS)
Present
Timoshenko beam

(f)

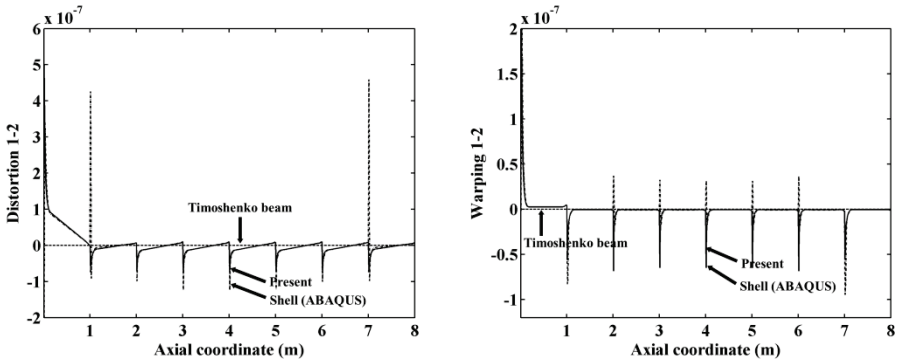

(g)

(h)

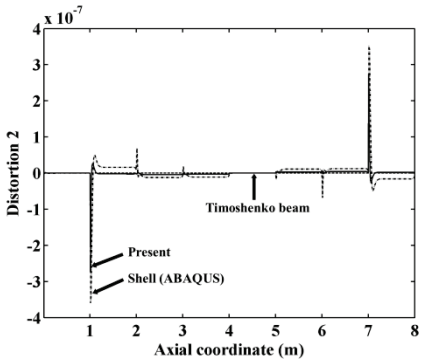

(e)

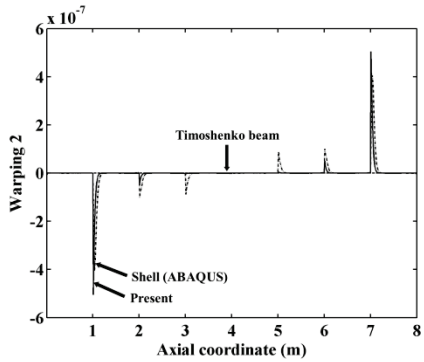

(f)

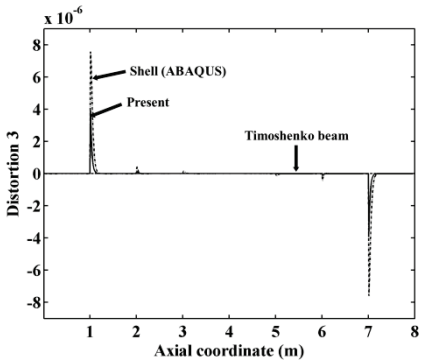

(e)

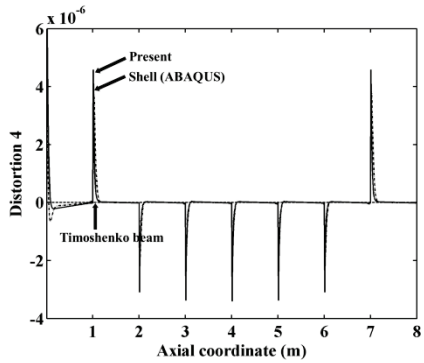

(f)

Fig. 5.12 Numerical results for the eight box beams-joint structure under transverse force $(F_x)_1$=100 N: (a) problem description (L=1000 mm, b=50 mm,

h=100 mm, t=2 mm, ϕ_k= 45° (k=1, 2, …, 8)), (b) axial displacement U_z, (c) transverse displacement U_x, (d) in-plane bending/shear rotation θ_y, (e) distortion 1-1 χ_1^1, (f) warping 1-1 W_1^1, (g) distortion 1-2 χ_1^2, (h) warping 1-2 W_1^2, (i) distortion 2 χ_2, (j) warping 2 W_2, (k) distortion 3 χ_3, (l) distortion 4 χ_4.

The joint angle of Beam k ($k = 1, 2, \cdots, 8$) in the beams-joint structure of Fig. 5.12(a) is $\phi_k = (\frac{360}{8}) \times (k-1)$, so the angle between two adjacent beams is uniformly 45°. All box beams constituting the structure are identical. The length of those beams is $L = 1000$ mm, and the dimensions of the beam cross-sections are $b = 50$ mm, $h = 100$ mm, and $t = 2$ mm, respectively. The material properties of those beams are Young's modulus $E = 200$ Gpa and Poisson's ratio $\nu = 0.3$. The end of Beam 1 denoted by A is subjected to a transverse force $(F_x)_1 = 100$ N, and is assumed to be rigid. The ends of the other box beams (B-H) are all fixed.

The results are given in Figs. 5.12(b-l). As in Fig. 5.9, the range of the axial coordinates, ($k-1, k$; $k = 1, 2, \cdots, 8$), corresponds to Beam k. Examining the results on the basis of those from the shell analysis, the analysis using the Timoshenko beam theory highly overestimates the stiffness of the structure, as observed in the previous result. However, the proposed method can predict the response of the structure almost as accurately as those from the shell analysis, even though the number of box beams connected at the joint is significantly increased.

We now investigate if accurate results can be still obtained by the proposed

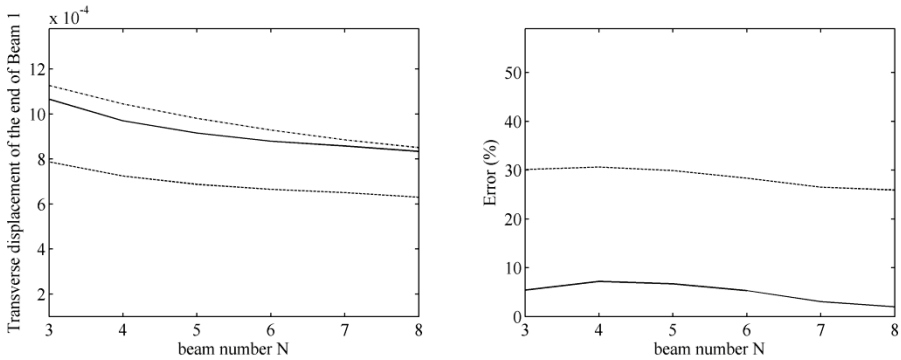

(a) (b)

Fig. 5.13 (a) Numerical results for the box beams-joint structures with various numbers of box beams (N) ranging $3 \leq N \leq 8$, (b) percent errors for one-dimensional analyses with respect to the result from shell analysis.

method when the number of box beams connected at the joint is changed. To do this, problems that are defined based on the first example in Case study 2 are varied by changing the number of box beams connected at the joint, i.e. N is in a range $3 \leq N \leq 8$. The joint angle of Beam k ($k = 1, 2, \cdots, N$) is $\phi_k = (360/\mathrm{N}) \times (k-1)$, and the angle between the two adjacent beams is uniformly $(360/N)^\circ$.

The results are given in Fig. 5.13. The graph in Fig. 5.13 represents the variation of torsional rotation $(\theta_z)_1$ at the end A of Beam 1 when N is increased. From the results, it can be found that the proposed approach can provide accurate results for a box beams-joint structure composed of various numbers of box beams. Lastly, the problem with more complicated boundary conditions as depicted in Fig. 5.14(a) is considered; the structure shown in Fig. 5.14(a) is equal to the structure in

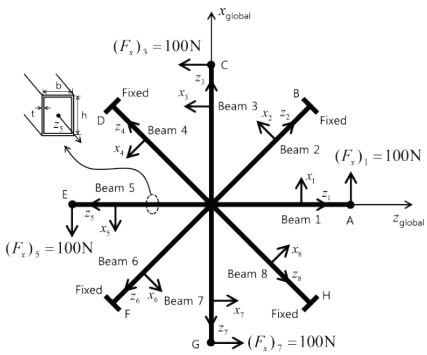
x_{global}
$(F_x)_3 = 100N$
C
Fixed
B
Fixed
D
Beam 3
Beam 4
Beam 2
$(F_x)_1 = 100N$
Beam 5
E
Beam 1
A
z_{global}
$(F_x)_5 = 100N$
Beam 6
Beam 8
Fixed
F
Beam 7
H
Fixed
G
$(F_x)_7 = 100N$

(a)

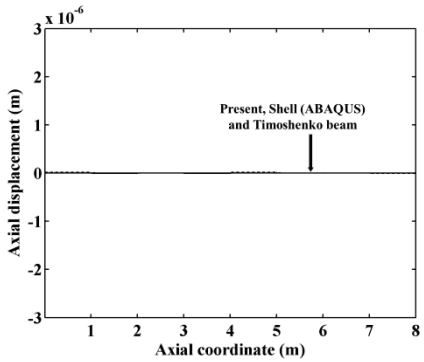
x 10^-6
Present, Shell (ABAQUS) and Timoshenko beam
Axial displacement (m)
Axial coordinate (m)

(b)

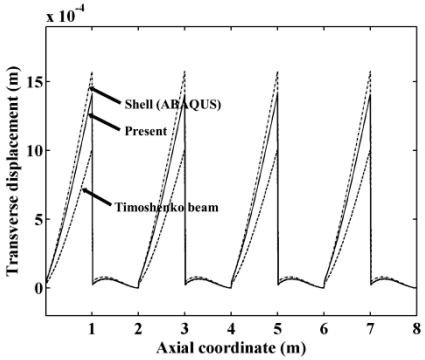
x 10^-4
Shell (ABAQUS)
Present
Timoshenko beam
Transverse displacement (m)
Axial coordinate (m)

(c)

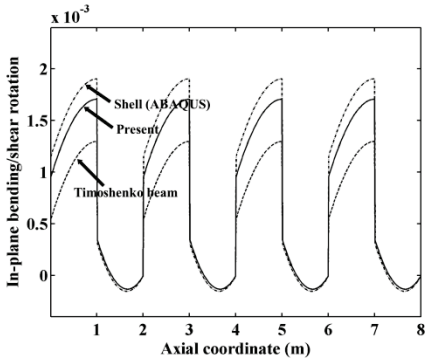
x 10^-3
Shell (ABAQUS)
Present
Timoshenko beam
In-plane bending/shear rotation
Axial coordinate (m)

(d)

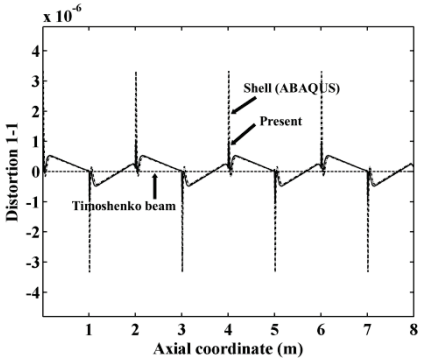
x 10^-6
Shell (ABAQUS)
Present
Timoshenko beam
Distortion 1-1
Axial coordinate (m)

(e)

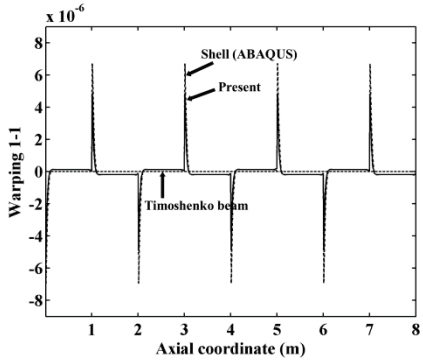
x 10^-6
Shell (ABAQUS)
Present
Timoshenko beam
Warping 1-1
Axial coordinate (m)

(f)

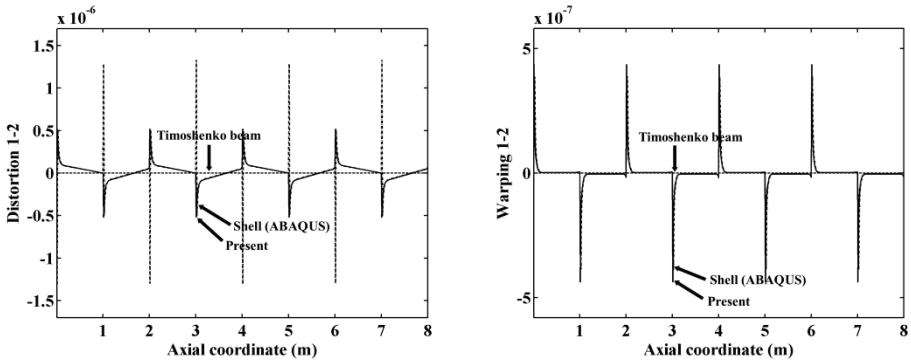

(g)

(h)

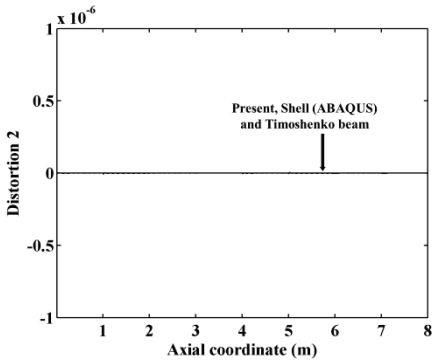

(e)

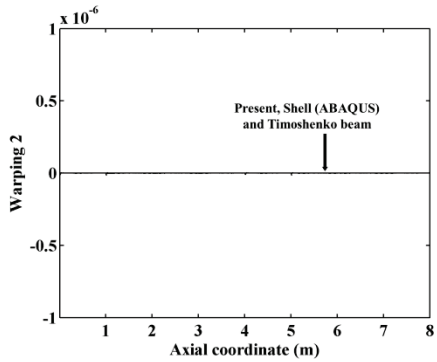

(f)

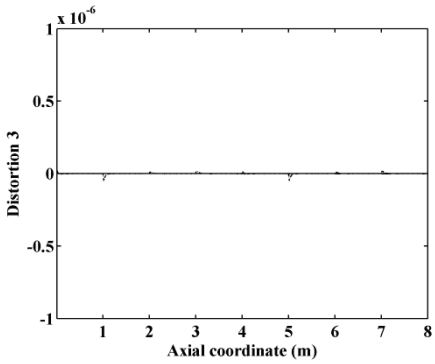

(e)

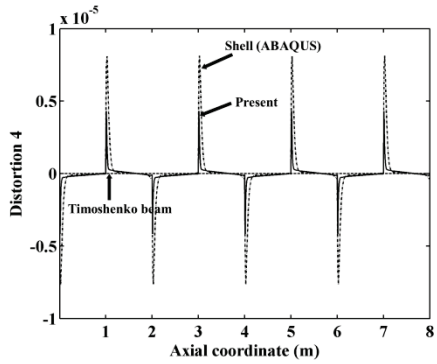

(f)

Fig. 5.14 Numerical results for the eight box beams-joint structure with more complicated boundary conditions: (a) problem description (L=1000 mm, b=50

mm, h=100 mm, t=2 mm, ϕ_k= 45° (k=1, 2, …, 8)), (b) axial displacement U_z, (c) transverse displacement U_x, (d) in-plane bending/shear rotation θ_y, (e) distortion 1-1 χ_1^1, (f) warping 1-1 W_1^1, (g) distortion 1-2 χ_1^2, (h) warping 1-2 W_1^2, (i) distortion 2 χ_2, (j) warping 2 W_2, (k) distortion 3 χ_3, (l) distortion 4 χ_4.

the first example of case study 2. Observing the result given in Figs. 5.14(b-l), it can be found that the proposed approach can provide the correct result even where complicated boundary conditions are considered.

5.6 Conclusions

When a three or more box beams-joint structure is subjected to in-plane bending or longitudinal force, a one-dimensional analysis method being capable of interpreting the flexible response of the structure is established. To take into account the influence of cross-sectional deformations on the flexible response of the joint, the higher-order beam theory considering those cross-sectional deformations as independent degrees of freedom is employed; To represent accurate joint flexibility, extensional warping W_2, extensional distortion χ_2 and bending distortion χ_4 are newly introduced in this study, and more precisely determined bending warpings (W_1^1, W_1^2) and bending distortions (χ_1^1, χ_1^2) are employed instead of (χ_1^g, W_1^g) in Choi and Kim [23]. The main difficulty in developing the desired analysis method is to determine the joint matching conditions among the 11 field variables of the employed higher-order beam theory. To derive the exact joint

matching conditions, joint equilibrium conditions of the generalized forces $\tilde{\mathbf{F}} = \{ F_z, F_x, M_y, Q_1^g, B_1^g, Q_2, B_2, Q_3, Q_4 \}^{\mathrm{T}}$ which are work conjugate of the field variables $\tilde{\mathbf{U}} = \{ U_z, U_x, \theta_y, \chi_1^g, W_1^g, \chi_2, W_2, \chi_3, \chi_4 \}^{\mathrm{T}}$ were first derived. Summarizing the procedure briefly, each force of $\tilde{\mathbf{F}}$ was expressed by the traditional (sectional) resultants acting on the entire cross-section or the so-called "edge resultants" [22] acting on the edge of the section. Then, joint equilibrium conditions concerning those sectional resultants or edge resultants were found based on the results in Choi and Kim [23], and extending those conditions, the joint equilibrium conditions applicable to three or more box beams-joint structures were derived. Considering the principle of virtual work, thereafter, the joint matching conditions for $\tilde{\mathbf{U}}$ that are capable of representing the flexible response of the three or more box beams-joint structure were theoretically derived from the determined equilibrium conditions. Lastly, the desired joint matching conditions for $\mathbf{U} = \{ U_z, U_x, \theta_y, \chi_1^1, W_1^1, \chi_1^2, W_1^2, \chi_2, W_2, \chi_3, \chi_4 \}^{\mathrm{T}}$ are derived from those for $\tilde{\mathbf{U}}$ through the comparison between ($\chi_1^1, W_1^1, \chi_1^2, W_1^2$) and (χ_1^g, W_1^g). Several numerical examples checking the accuracy and the validity of the proposed method were considered, and it was demonstrated that the proposed method can interpret the response of the three or more box beams-joint structures under in-plane loads as accurately as the ABAQUS shell analysis, regardless of the number of box beams, the joint angles, and the aspect ratios of the box beams cross-section. The proposed method has advantages against the shell analysis such as convenience for

modeling, the ease of modeling changes and significantly fast analysis. When introducing the proposed method with optimization design techniques, therefore, a faster and efficient initial design process of vehicle can be expected. In addition, the proposed methodologies for determining the higher-order deformation degrees or for deriving the joint matching conditions can be expected to be important foundations for expanding the scope of structures interpreted by using the higher-order beam theory-based method to a general three-dimensional thin-walled beams-joint structure.

Appendix A

Explicit expressions for the shape function $\psi_p^\alpha(s)$ ($p = n, s, z$; $\alpha = U_z, U_x, \theta_y, \chi_1^1, W_1^1, \chi_1^2, W_1^2, \chi_2, W_2, \chi_3, \chi_4$) are given. For convenience, $\psi_p^\alpha(s)$ are separately defined on each edge, and $\psi_p^\alpha(s_j)$ ($j = 1, 2, 3, 4$) represent the shape function on Edge *j*. The tangential coordinate s_j is measured from the center of Edge *j* along the contour line.

$$\psi_z^{U_z}(s_j) = 1 \qquad \text{(for } j = 1,\ 2,\ 3,\ 4) \qquad (5.A1)$$

$$\begin{aligned} \psi_n^{U_x}(s_j) &= (-1)^{(j-1)/2} \quad \text{(for } j = 1,\ 3) \quad \text{and} \quad 0 \quad \text{(for } j = 2,\ 4) \\ \psi_s^{U_x}(s_j) &= 0 \quad \text{(for } j = 1,\ 3) \quad \text{and} \quad (-1)^{(j)/2} \quad \text{(for } j = 2,\ 4) \end{aligned} \qquad (5.A2)$$

$$\psi_z^{\theta_y}(s_j) = (-1)^{(j+1)/2}\frac{b}{2} \ \text{(for } j = 1,\ 3) \quad \text{and} \quad (-1)^{(j-2)/2} s_j \ \text{(for } j = 2,\ 4) \qquad (5.A3)$$

$$\psi_n^{\chi_1^1}(s_j) = (-1)^{(j-1)/2} \times \{\frac{2}{bh^3} s_j^4 - \frac{3}{bh} s_j^2 + \frac{5h}{8b}\} \qquad \text{(for } j = 1,\ 3)$$

$$= (-1)^{(j)/2} \times \{\frac{2}{b} s_j\} \qquad \text{(for } j = 2,\ 4) \qquad (5.A4)$$

$$\psi_s^{\chi_1^1}(s_j) = (-1)^{(j-1)/2} \times \{\frac{2}{h} s_j\} \qquad \text{(for } j = 1,\ 3)$$

$$= 0 \qquad \text{(for } j = 2,\ 4)$$

$$\psi_z^{W_1^1}(s_j) = (-1)^{(j-1)/2} \times (-\frac{4}{h^2}) \times \{s_j^2 - \frac{h^2(b+h)}{4(b+3h)}\} \qquad \text{(for } j = 1,\ 3)$$

$$= (-1)^{(j-2)/2} \times (-\frac{4}{h^2}) \times \{-\frac{h^3}{b(b+3h)} s_j\} \qquad \text{(for } j = 2,\ 4) \qquad (5.A5)$$

$$\psi_n^{\chi_1^2}(s_j) = (-1)^{(j-1)/2} \qquad \text{(for } j = 1,\ 3)$$

$$= 0 \qquad \text{(for } j = 2,\ 4)$$

$$\psi_s^{\chi_1^2}(s_j) = 0 \qquad \text{(for } j = 1,\ 3) \qquad (5.A6)$$

$$= (-1)^{(j-2)/2} \times (\frac{12}{b^2}) \times \{-\frac{1}{2} s_j{}^2 + \frac{b^2}{24}\} \qquad \text{(for } j = 2,\ 4)$$

$$\psi_z^{W_1^2}(s_j) = (-1)^{(j-1)/2} \times (-\frac{4}{h^2}) \times \{s_j^2 - \frac{h^2}{20}\} \qquad \text{(for } j = 1,\ 3)$$

$$= (-1)^{(j-2)/2} \times (-\frac{4}{h^2}) \times \{-\frac{2h^2(h+2b)}{b^4} s_j{}^3 + \frac{h^2(5h+6b)}{10b^2} s_j\} \qquad (5.A7)$$

$$\text{(for } j = 2,\ 4)$$

$$\psi_n^{\chi_2}(s_j) = -\frac{b}{h} \qquad \text{(for } j = 1,\ 3)$$

$$= -1 \qquad \text{(for } j = 2,\ 4) \qquad (5.A8)$$

$$\psi_s^{\chi_1^2}(s_j) = -\frac{2}{h} s_j \qquad \text{(for } j = 1,\ 2,\ 3,\ 4)$$

$$\psi_z^{W_2}(s_j) = (-\frac{8}{h^2}) \times \{\frac{1}{2} s_j^2 + \frac{2b^3 - 3bh^2 - h^3}{24(b+h)}\} \qquad \text{(for } j = 1,\ 3)$$

$$= (-\frac{8}{h^2}) \times \{\frac{1}{2} s_j^2 + \frac{2h^3 - 3b^2h - b^3}{24(b+h)}\} \qquad \text{(for } j = 2,\ 4) \qquad (5.A9)$$

$$\psi_n^{\chi_3}(s_j) = \frac{384(b+h)}{h^4(5b+h)} \times \{-\frac{1}{24}s_j^4 + \frac{h^2(3b+h)}{48(b+h)}s_j^2 - \frac{h^4(5b+h)}{384(b+h)}\} \qquad \text{(for } j=1,\ 3)$$

$$= \frac{384(b+h)}{h^4(5b+h)} \times \{-\frac{h^3}{24(b+h)}s_j^2 + \frac{b^2h^3}{96(b+h)}\} \qquad \text{(for } j=2,\ 4)$$

$$\psi_s^{\chi_3}(s_j) = 0 \qquad \text{(for } j=1,\ 2,\ 3,\ 4)$$

(5.A10)

$$\psi_n^{\chi_4}(s_j) = (-1)^{(j-1)/2} \times \{-\frac{32}{bh(5b+3h)}\} \times \{-\frac{b(b+3h)}{2h^3}s_j^4 + \frac{3b(b+h)}{4h}s_j^2 - \frac{bh(5b+3h)}{32}\}$$

(for $j=1,\ 3$)

$$= (-1)^{(j-2)/2} \times \{-\frac{32}{bh(5b+3h)}\} \times \{s_j^3 - \frac{b^2}{4}s_j\} \qquad \text{(for } j=2,\ 4)$$

$$\psi_s^{\chi_4}(s_j) = 0 \qquad \text{(for } j=1,\ 2,\ 3,\ 4)$$

(5.A11)

where the ranges of s_j ($j=1, 2, 3, 4$) are $-\frac{h}{2} \le s_1,\ s_3 \le \frac{h}{2}$ and $-\frac{b}{2} \le s_2,\ s_4 \le \frac{b}{2}$.

The following orthogonality conditions hold among ($\psi_z^{U_z}$, $\psi_z^{\theta_y}$, $\psi_z^{W_1^1}$, $\psi_z^{W_1^2}$, $\psi_z^{W_2}$)

$$\iint_S \psi_z^{\alpha_1}(s) \cdot \psi_z^{\alpha_2}(s)\ dsdn = \sum_{j=1}^{4} \{ \iint_{Edge\ j} \psi_z^{\alpha_1}(s_j) \cdot \psi_z^{\alpha_2}(s_j)\ dsdn \} = 0$$

(5.A12)

$$(\alpha_1,\ \alpha_2 = U_z,\ \theta_y,\ W_1^1,\ W_1^2,\ W_2\ ;\ \alpha_1 \ne \alpha_2)$$

, and ($\psi_s^{U_x}$, $\psi_s^{\chi_1^1}$, $\psi_s^{\chi_1^2}$, $\psi_s^{\chi_2}$) also meet the following orthogonality conditions.

$$\iint_S \psi_s^{\alpha_3}(s) \cdot \psi_s^{\alpha_4}(s)\ dsdn = \sum_{j=1}^{4} \{ \iint_{Edge\ j} \psi_s^{\alpha_3}(s_j) \cdot \psi_s^{\alpha_4}(s_j)\ dsdn \} = 0$$

(5.A13)

$$(\alpha_3,\ \alpha_4 = U_x,\ \chi_1^1,\ \chi_1^2,\ \chi_2\ ;\ \alpha_3 \ne \alpha_4)$$

Lastly, one can show that the following orthogonality conditions hold between

($\psi_n^{\chi_3}$, $\psi_n^{\chi_4}$)

$$\iint_S (-n\cdot\dot{\psi}_n^{\chi_3})\cdot(-n\cdot\dot{\psi}_n^{\chi_4})\ dsdn = \sum_{j=1}^{4}\{\iint_{Edge\ j}(-n\cdot\dot{\psi}_n^{\chi_3})\cdot(-n\cdot\dot{\psi}_n^{\chi_4})\ dsdn\} = 0 \quad (5.A14)$$

References

[1] Gere JM, Timoshenko SP. Mechanics of materials. 4th ed. Boston: PWS Pub. Co.; 1997.

[2] Timoshenko SP, Goodier JN. Theory of elasticity. 3rd ed. New York: McGraw-Hill Pub. Co.; 1970.

[3] Vlasov VZ. Thin-walled elastic beams. Jerusalem: Israel Program for Scientific Translations; 1961.

[4] Boswell LF, Zhang SH. A box beam finite element for the elastic analysis of thin-walled structures. Thin-Walled Struct 1983;1:353-83.

[5] Boswell LF, Zhang SH. The effect of distortion in thin-walled box-spine beams. Int J Solids Struct 1984;20:845-62.

[6] Kim JH, Kim YY. Analysis of thin-walled closed beams with general quadrilateral cross sections. J Appl Mech-Trans ASME 1999;66:904-12.

[7] Kim YY, Kim JH. Thin-walled closed box beam element for static and dynamic analysis. Int J Numer Methods Eng 1999;45:473-90.

[8] Kim JH, Kim YY. One-dimensional analysis of thin-walled closed beams having general cross-sections. Int J Numer Methods Eng 2000;49:653-68.

[9] Kim JH, Kim YY. Thin-walled multicell beam analysis for coupled torsion, distortion, and warping deformations. J Appl Mech-Trans ASME 2001;68:260-9.

[10] Chang DC. Effects of flexible connections on body structural response. SAE Technical Paper 1974; No. 740041.

[11] Rao MK, Zebrowski MP, Crabb HC. Automotive body joint analysis for improved vehicle response. Proc. Int. Symp. Automotive Technology and Automation 1983;2:953-74.

[12] Lee K, Nikolaidis E. A two-dimensional model for joints in vehicle structures. Comput Struct 1992;45:775-84.

[13] Bylund N. Fast and economic stiffness evaluation of mechanical joints. SAE Technical Paper 2003;1: No. 2751.

[14] Donders S, Takahashi Y, Hadjit R, Van Langenhove T, Brughmans M, Van Genechten B et al. A reduced beam and joint concept modeling approach to optimize global vehicle body dynamics. Finite Elem Anal Des 2009;45:439-55.

[15] Kim YY, Kim Y. A one-dimensional theory of thin-walled curved rectangular box beams under torsion and out-of-plane bending. Int. J. Numer. Methods Eng. 2002;53:1675-93.

[16] Kim Y, Kim YY. Analysis of thin-walled curved box beam under in-plane flexure. Int. J. Solids Struct 2003;40:6111-23.
[17] Jang G-W, Kim KJ, Kim YY. Higher-order beam analysis of box beams connected at angled joints subject to out-of-plane bending and torsion. Int J Numer Methods Eng 2008;75:1361-84.
[18] Jang G-W, Kim YY. Higher-order in-plane bending analysis of box beams connected at an angled joint considering cross-sectional bending warping and distortion. Thin-Walled Struct 2009;47:1478-89.
[19] Jang G-W, Kim YY. Vibration analysis of piecewise straight thin-walled box beams without using artificial joint springs. J Sound Vibr 2009;326:647-70.
[20] Choi S, Jang G-W, Kim YY. Exact matching condition at a joint of thin-walled box beams under out-of-plane bending and torsion. J Appl Mech-Trans ASME 2012;79:051018.
[21] Jang G-W, Choi S, Kim YY. Analysis of Three Thin-Walled Box Beams Connected at a Joint under Out-of-Plane Bending Loads. J Eng Mech 2013;139:1350-61.
[22] Choi S, Kim YY. Exact Matching at a Joint of Multiply-Connected Box Beams under Out-of-Plane Bending and Torsion. Eng Struct (under review).
[23] Choi S, Kim YY. Analysis of two box beams-joint systems under in-plane bending and axial loads by one-dimensional higher-order beam theory. Int. J. Solids Struct. (Submitted)
[24] Hibbett HD, Karlsson BI, Sorensen EP. ABAQUS/standard: User's Manual. 1998.
[25] Reddy JN. Theory and analysis of elastic plates. Philadelphia (PA): Taylor and Francis; 1999.
[26] Bauchau OA, Craig JI. Structural analysis: with applications to aerospace structures. New York: Springer; 2009.
[27] Babuška I. The finite element method with Lagrangian multipliers. Numer Math 1973;20:179-92.

CHAPTER 6.
Applications

6.1 Modal Analysis

A high computational cost is required to calculate natural mode shapes and frequencies of a thin-walled box beams-joint system using the detailed shell model. If the proposed one-dimensional approach can be applicable to the modal analysis of the box beams-joint system, the advantage of the proposed approach against the detailed shell analysis will be even more pronounced.

The modal analysis of the underbody structure shown in Fig. 6.1 is conducted by using the proposed analysis method. Sixteen field variables introduced in Chapter 3 and Chapter 5 are employed as the degrees of freedom of the higher-order beam theory, and the joint matching conditions derived in Chapter 3 and Chapter 5 are applied. The mass matrix for the box beam element is derived by following the procedure given in Jang and Kim [1].The material density ρ of the

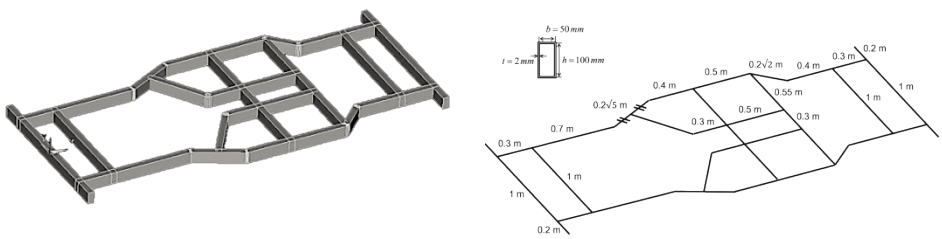

Fig. 6.1 a simplified beam model of the underbody structure

box beam is $7850\ \mathrm{kg/m^3}$. To check the accuracy of the proposed method, the analysis results of the proposed method are compared with those obtained by the detailed shell analysis and the Timoshenko beam analysis.

Table. 6.1 Modal analysis results for the underbody structure shown in Fig. 6.1

Mode		Shell (ABAQUS)	Proposed method	Timoshenko beams
1	out-of-plane 1st torsional mode	16.913	16.486 (2.5%)	34.072 (101.5%)
2	out-of-plane 1st bending mode	22.042	22.488 (2.0%)	37.978 (72.3%)
3	out-of-plane 2nd torsional mode	38.930	38.276 (1.7%)	74.172 (90.5%)
4	in-plane 1st bending mode	51.091	52.217 (2.2%)	65.723 (28.6%)
5	out-of-plane 2nd bending mode	53.236	54.367 (2.1%)	91.972 (72.8%)
6	in-plane 2nd bending mode	72.009	72.921 (1.3%)	93.262 (29.5%)
7	out-of-plane 3rd torsional mode	82.772	82.906 (0.2%)	142.03 (71.6%)
8	in-plane 1st extensional mode	99.366	100.88 (1.5%)	126.21 (27.0%)
9	out-of-plane 1st local bending mode	114.44	115.55 (1.0%)	158.26 (38.3%)
10	in-plane 3rd bending mode	123.22	123.20 (0.1%)	168.72 (36.9%)
Average Error (Maximum Error)		-	1.4% (2.5%)	56.9% (101.5%)

Observing the results given in Table. 6.1, the Timoshenko beam model significantly overestimates the dynamic stiffness of the underbody structure (the maximum error is 101.5%). In addition, the order of the lowest 10 natural modes is calculated incorrectly. Meanwhile, one can find that the proposed approach can predict the natural frequencies for the lowest 10 modes of the beam-joint system accurately (the maximum error is 2.5%). Through the example study, therefore, it can be found that the one-dimensional analysis method established in this study can be applicable to the modal analysis of thin-walled box beam structures.

The box beams connected at a joint are assumed to be identical in this study. However, the proposed analysis method is applicable to the box beams-joint systems consisting of the box beams with different cross-section dimensions. The joint matching conditions for the mentioned systems are identical, except that the common width b and height h of the cross-section are substituted by the width b_k and the height h_k (k=1, 2, …, N; N≥3) of each beam member (e.g. beam k).

To check the validity of the proposed method, the modal analysis of the T-joint structure shown in Fig. 6.2 is conducted. The widths of Beam 1 and 2 are b_1= b_2= 0.1 m, and the heights of those beams are h_1= h_2= 0.05 m. The width and height of Beam 3 are b_3 = 0.075 m and h_3 = 0.05 m, respectively. The dimensions of the T-joint structure considered in this study are identical to those composed with Rockers and B pillar in the simplified side frame structure [2].The analysis results of the proposed method are compared with those obtained by the detailed shell

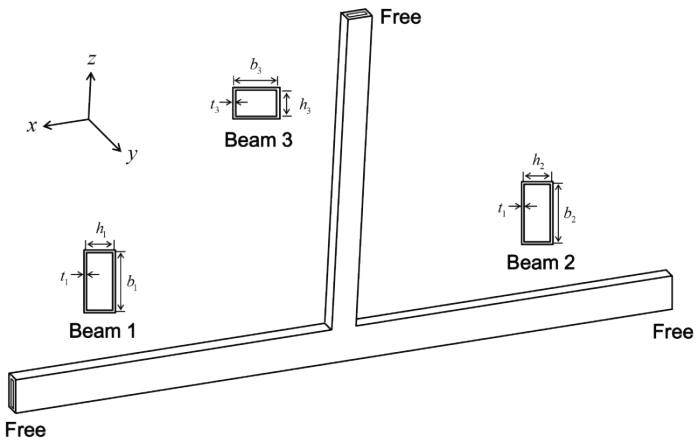

Fig. 6.2 T-joint structure consisting of the box beams with different cross-section dimensions

analysis and the Timoshenko beam analysis.

Table. 6.2 Modal analysis results for the T-joint structure shown in Fig. 6.2

Mode		Shell (ABAQUS)	Proposed method	Timoshenko beams
1	in-plane 1st bending mode	86.887	86.786 (0.1%)	92.625 (6.6%)
2	out-of-plane 1st bending mode	90.372	88.097 (2.5%)	91.511 (1.3%)
3	out-of-plane 1st torsional mode	105.79	104.85 (0.9%)	249.49 (135.8%)
4	out-of-plane 2nd torsional mode	129.21	122.77 (5.0%)	263.84 (104.2%)
5	in-plane 2nd bending mode	134.70	134.91 (0.2%)	137.27 (1.9%)
6	out-of-plane 3nd torsional mode	232.94	233.78 (0.4%)	466.37 (100.2%)
7	out-of-plane 4th torsional mode	246.63	248.15 (0.6%)	530.19 (115.0%)
8	out-of-plane 2nd bending mode	269.58	267.97 (0.6%)	633.81 (135.1%)
9	out-of-plane 3rd bending mode	302.06	299.56 (0.8%)	639.06 (111.6%)
10	out-of-plane 5th torsional mode	321.65	318.64 (0.9%)	828.10 (157.8%)
Maximum Error		-	5.0%	157.8%

Observing the results given in Table. 6.2, the Timoshenko beam model overestimates (more than twice) the dynamic stiffness of the T-joint structure and calculates the order of the lowest 10 natural modes incorrectly. On the other hand, the proposed method can interpret the accurate dynamic responses of the T-joint structure comparable to those by the shell analysis (the maximum error is 5.0%). Through the example case, therefore, one can find that the proposed approach is applicable to the box beams-joint systems consisting of different box beam members.

Some case studies for the T-joint structures (Fig. 6.3) are conducted to check the limitations of the proposed analysis method. The three box beams of the T-joint structures are assumed to be identical. The box beam member of the length

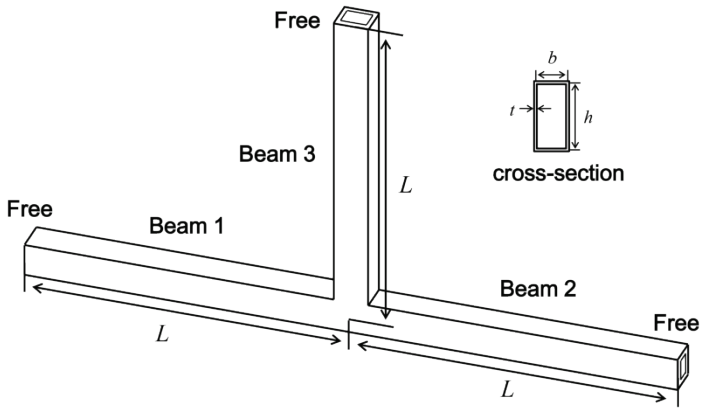

Fig. 6.3 T-joint structures consisting of three identical box beams

L=500 mm, width b= 50 mm, height h=50 mm, and thickness t=1 mm is considered as the reference (or standard) member for the case studies based on Ref. [2].

The limitation of the beam length to width ratio (L/b) is investigated through the modal analysis of the T-joint structures. The range of L/b for the considered T-

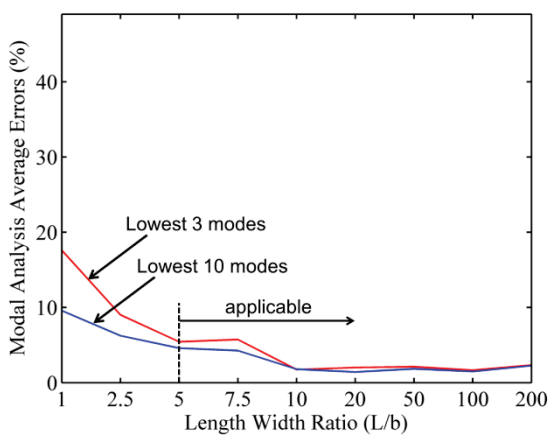

Fig. 6.4 Modal analysis errors for the T-joint structures with various length-width ratios (L/b)

joint structures is $1 \leq L/b \leq 200$, and other dimensions of the beam members are equal to those of the reference member.

The average errors of the predicted natural frequencies for the lowest three and ten modes are given in Fig. 6.3. Those errors are calculated based on the results by the shell analysis. The errors of the proposed method are around 2% when the ratio L/b is greater than ten. It is worth mentioning that the results of the proposed method are converged to those of the Timoshenko beam analysis when the ratio L/b is greater than 100 and that the results of the shell analysis are also converged to those of the Timoshenko beam analysis because the effects of the cross-sectional deformations are attenuated. Therefore, one can find that the proposed method does not have the upper limit for the beam length to width ratio L/b.

Meanwhile, the errors are increased rapidly when the ratio L/b is less than five. The reason is that the joint part becomes relatively larger in the T-joint structures when $L/b \leq 5$ while the joint is still modeled as a common point in the proposed method (the structural elements are normally regarded as the beams when $L/b \geq 10$). Therefore, it can be found that the proposed method cannot give accurate responses of the box beam systems when the ratio L/b of the box beams is less than 5.

The limitation of the thickness (t) is investigated for the next case study. The range of t for the considered T-joint structures is 0.01 mm$\leq t \leq$20 mm. The length is L=1000 mm and the other dimensions of box beam cross-section are equal to those of reference member and the length L of the box beams is L=1000 mm. Likewise, the modal analysis of the T-joint structures are conducted and the results of the

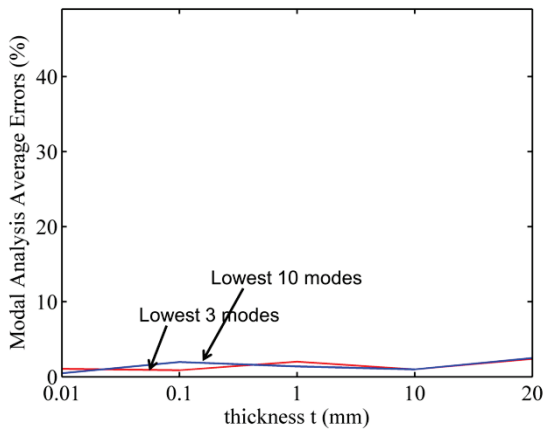

Fig. 6.5 Modal analysis errors for the T-joint structures with various thickness *t*

proposed method are compared with those by the shell analysis.

The average errors of the predicted natural frequencies for the lowest three and ten modes of the considered T-joint problems are given in Fig. 6.4. Observing the results, one can find that the proposed method do not have the limit for the box beam thickness *t*. Interestingly, the lowest ten modes are the local modes representing the vibrations of the box beam edges when the thickness *t* is 0.01 mm while the effects of the cross-sectional deformations are attenuated when $t \geq 10$ mm, and it is shown that the proposed method can express the behavior of the box beam system in both the limit cases.

Lastly, the limitation for the aspect ratio (h/b) of the box beam cross-section is investigated. The range of (h/b) for the considered T-joint structures is $1/10 \leq h/b \leq 10$, and other dimensions of the beam members are commonly L=1000 mm and t= 1 mm.

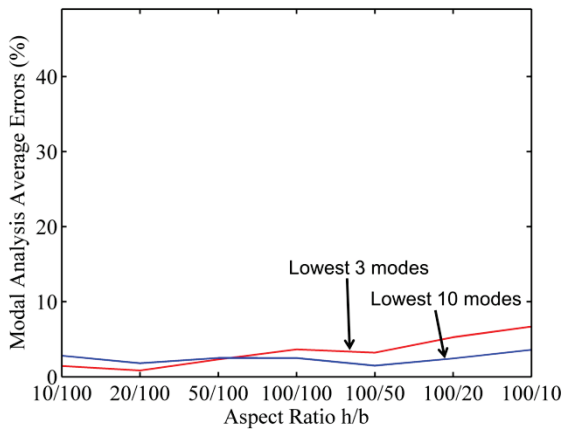

Fig. 6.6 Modal analysis errors for the T-joint structures with various aspect ratios (*h*/*b*)

The average errors of the predicted natural frequencies for the lowest three and ten modes of the considered T-joint problems are given in Fig. 11. Observing the results, one can find that the proposed method can capture the accurate dynamic behavior of the box beam systems even though the limit case of the aspect ratio *h/b* is considered (the average errors of the lowest three and ten modes are 6.5% and 3.6% respectively when *h/b* =10). Therefore, this case study shows that the proposed method do not have the limit for the aspect ratio *h/b* of box beam cross-section.

6.2 Extended Higher-Order Beam Model for the 3D Thin-Walled Box Beams-Shells Structures.

The proposed one-dimensional analysis can be employed for the accurate and

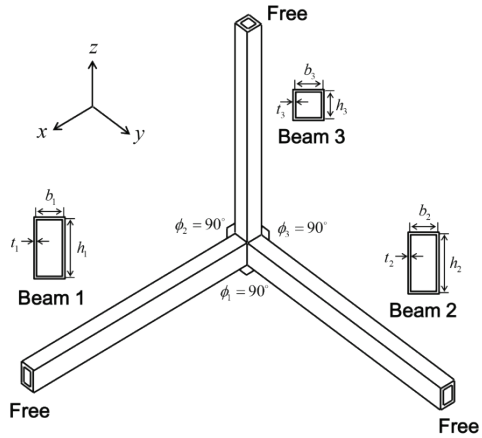

Fig. 6.7 A three-dimensional three box beams-joint system

efficient analysis and design of the automotive whole body structures if the analysis method is applicable to the three-dimensional box beams-joint systems. To this end, the exact matching conditions at a joint of the box beams being located in three-dimensional space are required. To check the possibility that the proposed approach for the derivation of the joint matching conditions can be extended to the joint of the three-dimensional box beams-joint systems, the joint matching conditions for the system shown in Fig. 6.7 are derived by employing the proposed approach. The higher-order beam theory considering torsional warping and distortion (Fig. 6.8) in addition to the six Timoshenko beam kinematic variables (or rigid-body motions) is employed. The distinctive feature of the joint matching conditions derived for the joint shown in Fig. 4 is that the torsional warping as well as the torsional distortion is coupled with the variables of the box beam rigid-body motions. The approach proposed in this paper is directly employed to the derivation

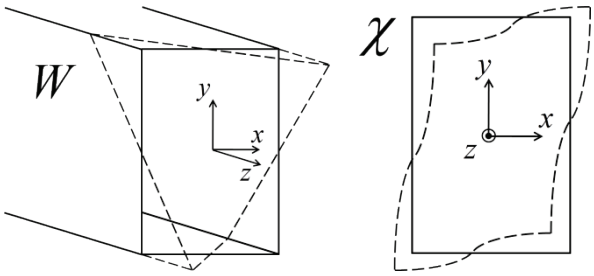

Fig. 6.8 Torsional warping W and distortion χ

of the matching conditions although additional considerations are introduced to derive the joint matching conditions including those coupling relations.

The modal analysis of the system shown in Fig. 6.7 is conducted to check the validity of the derived joint matching conditions, and the results of the proposed method are compared with those obtained by the shell analysis and the Timoshenko

Table. 6.3 Modal analysis results for the three-dimensional three box beams-joint system shown in Fig. 6.7

Mode	Shell (ABAQUS)	Proposed method	Timoshenko beams
1	43.8	47.0 (7.4%)	69.9 (59.6%)
2	56.3	57.2 (1.6%)	72.2 (28.2%)
3	66.1	65.7 (0.6%)	85.7 (29.6%)
4	267.1	266.1 (0.4%)	274.9 (2.9%)
5	290.1	291.7 (0.5%)	323.8 (11.6%)
6	318.4	319.4 (0.3%)	331.5 (4.1%)
7	321.7	320.6 (0.3%)	394.7 (22.7%)
8	408.4	405.8 (0.6%)	468.9 (14.8%)
9	414.0	420.3 (1.5%)	512.3 (23.7%)
10	476.0	475.7 (0.1%)	632.9 (33.0%)
Maximum Error	-	7.4%	59.6%

beam analysis.

Observing the results shown in Table. 6.3, one can find that the proposed method can calculate the lowest 10 natural frequencies of the considered system as accurately as those obtained by the shell analysis while the Timoshenko beam analysis highly overestimates the stiffness of the considered system. Because only two cross-sectional deformations (i.e. torsional warping and distortion) are considered as the higher-order deformation degrees among those introduced in this study, slightly inaccurate natural frequency of the first mode is calculated by the proposed method. More accurate result can be expected when more higher-order deformation degrees are employed. Through this example study, one can find that the one-dimensional analysis method established in this study can be extended for the analysis method of three-dimensional thin-walled box beam structures.

The automobile body structures can be simplified as the structures consisting of thin-walled box beams and shells [2]. Because the stiffnesses of the body structures such as the torsional stiffness are varied significantly depending on the presence or absence of the shells [2], establishing the analysis method for the structures consisting of box beams and shells is important to evaluate the static or dynamic stiffnesses of the body structures correctly.

Using the proposed one-dimensional approach, one can establish the analysis method for the box beams-shells structures modeling the box beams-joint system parts by the higher-order beam elements and modeling the shell parts by the detailed shell elements. The key problem in regard of this study is defining the

matching conditions between the degrees of the higher-order beam elements and those of the shell elements at the intersections of the box beams and the shells. The higher-order beam theory employed in this study can express the three-dimensional displacements ($\tilde{u}_n, \tilde{u}_s, \tilde{u}_z$) at a generic point ($n, s, z$) on the box beam member using the one-dimensional field variables and their shape functions. For examples, the three-dimensional displacements ($\tilde{u}_n, \tilde{u}_s, \tilde{u}_z$) expressed by the one-dimensional field variables $\mathbf{U} = \{U_y, \theta_x, \theta_z, W, \chi\}^{\mathrm{T}}$ representing the out-of-plane deformations are as:

$$\tilde{u}_n(n, s, z) = u_n, \quad \tilde{u}_s(n, s, z) = u_s - n\frac{\partial u_n}{\partial s}, \quad \tilde{u}_z(n, s, z) = u_z - n\frac{\partial u_n}{\partial z} \tag{6.1}$$

where (u_n, u_s, u_z) represent the displacements on the contour line ($n = 0$), and they are defined as:

$$u_n(s, z) = \psi_n^{U_y}(s)\cdot U_y(z) + \psi_n^{\theta_x}(s)\cdot \theta_x(z) + \psi_n^{\theta_z}(s)\cdot \theta_z(z) + \psi_n^{W}(s)\cdot W(z) + \psi_n^{\chi}(s)\cdot \chi(z) \tag{6.2a}$$

$$u_s(s, z) = \psi_s^{U_y}(s)\cdot U_y(z) + \psi_s^{\theta_x}(s)\cdot \theta_x(z) + \psi_s^{\theta_z}(s)\cdot \theta_z(z) + \psi_s^{W}(s)\cdot W(z) + \psi_s^{\chi}(s)\cdot \chi(z) \tag{6.2b}$$

$$u_z(s, z) = \psi_z^{U_y}(s)\cdot U_y(z) + \psi_z^{\theta_x}(s)\cdot \theta_x(z) + \psi_z^{\theta_z}(s)\cdot \theta_z(z) + \psi_z^{W}(s)\cdot W(z) + \psi_z^{\chi}(s)\cdot \chi(z) \tag{6.2c}$$

Therefore, one can define the matching conditions between the degrees of the box beam elements and those of the shell elements at the intersections by using the three-dimensional displacements given in Eq. (6.1) [3].

6.3 Optimization of Thin-Walled Box Beams-Joint Systems Using the Higher-Order Beam Analysis

A one-dimensional analysis approach being able to capture the behavior of thin-walled box beam structures correctly is required to carry out the design optimization of the thin-walled box beam structures. The classical Timoshenko beam analysis may be employed in the optimization of the box beam-joint system, but a reliable optimum solution cannot be expected because the responses of the system are not correctly evaluated. In fact, Kim et al. [4] have recently shown that two optimal solutions are obviously different when the same topology optimization problem is solved by using two different analysis approaches: the higher-order beam analysis [5] and the Timoshenko beam analysis, and they have proven the superiority of the design results obtained by the higher-order beam analysis through the comparison of the performances of the two design results by using the detailed shell analysis. Because the higher-order beam analysis being able to capture the accurate behavior of the beam-joint systems consisting of more than four box beams and under both in-plane and out-of-plane loads is finally established in this study, therefore, more advanced topology designs can be obtained by employing the proposed analysis method to the topology optimization of thin-walled box beam structures.

Meanwhile, there is a difficulty in the topology optimization using the higher-order beam theory that the joint matching conditions should be redefined when

some of box beams connected at a joint are disappeared in the process of the topology optimization. To solve this problem, Kim et al. [4] considered the combinations of the joint matching conditions for all possible connectivity of the box beams meeting at a joint, and employing the stacking method, they established the design approach which can automatically consider the appropriate joint matching conditions even though the connectivity of the box beams at a joint is varied in the optimization process. However, the number of box beams connected at a joint is limited to four or less in Kim et al. [4] because the combinations of the joint matching conditions are significantly increased when more than four box beams are connected at a joint. Therefore, additional considerations are required to establish a design approach applicable to more general topology optimization of the thin-walled box beam structures.

6.4 Adjustment of the Joint Matching Conditions Based on the Experimental Results

There have been efforts [6-8] to establish the analysis methods which can predict accurate responses of vehicle body structures comparable to the experiment results by using the joint springs. Those rotational spring concepts are mainly applied to the kinematic variables which represent the rotations of the box beam cross-section to express the additional joint flexibilities.

On the other hand, it has been shown in this study that the additional rotations of

box beam cross-sections at the joints are induced by the coupling effects with the higher-order deformation degrees. The coupling relations which are theoretically derived in this study are as:

$$(\Theta_x)_k = (\theta_x)_k\,; \quad (\Theta_z)_k = (\theta_z)_k - \frac{2b}{b+h}\chi_k \tag{6.3a}$$

$$(\Theta_y)_k = (\theta_y)_k + \frac{4h}{b(b+3h)}(W_1^1)_k - \frac{4h}{5b^2}(W_1^2)_k \tag{6.3b}$$

where ($(\Theta_x)_k, (\Theta_y)_k, (\Theta_z)_k$) represent the magnitudes of the cross-sectional rotations of Beam k (k=1, 2, …, N; N≥3) at a joint. One can find that additional rotation in z-direction at a joint is induced by the torsional distortion χ and that additional rotation in y-direction at a joint is induced by the bending warpings W_1^1 and W_1^2 (Fig. 6.9). Therefore, the accurate responses of the box beams-joint systems comparable to the experimental results can be obtained by the proposed method if the magnitudes of (χ, W_1^1, W_1^2) generated at the joints of the actual box

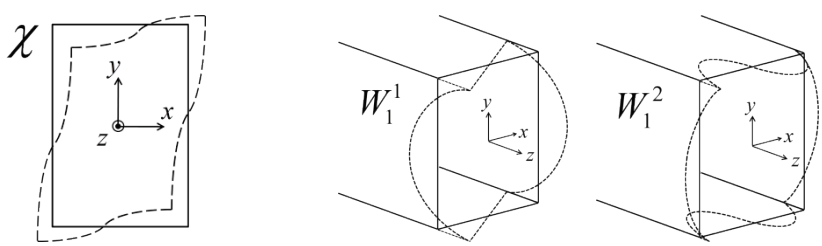

(a) (b)

Fig. 6.9 Cross-sectional deformations which are coupled with the rigid-body rotations at a joint: (a) torsional distortion χ, (b) bending warpings W_1^1, W_1^2

beam structures can be exactly evaluated by the proposed method. Due to various factors, however, the magnitudes of (χ, W_1^1, W_1^2) at an actual joint could be different with those calculated by the proposed numerical approach, and an accurate analysis model can be established by applying the correction factors to the variables (χ, W_1^1, W_1^2) in the proposed method. The correction factors for (χ, W_1^1, W_1^2) can be exactly obtained through the approaches given in Refs. [6-8].

References

[1] Jang G-W, Kim YY. Vibration analysis of piecewise straight thin-walled box beams without using artificial joint springs. J Sound Vibr 2009;326:647-70.

[2] Malen DE. Fundamentals of automobile body structure design. Warrendale(PA): SAE International.; 2011.

[3] Kim JH, Kim HS, Kim DW, Kim YY. 2002, New accurate efficient modeling techniques for the vibration analysis of T-joint thin-walled box structures. Int J Solid Struct 2002;39:2893-909.

[4] Kim DM, Kim SI, Choi S, Jang GW, Kim YY. Topology optimization of thin-walled box beam structures based on the higher-order beam theory. Int J Numer Meth Engng 2015 (online published). DOI: 10.1002/nme.5143.

[5] Jang G-W, Choi S, Kim YY. Analysis of Three Thin-Walled Box Beams Connected at a Joint under Out-of-Plane Bending Loads. J Eng Mech 2013;139:1350-61.

[6] Chang DC. Effects of flexible connections on body structural response. SAE Technical Paper 1974; No. 740041.

[7] Lee K, Nikolaidis E. A two-dimensional model for joints in vehicle structures. Comput Struct 1992;45:775-84.

[8] El-Sayed MEM. Calculation of joint spring rates using finite element formulation. Comput Struct 1989;33:977-81.

ABSTRACT (KOREAN)

다중 연결된 직사각 박판보에 관한 고차 보 이론 기반의 통합 해석 연구

최 수 민
서울대학교 대학원
기계항공공학부

조인트를 갖는 직사각 박판보 시스템의 거동을 올바르게 해석하는 일차원 보 해석 모델을 구축하기 위해서는 i) 보 부재 및 조인트의 유연한 거동을 유발하는 주요 단면변형들을 추가적인 기구학적 자유도로 포함하는 고차 보 이론의 개발과 함께 ii) 조인트에서 고려하는 기구학적 자유도들 사이의 역학적 관계를 나타내는 엄밀한 매칭 조건의 유도가 요구된다. 특히, 세 개 이상의 보 부재들이 한 개의 조인트에 다중으로 연결될 경우 전체 시스템의 강성을 결정할 만큼 매우 유연한 거동이 조인트에서 관찰되는데, 조인트에 연결된 보 부재의 개수 및 그들이 이루는 조인트 각에 따라 그 거동의 양상이 크게 달라지는 어려움이 있어 다양한 직사각 박판보-조인트 시스템들의 거동을 엄밀하게 해석하는 일관된 일차원 보 해석 모델은 아직 제안된 바 없다. 이러한 연구 배경 하에 본 연구에

서는 최초로 다중으로 연결된 직사각 박판보-조인트 시스템에 적용 가능한 일차원 고차 보 해석 모델을 구축하였다. 주목할 점은 본 연구에서는 기존에 알려진 합력들과 함께 소위 “모서리 합력”이라는 새로운 개념을 도입하여 조인트에 역학적으로 타당한 평형 관계를 정의하였으며, 정의된 평형 관계에 에너지 기법을 적용하여 결과적으로 엄밀한 조인트 매칭 조건을 이론적으로 유도해냈다는 것이다. 이러한 과정을 통해 유도된 조인트 매칭 조건은 조인트에 연결된 보의 개수 및 그들이 이루는 조인트 각에 무관하게 항상 적용 가능하다. 이와 더불어, 본 연구에서는 시스템에 면 내 하중이 작용할 때 관찰되는 조인트의 유연성을 엄밀하게 표현하기 위해 기존에 제안된 벤딩 워핑 및 벤딩 디스토션과 같은 고차 변위들을 좀 더 정확하게 재 정의하였으며, 그와 함께 그 동안 고려되지 않았던 새로운 고차 변위들을 추가적으로 고차 보 이론에 도입하였다. 제안하는 일차원 해석 모델의 정확성 및 유효성을 검증하기 위해 몇 가지 주요한 수치 예제들을 해석해 보았으며, 그를 통해 제안하는 해석 모델이 직사각 박판보-조인트 시스템들의 거동을 쉘 요소 기반 상세 모델의 해석만큼 정확하게 예측함을 확인하였다.

주요어: 직사각 박판보, 고차 보 이론, 조인트 평형, 조인트 매칭 조건

학 번: 2009-20732